

# Electrons and Optical Phonons in Mesoscopic Semiconductor Heterostructures

Der Fakultät für Mathematik, Naturwissenschaften und Informatik  
der Brandenburgischen Technischen Universität Cottbus

zur Erlangung des akademischen Grades

Doktor der Naturwissenschaften  
(Dr. rer. nat.)

genehmigte Dissertation

vorgelegt von

Diplom-Physikerin  
Elena Roxana Racec, geb. Țepuș

geboren am geboren am 02.01.1972 in Filipeștii de Tîrg, Rumänien

Gutachter: Prof. Dr. rer. nat. habil. E. Sigmund

Prof. Dr. rer. nat. habil. H. Heyszenau

Prof. Dr. D. E. N. Brancuș

Tag der mündliche Prüfung: 16.07.2002



## Abstract

We analyze here some electron properties and lattice dynamics in semiconductor heterostructures, pointing out the dramatic changes relative to the bulk properties due to the existence of the interfaces in these systems.

The first part of the study is devoted to the electron scattering phenomena in noninteracting open systems and to the transport properties described in the Landauer-Büttiker formalism. The physics of open systems is often dominated by resonances; we relate the isolated and interacting transport resonances with poles of the S matrix in the complex energy plane. We develop a resonant theory of transport and apply it first to the conductance through a quantum dot embedded in a quantum wire. We find two basic contributions to the conductance: first, a resonant one described by a Fano profile with a complex asymmetry parameter and second, a noncoherent background which can be assumed as a constant in the case of small overlap of the conductance peaks. We establish a method to reconstruct the S-matrix from the experimental conductance data. As a second application we analyze the capacitance of a two dimensional electron gas formed in a MIS-type semiconductor heterostructure. The measured step in the C-V characteristic associated to the formation of a field induced two-dimensional electron gas is due to the formation of an intermediate resonance in the energetic domain of the occupied scattering states. This is a separate type of resonance with distinct characteristics: in contrast to the quasibound state i) it is localized in the space between the probe and the isolated quantum system, ii) its energy lies in the classically allowed regime, and iii) its line shape is strongly asymmetric. Excellent quantitative agreement with the experimental capacitance measurements is obtained.

In the second part of the study we illustrate how the optical phonon spectra and the electron-optical phonon interaction are modified in a strained semiconductor heterostructure relative to their isotropic bulk constituents. In contrast to an isotropic system for a double heterostructure, for which the median layer is uniaxial, four major new features are found: i) the degeneracy of the normal modes confined in the uniaxial layer is lifted, the frequencies being distributed in two domains which correspond to the frequencies of the so-called quasilongitudinal and quasitransverse modes of the uniaxial bulk systems; ii) for some strong anisotropy the character of some modes (interface or confined) depends on the domain of values of the in-plane wave vector; iii) an electron placed outside the uniaxial layer interacts strongly with the confined modes; iv) for some strong anisotropy the interaction between an electron situated inside the uniaxial layer and the quasitransverse modes is unexpectedly large. The results are particularized for double heterostructures InP/GaAs/InP grown on the faces (001) and (111) of the substrate.



# Contents

<b>1</b>	<b>Introduction</b>	<b>3</b>
<b>2</b>	<b>Ballistic Transport in Mesoscopic Systems</b>	<b>5</b>
2.1	Ballistic and Diffusive Regimes of Transport . . . . .	5
2.2	Mesoscopic Semiconductor Heterostructures . . . . .	8
2.3	One-Particle Electronic States . . . . .	13
2.3.1	Potential Energy for the Electrons . . . . .	13
2.3.2	R Matrix Method for Solving 1D Scattering Problems . . . . .	16
2.3.3	Electronic Wave Functions . . . . .	28
2.4	Noninteracting Low-Dimensional Electron Gas . . . . .	28
2.4.1	Multi-Electron System . . . . .	28
2.4.2	Electrical Charge- and Current Density . . . . .	30
2.4.3	System in Thermodynamic Equilibrium . . . . .	33
2.5	Electronic Transport . . . . .	35
2.6	Summary . . . . .	36
<b>3</b>	<b>Applications</b>	<b>37</b>
3.1	Conductance through a Quantum Dot . . . . .	37
3.2	Capacitance of a Field Induced 2DEG . . . . .	45
<b>4</b>	<b>Resonances in Transport Phenomena</b>	<b>53</b>
4.1	Analyticity Properties of the S Matrix . . . . .	54
4.1.1	Resonant States in the R Matrix Theory . . . . .	55
4.2	Conductance Resonances in a Quantum Dot . . . . .	56
4.2.1	Fano Resonances in Transmission . . . . .	58
4.2.2	Coherent and Noncoherent Contributions . . . . .	66
4.2.3	Comparison with Experimental Data . . . . .	68
4.3	Capacitance of a Field Induced 2DEG . . . . .	72
4.4	Summary . . . . .	77
<b>5</b>	<b>Optical Phonons in Uniaxial Slabs</b>	<b>79</b>
5.1	Equations of Motion . . . . .	80
5.2	Normal Modes . . . . .	84
5.2.1	s-Polarized Phonon Modes . . . . .	84

5.2.2	<i>p</i> -Polarized Phonon Modes . . . . .	84
5.3	Hamiltonian of the Optical Phonon Field . . . . .	92
5.4	Electron-Phonon Interaction . . . . .	94
5.4.1	Interaction with the Surface Modes . . . . .	95
5.4.2	Interaction with the Confined Modes . . . . .	96
5.5	Normal Modes for Different Uniaxial Materials . . . . .	96
5.5.1	Uniaxial Materials with Surface Modes . . . . .	98
5.5.2	Uniaxial Materials without Surface Modes . . . . .	112
5.6	Summary . . . . .	116
<b>6</b>	<b>Optical Phonons in Uniaxial Double Heterostructures</b>	<b>117</b>
6.1	Geometry of the Problem . . . . .	118
6.2	Equation of Motion . . . . .	119
6.3	Normal Modes . . . . .	120
6.3.1	Interface Modes . . . . .	120
6.3.2	Normal Modes Confined in the Uniaxial Layer . . . . .	121
6.3.3	Half-Space Modes . . . . .	123
6.4	Hamiltonian of the Optical Phonon Field . . . . .	124
6.5	Electron-Phonon Interaction . . . . .	124
6.6	Bisotropically Strained Double Heterostructures . . . . .	125
6.6.1	Heterostructures Grown on the Face (001) . . . . .	126
6.6.2	Heterostructures Grown on the Face (111) . . . . .	130
6.7	Summary . . . . .	133
<b>7</b>	<b>Conclusions</b>	<b>135</b>
<b>A</b>	<b>Hamilton Operator of a Bound System</b>	<b>139</b>
<b>B</b>	<b>Unitarity of the <math>\tilde{S}</math>-matrix</b>	<b>145</b>
	<b>Bibliography</b>	<b>147</b>

# Chapter 1

## Introduction

Nanostructures based on semiconductor heterostructures are nowadays commonly used in electronic and optoelectronics devices [1, 2]. On the other hand, physical phenomena related to semiconductor nanostructures, such as the confinement of electron in zero, one, and two dimensions, are of great interest and have contributed to the definition of new concepts in condensed matter physics [3, 4, 5]. A proper theoretical description of semiconductor nanostructures is, thus, of crucial importance since it allows for investigating fundamental physics and for optimizing nanostructure-based devices.

In his lecture addressed on the occasion of the 2000 Nobel Prize award [4], Herbert Kroemer has defined the heterostructures as "heterogenous semiconductor structures built from two or more different semiconductors, in such a way that the transition region or interface between the different materials plays an essential role in any device action. Often, it may be said that the interface is the device". Modern methods of epitaxial growth [6] molecular beam epitaxy (MBE) and metal-organic chemical vapor deposition (MOCVD), have provided the capability of fabricating a huge variety of heterostructures of different semiconductors compounds with interfaces of atomic precision.

The existence of the interfaces in semiconductor heterostructure yields dramatic changes of the electron properties and of the lattice dynamics. Some aspects of these modifications and their effects on the transport properties are analyzed in this work. The thesis is structured as follows:

In Chap. 2 we describe the general theoretical basis of our approach for ballistic transport in mesoscopic systems. Our interest is focused on open quantum systems coupled to the contacts not only by tunnel barriers but also through classically allowed energy channels for the electron motion. We develop a model based on the independent electron approach and, to keep the mathematical complications to a minimum, we concentrate on the behavior of the effectively one dimensional systems at low temperatures and in zero magnetic field. We make use of the general S matrix theory [7, 8, 9] to reformulate the scattering problem for a system with nonspherical symmetry. To calculate the scattering wave functions of the electrons in

semiconductor heterostructure we use the R matrix representation of the scattering matrix [10, 11, 12]. All transport properties of the system are derived from the scattering matrix and from the wave functions in the framework of the Landauer-Büttiker formalism.

In Chap. 3 we calculate as examples the conductance through a quantum dot embedded in a quantum wire [13] and the capacitance of a two dimensional electron gas formed in a MIS-type semiconductor heterostructure [14], based on the transport theory developed in the previous chapter. These two particular systems allow for a continuous variation of the coupling between the active region (scattering system or quantum system) and the contacts.

In Chap. 4 we present in detail an analytical theory of the transport resonances which is derived from the poles of the scattering matrix in the complex energy plane [13]. As an advantage, the R matrix approach used here permits a convenient separation of the singular part in S matrix and, thus, allows for a very simple method to find the poles associated with all types of resonances: quasibound states, Fowler-Nordheim and Fabry-Perot resonances. The particular representation of the S matrix in terms of the R matrix also allows for a systematic expansion of the scattering matrix in a consistent Laurent series around every pole and, after that, for a linearization of the problem for quasi-isolated resonances [13]. The result is a Fano line shape with a complex asymmetry parameter which is the most general description of a resonance in terms of a single level interacting with a constant background. To exemplify this resonance line shape we analyze the two systems presented in Chap. 3.

In order to elucidate the role of the uniaxial anisotropy on the spectra of optical phonons and, in turn, on the electron-phonon interaction, we discuss in Chap. 5 a simple system, namely a uniaxial semiconductor slab with the optical axis directed along the normal to the surfaces. We use the dielectric continuum model of Born and Huang [15] with electrostatic boundary conditions. Investigation of the normal modes have been carried out excluding the retardation of the Coulomb interaction. The obtained results are particularized for slabs made from natural uniaxial materials, namely CdS, PbI<sub>2</sub> and SnS<sub>2</sub>, and the particular characteristics of each type of uniaxial anisotropy are pointed out.

In Chap. 6 we analyze the optical phonon modes of a double semiconductor heterostructure having as median layer an anisotropic uniaxial polar material with the optical axis directed along the normal to the interfaces. Similarly to the case of the uniaxial slab, the eigenfrequencies and the eigenvectors of the optical phonon field, as well as the electron-optical phonon coupling functions, are obtained in the context of the dielectric continuum model. Using the bisotropic strain model for the pseudo-morphic layer uniaxially distorted [16], we discuss here the dispersion laws of the phonon modes and their interaction with the conduction electrons for the InP/GaAs/InP heterostructures grown on the faces (001) and (111) of the substrate. We analyze the systems presented in Ref. [17] for which there are no effects induced by relaxation.



# Chapter 2

## Ballistic Transport in Mesoscopic Systems

### 2.1 Ballistic and Diffusive Regimes of Transport

In the simplest case of *ballistic transport* in mesoscopic semiconductor structures, one may assume that particles move from a reservoir (*source contact*) to another (*drain contact*) through the "active region" without scattering, except for possible reflection from barriers, inside this region or from the region boundaries.

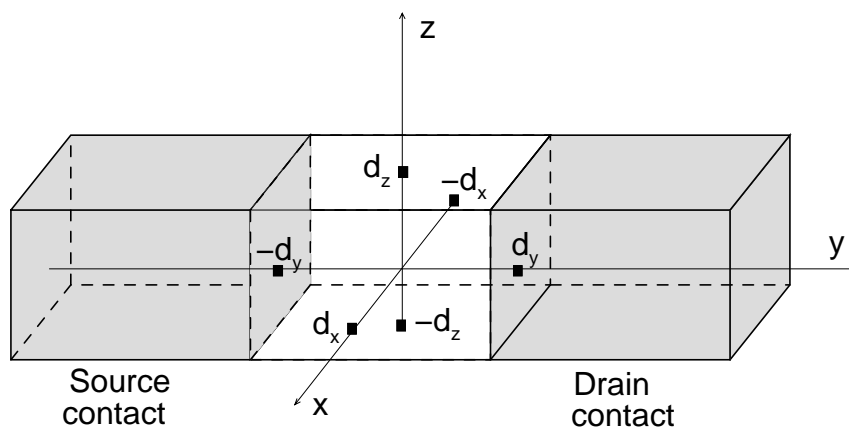


Figure 2.1: A system relevant for the transport properties sandwiched between source and drain contact. The system is confined in a box with the sizes  $2d_x$ ,  $2d_y$  and  $2d_z$ .

In the opposite limit the transport is *diffusive* and corresponds to the particle movement through a disordered system, in which the impurities act as elastic scatterers for the carriers [2].

Following Ando [1], we introduce some length scales characterizing mesoscopic systems which allow for a definition of the two transport regimes.

### System size

Consider the "active region" between contacts as a box with size  $2d_x \times 2d_y \times 2d_z$  (for simplicity we suppose  $d_x < d_y < d_z$ ). The energy of a particle in this box is given by

$$E(n_x, n_y, n_z) = \frac{\hbar^2}{2m} \left[ \left( \frac{\pi n_x}{2d_x} \right)^2 + \left( \frac{\pi n_y}{2d_y} \right)^2 + \left( \frac{\pi n_z}{2d_z} \right)^2 \right],$$

where  $n_x, n_y, n_z$  are integers.

When many electrons are confined into a box we also have to consider the charge energy  $E_C$ , due to the Coulomb interaction among electrons, in addition to the quantum mechanical quantization energy  $E(n_x, n_y, n_z)$  given above. The typical charge energy required for adding or removing an electron is  $E_C = e^2/8\pi\epsilon_0 d$   $d \sim d_x \sim d_y \sim d_z$ .

### Fermi Wavelength

The Fermi wavelength

$$\lambda_F = \frac{2\pi}{k_F}.$$

is directly related to the Fermi wave vector  $k_F$  and, thus, to the electron density  $n$ . At zero temperature, electrons occupy states specified by the wave vector  $\mathbf{k}$  with  $|\mathbf{k}| \leq k_F$  and

$$n = \begin{cases} \frac{2}{(2\pi)^3} \frac{4\pi}{3} k_F^3, & \text{for 3D systems} \\ \frac{2}{(2\pi)^2} \pi k_F^2, & \text{for 2D systems} \\ \frac{2}{(2\pi)} 2k_F, & \text{for 1D systems} \end{cases},$$

where the factor 2 comes from the electron spin. In typical metals such as Cu and Ag ( $n \simeq 10^{22} \text{ cm}^{-3}$  at  $T=300\text{K}$ ), Fermi wavelength is of the order of a few angstroms and, in semiconductors such as 2D systems realized in GaAs/AlGaAs heterostructures, we have  $\lambda_F \simeq 400\text{\AA}$  for the electron concentration  $n \simeq 3 \times 10^{11} \text{ cm}^{-2}$ .

The system in Fig. (2.1) can roughly be categorized as bulk system or as mesoscopic system, depending on the relative magnitude of  $d_x, d_y, d_z$ , and  $\lambda_F$ :

1. Macroscopic system (bulk system or 3D) for  $\lambda_F \ll d_x < d_y < d_z$
2. Mesoscopic system for which the size is large compared to the microscopic (atomic) scale but small compared to the macroscopic scale[2].
  - Quasi 2D (thin film) for  $\lambda_F \sim d_x \ll d_y < d_z$
  - 2D (MOSFET, heterostructure) for  $d_x < \lambda_F \ll d_y < d_z$
  - Quasi 1D (quantum wire) for  $d_x < d_y \sim \lambda_F \ll d_z$
  - 1D for  $d_x < d_y < \lambda_F \ll d_z$
  - 0D (quantum dot) for  $d_x < d_y < d_z \ll \lambda_F$

### Mean Free Path

Transport in large macroscopic systems is studied using the Boltzmann equation[18], which introduces the important length scale called the mean free path  $\Lambda$ . The mean free path is the average orbit-length covered by an electron before being scattered into a different wave vector direction. At sufficiently low temperatures, the transport is determined by electrons with energies around Fermi energy  $E_F$  and, therefore, we have

$$\Lambda = v_F \tau,$$

where  $v_F$  is the Fermi velocity and  $\tau$  is the relaxation time. The conductivity is usually written as

$$\sigma = \frac{ne^2\tau}{m^*},$$

where  $n$  is the electron concentration and  $m^*$  the effective electron mass.

An electron makes a ballistic motion without being scattered on a scale smaller than the mean free path, but it makes a diffusive motion on the scale larger than  $\Lambda$ . The diffusive motion is characterized by the diffusion coefficient  $D$ , given in the limit of low temperatures by

$$D = v_F^2 \tau = \frac{\Lambda^2}{\tau} = \Lambda v_F.$$

The transport through mesoscopic systems is divided into the diffusive and ballistic regimes, depending on the relative magnitude of the mean free path  $\Lambda$  and the system size  $2d$ . In the diffusive regime ( $\Lambda \ll 2d$ ), the transport can be understood as diffusive process and is essentially independent of the form of the system. In the ballistic regime ( $\Lambda \gg 2d$ ), the electron makes a ballistic motion inside the system and the system boundary plays the role of scatterer instead of impurities.

Metallic wire or dots usually have  $\Lambda \sim 100\text{\AA}$ , and the system size is larger. Because Fermi wavelength ( $\lambda_F \sim 1 - 2\text{\AA}$ ) is much smaller than the system size, the quantization of the energy levels is not important except for very low temperatures, when the separation between nearest neighbor energy levels becomes comparable to  $k_B T$  (where  $T$  is the temperature and  $k_B$  the Boltzmann constant). In the metallic dots, therefore, the most important energy scale is the charge energy due to the Coulomb interaction.

In semiconductor heterostructures having a high quality the mean free path can be as large as  $50\ \mu\text{m}$  and ballistic transport occurs. Further, the Fermi wave length is large ( $\lambda_F \sim 300 - 500\text{\AA}$ ) and can be comparable to the system size. The quantization due to the system confinement plays a very important role.

### Phase Coherence Length

We consider an electron system whose motion is described by a single Schrödinger equation. However, in real semiconductors an electron interacts with many other degrees of freedom (for example other electrons or lattice vibrations) and changes its energy. The phase of the electron is destroyed by such dynamical interactions and

the distance over which an electron maintains its phase memory is called the phase coherence length. For the phase relaxation time  $\tau_\phi$  determined by the inelastic scattering, the phase coherence length is given by  $L_\phi = \sqrt{D\tau_\phi} = \Lambda\sqrt{\tau_\phi/\tau}$  in the diffusive regime and  $L_\phi = v_F\tau_\phi$  in the ballistic regime.

In mesoscopic systems, sizes can be comparable to or smaller than the phase coherence length. Usually, observed quantities in macroscopic systems are the average over ensembles of various systems, since each system consists of many subsystems described by independent Schrödinger equations. When the phase coherence becomes comparable to the system size, then the whole system is governed by a single Schrödinger equation and observed quantities are not averaged out.

The temperature is another important factor which can contribute to the loss of phase coherence. At nonzero temperatures, transport properties are determined by a thermal average for states having an energy lying in the interval  $(E_F - k_B T, E_F + k_B T)$ . This means that the electron loses its phase memory after a time interval of the order of  $\hbar/k_B T$ . The size corresponding to this time interval is the thermal diffusion length given by

$$L_T = \sqrt{\frac{D\hbar}{k_B T}},$$

when the electron makes a random walk characterized by the diffusion constant  $D$ .

## 2.2 Mesoscopic Semiconductor Heterostructures

The generic system that we analyze further is a semiconductor heterostructure where the charge carriers are introduced either by modulation doping, or they flow in and out of the system through heavily doped (metallic) contacts. Transport in these systems can roughly be divided into two categories: perpendicular transport and parallel transport, according to whether the motion of charge carriers is perpendicular or parallel to the layers that form the heterostructure.

### Perpendicular Transport

We present first the two systems that have dominated the research in low-dimensional physics: MIS-type (metal-insulator-semiconductor) heterostructure and modulation-doped heterostructure. In both of them a two dimensional electron gas (2DEG) is developed.

In the MIS-type systems the 2DEG is confined to the interface between a semiconductor and an insulator (as in silicon MOSFETs) or to the interface between two different semiconductors (as in GaAs/AlGaAs MIS-type heterostructures, presented in Fig. 2.2). The external electric field pushes the electrons against a highly impenetrable barrier; they can move along the plane of the interface but are bound to it in the perpendicular direction [5].

In the modulation doped GaAs/AlGaAs heterostructures (see Fig. 2.3), one can separate the mobile electrons from their parent impurities by confining them to

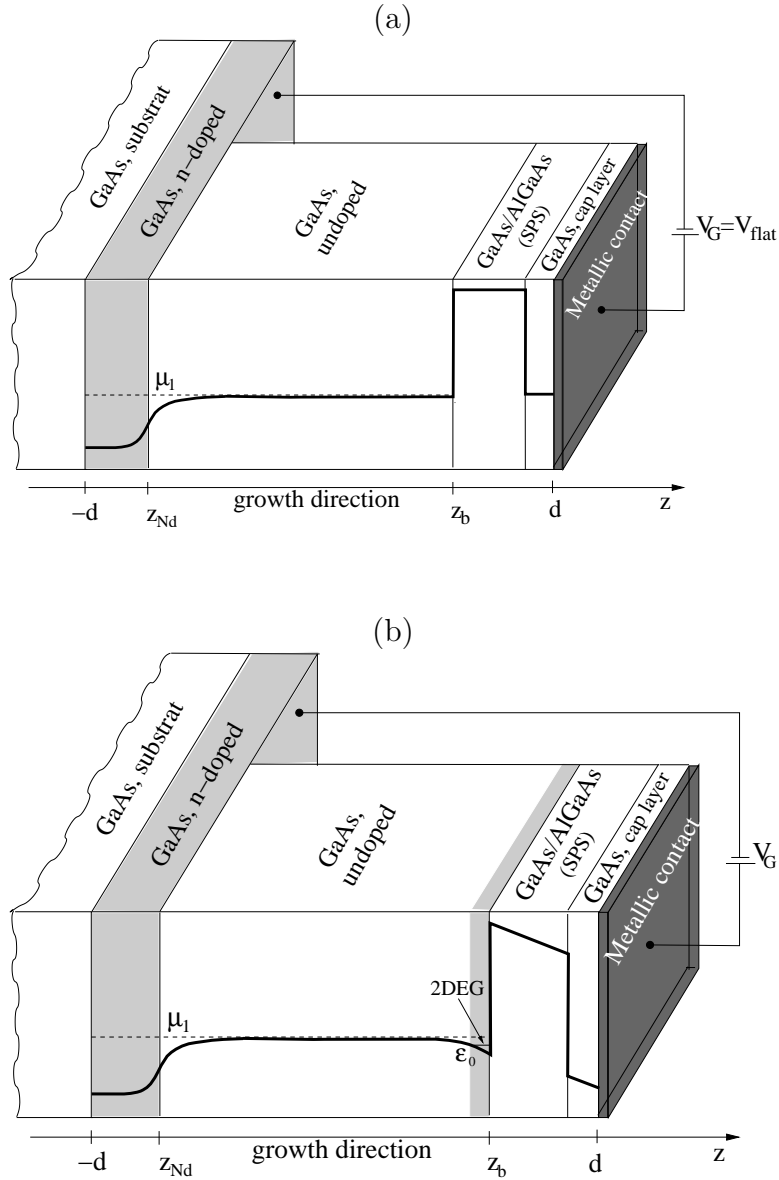


Figure 2.2: A GaAs/AlGaAs MIS-type heterostructure. Schematic illustration of the conduction band diagram for (a)  $V_G = V_{\text{flat}}$  for which the "flat band" condition is satisfied and (b) for a value  $V_G$  of the gate voltage for which the field-induced two dimensional electron gas appears in front of the blocking barrier[14].

different neighboring layers. Each Si atom introduced in the AlGaAs layer easily loses its additional electron, which, in turn, becomes a conduction electron. Seeking the energetically lowest state, the electron "falls down" into the GaAs layer whose conduction band lays about 300 meV under the AlGaAs conduction band. The attraction from all positively charged silicon ions pulls the mobile electrons against the AlGaAs barrier. The carriers become quantum mechanically bound to the interface, but remain mobile within the plane transverse to the growth direction [5]. The motion at the interface is not perturbed from the scattering or impurities. The selective doping principle has become incorporated into the high-electron-mobility transistor (HEMT).

In both structures, we have electrons that are "trapped" at an interface, but move without scattering (with metallic-like conduction properties) along the interface. The physics of these electron systems has been of wide interest, while attempts to improve the performance of these structures as devices have led to many of the new materials and device technologies. Historically, the Si-SiO<sub>2</sub> system dominated research in the 1970s [20], while the GaAs/AlGaAs heterojunction dominated research in the 1980s. A lucky combination of a number of properties, i.e., a small effective mass and wide energy gap, effective radiative recombination, a sharp optical absorption edge due to the "direct" band structure, a high mobility at the absolute minimum of the conduction band, ensured for GaAs a central place in the semiconductor physics and electronics. Since the high mobility electron systems are obtained in semiconductors only by using heterostructures between a GaAs layer serving as active region and a wide band gap semiconductor acting as barrier, the most promising system is the GaAs/AlGaAs multilayer nanostructure. The reason is the "Great Crystallographic Accident" that AlAs, GaAs and the (Al,Ga)As alloy systems have the same lattice parameter [3, 4].

Such high-electron-mobility heterostructures very often form the basis for fabricating the quantum waveguide and quantum dot structures. The primary focus of our attention is on the transport properties in nanostructures; quantum dots provide some of the most interesting experiments in this regard. Rich phenomena are observed not only because of quantum confinement and the resonant structures associated with this confinement, but also due to the granular nature of the electron charge. In contrast to the quantum wells and quantum wires, quantum dots are sufficiently small that even the introduction of a single electron is sufficient to change the transport properties, due to the charging energy associated with this extra electron.

If we restrict our analysis only to the perpendicular transport, there have been several experiments on quantum dot structures containing only a few electrons. These include the two-terminal asymmetric double barrier tunneling structure [21] and the gated double barrier tunneling structure [22], used for analyzing transport properties, and the vertically gated modulation-doped heterostructure [23] used for capacitance measurements. As an example, we present in Fig. 2.4 the schematic diagram of the vertical quantum dot obtained by Schmidt et al [21] adding a lateral

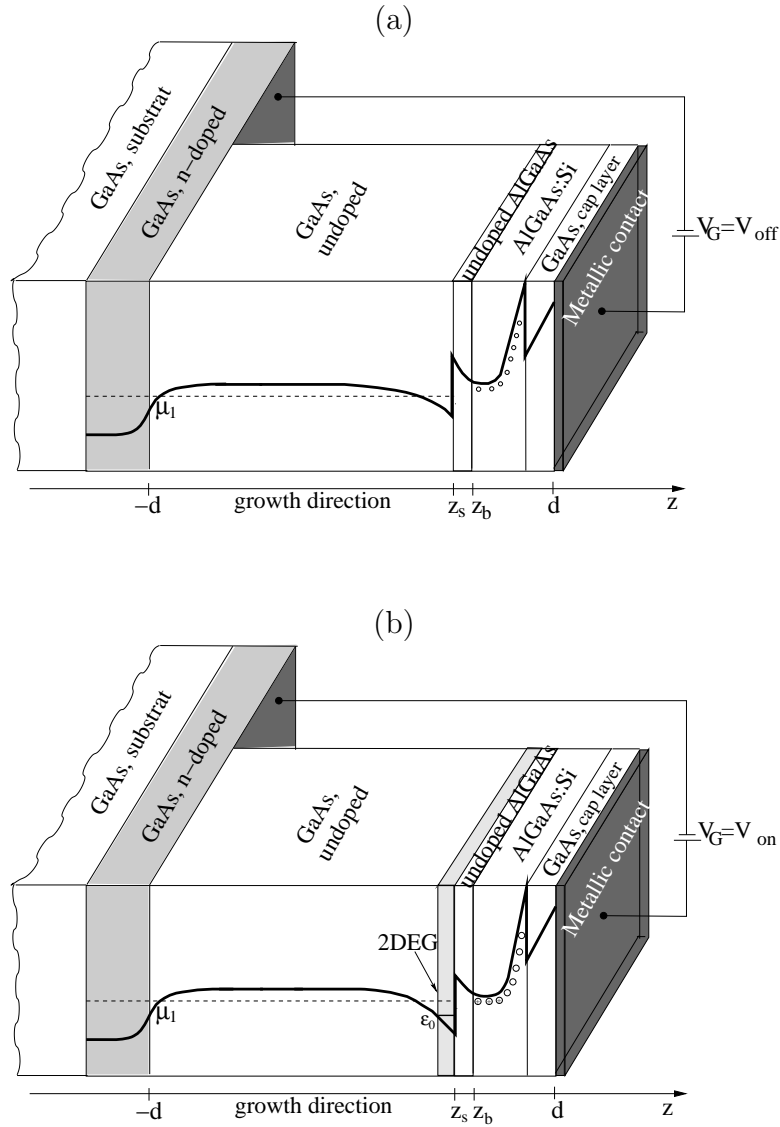


Figure 2.3: A GaAs/AlGaAs modulation doped heterostructure. Schematic illustration of the conduction band diagram for (a) normally off ( $V_G = V_{\text{off}}$ ) and (b) normally on ( $V_G = V_{\text{on}}$ ) device (in accord with Weisbuch and Vinter [19]). In the first case the impurity level lays far from the chemical potential of the structure and the probability to have ionized donors is small. Consequently, the concentration of the conduction electrons at the interface is negligible. With increasing applied voltage on the gate the edge of the conduction band goes down and the ionization probability increases. Conduction electrons are generated and they move to the neighboring GaAs layer, where they can occupy lower energy levels. The positive charge of the ions confines the electrons in the GaAs layer.

confinement to a double barrier heterostructure. The dot has the shape of a disk with a diameter roughly 10 times the thickness. In such a submicrometer-diameter resonant tunneling diode, the potential in the transport direction is given by two asymmetric barriers which isolate the dot from the contacts. The lateral potential has a cylindrical symmetry with a rather soft boundary profile, which can be approximated by a harmonic potential. Consequently, the electrons are accumulated in the dot and manifest atom-like properties.

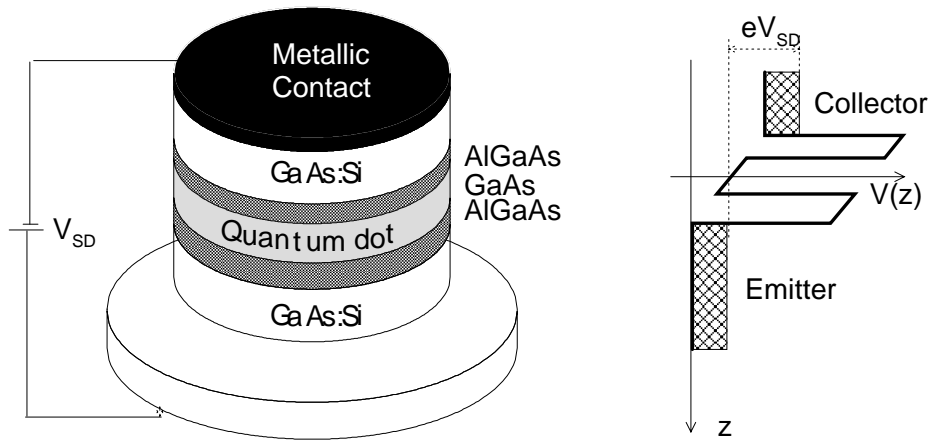


Figure 2.4: Left side: Schematic representation of a two-terminal asymmetric double barrier tunneling structure [21]. Right side: Sketch of the energy diagram for finite bias voltage.

### Parallel Transport

In the case of parallel transport, an infinite variety of structures can be envisioned: quantum point contacts [24], quantum wires [25], and quantum dots [2]. Assuming we start with a 2DEG heterostructure, confinement of the 2DEG in another direction can be realized by etching the heterostructure or by using an electrostatic potential due to metal gates (split-gate technique). By adjusting the gate potential it is possible to deplete the underlying two-dimensional electron gas, and, thus, to introduce spatial modulation of the two-dimensional charge density.

As an example, we present here the single electron transistor (SET) used by Kastner and coworkers [26] for studies of the Kondo effect and the Fano resonances in transport. A SET consists of a small droplet of electrons coupled to two conducting leads by tunnel barriers. The droplet is created in a 2DEG that forms at the interface of a high electron mobility GaAs/AlGaAs heterostructure. Applying a negative voltage to two pairs of split gate electrodes depletes the 2DEG underneath them and forms the two tunnel barriers. The barriers separate the droplet of electrons from the 2DEG region on either side, and these regions act as leads. The heights of the two



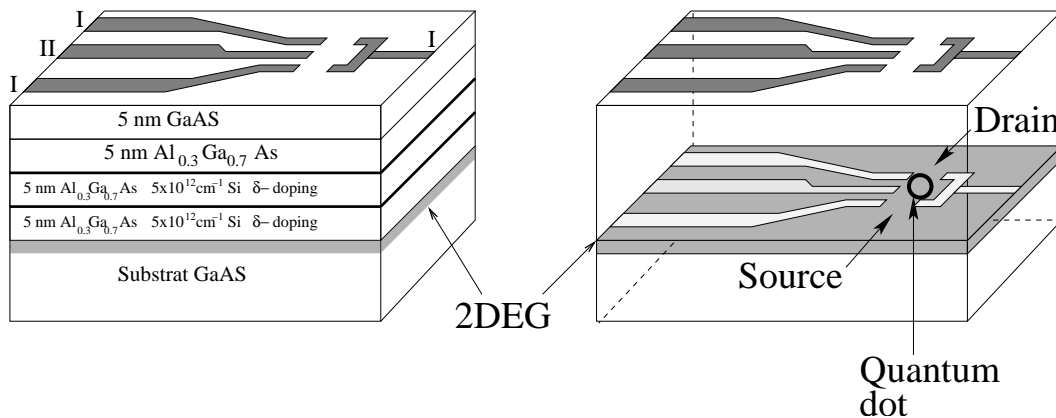


Figure 2.5: Schematic representation of the SET described in Ref, [26] (left side) and the two dimensional electron gas and the depletion regions generated by the top split gates in plane of the 2DEG.

barriers can be modified independently by changing the voltage on the respective constriction electrodes (denoted by I in Fig. 2.5). Also, the potential energy of the electrons on the droplet can be shifted relative to the chemical potentials in the leads, by using an additional plunger gate electrode (denoted by II in Fig. 2.5). The electrons in this system move in a potential which has a very complicated dependence on the position but, in the first approximation, one can consider a total confinement in the lateral directions (perpendicular on the transport direction) and a two barrier potential between source and drain.

## 2.3 One-Particle Electronic States

We begin the analysis of the electronic states in mesoscopic heterostructures, by developing a model based on the independent (quasi)electron approach; This approach is perfectly justified at least in the case of the open quantum systems that are coupled to the contacts (particles reservoirs) through particle exchange [27].

### 2.3.1 Potential Energy for the Electrons

The wave function, which describes the electronic state of energy  $E$ , is a solution of the Schrödinger equation:

$$\left[ \frac{1}{2m^*} \vec{P}^2 + V_{eff}(\vec{r}) - E \right] \Psi(E, \vec{r}) = 0, \quad (2.1)$$

where  $\vec{P}$  is the momentum operator,  $V_{eff}(\vec{r})$  is the effective potential energy which is a sum of the heterojunction conduction band discontinuities, the electrostatic

potential due to the ionized donors and acceptors, the self-consistent Hartree and exchange potentials due to free carriers and external potentials. In Fig. 2.6 is presented the potential energy of an effectively one dimensional structure, without external electric field, considering the electrostatic interaction among charges in the system.

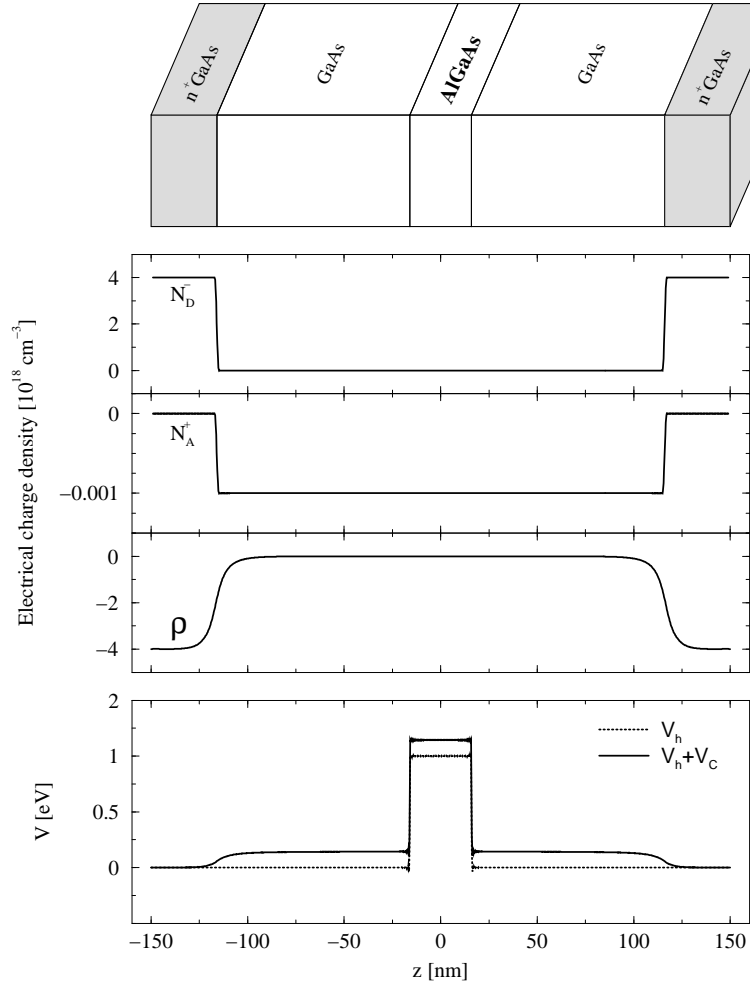


Figure 2.6: Upper part: Schematic illustration of the system geometry. Middle part: Electrical charge distribution in the structure, fixed charge of the ionized donors and acceptors,  $N_D^-$  and  $N_A^+$ , respectively and electronic mobile charge  $\rho$ . Lower part: Potential energy in which the electrons move, given by the heterostructure band off-sets ( $V_h$ ) and Coulomb interaction ( $V_C$ ). [28]

The electronic states in mesoscopic systems are easily described within the effective mass approximation whose validity requires that the envelope function  $\Psi(E, \vec{r})$  be slowly varying over dimensions comparable to the unit cell of the crystal [29].

The system (active region and contacts) is considered isotropic and its dimensions ( $2L_x, 2L_y, 2L_z$ ) large enough to be extended to infinity ( $d \ll L_x, L_y, L_z, d$  being the size of the active region).

Further, we restrict our analysis to the case of semiconductor nanostructures, in which the current flows only in one direction, from source to drain contact, called transport direction; any kind of residual current is neglected. This means that the electrons are either bound in the lateral directions or freely moving in a plane perpendicular to the transport direction, so that the mean value of the lateral current is zero. Consequently, the potential energy in which the electrons move should have a perpendicular component  $V_{\perp}(\vec{r})$ , which we assume independent of the coordinate in the transport direction, i.e.  $V_{\perp}(\vec{r}) \equiv V_{\perp}(\vec{r}_{\perp})$ . For the structures which contain only a 2DEG and no lateral modulation (see. Figs. 2.2 and 2.3)  $V_{\perp}(\vec{r}_{\perp}) = 0$ , whereas for quantum dots  $V_{\perp}(\vec{r}_{\perp})$  is considered either a parabolic or a square infinite well potential energy. We assume, also, that except for this overall component  $V_{\perp}(\vec{r}_{\perp})$ , there is no other lateral potential which can supplementary confine the electrons in a certain region of the structure. Thus, the potential energy is separable,

$$V_{eff}(\vec{r}) = V(z) + V_{\perp}(\vec{r}_{\perp}). \quad (2.2)$$

This special form of  $V_{eff}(\vec{r})$  seems to be a strong restriction and it is not easy to imagine its validity in the case of structures with very complicate geometry, like the dot realized by Göres et al [26, 30] (see Fig. 2.5), but it is the price payed for a good analytical description of the transport phenomena in semiconductor nanostructures.

Due to the separable form of the potential, a particular solution of the Schrödinger equation (2.1) associated to the energy  $E$  is

$$\Psi_{\nu,i}^{(s)}(E; \vec{r}) = \phi_{\nu,i}(\vec{r}_{\perp}) \psi^{(s)}(\epsilon, z), \quad (2.3)$$

where  $\nu$  indexes the energy levels associated with the motion in the lateral directions,  $i$  corresponds to the degeneracy of the level  $\epsilon'_{\perp}$ ,  $\epsilon = E - \epsilon'_{\perp}$ , and  $s$  is the degeneracy index for the electron motion in the transport direction. The functions  $\phi_{\nu,i}(\vec{r}_{\perp})$  and energies  $\epsilon'_{\perp}$  are the solutions of the eigenvalue problem

$$\left[ \frac{1}{2m^*} \vec{P}_{\perp}^2 + V_{\perp}(\vec{r}_{\perp}) - \epsilon'_{\perp} \right] \phi_{\nu,i}(\vec{r}_{\perp}) = 0. \quad (2.4)$$

The Hamilton operator for this problem is a Hermitian one and, consequently, the eigenfunction set  $\{\phi_{\nu,i}(\vec{r}_{\perp})\}_{(\nu,i)}$  forms a basis for which the orthogonality and completeness relations

$$\begin{aligned} \int d\vec{r}_{\perp} \phi_{\nu,i}^*(\vec{r}_{\perp}) \phi_{\nu',i'}(\vec{r}_{\perp}) &= \delta_{\nu\nu'} \delta_{ii'}, \\ \sum_{\nu} \sum_i \phi_{\nu,i}^*(\vec{r}_{\perp}) \phi_{\nu,i}(\vec{r}'_{\perp}) &= \delta(\vec{r}_{\perp} - \vec{r}'_{\perp}) \end{aligned} \quad (2.5)$$

are valid. The indexes  $(\nu, i)$  are generic; for a free electron system in a plane perpendicular to the transport direction these indexes should be replaced by a 2D wave

vector  $\vec{k}_\perp$ . The energy spectrum becomes continuous ( $\epsilon_\perp = \hbar^2 k_\perp^2 / 2m^*$ ). Thus, in Eqs. (2.5)  $\delta_{\nu\nu'}\delta_{ii'}$  is transformed into  $\delta(\vec{k}_\perp - \vec{k}'_\perp)$  and the sums over  $\nu$  and  $i$  become an integral over  $\vec{k}_\perp$ . Each energy level  $\epsilon_\perp$  is degenerate with an infinite degeneracy. In the opposite limit, for a complete confinement of the system in the lateral directions, the energy levels are discrete and nondegenerate, and  $(\nu, i)$  is substituted by a quantum number.

The  $z$ -dependent function in the expression (2.3) is a solution to the one dimensional eigenvalues problem:

$$\left[ \frac{1}{2m^*} P_z^2 + V(z) - \epsilon \right] \psi^{(s)}(\epsilon, z) = 0. \quad (2.6)$$

For all systems, which are included in the category of nanostructures, the potential energy  $V(z)$  has some common properties. There is an active region (see Fig. 2.1) which is small at the scale of the whole system. Inside this region, the electrons are elastically scattered from interfaces between different layers or between allowed and not allowed (depletion) domains of the 2DEG. This region is called "scattering region" and it is embedded between two contacts, which are practically semi-infinite homogeneous semiconductors, and the electrons inside move in a potential energy given only by the bulk conduction band structure. Thus, from the mathematical point of view, the potential energy  $V(z)$  should be a function which varies considerably over small distances inside the "scattering region" and is constant outside, i.e.  $V(z < -d) = V_1$  and  $V(z > d) = V_2$ , where  $\pm d$  are the limits of the "scattering region". It can not be established a relation between the surfaces of the scattering region and the interfaces between layers or domains of the 2DEG. Each interface can cause elastic scatterings and should be included in the scattering region. Thus, the planes  $z = \pm d$  are chosen inside the homogeneous materials of the contacts, far enough from any interface and, of course, the choice is not unique.

In addition, we assume some mathematical properties for the potential energy  $V(z)$ ; this function is considered continuous for all values of the  $z$ -coordinate and satisfying the condition  $V(z) \geq -az^2 - b$ , where  $a, b > 0$ , which ensures the self-adjointness of the Hamilton operator [9] of the problem (2.6).

### 2.3.2 R Matrix Method for Solving 1D Scattering Problems

The above considerations about the potential energy, in which the electrons move, allow us to reduce the Schrödinger equation to the effectively one dimensional eigenvalue problem (2.6). This problem is essentially a scattering problem for a particle with the mass  $m^*$ , in a potential with nonspherical symmetry, and it is usually solved in the scattering matrix approach [31].

In the stationary description of the scattering process, it is assumed that the wave function of the system at large distances from the scattering center is a superposition of the incident and scattered waves [32]. In our case, the electrons are elastically scattered inside the domain  $[-d, d]$  and one may consider, for all points outside this

region, the  $z$ -dependent part of the wave function as a sum of an incoming- and an outgoing exponential functions:

$$\psi(\epsilon, z) = \begin{cases} \psi^{in}(\epsilon, -d) \exp[ik_1(z+d)] + \psi^{out}(\epsilon, -d) \exp[-ik_1(z+d)], & z \leq -d \\ \psi_{in}(\epsilon, z), & |z| < d \\ \psi^{in}(\epsilon, d) \exp[-ik_2(z-d)] + \psi^{out}(\epsilon, d) \exp[ik_2(z-d)], & z \geq d \end{cases} \quad (2.7)$$

where

$$k_s(\epsilon) = \sqrt{\frac{2m^*}{\hbar^2}(\epsilon - V_s)}, \quad s = 1, 2. \quad (2.8)$$

If  $\epsilon > V_s$  then  $k_s$  is a nonzero positive number according to the definition of the real square root function. However, if  $\epsilon < V_s$ , we have to take the first branch of the complex square root function, so that  $k_s = i\lambda_s$ , where  $\lambda_s$  is a positive real number.

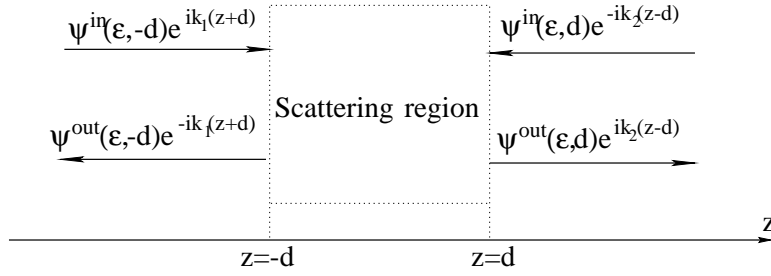


Figure 2.7: Incoming and outgoing parts of the wave function  $\psi(\epsilon, z)$

The expansion coefficients  $\psi^{in/out}(\epsilon, \pm d)$  in Eq. (2.7) are, generally, complex numbers and for a fixed energy  $\epsilon$  can not be all independent. Each wave function and its first derivative have to satisfy the continuity conditions at  $z = \pm d$ ,

$$\lim_{z \nearrow \pm d} \psi(\epsilon, z) = \lim_{z \searrow \pm d} \psi(\epsilon, z), \quad (2.9)$$

$$\lim_{z \nearrow \pm d} \frac{d}{dz} \psi(\epsilon, z) = \lim_{z \searrow \pm d} \frac{d}{dz} \psi(\epsilon, z). \quad (2.10)$$

However, in the case of an arbitrary dependence on  $z$  of the potential energy between  $z = -d$  and  $z = d$ , we can not directly use these conditions because the function inside the scattering region,  $\psi_{in}(\epsilon, z)$ , is not yet known.

For energies smaller than the minimum of the potential energy  $V(z)$ , the solution given by Eq. (2.7) should be zero and  $\psi^{in/out}(\epsilon, \pm d) = 0$ . If the energies are greater than  $\min[V(z)]$ , the eigenvalue spectrum of the one dimensional Schrödinger equation (2.6) has a discrete part for  $\min(V_1, V_2) > \epsilon > \min[V(z)]$ , associated with bound states, and a continuous part for  $\epsilon > \min(V_1, V_2)$ , corresponding to the scattering

states. Further we assume  $V(z) \geq \min(V_1, V_2)$ ,  $\forall z \in \mathbf{R}$ ; we are interested here in describing elastic processes which contribute to the transport phenomena and, in this case, the bound states do not play any role. As it is shown in Ref. [9], Chap. 4, this condition imposed on the potential energy leads to a Hamilton operator of the 1D scattering problem (2.6) which is self-adjoint.

### Definition of the S Matrix

If we consider a free particle ( $V(z) \rightarrow 0$ ,  $\forall z$ ), the energy density operator is

$$H_0 = -\frac{\hbar^2}{2m^*} \frac{d^2}{dz^2} = \frac{1}{2m^*} P_z^2 \quad (2.11)$$

and it is obvious that it commutes with the momentum operators  $P_z$ . It results immediately that the eigenfunctions of  $P_z$

$$\begin{aligned} \psi_0^{(1)}(\epsilon, z) &= \frac{1}{\sqrt{2\pi}} \exp [ikz], \\ \psi_0^{(2)}(\epsilon, z) &= \frac{1}{\sqrt{2\pi}} \exp [-ikz] \end{aligned} \quad (2.12)$$

associated with the eigenvalues  $\pm k = \pm\sqrt{2m^*\epsilon/\hbar^2}$  are also eigenfunctions of  $H_0$ , corresponding to the eigenvalue  $\epsilon = \hbar^2 k^2 / 2m^* > 0$ . For a fixed energy  $\epsilon$  there are two independent solutions of the free particle eigenvalue problem and, thus, for a particle in a scattering potential there should be at most two independent solutions that correspond to the same energy  $\epsilon$  (the scattering potential represents a constriction for the particle and can only reduce the degrees of freedom). Consequently, there are at most two independent expansion coefficients in Eq. (2.7) and we choose them  $\psi^{in}(\epsilon, \pm d)$ . The coefficients corresponding to the outgoing waves in Eq. (2.7) should be functions of  $\psi^{in}(\epsilon, \pm d)$ ,

$$\begin{pmatrix} \psi^{out}(\epsilon, -d) \\ \psi^{out}(\epsilon, +d) \end{pmatrix} = \begin{pmatrix} S(\epsilon; -d, -d) & S(\epsilon; -d, +d) \\ S(\epsilon; +d, -d) & S(\epsilon; +d, +d) \end{pmatrix} \begin{pmatrix} \psi^{in}(\epsilon, -d) \\ \psi^{in}(\epsilon, +d) \end{pmatrix}. \quad (2.13)$$

This matrix contains all the information about the collisions in the system [9], Chap. 4, and is called the scattering matrix (S matrix); it is defined for each value of the energy  $\epsilon$  associated with the motion of the electron in the transport direction.

If there is no scattering ( $V(z) \rightarrow 0$ ), the scattering functions given by Eq. (2.7) with the conditions  $V_1, V_2 \rightarrow 0$  and  $d \rightarrow 0$  should be equivalent with those in Eqs. (2.12). For a free particle the energy levels are degenerate, with the order of degeneracy two, and for each energy  $\epsilon$  there are two wave functions corresponding to particles incident from the left and right side, respectively.

For a particle coming from the left side,

$$\begin{pmatrix} \psi^{in}(\epsilon, -d) \\ \psi^{in}(\epsilon, d) \end{pmatrix} = C_1 \begin{pmatrix} 1 \\ 0 \end{pmatrix}, \quad (2.14)$$

in the limit  $V_1, V_2 \rightarrow 0$  ( $k_1 = k_2 = k$ ) we obtain from Eq. (2.7) the wave function outside the scattering region of the form

$$\psi(\epsilon, z) = \begin{cases} C_1 \exp[ik(z+d)] + \psi^{out}(\epsilon, -d) \exp[-ik(z+d)], & z \leq -d \\ \psi^{out}(\epsilon, d) \exp[ik(z-d)], & z \geq d \end{cases}. \quad (2.15)$$

The limit  $d \rightarrow 0$  in the above expression yields exactly the first function of Eqs. (2.12), corresponding to a free particle, if

$$\lim_{d \rightarrow 0} \begin{pmatrix} \psi^{out}(\epsilon, -d) \\ \psi^{out}(\epsilon, d) \end{pmatrix} = C_1 \begin{pmatrix} 0 \\ 1 \end{pmatrix} \quad (2.16)$$

and  $C_1 = 1/\sqrt{2\pi}$ .

It can be analogously demonstrated that, for a particle coming from the right side,

$$\begin{pmatrix} \psi^{in}(\epsilon, -d) \\ \psi^{in}(\epsilon, d) \end{pmatrix} = C_2 \begin{pmatrix} 0 \\ 1 \end{pmatrix}, \quad (2.17)$$

the second function of Eqs. (2.12) is obtained from Eq. (2.7) in the free particle limit, if

$$\lim_{d \rightarrow 0} \begin{pmatrix} \psi^{out}(\epsilon, -d) \\ \psi^{out}(\epsilon, d) \end{pmatrix} = C_2 \begin{pmatrix} 1 \\ 0 \end{pmatrix} \quad (2.18)$$

and  $C_2 = 1/\sqrt{2\pi}$ .

So, if the particle becomes free, the S matrix should be of the form  $\begin{pmatrix} 0 & 1 \\ 1 & 0 \end{pmatrix}$ .

For an arbitrary potential  $V(z)$ , we do not know how the S matrix looks like, but the scattering processes make it more complex than above. Although its elements should strongly depend on the form of the scattering potential, there are a few general properties of this matrix, that will be derived further.

### Wave functions outside the scattering region

The expression of the wave function, for points outside the scattering region, is given by Eq. (2.7) and we analyze it in detail for the continuous region of the energy spectrum of the equation (2.6).

- $\epsilon \geq \max(V_1, V_2)$

For a fixed energy  $\epsilon$ , there are two independent solutions of equation (2.6). This is not a unique way of defining these eigenfunctions, but we prefer to use the so called scattering functions. The first one corresponds to a particle coming from the left side of the system (see Eq. (2.14)) and is obtained from the general expression (2.7) and the definition (2.13) of the S matrix:

$$\psi^{(1)}(\epsilon, z) = \frac{1}{\sqrt{2\pi}} \begin{cases} \exp [ik_1(z + d)] + S(\epsilon; -d, -d) \exp [-ik_1(z + d)], & z \leq -d \\ S(\epsilon; d, -d) \exp [ik_2(z - d)], & z \geq d \end{cases}. \quad (2.19)$$

Generally, the wave functions are solutions of a differential equation and are defined up to a constant factor. In the above expression, we fix this constant, so that, in the limit  $V(z) \rightarrow 0$ , the scattering function (2.19) becomes an eigenfunction of the momentum operator  $P_z$ .

In the present calculation we only analyze the elastic scattering processes, so that an incident particle with the energy  $\epsilon$  can be either transmitted or reflected from the potential  $V(z)$ . In this case, we can identify the element  $S(\epsilon; -d, -d)$  of the S matrix with the reflection amplitude,  $r^{(1)}(\epsilon)$ , and the element  $S(\epsilon; d, -d)$  with the transmission amplitude,  $t^{(1)}(\epsilon)$ , of the particle coming from the left side of the system.

The second scattering function is given by

$$\psi^{(2)}(\epsilon, z) = \frac{1}{\sqrt{2\pi}} \begin{cases} S(\epsilon; -d, d) \exp [-ik_1(z + d)], & z \leq -d \\ \exp [-ik_2(z - d)] + S(\epsilon; d, d) \exp [ik_2(z - d)], & z \geq d \end{cases} \quad (2.20)$$

and corresponds to a particle coming from the right side of the system for which Eq. (2.17) is valid. The reflection and transmission amplitudes for such a particle are  $r^{(2)}(\epsilon) = S(\epsilon; d, d)$  and  $t^{(2)}(\epsilon) = S(\epsilon; -d, d)$ , respectively.

- $\max(V_1, V_2) > \epsilon \geq \min(V_1, V_2)$

We consider  $V_1 \geq V_2$  and it follows that  $k_2$  is a pure real- and  $k_1$  a pure imaginary number for energies between  $V_2$  and  $V_1$ . Because the wave function has finite values for each  $z$  and each energy, the coefficient  $\psi^{in}(\epsilon, -d)$  should be zero. In this case, there is only one scattering function for a fixed energy  $\epsilon$



and outside the scattering region it has the expression

$$\psi^{(2)}(\epsilon, z) = \frac{1}{\sqrt{2\pi}} \begin{cases} S(\epsilon; -d, d) \exp[-ik_1(z+d)], & z \leq -d \\ \exp[-ik_2(z-d)] + S(\epsilon; d, d) \exp[ik_2(z-d)], & z \geq d \end{cases}, \quad (2.21)$$

which corresponds to a particle coming from the right side of the system. The reflection and transmission amplitudes for this particle are  $r^{(2)}(\epsilon) = S(\epsilon; d, d)$  and  $t^{(2)}(\epsilon) = S(\epsilon; -d, d)$ , respectively.

The condition  $V_1 > \epsilon \geq V_2$  implies that  $k_1$  is a purely imaginary number and the wave function corresponding to the energy  $\epsilon$  decays exponentially into the left region, outside the scattering system ( $z < -d$ ). The corresponding state is called quasibound state. In this case, the energy level  $\epsilon$  is not degenerate anymore. The time translational invariance requires that  $(\psi^{(2)}(\epsilon, z))^*$  is also a solution of the 1D Schrödinger equation (2.6) corresponding to the energy  $\epsilon$ . That means  $(\psi^{(2)}(\epsilon, z))^* = c\psi^{(2)}(\epsilon, z)$ , where  $c$  is a constant, and  $r^{(2)}(\epsilon) = 1$ ,  $t^{(2)}(\epsilon) \in \mathbf{R}$ .

The constant  $1/\sqrt{2\pi}$  is chosen only to have a similar expression as in Eq. (2.20); if the particle becomes free, the quasibound states do not exist anymore and there is no supplementary condition to determine the constant up to which the wave function is defined.

Analogously, in the case  $V_1 < V_2$ , the eigenfunction corresponding to the energy  $\epsilon$  is given as

$$\psi^{(1)}(\epsilon, z) = \frac{1}{\sqrt{2\pi}} \begin{cases} \exp[ik_1(z+d)] + S(\epsilon; -d, -d) \exp[-ik_1(z+d)], & z \leq -d \\ S(\epsilon; d, -d) \exp[ik_2(z-d)], & z \geq d \end{cases}. \quad (2.22)$$

It describes a particle coming from the left side of the system characterized by the reflection and transmission amplitudes  $r^{(1)}(\epsilon) = S(\epsilon; -d, -d)$  and  $t^{(1)}(\epsilon) = S(\epsilon; d, -d)$ , respectively. The condition  $V_1 < \epsilon \leq V_2$  implies that  $k_2$  is a purely imaginary number and the function describes a quasibound state exponentially decaying in the region  $z > d$ , and with  $r^{(1)}(\epsilon) = 1$ ,  $t^{(1)}(\epsilon) \in \mathbf{R}$ .

We can conclude that the scattering functions correspond to the continuous energy spectrum of the Schrödinger equation and are given by

$$\psi^{(1)}(\epsilon, z) = \frac{\theta(\epsilon - V_1)}{\sqrt{2\pi}} \begin{cases} \exp [ik_1(z + d)] + S(\epsilon; -d, -d) \exp [-ik_1(z + d)], & z \leq -d \\ S(\epsilon; d, -d) \exp [ik_2(z - d)], & z \geq d \end{cases}, \quad (2.23)$$

$$\psi^{(2)}(\epsilon, z) = \frac{\theta(\epsilon - V_2)}{\sqrt{2\pi}} \begin{cases} S(\epsilon; -d, d) \exp [-ik_1(z + d)], & z \leq -d \\ \exp [-ik_2(z - d)] + S(\epsilon; d, d) \exp [ik_2(z - d)], & z \geq d \end{cases}. \quad (2.24)$$

for points outside the scattering region. The step functions

$$\theta(\epsilon - V_s) = \begin{cases} 1, & \epsilon > V_s \\ 0, & \epsilon < V_s \end{cases}, \quad s = 1, 2, \quad (2.25)$$

ensure that, in the domain of the quasibound states ( $\min(V_1, V_2) < \epsilon \leq \max(V_1, V_2)$ ), there is only one scattering function for each energy  $\epsilon$ . We define further the  $2 \times 2$  matrix  $\Theta(\epsilon)$  as

$$\Theta(\epsilon) = \begin{pmatrix} \theta(\epsilon - V_1) & 0 \\ 0 & \theta(\epsilon - V_2) \end{pmatrix} \quad (2.26)$$

and write the wave functions into a very useful matrix form:

$$\begin{pmatrix} \psi^{(1)}(\epsilon, z < -d) \\ \psi^{(2)}(\epsilon, z < -d) \end{pmatrix} = \frac{\Theta(\epsilon)}{\sqrt{2\pi}} \left[ \begin{pmatrix} \exp [ik_1(z + d)] \\ 0 \end{pmatrix} + \mathbf{S}^t(\epsilon) \begin{pmatrix} \exp [-ik_1(z + d)] \\ 0 \end{pmatrix} \right] \quad (2.27)$$

for  $z < -d$  and

$$\begin{pmatrix} \psi^{(1)}(\epsilon, z > d) \\ \psi^{(2)}(\epsilon, z > d) \end{pmatrix} = \frac{\Theta(\epsilon)}{\sqrt{2\pi}} \left[ \begin{pmatrix} 0 \\ \exp [-ik_2(z + d)] \end{pmatrix} + \mathbf{S}^t(\epsilon) \begin{pmatrix} 0 \\ \exp [ik_2(z + d)] \end{pmatrix} \right] \quad (2.28)$$

for  $z > d$ .  $\mathbf{S}^t(\epsilon)$  is the transpose of the S matrix.

### Wave functions inside the scattering region

In the case of a general potential inside the scattering region, we can not represent the wave functions  $\psi_{\text{in}}^{(s)}(\epsilon, z)$  by elementary functions and it is necessary to expand

them into a basis of eigenfunctions of a solvable problem. In the R matrix formalism the Wigner-Eisenbud basis is considered, i.e. the eigenbasis of the Hamilton operator corresponding to the closed counterpart of the studied scattering problem. This method, intensively used in the nuclear reaction theory [33, 34], became also important in the last ten years for describing transport phenomena [27],[10]-[12].

### Wigner-Eisenbud problem

We consider an electron of mass  $m^*$ , moving in the potential  $V(z)$  given in Eq. (2.6), but, contrary to the scattering problem described there, confined between  $z = -d$  and  $z = d$ . The corresponding eigenvalue problem, called Wigner-Eisenbud problem, is

$$\left[ -\frac{\hbar^2}{2m^*} \frac{d^2}{dz^2} + V(z) - \epsilon_l \right] \chi_l(z) = 0 \quad (2.29)$$

with the boundary conditions

$$\left. \frac{d\chi_l}{dz} \right|_{z=\pm d} = 0 \quad (2.30)$$

and with  $\chi_l(z)$  defined only for  $z \in [-d, d]$ . As it is shown in Appendix A the Hamilton operator for this problem is self-adjoint and allows for a discrete ( $l \geq 1$ ,  $l \in \mathbf{N}$ ) and nondegenerate energy spectrum. The corresponding eigenfunctions can be chosen as real functions and we impose that they be normalized. The self-adjointness of the Hamiltonian ensures that the eigenfunctions constitute a basis for which the orthogonality and the completeness relations are valid,

$$\int_{-d}^d dz \chi_l(z) \chi_{l'}(z) = \delta_{ll'}, \quad (2.31)$$

and

$$\sum_{l=1}^{\infty} \chi_l(z) \chi_l(z') = \delta(z - z'), \quad (2.32)$$

respectively.

### Definition of the R Function and R Matrix

We expand the wave functions inside the scattering region ( $z \in [-d, d]$ ) in terms of the Wigner-Eisenbud functions

$$\psi^{(s)}(\epsilon, z) = \sum_{l=1}^{\infty} a_l^{(s)}(\epsilon) \chi_l(z) \quad (2.33)$$

and the expansion coefficients  $a_l^{(s)}$  are given by

$$a_l^{(s)}(\epsilon) = \int_{-d}^d dz \chi_l(z) \psi^{(s)}(\epsilon, z) \quad (2.34)$$

for each  $s = 1, 2$  and  $l \geq 1$ .

The wave functions and the Wigner-Eisenbud functions satisfy the same differential equation inside the scattering region but the boundary conditions are different; the derivative of the Wigner-Eisenbud functions vanishes at  $z = \pm d$  while the wave functions and their derivatives verify the continuity conditions (2.9) and (2.10), at the edges of the scattering domain, i.e.

$$\begin{pmatrix} \psi^{(1)}(\epsilon, -d) & \psi^{(1)}(\epsilon, d) \\ \psi^{(2)}(\epsilon, -d) & \psi^{(2)}(\epsilon, d) \end{pmatrix} = \frac{\Theta(\epsilon)}{\sqrt{2\pi}} [\mathbf{1} + \mathbf{S}^t(\epsilon)] \quad (2.35)$$

and

$$\begin{pmatrix} -\frac{d\psi^{(1)}}{dz}(\epsilon, z)\Big|_{z=-d} & \frac{d\psi^{(1)}}{dz}(\epsilon, z)\Big|_{z=d} \\ -\frac{d\psi^{(2)}}{dz}(\epsilon, z)\Big|_{z=-d} & \frac{d\psi^{(2)}}{dz}(\epsilon, z)\Big|_{z=d} \end{pmatrix} = -\frac{i}{\sqrt{2\pi}} \frac{\pi}{2d} \Theta(\epsilon) [\mathbf{1} - \mathbf{S}^t(\epsilon)] \mathbf{K}(\epsilon) \quad (2.36)$$

as follows from the expressions (2.27) and (2.28) of the wave functions outside the scattering region particularized for  $z = \pm d$ . The  $2 \times 2$  matrix  $\mathbf{K}(\epsilon)$  is the dimensionless wave vector matrix defined by

$$K(\epsilon) = \begin{pmatrix} \frac{k_1}{\pi/2d} & 0 \\ 0 & \frac{k_2}{\pi/2d} \end{pmatrix}. \quad (2.37)$$

Now we have to calculate the expansion coefficients  $a^{(s)}(\epsilon)$  in Eq. (2.33). The start relations are the Schrödinger equation (2.6) and the equation (2.29) satisfied by the Wigner Eisenbud functions. We multiply them by  $\chi_l(z)$  and  $\psi^{(s)}(\epsilon, z)$ , respectively, and integrate them over  $z$  between  $z = -d$  and  $z = d$ . Subtracting one from the other we find

$$\begin{aligned} & -\frac{\hbar^2}{2m^*} \left[ \int_{-d}^d dz \chi_l(z) \frac{d^2}{dz^2} \psi^{(s)}(\epsilon, z) - \int_{-d}^d dz \psi^{(s)}(\epsilon, z) \frac{d^2}{dz^2} \chi_l(z) \right] \\ & = (\epsilon - \epsilon_l) \int_{-d}^d dz \chi_l(z) \psi^{(s)}(\epsilon, z), \end{aligned} \quad (2.38)$$

Performing an integration by parts on the left side of the above equation and identifying the integral on the right side with the coefficient  $a_l^{(s)}$ , defined by (2.34), we obtain

$$a_l^{(s)}(\epsilon) = \frac{\hbar^2}{2m^*} \frac{\chi_l(-d)}{\epsilon - \epsilon_l} \frac{d}{dz} \psi^{(s)}(\epsilon, z) \Big|_{z=-d} - \frac{\hbar^2}{2m^*} \frac{\chi_l(d)}{\epsilon - \epsilon_l} \frac{d}{dz} \psi^{(s)}(\epsilon, z) \Big|_{z=d}. \quad (2.39)$$

Feeding this expression into the definition (2.33) of the wave function it follows that

$$\psi^{(s)}(\epsilon, z) = R(\epsilon; -d, z) \frac{2d}{\pi} \frac{d}{dz} \psi^{(s)}(\epsilon, z) \Big|_{z=-d} - R(\epsilon; d, z) \frac{2d}{\pi} \frac{d}{dz} \psi^{(s)}(\epsilon, z) \Big|_{z=d}, \quad (2.40)$$

where the R function is defined as

$$R(\epsilon; z, z') = \frac{\hbar^2}{2m^*} \frac{\pi}{2d} \sum_{l=1}^{\infty} \frac{\chi_l(z)\chi_l(z')}{\epsilon - \epsilon_l}. \quad (2.41)$$

The above expression of the R function has the advantage of being dimensionless. The Wigner Eisenbud functions are normalized (see Eq. (2.31)) and, consequently,  $\chi_l(z)\chi_l(z')2d/\pi$  is a dimensionless quantity.  $R(\epsilon; z, z')$  can be written into an equivalent form

$$R(\epsilon; z, z') = \frac{\hbar^2}{2m^*} \left( \frac{\pi}{2d} \right)^2 \sum_{l=1}^{\infty} \frac{\chi_l(z)\chi_l(z') 2d/\pi}{\epsilon - \epsilon_l}, \quad (2.42)$$

which is evidently dimensionless because the expression in front of the sum represents the first energy level of a particle, in an infinite quantum well with the width  $2d$ .

We put, further, the scattering functions for each  $z$  inside the scattering region into a matrix form

$$\begin{pmatrix} \psi^{(1)}(\epsilon, z) \\ \psi^{(2)}(\epsilon, z) \end{pmatrix} = \frac{i}{\sqrt{2\pi}} \Theta(\epsilon) [\mathbf{1} - \mathbf{S}^t(\epsilon)] \mathbf{K}(\epsilon) \begin{pmatrix} R(\epsilon; -d, z) \\ R(\epsilon; d, z) \end{pmatrix} \quad (2.43)$$

The derivatives of  $\psi^{(s)}(\epsilon, z)$  at  $z = \pm d$  were substituted by their expressions given in Eq. (2.36). Thus, the values of the functions at the edges of the scattering domain,

$$\begin{pmatrix} \psi^{(1)}(\epsilon, -d) & \psi^{(1)}(\epsilon, d) \\ \psi^{(2)}(\epsilon, -d) & \psi^{(2)}(\epsilon, d) \end{pmatrix} = \frac{i}{\sqrt{2\pi}} \Theta(\epsilon) [\mathbf{1} - \mathbf{S}^t(\epsilon)] \mathbf{K}(\epsilon) \mathbf{R}^t(\epsilon), \quad (2.44)$$

are elegantly given by the R matrix

$$\mathbf{R}(\epsilon) = \begin{pmatrix} R(\epsilon; -d, -d) & R(\epsilon; d, -d) \\ R(\epsilon; -d, d) & R(\epsilon; d, d) \end{pmatrix}. \quad (2.45)$$

### Relation between R- and S Matrix

The scattering functions should also be continuous at the edges of the scattering system (see Eqs. (2.9)) and we exploit this condition to determine the relation between R and S matrix. Equating the two expressions (2.35) and (2.44) of these functions at  $z = \pm d$  we infer

$$\mathbf{S}(\epsilon) = \mathbf{1} - 2[\mathbf{1} + i\mathbf{R}(\epsilon)\mathbf{K}(\epsilon)]^{-1} \quad (2.46)$$

for each value of the energy  $\epsilon$ . As was shown in the first part of this section, the elements of the S matrix defined by (2.13) are, in fact, the reflection and transmission amplitudes for the particles coming from the left and right side of the system,

$$\mathbf{S}(\epsilon) = \begin{pmatrix} r^{(1)}(\epsilon) & t^{(2)}(\epsilon) \\ t^{(1)}(\epsilon) & r^{(2)}(\epsilon) \end{pmatrix}. \quad (2.47)$$

However, for describing transport phenomena in semiconductors in the frame of the Landauer-Büttiker formalism [31], the reflection and transmission coefficients (probabilities),

$$R^{(1)}(\epsilon) = \frac{\text{reflected flux}}{\text{incident flux}} = |r^{(1)}(\epsilon)|^2, \quad R^{(2)}(\epsilon) = |r^{(2)}(\epsilon)|^2, \quad (2.48)$$

$$T^{(1)}(\epsilon) = \frac{\text{transmitted flux}}{\text{incident flux}} = \left| \frac{k_2}{k_1} \right| |t^{(1)}(\epsilon)|^2, \quad T^{(2)}(\epsilon) = \left| \frac{k_1}{k_2} \right| |t^{(2)}(\epsilon)|^2 \quad (2.49)$$

play a central role. We introduce further another matrix,

$$\tilde{\mathbf{S}}(\epsilon) = \mathbf{K}^{1/2}(\epsilon) \mathbf{S}(\epsilon) \mathbf{K}^{-1/2}(\epsilon), \quad (2.50)$$

which is actually the current scattering matrix [12], having the property that

$$\begin{aligned} |\tilde{\mathbf{S}}_{11}(\epsilon)|^2 &= R^{(1)}(\epsilon), & |\tilde{\mathbf{S}}_{12}(\epsilon)|^2 &= T^{(2)}(\epsilon), \\ |\tilde{\mathbf{S}}_{21}(\epsilon)|^2 &= T^{(1)}(\epsilon), & |\tilde{\mathbf{S}}_{22}(\epsilon)|^2 &= R^{(2)}(\epsilon). \end{aligned} \quad (2.51)$$

The relation (2.46) between R and S matrix can be rewritten into an equivalent form

$$\tilde{\mathbf{S}}(\epsilon) = \mathbf{1} - 2 [\mathbf{1} + i\mathbf{\Omega}(\epsilon)]^{-1} \quad (2.52)$$

where the matrix  $\mathbf{\Omega}$  of rank two is defined as

$$\mathbf{\Omega}(\epsilon) = \mathbf{K}^{1/2}(\epsilon) \mathbf{R}(\epsilon) \mathbf{K}^{1/2}(\epsilon) = \frac{\hbar^2}{2m^*} \left( \frac{\pi}{2d} \right)^2 \sum_{l=1}^{\infty} \frac{\boldsymbol{\omega}_l(\epsilon)}{\epsilon - \epsilon_l}, \quad (2.53)$$

with

$$(\boldsymbol{\omega}_l(\epsilon))_{ij} = \left( \frac{k_i}{\pi/2d} \right)^{1/2} \left( \frac{k_j}{\pi/2d} \right)^{1/2} \frac{2d}{\pi} \chi_l((-1)^i d) \chi_l((-1)^j d), \quad i, j = 1, 2 \quad (2.54)$$

for all  $l \geq 1$ . Per construction,  $\mathbf{\Omega}$  is a symmetrical matrix with real elements in the domain of the scattering states with  $\epsilon > \max(V_1, V_2)$ . These properties lead to the unitarity of the current scattering matrix,

$$\tilde{\mathbf{S}}(\epsilon) \tilde{\mathbf{S}}^\dagger(\epsilon) = \tilde{\mathbf{S}}^\dagger(\epsilon) \tilde{\mathbf{S}}(\epsilon) = \mathbf{1} \quad (2.55)$$

for  $\epsilon \geq \max(V_1, V_2)$  which includes the reciprocity relations,

$$R^{(1)}(\epsilon) = R^{(2)}(\epsilon) = R(\epsilon), \quad (2.56)$$

$$T^{(1)}(\epsilon) = T^{(2)}(\epsilon) = T(\epsilon), \quad (2.57)$$

and the well-known relation of the flux conservation: the incident flux equals the reflected flux plus the transmitted flux,

$$R(\epsilon) + T(\epsilon) = 1. \quad (2.58)$$

Feeding the relation (2.52) between R and S matrix into the expressions (2.27), (2.28) and (2.43), we obtain the scattering functions in the whole system, in terms of the Wigner-Eisenbud functions and energies:

$$\begin{pmatrix} \psi^{(1)}(\epsilon, z) \\ \psi^{(2)}(\epsilon, z) \end{pmatrix} = \frac{2\Theta(\epsilon)}{\sqrt{2\pi}} \left[ \begin{pmatrix} \cos[k_1(z+d)] \\ 0 \end{pmatrix} - \mathbf{K}^{1/2} [\mathbf{1} + i\mathbf{\Omega}]^{-1} \mathbf{K}^{-1/2} \begin{pmatrix} \exp[-ik_1(z+d)] \\ 0 \end{pmatrix} \right] \quad (2.59)$$

for  $z < -d$ ,

$$\begin{pmatrix} \psi^{(1)}(\epsilon, z) \\ \psi^{(2)}(\epsilon, z) \end{pmatrix} = \frac{2i}{\sqrt{2\pi}} \Theta(\epsilon) \mathbf{K}^{1/2} [\mathbf{1} + i\mathbf{\Omega}]^{-1} \mathbf{K}^{1/2} \begin{pmatrix} R(\epsilon; -d, z) \\ R(\epsilon; d, z) \end{pmatrix} \quad (2.60)$$

for  $|z| < d$  and

$$\begin{pmatrix} \psi^{(1)}(\epsilon, z) \\ \psi^{(2)}(\epsilon, z) \end{pmatrix} = \frac{2\Theta(\epsilon)}{\sqrt{2\pi}} \left[ \begin{pmatrix} 0 \\ \cos[k_2(z+d)] \end{pmatrix} - \mathbf{K}^{1/2} [\mathbf{1} + i\mathbf{\Omega}]^{-1} \mathbf{K}^{-1/2} \begin{pmatrix} 0 \\ \exp[ik_2(z+d)] \end{pmatrix} \right] \quad (2.61)$$

for  $z > d$ .

Thus, we only have to solve the closed counterpart of the scattering problem in order to find the scattering functions of the open system.

The scattering functions  $\psi^{(s)}(\epsilon, z)$  form an orthogonal and complete system for a potential energy  $V(z)$  which does not allow bound states [35]. They are eigenfunctions of the Hamilton operator and the self-adjointness of this operator allows us to consider the set as complete,

$$\begin{aligned} & \int_0^\infty dk_1 \left( \psi^{(1)}(\epsilon; z) \right)^* \psi^{(1)}(\epsilon; z') \\ & + \int_0^\infty dk_2 \left( \psi^{(2)}(\epsilon; z) \right)^* \psi^{(2)}(\epsilon; z') = \delta(z - z'). \end{aligned} \quad (2.62)$$

The relation (2.8) between the wave vectors  $k_1$ ,  $k_2$  and the energy  $\epsilon$  leads to an equivalent form of the completeness condition

$$\sum_{s=1,2} \int_{V_s}^\infty d\epsilon g_s(\epsilon) \left( \psi^{(s)}(\epsilon; z) \right)^* \psi^{(s)}(\epsilon; z') = \delta(z - z'), \quad (2.63)$$

where

$$g_s(\epsilon) = \frac{m^*}{\hbar^2 k_s(\epsilon)}, \quad s = 1, 2 \quad (2.64)$$

defines the 1D density of states. The orthogonality condition is written as

$$\int_{-\infty}^{\infty} dz \left( \psi^{(s)}(\epsilon, z) \right)^* \psi^{(s')}(\epsilon', z) = \delta_{ss'} \delta(k_s(\epsilon) - k_{s'}(\epsilon')) \quad (2.65)$$

or as

$$\int_{-\infty}^{\infty} dz \left( \psi^{(s)}(\epsilon, z) \right)^* \psi^{(s')}(\epsilon', z) = \delta_{ss'} \delta(\epsilon - \epsilon') / g_s(\epsilon). \quad (2.66)$$

### 2.3.3 Electronic Wave Functions

The above discussion about the eigenvalue problems associated with the electron motion in the lateral- and in the transport direction allows us to conclude that the functions  $\phi_{\nu,i}(\vec{r}_{\perp})\psi^{(s)}(\epsilon, z)$  form a basis, where  $\phi_{\nu,i}(\vec{r}_{\perp})$  are defined by Eq. (2.4) and the scattering functions  $\psi^{(s)}(\epsilon, z)$  by Eqs. (2.59)-(2.61) Each wave function  $\Psi(E, \vec{r})$  which describes an electron of energy  $E$  can be expanded in terms of this basis,

$$\Psi(E, \vec{r}) = \sum_{\nu,i,s} c_{\nu,i}^{(s)}(E) \phi_{\nu,i}(\vec{r}_{\perp}) \psi^{(s)}(E - \epsilon'_{\perp}, z), \quad (2.67)$$

where  $c_{\nu,i}^{(s)}(E)$  are constants. The energy levels  $E$  are degenerate, the order of degeneracy being infinite; if  $E$  is fixed the energies associated with the motion in the lateral direction  $\epsilon'_{\perp}$  define the different channels for the electron [37]. In our simple model, in which the potential energy is separable, the channels do not interact with each other and an electron incident in the scattering system through a channel  $\epsilon'_{\perp}$  is either reflected or transmitted on the same channel.

## 2.4 Noninteracting Low-Dimensional Electron Gas

The conduction electrons in a semiconductor are considered as an electron gas embedded in a positively charged medium which maintains the overall charge neutrality of the system. The simplest approximation for the description of an electron gas is to neglect all interactions: the Coulomb interaction of the electrons with each other and the interaction of the electrons with the positive background. Every electron is then independent from other electrons and subject only to external forces.

### 2.4.1 Multi-Electron System

We assume the noninteracting electron gas in a semiconductor heterostructure as an infinite system and apply the second quantization technique to the wave field



described by the Schrödinger equation. Each state of the system is described by the field operators  $\Psi(\vec{r})$  and  $\Psi^\dagger(\vec{r})$ . Using the eigenbasis of the one-particle Hamiltonian associated with the Schrödinger equation (2.1) we can represent  $\Psi(\vec{r})$  and  $\Psi^\dagger(\vec{r})$  in terms of the creation and destruction operators for the states  $(\nu, i, s, \epsilon)$  of the field,  $c_s^{\nu,i}(\epsilon)$  and  $(c_s^{\nu,i}(\epsilon))^\dagger$ , respectively. Thus,

$$\Psi(\vec{r}) = \sum_{\nu,i} \sum_{s=1,2} \int_{V_s}^{\infty} d\epsilon g_s(\epsilon) \phi_{\nu,i}(\vec{r}_\perp) \psi^{(s)}(\epsilon, z) c_s^{\nu,i}(\epsilon), \quad (2.68)$$

$$\Psi^\dagger(\vec{r}) = \sum_{\nu,i} \sum_{s=1,2} \int_{V_s}^{\infty} d\epsilon g_s(\epsilon) \phi_{\nu,i}^*(\vec{r}_\perp) \left( \psi^{(s)}(\epsilon, z) \right)^* (c_s^{\nu,i}(\epsilon))^\dagger \quad (2.69)$$

with the 1D density of states  $g_s(\epsilon)$ ,  $s = 1, 2$  defined by (2.64). The electrons in semiconductors are a system of fermions which have the property that any state may contain either no particle or one particle. This could be accomplished by making the fields anticommute:

$$\begin{aligned} \{\Psi(\vec{r}), \Psi^\dagger(\vec{r}')\} &= \delta(\vec{r} - \vec{r}'), \\ \{\Psi(\vec{r}), \Psi(\vec{r}')\} &= 0, \\ \{\Psi^\dagger(\vec{r}), \Psi^\dagger(\vec{r}')\} &= 0. \end{aligned} \quad (2.70)$$

The anticommutation relations may be satisfied if  $c_s^{\nu,i}(\epsilon)$  and  $(c_s^{\nu,i}(\epsilon))^\dagger$  verify their own anticommutation relations:

$$\begin{aligned} \{c_s^{\nu,i}(\epsilon), (c_{s'}^{\nu',i'}(\epsilon'))^\dagger\} &= \delta_{\nu\nu'} \delta_{ii'} \delta_{ss'} \delta(\epsilon - \epsilon') / g_s(\epsilon), \\ \{c_s^{\nu,i}(\epsilon), c_{s'}^{\nu',i'}(\epsilon')\} &= 0, \\ \{(c_s^{\nu,i}(\epsilon))^\dagger, (c_{s'}^{\nu',i'}(\epsilon'))^\dagger\} &= 0. \end{aligned} \quad (2.71)$$

The many-particle Hamiltonian of the electron system without mutual interaction,

$$\mathbf{H} = \int d\vec{r} \Psi^\dagger(\vec{r}) \left[ \frac{1}{2m^*} \vec{P}^2 + V_\perp(\vec{r}_\perp) + V(z) \right] \Psi(\vec{r}), \quad (2.72)$$

is, also, written in terms of the creation and destruction operators

$$\mathbf{H} = \sum_{\nu,i} \sum_{s=1,2} \int_{V_s}^{\infty} d\epsilon g_s(\epsilon) E_\nu(\epsilon) (c_s^{\nu,i}(\epsilon))^\dagger c_s^{\nu,i}(\epsilon) \quad (2.73)$$

with the energy of the single particle state labelled  $(\nu, i, s, \epsilon)$  defined as

$$E_\nu(\epsilon) = \epsilon'_\perp + \epsilon. \quad (2.74)$$

The electrons are indistinguishable particles and a dynamical state of the total system is completely determined by giving the occupation numbers  $n_s^{\nu,i}(\epsilon)$  of each single particle state  $(\nu, i, s, \epsilon)$ ,

$$|N\rangle = \bigotimes_{(\nu,i,s,\epsilon)} |n_s^{\nu,i}(\epsilon)\rangle. \quad (2.75)$$

According to Pauli principle, at most one particle can be in any state so that these occupation numbers are restricted to the values 0 or 1.

## 2.4.2 Electrical Charge- and Current Density

Creation and destruction operators are also used to describe other kinds of operators besides Hamiltonians. The electron charge density is defined as

$$\rho(\vec{r}) = 2e\Psi^\dagger(\vec{r})\Psi(\vec{r}) \quad (2.76)$$

and may be expressed in terms of creation and destruction operators:

$$\rho(\vec{r}) = 2e \sum_{\substack{\nu,i,s \\ \nu',i',s'}} \int_{V_s}^{\infty} d\epsilon g_s(\epsilon) \int_{V_{s'}}^{\infty} d\epsilon' g_{s'}(\epsilon') \phi_{\nu,i}^*(\vec{r}_\perp) \phi_{\nu',i'}(\vec{r}_\perp) \left( \psi^{(s)}(\epsilon, z) \right)^* \psi^{(s')}(\epsilon', z) \\ (c_s^{\nu,i}(\epsilon))^\dagger c_{s'}^{\nu',i'}(\epsilon'), \quad (2.77)$$

where  $e$  is the elementary electronic charge. The factor 2 comes from the spin degeneracy.

The standard quantum mechanical representation of the electrical current density is

$$\vec{j}(\vec{r}) = \frac{2e\hbar}{m^*} \text{Im} \left[ \Psi^\dagger(\vec{r}) \nabla \Psi(\vec{r}) \right] \quad (2.78)$$

and using the expressions (2.68) and (2.69) of the field operators one obtains:

$$\vec{j}(\vec{r}) = \frac{2e\hbar}{m^*} \sum_{\substack{\nu,i,s \\ \nu',i',s'}} \int_{V_s}^{\infty} d\epsilon g_s(\epsilon) \int_{V_{s'}}^{\infty} d\epsilon' g_{s'}(\epsilon') \text{Im} \left[ \phi_{\nu,i}^*(\vec{r}_\perp) \left( \psi^{(s)}(\epsilon, z) \right)^* \nabla \phi_{\nu',i'}(\vec{r}_\perp) \right. \\ \left. \psi^{(s')}(\epsilon', z) \right] (c_s^{\nu,i}(\epsilon))^\dagger c_{s'}^{\nu',i'}(\epsilon'). \quad (2.79)$$

If the electron system is in an eigenstate  $|N\rangle$  of the Hamilton operator, the mean values of the charge and current densities are

$$\rho(\vec{r}) = 2e \sum_{\nu,i,s} \int_{V_s}^{\infty} d\epsilon g_s(\epsilon) |\phi_{\nu,i}(\vec{r}_\perp)|^2 \left| \psi^{(s)}(\epsilon, z) \right|^2 n_s^{\nu,i}(\epsilon) \quad (2.80)$$

and

$$\begin{aligned} \vec{j}(\vec{r}) = & \frac{2e\hbar}{m^*} \sum_{\nu,i,s} \int_{V_s}^{\infty} d\epsilon g_s(\epsilon) \left\{ \hat{e}_z |\phi_{\nu,i}(\vec{r}_{\perp})|^2 \operatorname{Im} \left[ \left( \psi^{(s)}(\epsilon, z) \right)^* \frac{d}{dz} \psi^{(s)}(\epsilon, z) \right] \right. \\ & \left. + \left| \psi^{(s)}(\epsilon, z) \right|^2 \operatorname{Im} \left[ \phi_{\nu,i}^*(\vec{r}_{\perp}) \nabla_{\vec{r}_{\perp}} \phi_{\nu,i}(\vec{r}_{\perp}) \right] \right\} n_s^{\nu,i}(\epsilon), \end{aligned} \quad (2.81)$$

respectively, where  $\hat{e}_z$  is the unity vector of the  $z$  axis. Per construction, the states  $|N\rangle$  (defined in (2.75)) which correspond to different occupation number sets are orthogonal and, consequently,  $\langle N | (c_s^{\nu,i}(\epsilon))^{\dagger} c_{s',i'}^{\nu',i'}(\epsilon') | N \rangle = n_s^{\nu,i}(\epsilon) \delta_{\nu\nu'} \delta_{ii'} \delta_{ss'} \delta(\epsilon - \epsilon') / g_s(\epsilon)$ .

Further we analyze the component of the current density on the direction defined by the source- and drain contact. As results from Eq. (2.81)

$$\begin{aligned} j_z(\vec{r}_{\perp}, z < -d) = & \frac{2e}{h} \sum_{\nu,i} |\phi_{\nu,i}(\vec{r}_{\perp})|^2 \int_{V_m}^{\infty} d\epsilon \left\{ n_1^{\nu,i}(\epsilon) \left[ 1 - |r^{(1)}(\epsilon)|^2 \right] \right. \\ & \left. - n_2^{\nu,i}(\epsilon) \frac{k_1(\epsilon)}{k_2(\epsilon)} |t^{(2)}(\epsilon)|^2 \right\} \end{aligned} \quad (2.82)$$

in the source contact region and

$$\begin{aligned} j_z(\vec{r}_{\perp}, z > d) = & \frac{2e}{h} \sum_{\nu,i} |\phi_{\nu,i}(\vec{r}_{\perp})|^2 \int_{V_m}^{\infty} d\epsilon \left\{ n_1^{\nu,i}(\epsilon) \frac{k_2(\epsilon)}{k_1(\epsilon)} |t^{(1)}(\epsilon)|^2 \right. \\ & \left. - n_2^{\nu,i}(\epsilon) \left[ 1 - |r^{(2)}(\epsilon)|^2 \right] \right\} \end{aligned} \quad (2.83)$$

in the drain contact region, where  $V_m = \max(V_1, V_2)$ . The scattering wave functions  $\psi^{(s)}(\epsilon, z)$  were replaced by their expressions (2.59), (2.61) and  $g_s(\epsilon)$  by (2.64). The nondegenerate energy levels between  $\min(V_1, V_2)$  and  $\max(V_1, V_2)$  do not contribute to the current because the corresponding scattering functions are real and, therefore,  $\operatorname{Im} \left[ \left( \psi^{(s)}(\epsilon, z) \right)^* \frac{d}{dz} \psi^{(s)}(\epsilon, z) \right] = 0$ . For  $\epsilon > V_m$  the reflection and transmission amplitudes  $r^{(s)}(\epsilon)$  and  $t^{(s)}(\epsilon)$ ,  $s = 1, 2$ , are related to each other as follows from the unitarity condition (2.55) of the scattering matrix. Therefore, the current density in the contacts is given by

$$j_z(\vec{r}_{\perp}, z < -d) = \frac{2e}{h} \sum_{\nu,i} |\phi_{\nu,i}(\vec{r}_{\perp})|^2 \int_{V_m}^{\infty} d\epsilon T(\epsilon) \left[ n_1^{\nu,i}(\epsilon) - n_2^{\nu,i}(\epsilon) \right], \quad (2.84)$$

$$j_z(\vec{r}_{\perp}, z > d) = \frac{2e}{h} \sum_{\nu,i} |\phi_{\nu,i}(\vec{r}_{\perp})|^2 \int_{V_m}^{\infty} d\epsilon T(\epsilon) \left[ n_1^{\nu,i}(\epsilon) - n_2^{\nu,i}(\epsilon) \right], \quad (2.85)$$

where  $T(\epsilon)$  is the transmission probability defined in Eq. (2.49). The expressions of the current density for the two regions of the structure are identical and this fact proves the current conservation in the system.

Here we restrict our analysis only to the systems for which the electrons either move freely or are confined to both of the lateral directions. For the heterostructures with total lateral confinement, the energy levels  $\epsilon'_\perp$  are nondegenerate ( $i = 1$ ) and the time translational invariance allows us to choose the function  $\phi_{\nu,i}(\vec{r}_\perp)$  as real. It results immediately that  $\text{Im} [\phi_{\nu,i}^*(\vec{r}_\perp) \nabla_{\vec{r}_\perp} \phi_{\nu,i}(\vec{r}_\perp)] = 0$  and the lateral component of the current density vanishes. In this case it is convenient to define the electrical current in the transport direction,

$$I(z) = \int d\vec{r}_\perp j_z(\vec{r}_\perp, z). \quad (2.86)$$

Using the normalization condition of the functions  $\phi_{\nu,i}(\vec{r}_\perp)$  (second Eq. (2.5)) we find

$$I(z < -d) = \frac{2e}{h} \sum_\nu \int_{V_m}^\infty d\epsilon T(\epsilon) [n_1^\nu(\epsilon) - n_2^\nu(\epsilon)], \quad (2.87)$$

$$I(z > d) = \frac{2e}{h} \sum_\nu \int_{V_m}^\infty d\epsilon T(\epsilon) [n_1^\nu(\epsilon) - n_2^\nu(\epsilon)], \quad (2.88)$$

In the opposite limit, for a free electron gas in a plane perpendicular to the transport direction, we can define a 2D wave vector  $\vec{k}_\perp$  and  $\sum_{\nu,i} \dots \rightarrow \int d\vec{k}_\perp \dots$ ,  $\phi_{\nu,i}(\vec{r}_\perp) \rightarrow \phi(\vec{k}_\perp, \vec{r}_\perp) = \frac{1}{2\pi} e^{i\vec{k}_\perp \cdot \vec{r}_\perp}$ , and  $n_s^{\nu,i}(\epsilon) \rightarrow n_s(\vec{k}_\perp, \epsilon)$ . From here it follows directly that  $\text{Im} [\phi_{\nu,i}^*(\vec{r}_\perp) \nabla_{\vec{r}_\perp} \phi_{\nu,i}(\vec{r}_\perp)] \rightarrow \vec{k}_\perp / (2\pi)^2$  and the components of the current density become

$$\vec{j}_\perp(\vec{r}) = \frac{2e}{(2\pi)^2 \hbar} \int d\vec{k}_\perp \sum_s \int_{V_s}^\infty d\epsilon \frac{k_\perp}{k_s(\epsilon)} |\psi^{(s)}(\epsilon, z)|^2 n_s(\vec{k}_\perp, \epsilon), \quad (2.89)$$

and

$$j_z(\vec{r}_\perp, z < -d) = \frac{2e}{(2\pi)^2 \hbar} \int d\vec{k}_\perp \int_{V_m}^\infty d\epsilon T(\epsilon) [n_1(\vec{k}_\perp, \epsilon) - n_2(\vec{k}_\perp, \epsilon)], \quad (2.90)$$

$$j_z(\vec{r}_\perp, z > d) = \frac{2e}{(2\pi)^2 \hbar} \int d\vec{k}_\perp \int_{V_m}^\infty d\epsilon T(\epsilon) [n_1(\vec{k}_\perp, \epsilon) - n_2(\vec{k}_\perp, \epsilon)]. \quad (2.91)$$

We can also imagine other types of heterostructures for which the electron motion is free on one of the two lateral directions but confined on the other one and the expression (2.81) of the current density can be easily particularized for each situation.

### 2.4.3 System in Thermodynamic Equilibrium

We consider now the electron gas in contact with a reservoir with which the system can exchange particles and thermal energy. This approach, due to Gibbs, simplifies the mathematics greatly. In this situation, both the energy and the particle number of the system will fluctuate, but, generally, the fluctuations will be negligibly small for a macroscopic system [38]. We have assumed here the geometrical dimensions of the whole semiconductor heterostructure large in comparison to the size of the scattering region ( $L_x, L_y, L_z \gg d$ ). Thus, in the limit of the thermodynamic equilibrium, the particle number and the energy of the system can be considered approximatively constant.

For any given value of the particle number  $N$ , a state of the electron gas is specified by a set  $\{n_s^{\nu,i}(\epsilon)\}_{(\nu,i,s,\epsilon)}$  of the occupation numbers which satisfies  $N = \sum_{\nu,i,s} \int_{V_s}^{\infty} g_s(\epsilon) n_s^{\nu,i}(\epsilon)$ . For the open system which exchanges particles with the reservoir,  $N$  varies and a state of the system is described by a linear combination of the eigenvectors (2.75) of the number operator,

$$|\Psi\rangle = \sum_{\{n_s^{\nu,i}(\epsilon)\}_{(\nu,i,s,\epsilon)}} p \left( \{n_s^{\nu,i}(\epsilon)\}_{(\nu,i,s,\epsilon)} \right) \bigotimes_{(\nu,i,s,\epsilon)} |n_s^{\nu,i}(\epsilon)\rangle \quad (2.92)$$

The summation is made over all sets of occupation numbers for all possible values of  $N$ , i.e. each  $n_s^{\nu,i}(\epsilon)$  takes the values 0 and 1. The statistical and thermodynamic descriptions of the system in equilibrium lead to the probability to find the system in the state described by the occupation number set  $\{n_s^{\nu,i}(\epsilon)\}_{(\nu,i,s,\epsilon)}$ ,

$$\left| p \left( \{n_s^{\nu,i}(\epsilon)\}_{(\nu,i,s,\epsilon)} \right) \right|^2 = \frac{1}{Z(T, V, \mu)} \exp \left[ - \sum_{\nu,i,s} \int_{V_s}^{\infty} d\epsilon g_s(\epsilon) n_s^{\nu,i}(\epsilon) (E_\nu(\epsilon) - \mu) / k_B T \right] \quad (2.93)$$

with the grand partition function

$$Z(T, V, \mu) = \sum_{\{n_s^{\nu,i}(\epsilon)\}_{(\nu,i,s,\epsilon)}} \exp \left[ - \sum_{\nu,i,s} \int_{V_s}^{\infty} d\epsilon g_s(\epsilon) n_s^{\nu,i}(\epsilon) (E_\nu(\epsilon) - \mu) / k_B T \right], \quad (2.94)$$

where  $T$  is the temperature of the system,  $V$  the volume,  $\mu$  the chemical potential and  $k_B$  the Boltzmann constant. The system and the reservoir have the same temperature and chemical potential, at equilibrium.

Given the temperature  $T$  and volume  $V$ , the mean total number of the electrons in the system is defined as

$$\bar{N} = \langle \Psi | \sum_{\nu,i,s} \int_{V_s}^{\infty} d\epsilon g_s(\epsilon) \left( c_s^{\nu,i}(\epsilon) \right)^\dagger c_s^{\nu,i}(\epsilon) | \Psi \rangle \quad (2.95)$$

and, using the expression (2.94) of the grand partition function, produces

$$\bar{N} = \sum_{\nu, i, s} \int_{V_s}^{\infty} d\epsilon g_s(\epsilon) f_{FD}(\epsilon + \epsilon'_{\perp} - \mu) \quad (2.96)$$

where  $f_{FD}(E - \mu)$  is the Fermi Dirac distribution function,

$$f_{FD}(E - \mu) = \frac{1}{\exp[(E - \mu)/k_B T] + 1}, \quad (2.97)$$

which can be identified with the mean occupation number of the single particle state  $(\nu, i, s, \epsilon)$  of energy  $E = \epsilon'_{\perp} + \epsilon$ . The fluctuation in  $\bar{N}$  due to the particle exchange with the reservoir are usually completely negligible. We can, then, think of  $\bar{N}$  as the actual number of particles in the system and consider Eq. (2.96) as determining the chemical potential  $\mu$  for a system of  $\bar{N}$  particles, in a volume  $V$  in equilibrium at temperature  $T$ .

The conduction electrons of a semiconductor are treated as a perfect gas obeying Fermi-Dirac statistics. The electron-electron and the electron-ion collision processes are quite limited by the distribution function, at least in the limit of low temperatures. After a collision, an electron should be scattered into an unoccupied single particle state. However, the energy distribution of the conduction electrons, given by the Fermi-Dirac distribution function, is such that the most final states energetically accessible in a collision are already occupied. In this way, we can partly justify the free electron model.

The mean value of the energy for the electron gas in contact with a reservoir at the temperature  $T$  is

$$\bar{\mathcal{E}} = \langle \Psi | H | \psi \rangle = \sum_{\nu, i, s} \int_{V_s}^{\infty} d\epsilon g_s(\epsilon) (\epsilon + \epsilon'_{\perp}) f_{FD}(\epsilon + \epsilon'_{\perp} - \mu) \quad (2.98)$$

where  $H$  is the Hamiltonian of the system given by (2.73). If the system is large enough, the energy fluctuations in conditions of thermodynamic equilibrium are negligible, and the energy of the system is sharply defined and given by the mean energy  $\bar{\mathcal{E}}$ . Also, the number of the particles, which have the same energy  $E$ , should be practical constant for  $\bar{\mathcal{E}}$  and  $\bar{N}$  without fluctuations.

To characterize the electron gas at thermodynamic equilibrium it is also important to evaluate the electrical charge in the system. The mean values of the operators  $\rho(\vec{r})$  (Eq. (2.77)) in the state  $|\Psi\rangle$  are not easy to calculate, even in the case of thermodynamic equilibrium. We consider, first, the ground state of the electron gas which is obtained for  $T \rightarrow 0$ . In this limit, the Fermi-Dirac distribution function becomes a step function,  $f_{FD}(\epsilon + \epsilon'_{\perp} - \mu) \rightarrow \theta(E_F - \epsilon - \epsilon'_{\perp})$ , where  $E_F$  denotes the Fermi energy, and gives directly the occupation numbers of this pure state,

$$\lim_{T \rightarrow 0} n_s^{\nu, i}(\epsilon) = \theta(E_F - \epsilon - \epsilon'_{\perp}) = \lim_{T \rightarrow 0} f_{FD}(\epsilon + \epsilon'_{\perp} - \mu). \quad (2.99)$$

Thus, the charge density of the electron gas in the ground state is given by the expressions (2.80), in which we replace  $n_s^{\nu,i}(\epsilon)$  by  $f_{FD}(\epsilon + \epsilon'_\perp - \mu)$ ,

$$\rho(\vec{r}) = 2e \sum_{\nu,i,s} \int_{V_s}^{\infty} d\epsilon g_s(\epsilon) |\phi_{\nu,i}(\vec{r}_\perp)|^2 |\psi^{(s)}(\epsilon, z)|^2 f_{FD}(\epsilon + \epsilon'_\perp - \mu) \quad (2.100)$$

This relation, rigorously demonstrated only in the limit  $T \rightarrow 0$ , is usually used to calculate the charge density at low temperatures.

The current density for the electron gas in thermodynamic equilibrium at  $T \rightarrow 0$  can be found analogously from Eqs. (2.87-2.91) and it obviously vanishes.

## 2.5 Electronic Transport

Many experiments in semiconductor physics measure the linear response to an external electric field on the device; linear response means that the signal is directly proportional to the intensity of the external perturbation, situation which usually corresponds to a low magnitude of the perturbing field. Such experiments yield information about the conductivity and the capacitance of the electron gas which is formed in semiconductor heterostructures. The main aim of this section is to connect the macroscopic physical quantities conductance and capacitance to the electronic wave functions, which are deduced through a fully quantum mechanical calculation.

To calculate the current in the Landauer-Büttiker formalism [31], the electrons can be thought of as two noninteracting Fermi-gases: First, the electrons coming from the source contact which occupy the single-particle scattering states with  $s = 1$  according to the Fermi-Dirac distribution function  $f_{FD}(E - \mu_1)$ , where  $\mu_1$  is the chemical potential of the source contact. Second, the electrons coming from the drain contact which occupy the single particle states indexed by  $s = 2$  according to the Fermi-Dirac distribution function  $f_{FD}(E - \mu_2)$ ,  $\mu_2 = \mu_1 - eV_{sd}$  being the chemical potential of the drain contact of the biased heterostructure. In the limit of low temperatures, we obtain from Eqs. (2.87-2.88) the current through the dot structure as

$$I(z) = \frac{2e}{h} \sum_{\nu} \int_{V_m}^{\infty} d\epsilon T(\epsilon) [f_{FD}(\epsilon'_\perp + \epsilon - \mu_1) - f_{FD}(\epsilon'_\perp + \epsilon - \mu_2)], \quad (2.101)$$

where  $T(\epsilon)$  is the transmission probability characterizing the scattering region of the system. It is convenient to write the above expression of the current into an equivalent form

$$I(z) = \frac{2e}{h} \int_{V_m}^{\infty} dE [f_{FD}(E - \mu_1) - f_{FD}(E - \mu_2)] \sum_{\nu} T(E - \epsilon'_\perp) \theta(E - \epsilon'_\perp), \quad (2.102)$$

in which the integration is made over the total energy of the electron and which has the advantage that it directly yields the conductance. The  $\theta$ -function serves to remove the channels with exponentially decaying wave functions in the contacts. In the linear response regime ( $V_{sd} \rightarrow 0$ ,  $V_1 = V_2 \equiv 0$ ) and for low temperatures ( $T \rightarrow 0$ ), we can expand the Fermi-Dirac function  $f_{FD}(E - \mu_2)$  in a Taylor series,  $f_{FD}(E - \mu_2) \rightarrow \theta(E - E_F) - \delta(E - E_F)eV_{sd}$ , and obtain [12] from Eq. (2.102)

$$G = \frac{2e^2}{h} \sum_{\nu} T(E_F - \epsilon_{\perp}^{\nu}) \theta(E_F - \epsilon_{\perp}^{\nu}). \quad (2.103)$$

In the limit of low temperatures the chemical potential becomes equal to the Fermi energy  $E_F$  of the electron gas in the source contact. It is seen that the conductance is the superposition of curves  $T(E_F - \epsilon_{\perp}^{\nu})$  in which the  $\nu$  dependence only results in an energy shift by  $\epsilon_{\perp}^{\nu}$ .  $T(\epsilon)$  is determined solely by the one-dimensional scattering problem Eq. (2.6).

## 2.6 Summary

After a short introduction about mesoscopic system and ballistic regime of transport we discuss in this chapter the scattering electronic states in semiconductor heterostructures using the R matrix representation of the scattering matrix [10, 11, 12]. The R matrix method, originally developed in the context of scattering cross sections in nuclear- and atomic physics [34], is a two step procedure: First, the R matrix is constructed in a time-consuming step solving Schrödinger equation with particular boundary conditions. We call the resulting eigenfunctions Wigner-Eisenbud functions and the eigenenergies Wigner-Eisenbud energies. Thus, the S matrix and the scattering states which contain information about transmission between incident and evanescent states are constructed in a relatively fast second step. This way it is possible to find analytical properties as well as to gain numerical advantages. Up to this point one has dealt with the effect of the heterostructure interfaces on the single electron states. The rest of the chapter deals with the electron gas considered as a many particle (noninteracting) system at equilibrium. The theory uses single particle scattering states to build up multi-particle states with the proper symmetry. The second quantization provides an elegant treatment of this problem. Further, we extend the validity of the expressions for the electron charge- and current density deduced at the thermodynamic equilibrium for the case of transport in the linear response regime at low temperatures. The occupation of the single particle electronic states is given by the Fermi-Dirac distribution function according to the Landauer-Büttiker formalism [31, 35]. Based on this theory developed here, we calculate the current which flows through an effectively one dimensional system and the conductance through this system.



# Chapter 3

## Applications

### 3.1 Conductance through a Quantum Dot

We consider an effectively one-dimensional system [13] as depicted in Fig. 3.1. The potential for the electrons has two components: the  $z$ -independent lateral confinement potential  $V_{\perp}(\vec{r}_{\perp})$ , which provides the one-dimensional character of the structure, and  $V(z)$  a double barrier potential separating a quantum dot from the rest of the system. As usual, we take  $V(z)$  as constant in the contacts,  $V(z < -d) = V_1$  for the source and  $V(z > d) = V_2$  for the drain. The potential difference  $eV_{\text{sd}} = V_1 - V_2$  results from an externally applied drain-source voltage. For simplicity, the contacts are assumed to be identical.

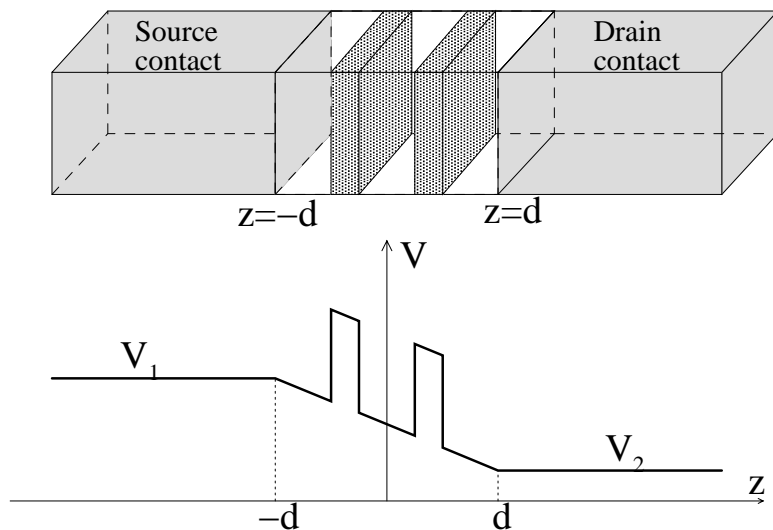


Figure 3.1: a.) Schematic illustration of the system geometry; b.)  $z$ -dependent part of the potential.

The conductance through the quantum dot is calculated in the Landauer-Büttiker formalism [31] as indicated at the end of Chap. 2. Thus, in the linear response regime ( $V_{sd} \rightarrow 0$ ,  $V_1 = V_2 \equiv 0$ ) and for low temperatures ( $T \rightarrow 0$ ), we can write

$$G = \frac{2e^2}{h} \sum_{\nu} T(E_F - \epsilon_{\perp}^{\nu}) \theta(E_F - \epsilon_{\perp}^{\nu}). \quad (3.1)$$

It is seen that the conductance is the superposition of curves  $T(E_F - \epsilon_{\perp}^{\nu})$  in which the  $\nu$  dependence only results in an energy shift by  $\epsilon_{\perp}^{\nu}$ .  $T(\epsilon)$  is determined solely by the one-dimensional scattering problem Eq. (2.6). Its general features are illustrated in Fig. 3.2: For small  $\epsilon$  the transmission is generally small and may have some isolated peaks at  $\epsilon_i$ . For  $\epsilon \sim V_{\max}$ , where  $V_{\max}$  is the maximum of  $V(z)$ , the transmission increases strongly to approach unity for larger energies.

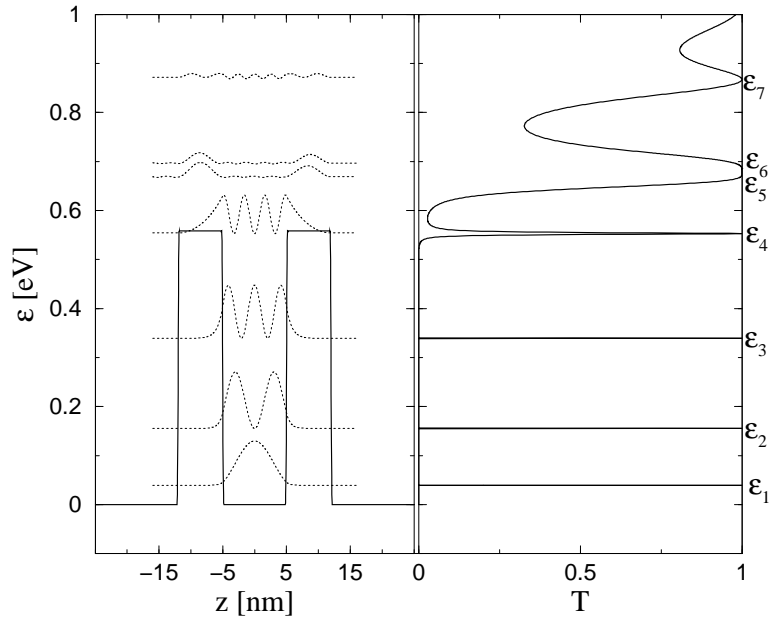


Figure 3.2: Left side: Assumed potential in a schematic plot (solid line), wave functions  $|\Psi^{(1)}|^2$  at the transmission maxima (dotted line); Right side: Transmission vs. energy.

In the experiments  $G$  and therefore  $T$  is probed at different energies by varying the voltage of an additional plunger gate. In the case of lateral tunneling, this additional gate is a top gate [30, 39] and, in the case of vertical tunneling, it is a side gate [22]. We use the following idealization for the total potential in presence of a varying gate voltage: The external potential created by the charges at the gate is screened out completely in the heavily doped contacts ( $|z| > d$ ) so that the total potential and  $E_F$  remain unchanged. In the scattering area ( $|z| < d$ )

the total potential can be idealized for small variations of the gate voltage as a varying potential offset  $V_g$ , so that  $V(z) \rightarrow V(z) + V_g$ . As shown in Fig. 3.3 the transmission probability of the double barrier system depends on the gate potential  $V_g$  and therefore the conductance  $G$  varies with  $V_g$ .

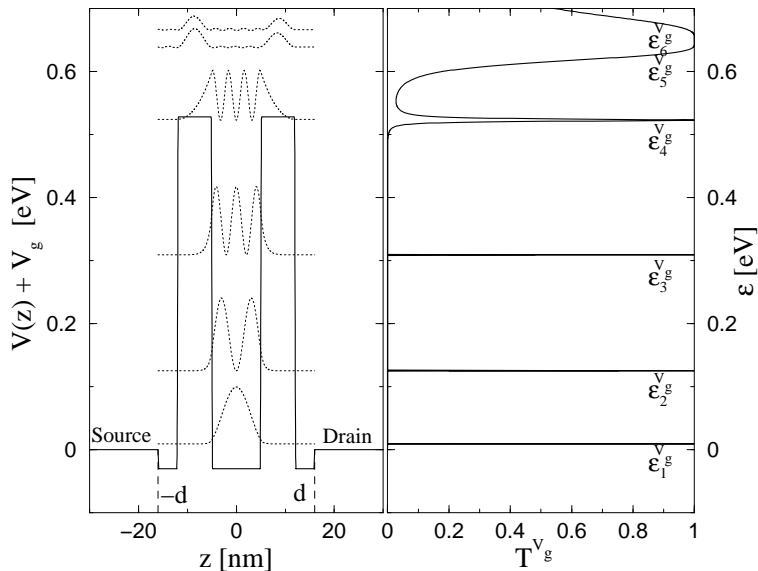


Figure 3.3: Left side: Variation of the total potential of our double-barrier test structure. The range of the source- and the drain contact is given by  $z < -d$  and  $z > d$ , respectively. The potential steps of height  $V_g$  (which is negative) at  $|z| = d$  ( $d=16$  nm) result from the voltage applied to the plunger gate. In dotted lines the wave functions  $|\psi^{(1)}|^2$  at the resonant energies  $\epsilon_i^{V_g}$ ,  $i = 1 \dots 6$  which are the positions of the transmission maxima calculated for the potential  $V(z) + V_g$ . Right side: Transmission  $T^{V_g}(\epsilon)$  as a function of energy calculated for the scattering potential  $V(z) + V_g$ .

We consider first a strongly confined system in the lateral directions, so that only the first energy level ( $\nu = 1$ ) satisfies the condition  $E_F - \epsilon_{\perp}^{\nu} \geq 0$ . In this case, the conductance is given as

$$G(V_g) = \frac{2e^2}{h} T^{V_g}(E_F - \epsilon_{\perp}^1), \quad (3.2)$$

where  $T^{V_g}(\epsilon)$  is the energy dependent transmission of the structure calculated with the potential  $V(z) + V_g$ . So, it can be seen that the conductance measurements directly provide information about the transmission of the scattering system. In Fig. 3.4 is presented the conductance of such a dot and the transmission curves corresponding to the conductance peaks. The conductance maxima are usually

referred to as resonances. We can assign to each peak in the curve  $G(V_g)$  the resonance index  $(1, i_0)$  by equating

$$\epsilon_{i_0}^{V_0} = E_F - \epsilon_{\perp}^1, \quad (3.3)$$

where  $V_g = V_0$  is the location of the conductance maximum and  $\epsilon_{i_0}^{V_0}$  is the energy of the  $i_0$ -th maximum of the curve  $T^{V_0}(\epsilon)$ . The conductance and transmission curves have similar forms but the expression (3.2) does not allow for obtaining an explicit dependence  $G = G(V_g)$  for the whole domain of the gate voltages. We can only provide an approach of the conductance in the vicinity of a sharp maximum at  $V_g = V_0$ . Following Eq. (2.29) the Wigner-Eisenbud functions  $\chi_l$  are unchanged by the transformation  $V(z) \rightarrow V(z) + V_g$  and the Wigner-Eisenbud energies become  $\epsilon_l \rightarrow \epsilon_l + V_g$ . We define for the linear response regime  $V_1 = V_2 = 0$  and  $k(\epsilon) = k_1(\epsilon) = k_2(\epsilon)$ . Then, according to Eq. (2.54) the matrices  $\omega_l$  are independent of  $V_g$ . We now consider a small voltage domain  $V_g = V_0 + \delta V$  around the conductance maximum, in which the sharp resonance extends. It then follows from Eqs. (2.53) and (2.54)

$$\begin{aligned} (\Omega^{V_g})_{ss'}(\epsilon) &= \sum_{l=1}^{\infty} \frac{(\omega_l(\epsilon))_{ss'}}{\epsilon - \epsilon_l - V_g} = \frac{\hbar^2}{2m^*} k(\epsilon) \sum_{l=1}^{\infty} \frac{\chi_l((-1)^s d) \chi_l((-1)^{s'} d)}{\epsilon - \epsilon_l - V_0 - \delta V} \\ &\approx \frac{\hbar^2}{2m^*} k(\epsilon - \delta V) \sum_{l=1}^{\infty} \frac{\chi_l((-1)^s d) \chi_l((-1)^{s'} d)}{(\epsilon - \delta V) - \epsilon_l - V_0} \\ &= (\Omega^{V_0})_{ss'}(\epsilon - \delta V), \end{aligned} \quad (3.4)$$

where  $\Omega^{V_g}$  is the matrix  $\Omega$  with allied potential shift  $V_g$ . From Eq. (3.4) it can be gathered that as long as we can approximate the slowly varying function  $k(\epsilon) \approx k(\epsilon - \delta V)$ , the gate-voltage dependence of  $\Omega$  can be absorbed in a simple shift of the energy argument of  $\Omega$ , at constant gate voltage. From Eqs. (2.52) and (3.4) we obtain  $\tilde{\mathbf{S}}^{V_g}(\epsilon^\nu) \approx \tilde{\mathbf{S}}^{V_0}(\epsilon^\nu - \delta V)$  and, therefore,

$$T^{V_g}(E_F - \epsilon_{\perp}^\nu) \approx T^{V_0}(E_F - \epsilon_{\perp}^\nu - \delta V). \quad (3.5)$$

Inserting this expression of the transmission around a maximum into Eq. (3.2), we can write

$$G(V_g) \simeq \frac{2e^2}{h} T^{V_0}(E_F - \epsilon_{\perp}^\nu - \delta V). \quad (3.6)$$

for the conductance around the maximum at  $V_g = V_0$ . In Fig. 3.5 it is shown that the relation (3.6) provides a good approximation for the conductance peak if the resonance is not too broad.

Following the analysis in Ref. [13] we examine further a dot embedded in a quantum wire with a weak lateral confinement. In this case, there are many eigenenergies of  $V_{\perp}(\vec{r}_{\perp})$  which satisfy the condition  $0 < \epsilon_{\perp}^\nu \leq E_F$  and, therefore, which contribute

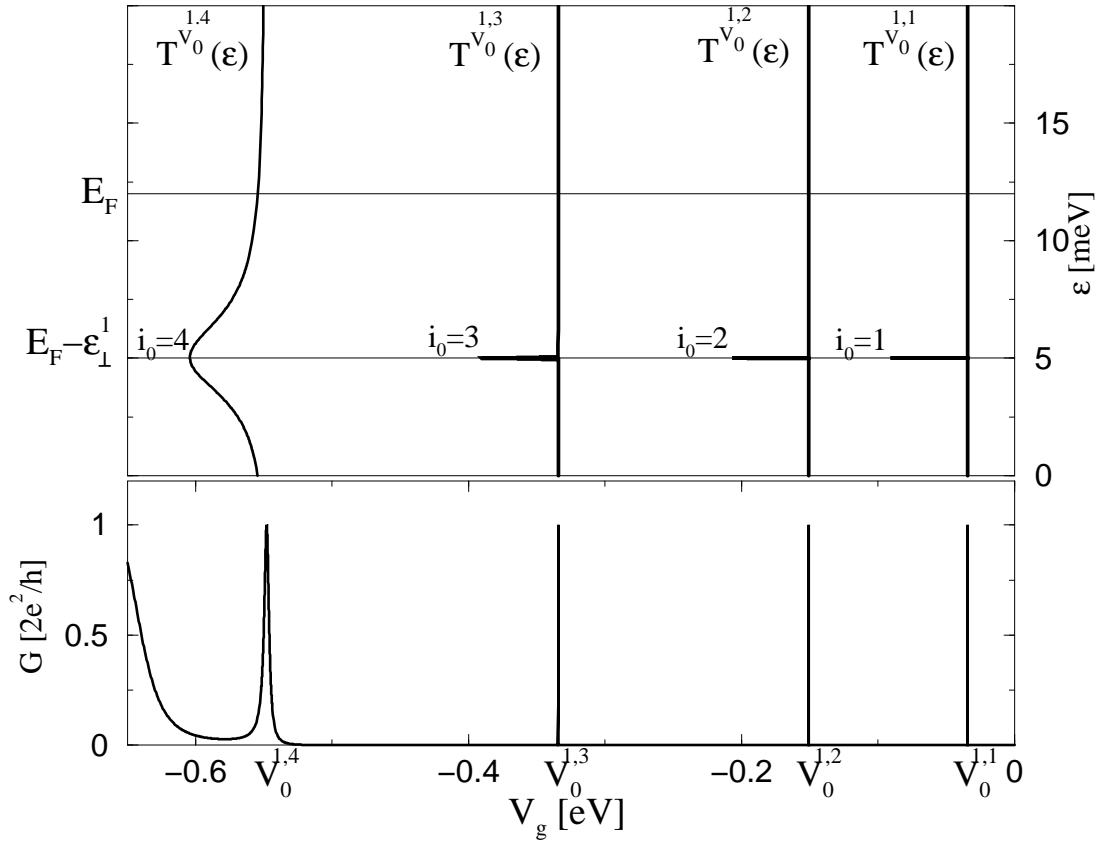


Figure 3.4: Lower part: Qualitatively illustration of the conductance as a function of the gate voltage for a strongly confined dot. The double barrier potential  $V(z)$  which separates the dot from the rest of the structure is given in Fig. 3.2. Upper part: Transmission vs. energy for the values of  $V_g$  which corresponds to the maxima of the conductance. The Fermi energy is fixed by the ionized donor concentration in the contacts,  $N_d^+ \simeq 4 \times 10^{18} \text{ cm}^{-3}$ . The lateral confinement potential of the structure is supposed so that only the first energy level is between 0 and  $E_F$  and has the value indicated on the graphic.

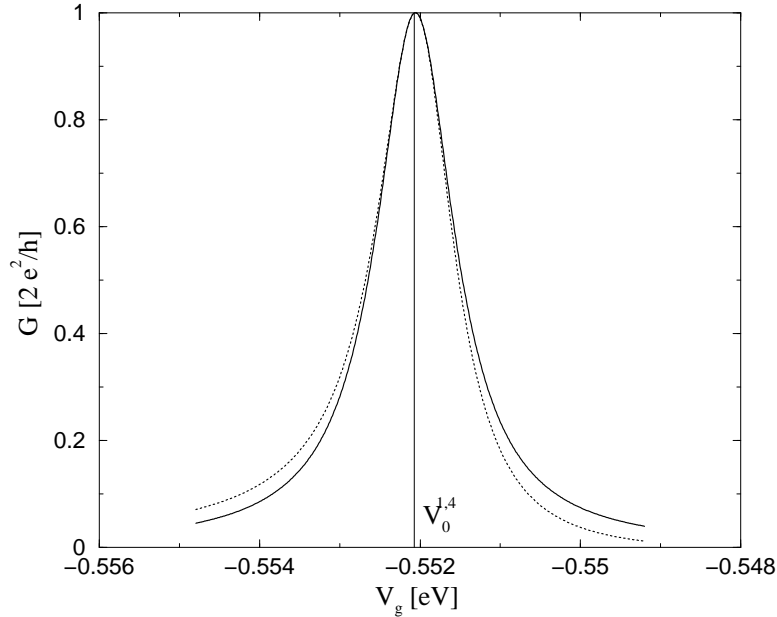


Figure 3.5: The conductance as a function of the gate potential  $V_g$  around the maximum  $i_0 = 4$  in Fig. 3.4; complete calculation (solid line) and approximative values (dotted line) given by Eqs. (3.2) and (3.6), respectively.

to the conductance according to Eq. (3.1). The sum in Eq. (3.1) represents an incoherent superposition of contributions stemming from different classes of resonances. Each class is characterized by the channel index  $\nu$ . As shown in Fig. 3.6 the existence of many open channels for the electron transport leads to a more complex structure of the conductance curve. Generally, to each conductance maximum at  $V_g = V_0$  a pair index  $(\nu_0, i_0)$  can be assigned, where  $\nu_0$  is the channel index and  $i_0$  the number of the maximum in the curve  $T^{V_0}(\epsilon)$ ; the two indices are connected through the equation

$$\epsilon_{i_0}^{V_0} = E_F - \epsilon_{\perp}^{\nu_0}. \quad (3.7)$$

If the conductance peak is narrow, the resonances with  $\nu \neq \nu_0$  provide a slowly varying noncoherent conductivity underground

$$G_{n.c.}(V_g) = \frac{2e^2}{h} \sum_{\nu \neq \nu_0} T^{V_g}(E_F - \epsilon_{\perp}^{\nu}), \quad (3.8)$$

in which the absolute squares of the transmission coefficients are added without phase-information. The resonant channel  $\nu_0$  produces a coherent contribution

$$G_c(V_g) = \frac{2e^2}{h} T^{V_g}(E_F - \epsilon_{\perp}^{\nu_0}), \quad (3.9)$$

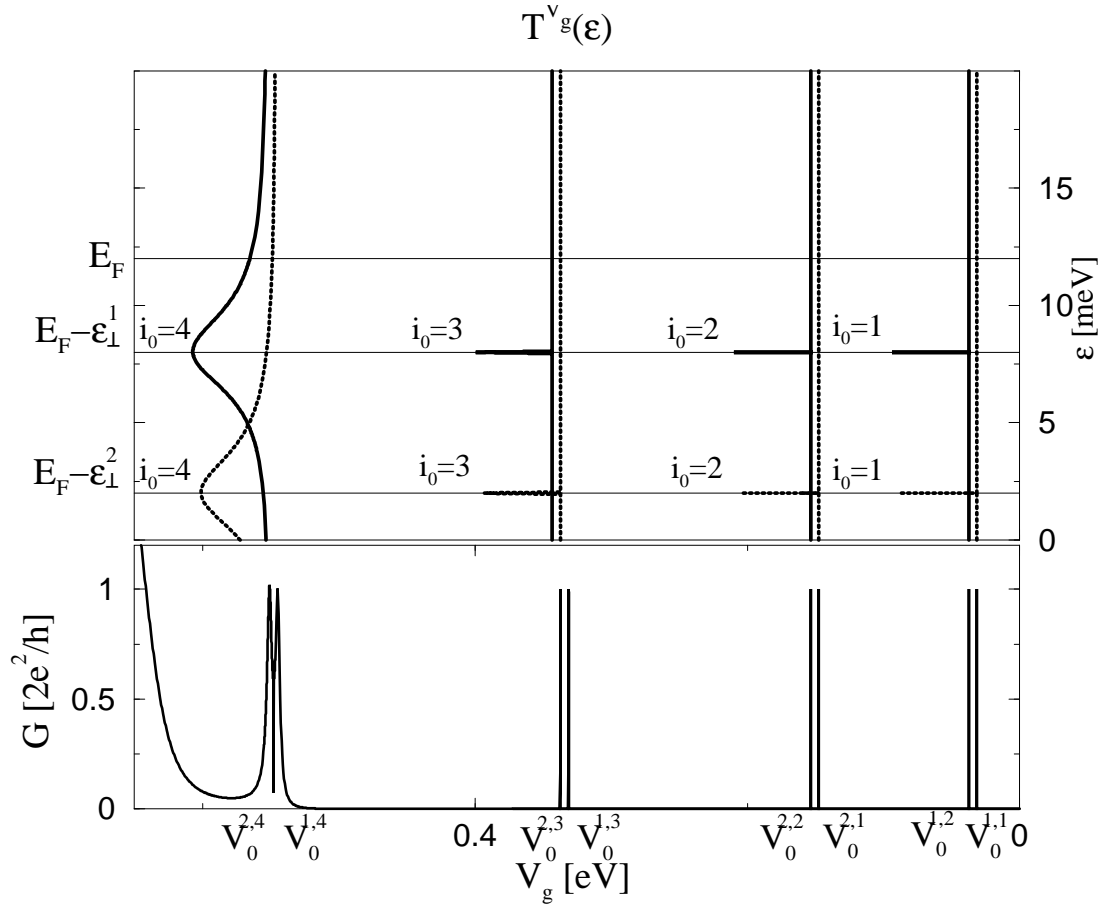


Figure 3.6: Lower part: Qualitative illustration of the conductance as a function of the gate voltage, for a dot isolated inside a quantum wire by the double barrier potential,  $V(z)$ , given in Fig. 3.2. The lateral confinement potential has two eigenenergies  $\epsilon_{\perp}^1$  and  $\epsilon_{\perp}^2$  which lie between 0 and  $E_F$ . Upper part: Transmission vs. energy for the values of  $V_g$  which correspond to the maxima of the conductance.

which can be approximated around a conductance maximum at  $V_g = V_0$  by the expression

$$G_c(V_g) \simeq \frac{2e^2}{h} T^{V_0}(E_F - \epsilon_{\perp}^{\nu_0} - \delta V), \quad (3.10)$$

based on the same argumentation as in the case of the single open transport channel (see Eq. (3.6));  $\delta V = V_g - V_0$ . For a small overlap of the peaks the noncoherent contribution to the conductance can be considered as constant and we obtain an explicit dependence of the conductance on the applied gate voltage

$$G(V_g) \simeq \frac{2e^2}{h} T^{V_0}(E_F - \epsilon_{\perp}^{\nu_0} - \delta V) + \frac{2e^2}{h} \sum_{\nu \neq \nu_0} T^{V_0}(E_F - \epsilon_{\perp}^{\nu}). \quad (3.11)$$

In Fig. 3.7 it is shown that the relation (3.11) provides a good approximation of the conductance inside the energy domain, in which a quasi-isolated resonance extends.

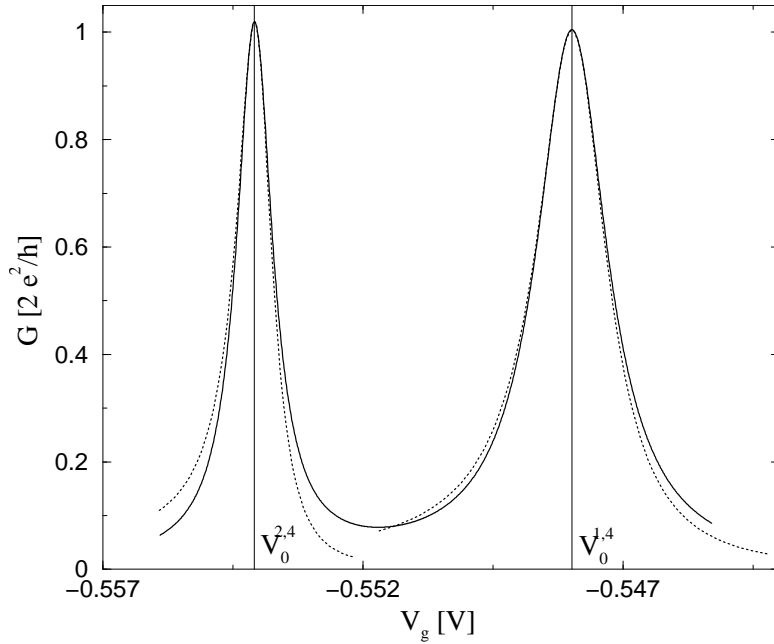


Figure 3.7: The conductance as a function of the gate potential  $V_g$  around the maxima  $\nu_0 = 1, i_0 = 4$  and  $\nu_0 = 2, i_0 = 4$  in Fig. (3.3); complete calculation (solid line) and approximative values (dotted line) given by Eqs. (3.1) and (3.11), respectively. For each maximum the coherent part of the conductance is  $G_c(V_0^{\nu_0,4}) = 2e^2/h$ ,  $\nu_0 = 1, 2$ . The noncoherent parts are  $G_{n.c.}(V_0^{1,4}) \simeq 0.009 e^2/h$  and  $G_{n.c.}(V_0^{2,4}) \simeq 0.038 e^2/h$ .



We have provided in this section a systematic treatment of the conductance through a quantum dot embedded in a quantum wire. In our system the potential is decoupled in the transport- and in the lateral direction which means that the scattering channels are also decoupled. In the frame of the Landauer-Büttiker formalism we find two basic contributions to the conductance: first, a resonant one depending on the gate voltage and second a noncoherent background which can be assumed as a constant in the case of small overlap of the conductance peaks. For a rigorous analysis of the voltage dependent part of the conductance we will use a S matrix description of the coherent transport, in which a Fano resonance is obtained from a pole of S matrix in the complex energy plane (see Chap. 4). The Fano function with a complex asymmetry parameter arises as the most general resonance line shape, under the assumption that the background can be considered constant over the entire width of the resonances.

## 3.2 Capacitance of a Field Induced 2DEG

Another general method for investigating mesoscopic systems constitutes the capacitance spectroscopy [23]. In a tunnel capacitor setup the scattering system is sandwiched between two voltage probes, one of which (the back gate) is strongly coupled to the quantum system while the other (the top gate) is decoupled by a large blocking barrier that suppresses charge transport between the contacts. Then, capacitance spectroscopy is based on the expectation that upon variation of the external voltage, a strong variation in the capacitance occurs when the chemical potential in the back contact reaches a resonance energy of the scattering system.

Further, we analyze the prototypical tunnel capacitor system depicted in Fig. 2.2. The considered AlAs/GaAs structure consists of a sequence of layers grown on a GaAs bulk material given by, first,  $n$ -GaAs layer as a back contact, second, intrinsic GaAs layer as a spacer, third, a short period  $Al_xGa_{1-x}As/GaAs$  superlattice as a blocking barrier and finally a metallization as a top gate. The band structure (see Fig. 3.8) resulting from self-consistent calculations [14, 40] shows for positive gate voltages  $V_G$  a potential pocket at the interface between the GaAs spacer and the blocking barrier, in which a two-dimensional electron gas is formed for large positive voltages.

The total potential of the scattering region is a sum of, first, the fixed potential of the band offsets in the heterostructure, second, the potential of the ionized impurities, and, third, the potential of the electron-electron interaction which we take in the Hartree approximation [14]. For the donors in the  $n$ -GaAs layer and the residual acceptors in the spacer layer we assume complete ionization and homogeneous distribution. The scattering potential has an effectively one-dimensional character,  $V = V(z)$ , and we assume it constant in contacts:  $V(z < -d) = V_1$  and  $V(z > d) = V_2$ . The source and drain regions of the structures act as particle reservoirs and are described by the chemical potentials  $\mu_1$  and  $\mu_2$  which are separated

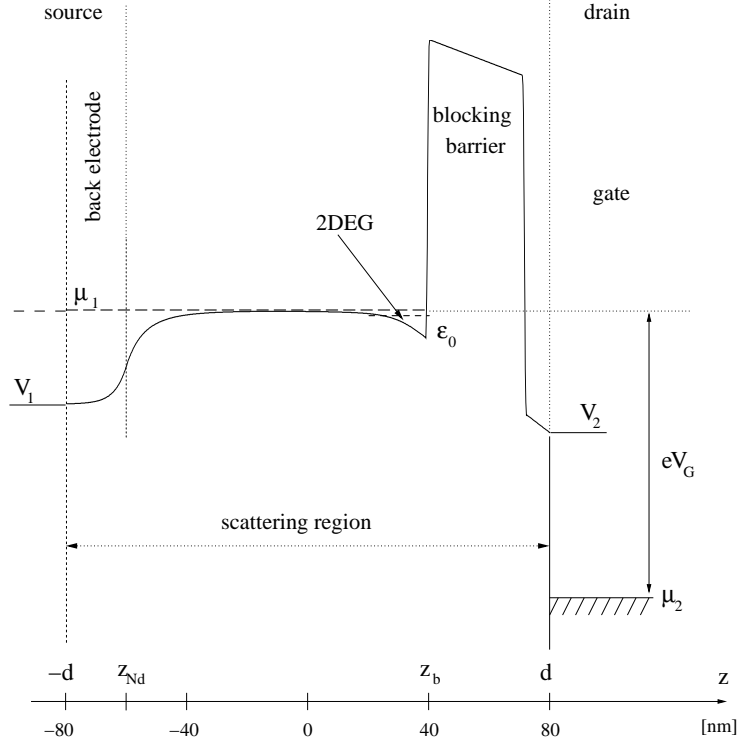


Figure 3.8: Band diagram from self-consistent calculation [14, 40] for the AlAs/GaAs heterostructure given in Fig. 2.2. The structure parameters correspond to the experiments in Ref. [41].

by the applied bias energy  $eV_G$ . The potential difference  $V_1 - V_2$  is determined by  $eV_G$  up to the value of the work function of the metal contact.

To find the charge density in the system we apply the Landauer-Büttiker picture [31] in which the occupation of each scattering state is given by the Fermi function  $f_{FD}(E - \mu_s)$ ,  $s = 1, 2$ . In the limit of low temperatures and based on the expression (2.100) we find

$$\rho(z) = 2e \int d\vec{k}_\perp \sum_s \int_{V_s}^{\infty} d\epsilon g_s(\epsilon) |\phi(\vec{k}_\perp, \vec{r}_\perp)|^2 |\psi^{(s)}(\epsilon, z)|^2 f_{FD} \left( \epsilon + \frac{\hbar^2 k_\perp^2}{2m^*} - \mu_s \right), \quad (3.12)$$

where  $\vec{k}_\perp$  is the 2D wave vector which characterizes the free motion of the electrons in the lateral directions and  $g_s(\epsilon)$  is the 1D density of states given by Eq. (2.64);  $\phi(\vec{k}_\perp, \vec{r}_\perp) = e^{i\vec{k}_\perp \vec{r}_\perp} / 2\pi$  and  $\psi^{(s)}(\epsilon, z)$  are the scattering functions given by Eqs. (2.59-2.61). It is convenient to replace the integration over  $k_\perp$  by an integration over the total energy of the electron,  $E = \epsilon + \frac{\hbar^2 k_\perp^2}{2m^*}$ , and the charge density in the system

becomes

$$\rho(z) = \frac{e}{\pi} \left( \frac{m^*}{\hbar^2} \right)^2 \sum_{s=1,2} \int_{V_s}^{\infty} d\epsilon \frac{|\psi^{(s)}(\epsilon, z)|^2}{k_s(\epsilon)} \int_{\epsilon}^{\infty} dE f_{FD}(E - \mu_s). \quad (3.13)$$

In Eq. (3.13) we can neglect the contribution of the right incident scattering states because the occupied states in the top contact lie about one electron volt below the conduction band edge in the back contact, due to the large work function of the gate metal [41].

The blocking barrier is now assumed to suppress charge transfer completely and we consider the limit of small frequencies. Then, the tunnel capacitor in Fig. 2.2 becomes equivalent to a simple plate capacitor [42]. Neglecting exponentially small charge penetration into the blocking barrier, the charge on the right plate,  $Q_R$ , is associated with the charge on the top gate. The charge on the left plate,  $Q_L = -Q_R$ , is the sum of all charges in the region  $-d < z < z_b$ , where  $z_b$  is the interface between the blocking barrier and *GaAs*-spacer layer. Using Gauss' law [14]  $Q_L$  can be evaluated as  $Q_L = -S\kappa(\partial V/\partial z)(z = z_b)$  where  $S$  is the area of the sample and  $\kappa$  is the dielectric permittivity of the layers. The capacitance is then readily found as

$$C = \left| \frac{\partial Q_L}{\partial V_G} \right| = \left| \frac{\partial Q_R}{\partial V_G} \right|. \quad (3.14)$$

Increasing the gate voltage, the potential energy at the interface between the *GaAs* spacer layer and the blocking barrier is lowered and new allowed states for the electrons appear. As the system is open for particle exchange with the source contact, the free states are immediately populated and the electron concentration inside the scattering system increases. Therefore, the variation of  $V_G$  changes the electronic component of  $Q_L$ ,

$$Q_L^e = \frac{e}{\pi} \left( \frac{m^*}{\hbar^2} \right)^2 \int_{-d}^{z_b} dz \int_{V_1}^{\infty} d\epsilon \frac{|\psi^{(1)}(\epsilon, z)|^2}{k_1(\epsilon)} \int_{\epsilon}^{\infty} dE f_{FD}(E - \mu_1). \quad (3.15)$$

The other charges in the system are fixed and their distribution can not be affected by changes in the potential energy, so that

$$C = \left| \frac{\partial Q_L^e}{\partial V_G} \right|. \quad (3.16)$$

Keeping in mind that our start expression for the charge density is valid only in the limit  $T \rightarrow 0$ , we can replace the chemical potential  $\mu_1$  by the Fermi energy of the source contact,  $E_F^{(1)} = V_1 + \hbar^2 (k_F^{(1)})^2 / 2m^*$ , and the electronic charge accumulated

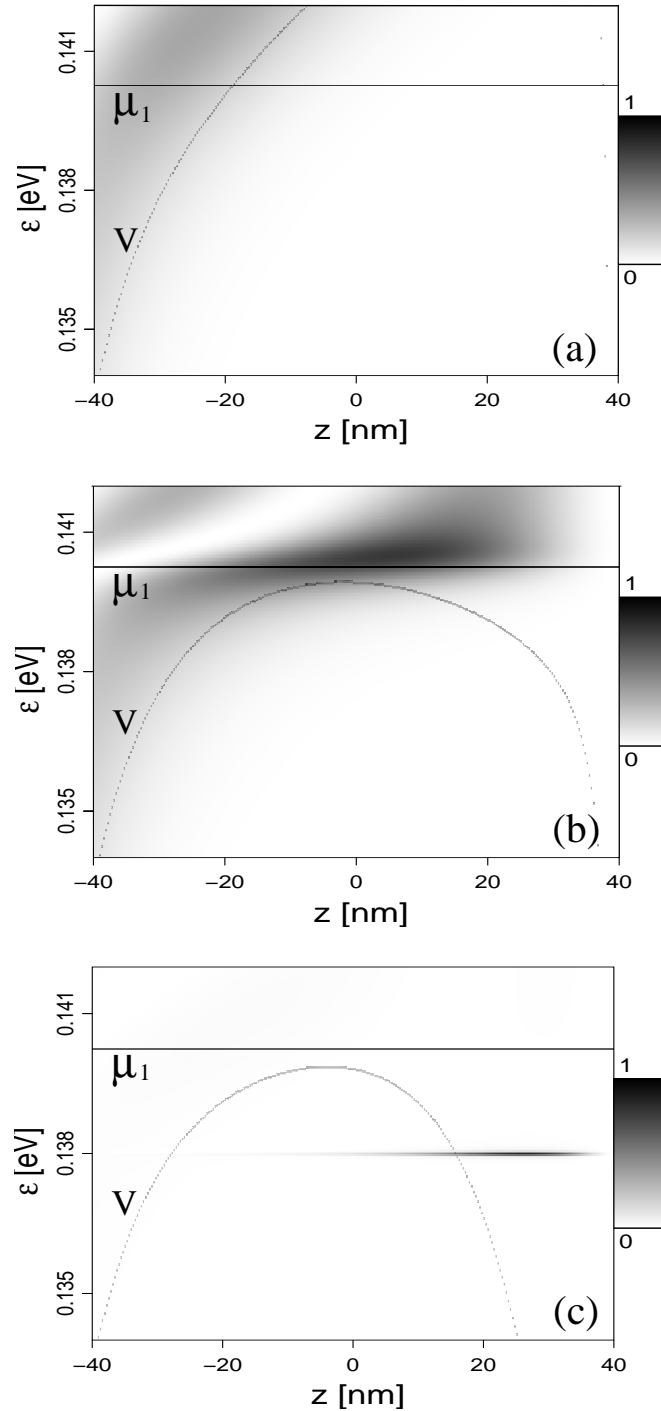


Figure 3.9: The energy- and space-dependence of the electron probability distribution density  $P_\epsilon(z)/P_{\max}$  for three values of applied bias: a.)  $V_g = -0.005V$ , b.)  $V_g = 0.01V$ , and c.)  $V_g = 0.06V$  [14].  $P_{\max} = P_{\epsilon_{\max}}(z_{\max})$  is the maximum value of  $P_\epsilon(z)$  in the considered energy and space domain, and depends on  $V_g$ . We can not keep the same units for all three plots because the total charge in the system varies with  $V_g$ .

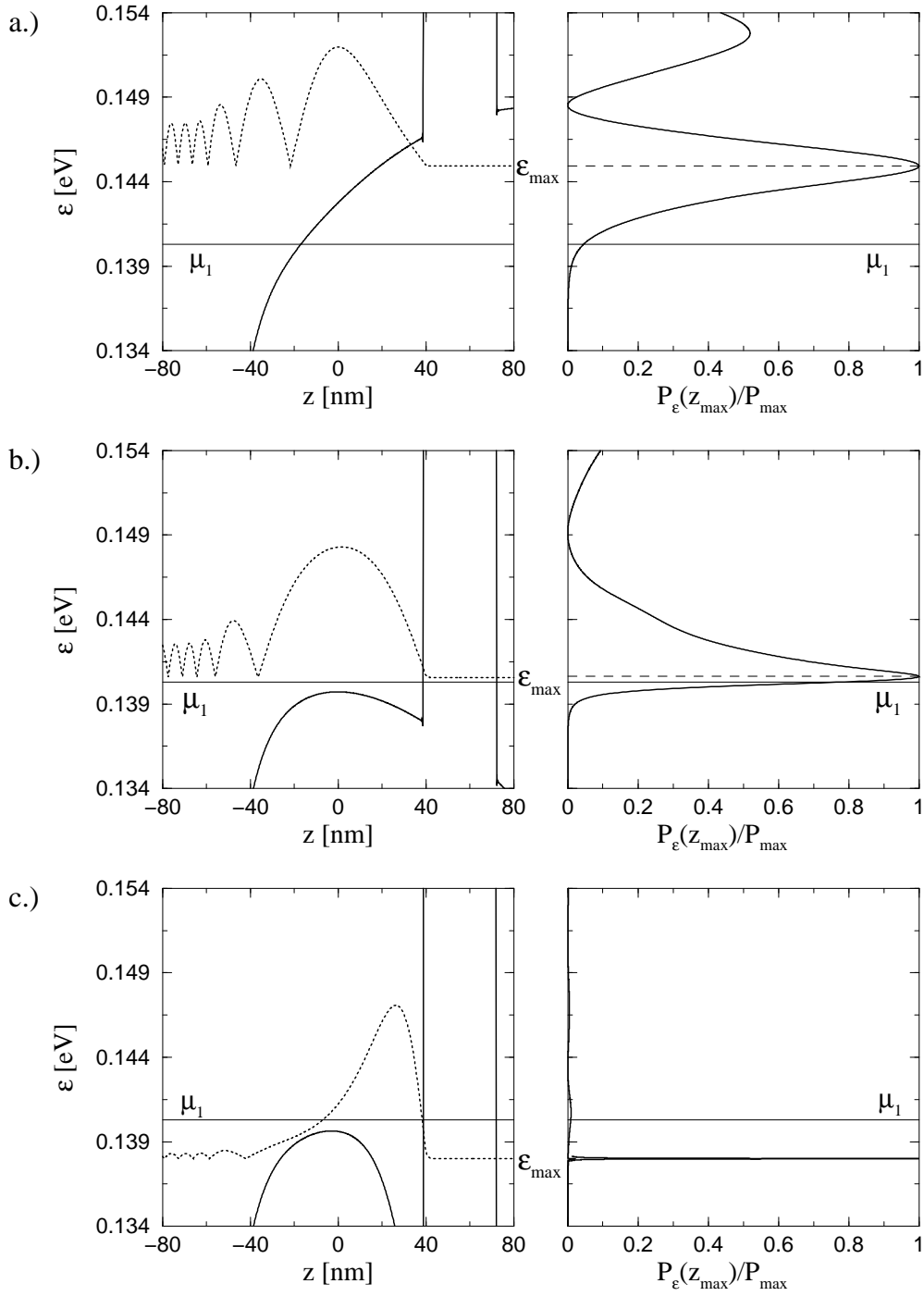


Figure 3.10: Left side: Potential energy (solid line) inside the scattering region ( $|z| \leq d$ ) of the system depicted in Fig. 2.2. Electron probability distribution density  $P_\epsilon(z)$  (dotted line) for  $\epsilon = \epsilon_{\max}$ . Right side: Probability distribution density at  $z = z_{\max}$ , normalized at its maximum value  $P_{\max} = P_{\epsilon_{\max}}(z_{\max})$ , for energies around the chemical potential. The three rows correspond to three values of applied bias: a.)  $V_g = -0.005V$ , b.)  $V_g = 0.01V$ , and c.)  $V_g = 0.06V$ .

in the scattering system is

$$Q_L^e = \frac{e}{2\pi} \frac{m^*}{\hbar^2} \int_{-d}^{z_b} dz \int_{V_1}^{E_F^{(1)}} d\epsilon \frac{\left(k_F^{(1)}\right)^2 - k_1^2(\epsilon)}{k_1(\epsilon)} \left|\psi^{(1)}(\epsilon, z)\right|^2. \quad (3.17)$$

To analyze the physical process that underlies the variation of  $Q_L^e$  with respect to  $V_G$ , we plot in Fig. 3.9 the energy- and space-dependence of the probability distribution density,  $P_\epsilon(z) = |\psi^{(1)}(\epsilon, z)|^2$ , to find an electron in the state  $\psi^{(1)}(\epsilon, z)$  in a volume element at the given  $z$ -coordinate. The scattering wave functions and consequently  $P_\epsilon(z)$  vary with the gate bias  $V_G$ . Because the work function of the metal contact is not precisely known we need to consider as the reference the gate bias energy  $eV_G^f$  which corresponds to the flat conduction band diagram defined through  $\lim_{z \nearrow z_b} dV/dz = 0$ ,  $\lim_{z \searrow z_b} dV/dz = 0$ . We analyze further the probability distribution density  $P_\epsilon(z)$  for different values of  $V_g = V_G - V_G^f$ . The capacitance of the 2DEG can be written as  $C = |\partial Q_L^e / \partial V_g|$ . Another important parameter for our system is the height of the wide and shallow barrier which is formed between the back contact and the blocking barrier (see Fig. 3.8),  $V_{\max} = \max_{-d \leq z < z_b} [V(z)]$ , and which also depend on the voltage. If  $V_g$  is negative, (Fig. 3.9 a.) the electrons are confined in the region close to the back contact and their density changes slightly with applied voltage. In this case  $V_{\max} \simeq V(z_b) \geq \mu_1$  as shown in Fig. 3.10 a.) and there is no particular energy structure of the scattering functions for energies which correspond to the occupied states ( $\epsilon \leq \mu_1$ ). In contrast, for positive values of  $V_g$  (Figs. 3.9 and 3.10 b.) and c.), there is a pronounced maximum of  $P_\epsilon(z)$  with a well defined width in energy and space. In this situation  $V_{\max}$  is below the chemical potential  $\mu_1$  and a classically allowed channel for the electrons is opened. For small positive values of  $V_g$  the maximum of  $P_\epsilon(z)$  lies in this channel. In  $z$ -direction the peak is centered around  $z_{\max}$ , which is close to the position of the maximum of the effective potential,  $V_{\max}$ . With increasing  $V_g$  a potential quantum well is formed at the interface between the spacer layer and the blocking barrier ( $z \simeq z_b$ ) and the position of the maximum of  $P_\epsilon(z)$  in  $z$ -direction,  $z_{\max}$  becomes close to  $z_b$ . (Figs. 3.9 c.) and 3.10 c.) left).  $P_\epsilon(z_{\max})$  has a sharp maximum which is located in an energy range with no classically allowed connection between the electrons in the quantum well and the back contact. (Figs. 3.9 c.) and 3.10 c.) right). It is usually said that the 2DEG is formed.

In the upper part of Fig. 3.11 we compare the experimental C-V-curve [41] to the results of our model [14]. For the numerical calculations, we use the parameters corresponding to the experiments in Ref. [41]: effective mass  $m^* = 0.066m_0$ ,  $\kappa_{GaAs} = \kappa_{AlGaAs} = 12.5\epsilon_0$ ,  $N_D - N_A = 4 \cdot 10^{18} \text{ cm}^{-3}$ , for  $z < z_{Nd}$ , and  $N_A - N_D = 10^{15} \text{ cm}^{-3}$ , for  $z_{Nd} < z < d$ , where  $N_D$  and  $N_A$  are the concentrations of the ionized donors and acceptors, respectively. We emphasize the excellent quantitative agreement between theory and experiment.

Qualitatively, the C-V-traces take the form of a broadened step located between a low-voltage,  $V_g < V_-$ , and a high-voltage,  $V_g > V_+$ , plateau. Both plateaus

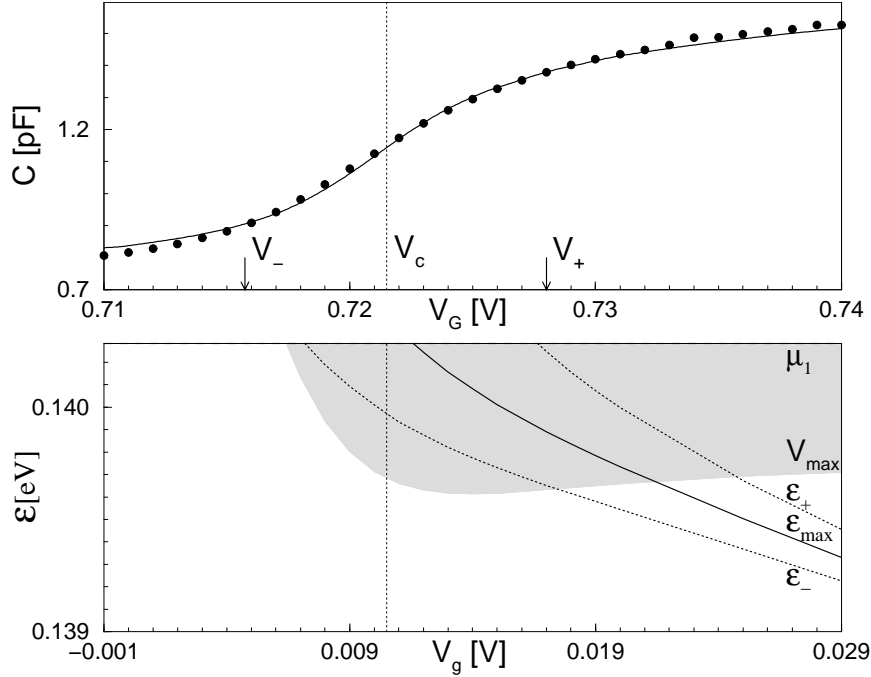


Figure 3.11: Upper part: The C-V curve, experimental data (filled circles) [41] and numerical calculation (solid line). Because the work function of the metal contact is not known precisely, we shift the theoretical voltage scale  $V_g$  with respect to the experimental one  $V_G$ , so that the centers of the steps coincide.  $V_g = 0$  corresponds to the flat band configuration. Lower part: resonance energy  $\epsilon_{\max}$  (solid line) and the energies  $\epsilon_{\pm}$  (dotted lines) at which  $P_{\epsilon}(z_{\max})$  takes half its maximum value  $P_{\max} = P_{\epsilon_{\max}}(z_{\max})$ . Shaded area: energies with  $\mu_1 > \epsilon > V_{\max}$ . Dotted vertical line indicates the center of the step.

have a small positive slope. We define the center of the step through the condition  $d^2C/dV_g^2 = 0$  and  $V_-$  and  $V_+$  correspond to the gate voltages where  $|dC/dV_g|$  takes half of its maximum value. From Fig. 3.11 it can be seen that the step in the C-V characteristic is located in a regime of gate voltages where  $V_{\max}$  is below the chemical potential in the back contact ( $V_{\max} < \mu_1$ ). Also, there are incident states with energies for which the classical motion between the back contact and the quantum well formed at the interface between GaAs spacer layer and blocking barrier is allowed. For these states the electron probability distribution density,  $P_{\epsilon}(z)$ , has a maximum in energy for each  $z$  with  $-d < z < z_b$ , as illustrated in Fig. 3.9 b.). In the lower part of Fig. 3.11 we show the position of the maximum of  $P_{\epsilon}(z_{\max})$ ,  $\epsilon_{\max}$ , and the energies  $\epsilon_{\pm}$  at which the absolute value of the wave function takes half the maximum value at constant  $z = z_{\max}$  (see Fig. 3.9). It can be seen that the center of the step in the C-V trace nearly coincides with the gate voltage at which

$\epsilon_{\max} = \mu_1$ . Furthermore, the voltage  $V_-$  occurs roughly at  $\epsilon_- = \mu_1$  and the onset of the high-voltage plateau  $V_+$  can be associated with  $\epsilon_+ = \mu_1$ .

We can conclude that with increasing applied voltage from  $V_-$  to  $V_+$  increases also the energetic overlapping of the classically allowed channel and the broad peak of  $P_e(z)$ . Consequently, the charge density, which is accumulated inside the scattering system, enhances gradually. The capacitance should follow the slow variation of the charge density, in contrast to a nearly closed system for which a jump in the capacitance occurs, when the chemical potential in the contact reaches a new energy level of the isolated quantum system. In the high voltage plateau ( $V_g > V_+$ ), the probability distribution density maximum in energy narrows considerably and migrates in an energy domain where the coupling to the back contact is possible only through tunneling. With increasing  $V_g$ , the wide and shallow tunneling barrier between the back contact and the electron gas accumulated at the interface between the spacer layer and the blocking barrier also increases, thus, decoupling the 2DEG from the contact. The system becomes equivalent with a plane capacitor with the plates given by the 2DEG and the top metallic gate.



# Chapter 4

## Resonances in Transport Phenomena

The notion of resonances, representing long-lived intermediate states of an open system to which bound states of its closed counterpart are converted, due to coupling to continua, is one of the most fundamental concepts in the domain of quantum scattering [43]. On a formal level resonances show up as poles of the scattering matrix occurring at complex energies  $\bar{E}_{0\lambda} = E_{0\lambda} - i\Gamma_\lambda/2$ , where  $E_{0\lambda}$  and  $\Gamma_\lambda$  are called position and width of the resonance, respectively [44].

In recent years, the study of resonances which appear in transport through semiconductor nanostructures has attracted considerable attention [26, 30, 45, 46, 47, 48, 49, 50, 51, 52]. Of particular interest are asymmetric resonances and antiresonances. In Fano theory both line shapes result from a coherent interaction of the resonance with a given background[53, 8]. To meet this condition, usually, a scenario is considered in which two transmission channels interfere: First, a resonant channel which is provided by a quasibound level, second, a background channel which is provided by a continuum of propagating states. In many studies the continuum of states is associated with a propagating mode in an electron waveguide[45]. The resonant channel can be established by a quasibound state in the binding potential of a donor impurity [46], by the  $\Gamma - X - \Gamma$  - channel in GaAs/AlAs/GaAs single-barrier structures [47] or by a resonantly coupled cavity[48]. An interesting variation of the latter case is the integration of the cavity in an Aharonov-Bohm ring[49]. A similar pattern as in Refs. [45]-[49] is followed in Ref. [50] analyzing magnetotransport across a quantum well. On the experimental side, a first study of Fano profiles in transport was reported very recently in conductance measurements on a single-electron transistor[30]. The measured resonances show typical features of asymmetric and antiresonant Fano profiles. However, there remain open the following questions: First, in agreement with the standard explanation for Fano resonances, there is a resonant part of the transmission which is well understood as a single-electron addition but no coherent background channel can be identified. Second, since there are minima in the conductance but no zeros, an incoherent contribution

to the conductance had to be assumed. As an alternative explanation a complex asymmetry parameter was proposed. Such a complex asymmetry parameter of the Fano distribution has been reported in a number of optical experiments[54, 55]. The aim of this chapter is to derive an analytical theory of transport resonances [13] and to identify in the experimental data the signature of the quasi-isolated resonances, which can be described by Fano functions with a complex asymmetry parameter [14, 13]. Conductance [30] and capacitance [41] measurements are available for high quality nanostructures and they prove directly the dominance of the resonances in the transport phenomena.

## 4.1 Analyticity Properties of the S Matrix

Following Bohm [8], we briefly summarize the analytic properties of the scattering matrix. The causality condition leads to analytic properties of the S matrix when the energy and momenta (or wave vector) of the electron are extended to complex values.  $\tilde{S}(\epsilon)$  is a meromorphic function on the two-sheeted Riemann surfaces with a branch point at  $\epsilon = 0$  and a cut from 0 to  $\infty$ . Bound states poles lie on the negative real axis of the "physical sheet", and except for them  $\tilde{S}(\epsilon)$  is an analytical function on the physical sheet. Further poles (of any order) may lie on the second, "unphysical sheet", coming from the possible zeros on the first sheet. Poles at various

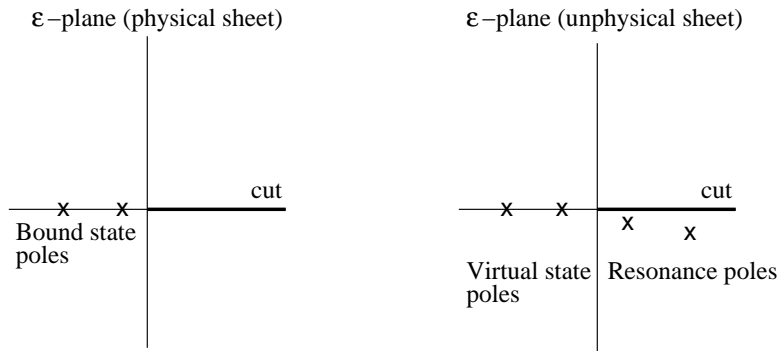


Figure 4.1: Left side: "Physical sheet" of the complex energy plane corresponding to the values of the wave vector  $k = \sqrt{2m^*\epsilon/\hbar^2}$  with  $\text{Im}[k] > 0$ . Poles of the scattering matrix associated with the bound states. Right side: "Unphysical sheet" of the complex energy plane corresponding to the values of the wave vector with  $\text{Im}[k] < 0$ . Poles of  $\tilde{S}(\epsilon)$  associated to the virtual states and to resonances.

locations on the "unphysical sheet" have various physical interpretations. Poles on the negative real axis of the unphysical sheet are called virtual state poles. A virtual state is one that would be bound if the interaction were more attractive. Poles of  $\tilde{S}(\epsilon)$  on the unphysical sheet, if they are close to the real axis, are of particular

importance. They are called resonance poles. However, it is believed that for an interaction that is effectively only in a region of the finite size, one has poles which then must be simple [8].

#### 4.1.1 Resonant States in the R Matrix Theory

Our theoretical development starts with the R matrix representation of the S matrix which is particularly well suited to the description of narrow resonances [43]. As it was demonstrated in the previous chapter, the two matrices are related to each other through the relation (see Eq. (2.52))

$$\tilde{\mathbf{S}}(\epsilon) = \mathbf{1} - 2[\mathbf{1} + i\mathbf{\Omega}(\epsilon)]^{-1}, \quad (4.1)$$

where the matrix  $\mathbf{\Omega}(\epsilon)$  is defined by (2.53). It is obvious that the resonance poles correspond to the zeros of the denominator function in the expression (4.1) of the  $\tilde{\mathbf{S}}$  matrix,

$$\det[\mathbf{1} + i\mathbf{\Omega}(\epsilon_{0\lambda} - i\Gamma_{\lambda}/2)] = 0. \quad (4.2)$$

According to the definition (2.53), the  $\mathbf{\Omega}$  matrix elements have single poles for each  $\epsilon = \epsilon_l$ ,  $l \geq 1$ , i.e. for each eigenenergy of the Hamiltonian corresponding to the scattering system isolated from the contacts. The Wigner Eisenbud energies  $\epsilon_l$  are real and are associated to the bound states. If the system is coupled to contacts the bound states are transformed into scattering states (maybe with a few exceptions depending on the particularities of  $V(z)$ ) and the poles should migrate in the lower part of the "unphysical sheet" of the complex energy plan.

We will first demonstrate that  $\epsilon_l$  are no singularities of the  $\tilde{\mathbf{S}}$  matrix. The matrix  $\mathbf{\Omega}$  given by Eq. (2.53) is split into a resonant part, which contains  $(\epsilon - \epsilon_{\lambda})^{-1}$ , and a regular matrix  $\mathbf{\Omega}_{\lambda}$ ,

$$\mathbf{\Omega}(\epsilon) = \frac{\boldsymbol{\omega}_{\lambda}(\epsilon)}{\epsilon - \epsilon_{\lambda}} + \sum_{\substack{n=1 \\ n \neq \lambda}}^{\infty} \frac{\boldsymbol{\omega}_n}{\epsilon - \epsilon_n} = \frac{\boldsymbol{\omega}_{\lambda}(\epsilon)}{\epsilon - \epsilon_{\lambda}} + \mathbf{\Omega}_{\lambda}(\epsilon). \quad (4.3)$$

This decomposition allows us to write

$$\begin{aligned} \mathbf{1} + i\mathbf{\Omega} &= \mathbf{1} + i\mathbf{\Omega}_{\lambda} + \frac{i\boldsymbol{\omega}_{\lambda}}{\epsilon - \epsilon_{\lambda}} \\ &= \left[ \mathbf{1}(\epsilon - \epsilon_{\lambda}) + i\boldsymbol{\omega}_{\lambda}(\mathbf{1} + i\mathbf{\Omega}_{\lambda})^{-1} \right] \frac{\mathbf{1} + i\mathbf{\Omega}_{\lambda}}{\epsilon - \epsilon_{\lambda}}. \end{aligned} \quad (4.4)$$

Taking into account that  $\det[\boldsymbol{\omega}_{\lambda}] = 0$  as follows from the definition (2.54), we obtain straightforwardly the determinant of the matrix  $\mathbf{1} + i\mathbf{\Omega}$ ,

$$\det[\mathbf{1} + i\mathbf{\Omega}] = \frac{\epsilon - \epsilon_{\lambda} - \bar{\mathcal{E}}_{\lambda}(\epsilon)}{\epsilon - \epsilon_{\lambda}} \mathcal{D}_{\lambda}(\epsilon) \quad (4.5)$$

with

$$\bar{\mathcal{E}}_\lambda(\epsilon) = -i\text{Tr}[\boldsymbol{\omega}_\lambda(\mathbf{1} + i\boldsymbol{\Omega}_\lambda)^{-1}], \quad (4.6)$$

and

$$\mathcal{D}_\lambda(\epsilon) = \det[\mathbf{1} + i\boldsymbol{\Omega}_\lambda]. \quad (4.7)$$

Now we can express the  $\tilde{\mathbf{S}}$ -matrix given by (2.52) in terms of  $\boldsymbol{\Omega}_\lambda$  and  $\boldsymbol{\omega}_\lambda$ ,

$$\tilde{\mathbf{S}}(\epsilon) = \frac{\mathbf{Z}_\lambda(\epsilon)}{\epsilon - \epsilon_\lambda - \bar{\mathcal{E}}_\lambda(\epsilon)}, \quad (4.8)$$

where the matrix  $\mathbf{Z}_\lambda(\epsilon)$  is defined as

$$\mathbf{Z}_\lambda(\epsilon) = \frac{\epsilon - \epsilon_\lambda}{\mathcal{D}_\lambda(\epsilon)} \left[ -1 - \det[\boldsymbol{\Omega}] + i(\boldsymbol{\Omega} - \boldsymbol{\Omega}^-) \right], \quad (4.9)$$

and  $\boldsymbol{\Omega}^- = \boldsymbol{\Omega}^{-1} \det[\boldsymbol{\Omega}]$ . In principle, the solutions of the equation  $\mathcal{D}_\lambda(\epsilon) = 0$  can not be associated with resonance poles of the  $\tilde{\mathbf{S}}$  matrix. As follows from the definition (4.6),  $\bar{\mathcal{E}}_\lambda(\bar{\epsilon}) \sim 1/\mathcal{D}(\bar{\epsilon})$  and becomes infinite for  $\mathcal{D}(\bar{\epsilon}) \rightarrow 0$ . So we can not directly say that  $\mathcal{D}_\lambda$  and  $\det[\mathbf{1} + i\boldsymbol{\Omega}]$  vanish at the same points. Even if the two functions have a common pole, it is expected to have a large imaginary part since  $\mathcal{D}_\lambda$  depends only through the regular and slowly varying function  $\boldsymbol{\Omega}_\lambda$ . Therefore, it is convenient to include  $\mathcal{D}_\lambda(\epsilon)$  in  $\mathbf{Z}_\lambda(\epsilon)$ .

The matrix  $\mathbf{Z}_\lambda$  and the function  $\bar{\mathcal{E}}_\lambda$  are related to each other through the unitarity requirement for the  $\tilde{\mathbf{S}}$  matrix which gives

$$\mathbf{Z}_\lambda \mathbf{Z}_\lambda^\dagger = \mathbf{Z}_\lambda^\dagger \mathbf{Z}_\lambda = \left| \epsilon - \epsilon_\lambda - \bar{\mathcal{E}}_\lambda(\epsilon) \right|^2. \quad (4.10)$$

The representation of the S-matrix in Eq. (4.8) is an exact reformulation of Eq. (2.52) and has the advantage that it directly yields the equation

$$\epsilon_{0\lambda} - i\Gamma_\lambda/2 - \epsilon_\lambda - \bar{\mathcal{E}}_\lambda(\epsilon_{0\lambda} - i\Gamma_\lambda/2) = 0 \quad (4.11)$$

to determine the positions  $\bar{\epsilon}_{0\lambda} = \epsilon_{0\lambda} - i\Gamma_\lambda/2$  of the poles in the complex energy plane. It is obvious that the expression (4.8) has no singularities for real energies in the interval  $(\epsilon_{\lambda-1}, \epsilon_{\lambda+1})$ . Coupling to the contacts leads to a nonzero imaginary part of the resonance energy and the stronger the coupling the larger the difference between the Wigner Eisenbud energies  $\epsilon_\lambda$  and the resonant energies  $\bar{\epsilon}_{0\lambda}$ .

## 4.2 Conductance Resonances in a Quantum Dot

In the following we are interested in the analysis of narrow transport resonances. They occur in the resonant part  $G_c$  of the conductance as given by Eq. (3.9). For

illustrative purposes and to check our analytical theory we consider  $T(\epsilon)$  for the double barrier system of Fig. 3.2 with an applied source-drain voltage  $V_{SD} = 200$  meV, as depicted in Fig. 4.2. In the structure of Fig. 4.2, the barriers are high enough so that the lowest three quasibound resonances (1-3) and the above lying Fowler-Nordheim-type resonance (4) are narrow and have little interaction. However, the approximation technique described below gives a very good description of the higher Fabry-Perot-type resonances (5 and 6) in the classically allowed transport regime as well. These resonances have a sizeable larger overlap.

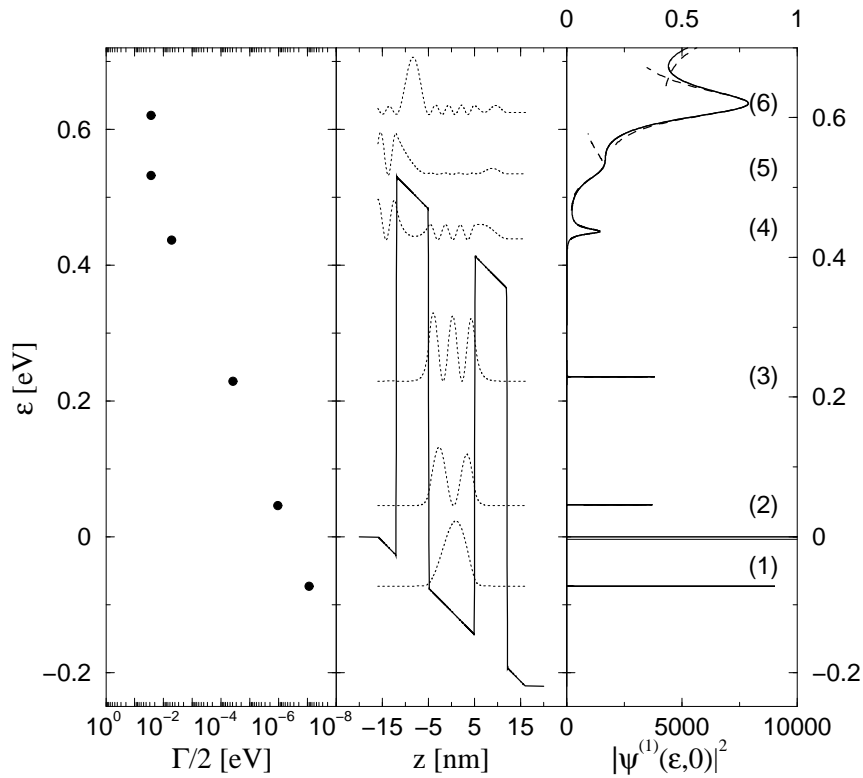


Figure 4.2: Middle: Assumed potential in a schematic plot (solid line), wave functions  $|\Psi^{(1)}|^2$  at the resonance energies (dotted lines). Left: Position of the poles of the  $S$ -matrix in the complex energy plane determined after Eqs. (4.12) and (4.13). Upper right: Transmission vs. energy from exact calculation (solid line) and approximation in Eq. (4.20) (dashed line). Lower right: Wave function  $|\Psi^{(1)}|^2$  in the middle of the quantum well ( $z = 0$ ) vs. energy from exact calculation.

### 4.2.1 Fano Resonances in Transmission

We are interested in narrow resonances for which  $\Gamma$  is a small quantity. Therefore, as a basic assumption for our theory of the resonant Fano line shape, we require the validity of the linearization of  $\bar{\mathcal{E}}_\lambda$  and implicitly  $\mathbf{Z}_\lambda$  in a domain of the complex energy plane that includes the pole  $\bar{\epsilon}_0$  and the part of the real axis which contains the transmission peak associated with the resonance; for simplicity, we omit further the index  $\lambda$  of the resonant pole.

After a first order expansion of  $\bar{\mathcal{E}}_\lambda(\epsilon_0 - i\Gamma/2)$  around  $\epsilon_0$  one obtains from Eq. (4.11)

$$\epsilon_0 = \epsilon_\lambda + \mathcal{E}_1(\epsilon_0) - \frac{\Gamma}{2} \frac{d\mathcal{E}_2}{d\epsilon} \Big|_{\epsilon=\epsilon_0}, \quad (4.12)$$

$$\Gamma = 2 \mathcal{E}_2(\epsilon_0) \left( 1 - \frac{d\mathcal{E}_1}{d\epsilon} \Big|_{\epsilon=\epsilon_0} \right)^{-1}, \quad (4.13)$$

where  $\mathcal{E}_1(\epsilon) = \text{Re} [\bar{\mathcal{E}}_\lambda(\epsilon)]$  and  $\mathcal{E}_2(\epsilon) = -\text{Im} [\bar{\mathcal{E}}_\lambda(\epsilon)]$ . Inserting Eq. (4.13) in Eq. (4.12) one obtains a nonlinear equation with a unique root for  $\epsilon_0$ . Our approach yields a simple and accurate numerical procedure to approximate the position of the poles of the S matrix in the complex energy plane, from which the shape of the lines directly follows. In Fig. (4.3b) it is demonstrated that the resonance energies of the lowest

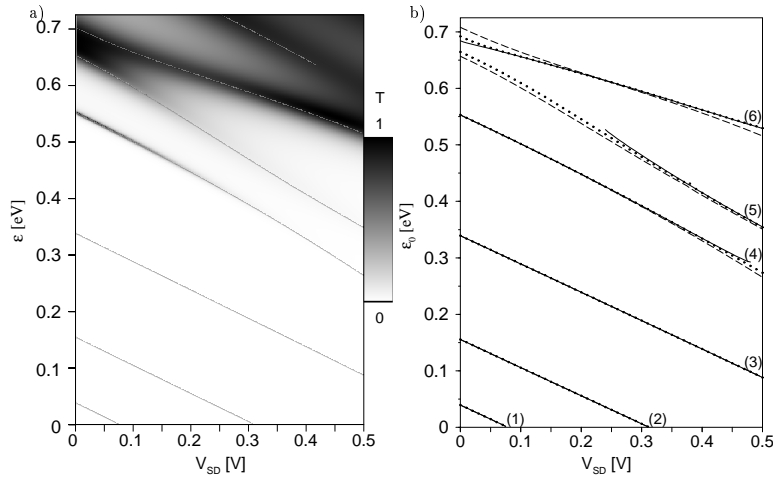


Figure 4.3: a.) Transmission as a function of  $V_{SD}$  and the kinetic energy  $\epsilon$ . b.) Energy of maximum transmission vs.  $V_{SD}$ : Complete calculation (solid lines),  $\epsilon_0$  given by Eqs. (4.12) and (4.13) (dashed lines), and values obtained in the Breit Wigner approximation, Eqs. (4.23) and (4.24), (dotted lines). The three lines coincide for the lowest three resonances.

levels are very well represented by our linear approximation.

To obtain the line shape of the resonance we employ a formal expansion of the  $\tilde{S}$ -matrix as given in Eq. (4.8) in a Laurent series around the pole  $\bar{\epsilon}_0 = \epsilon_0 - i\Gamma/2$ ,

$$\tilde{\mathbf{S}}(\bar{\epsilon}) = \frac{\mathbf{A}_{-1}}{\bar{\epsilon} - \epsilon_0 + i\Gamma/2} + \mathbf{A}_0 + \sum_{j=1}^{\infty} \mathbf{A}_j (\bar{\epsilon} - \epsilon_0 + i\Gamma/2)^j. \quad (4.14)$$

As usually done, we assume the poles to be simple [50, 51]. Here Eq. (4.8) ensures that the  $S$ -matrix is an analytic function in the resonance domain excepting the pole, condition which is required for the existence of the Laurent series. The resonance domain is defined as a region in the complex energy plane in the vicinity of  $\bar{\epsilon}_0$ , which includes usually the interval  $(\epsilon_0 - \Gamma/2, \epsilon_0 + \Gamma/2)$  on the real axis, and inside which we can linearize  $\bar{\mathcal{E}}_\lambda$  and  $\mathbf{Z}_\lambda$ . Thus, the derivatives up to the second order for these two functions at the points  $\bar{\epsilon}_0$  and  $\epsilon_0$  are very small and we can neglect them in the expression of the expansion coefficients of the Laurent series. Thus, the coefficients have the form

$$\mathbf{A}_{-1} \simeq \frac{\mathbf{Z}_\lambda(\epsilon_0) - i\Gamma/2 \left. \frac{d\mathbf{Z}_\lambda}{d\epsilon} \right|_{\epsilon=\epsilon_0}}{1 - \left. \frac{d\bar{\mathcal{E}}_\lambda}{d\epsilon} \right|_{\epsilon=\epsilon_0}}, \quad (4.15)$$

$$\mathbf{A}_0 \simeq \frac{\left. \frac{d\mathbf{Z}_\lambda}{d\epsilon} \right|_{\epsilon=\epsilon_0}}{1 - \left. \frac{d\bar{\mathcal{E}}_\lambda}{d\epsilon} \right|_{\epsilon=\epsilon_0}} \quad (4.16)$$

and  $\mathbf{A}_j \simeq 0, \forall j \geq 1$ . According to Eqs. (4.12) and (4.13)

$$1 - \left. \frac{d\bar{\mathcal{E}}_\lambda}{d\epsilon} \right|_{\epsilon=\epsilon_0} = \frac{\epsilon_0 - \epsilon_\lambda - \bar{\mathcal{E}}_\lambda(\epsilon_0)}{i\Gamma/2} \quad (4.17)$$

and  $\mathbf{A}_0$ , denoted by  $\tilde{\mathbf{S}}_{bg}$ , becomes identically with

$$\tilde{\mathbf{S}}_{bg} = \frac{i\Gamma/2}{\epsilon_0 - \epsilon_\lambda - \bar{\mathcal{E}}_\lambda(\epsilon_0)} \left. \frac{d\mathbf{Z}_\lambda}{d\epsilon} \right|_{\epsilon=\epsilon_0}. \quad (4.18)$$

From here it follows also  $\mathbf{A}_{-1} = i [\tilde{\mathbf{S}}(\epsilon_0) - \tilde{\mathbf{S}}_{bg}] \Gamma/2$ .

After the linearization of  $\bar{\mathcal{E}}_\lambda$  and  $\mathbf{Z}_\lambda$  we obtain

$$\tilde{\mathbf{S}}(\epsilon) \simeq i \frac{\tilde{\mathbf{S}}(\epsilon_0) - \tilde{\mathbf{S}}_{bg}}{e + i} + \tilde{\mathbf{S}}_{bg}, \quad (4.19)$$

where  $e = 2(\epsilon - \epsilon_0)/\Gamma$  and  $\epsilon_0$  and  $\Gamma$  are position and width of the resonance. Eq. (4.19) has a standard form [8, 51, 56, 57], but we can provide here an explicit expression for the nonresonant component of the scattering matrix,  $\tilde{\mathbf{S}}_{bg}$ . The first term in Eq. (4.19) represents the resonant part of  $\tilde{\mathbf{S}}$ . For each element of the matrix  $\tilde{\mathbf{S}}$  it is seen from Eq. (4.19) that the resonant part undergoes a phase change of  $\pi$  when the energy passes the resonance. In general, this produces a change between

constructive and destructive superposition of the resonant and the nonresonant part. Therefore, an asymmetric line is obtained.

From Eq. (4.19) a line shape of the transmission probability is deduced,

$$T(\epsilon) = \left| (\tilde{\mathbf{S}}(\epsilon))_{12} \right|^2 = T_{bg} \frac{[e + \text{Re}(q)]^2 + [\text{Im}(q)]^2}{e^2 + 1}, \quad (4.20)$$

where  $T_{bg} = \left| (\tilde{\mathbf{S}}_{bg})_{12} \right|^2$  is the background transmission. The right hand side of Eq. (4.20) is a Fano distribution (see Fig. 4.5) with a complex asymmetry parameter  $q$  given by

$$q = i \left( \tilde{\mathbf{S}}(\epsilon_0) \right)_{12} \left( \tilde{\mathbf{S}}_{bg} \right)_{12}^{-1}. \quad (4.21)$$

In the following, Eq. (4.20) will be referred to as the transmission in the Fano approximation. To prove the validity of this approach for the transmission line shape, we analyze in detail the first six maxima of the transmission curve corresponding to the double barrier system, given in Fig. 4.2. As can be seen from Fig. 4.4, in the resonance domains Eq. (4.20) provides a very good description of the peaks; for the first two maxima one can not see any difference between the curves corresponding to the exact calculation and Fano approximation. The exception is the fifth peak which can not be considered separated from the next one and therefore the required conditions for the Fano approximation are no longer fulfilled.

Often the background matrix  $\tilde{\mathbf{S}}_{bg}$  in Eq. (4.19) is assumed to be absent, leading to a symmetrical Wigner-Breit shape of the transmission peaks [58],

$$T(\epsilon) = \left| (\tilde{\mathbf{S}}(\epsilon))_{12} \right|^2 \simeq T(\epsilon_0) \frac{1}{e^2 + 1} = T(\epsilon_0) \frac{(\Gamma/2)^2}{(\epsilon - \epsilon_0)^2 + (\Gamma/2)^2}, \quad (4.22)$$

where  $T(\epsilon_0) = \left| (\tilde{\mathbf{S}}(\epsilon_0))_{12} \right|^2$ . For consistency, we have to neglect the first derivatives of  $\bar{\mathcal{E}}_\lambda(\epsilon)$  and  $\mathbf{Z}_\lambda(\epsilon)$  not only in the expression (4.19) of the  $\tilde{\mathbf{S}}$  matrix but also in Eqs. (4.12)-(4.13). Therefore, the position and the width of the resonance are determined by the equations

$$\epsilon_0 = \epsilon_\lambda + \mathcal{E}_1(\epsilon_0), \quad (4.23)$$

and

$$\Gamma = 2 \mathcal{E}_2(\epsilon_0), \quad (4.24)$$

respectively, where  $\mathcal{E}_1(\epsilon) = \text{Re} \left[ \bar{\mathcal{E}}_\lambda(\epsilon) \right]$  and  $\mathcal{E}_2(\epsilon) = -\text{Im} \left[ \bar{\mathcal{E}}_\lambda(\epsilon) \right]$ . Beside Eq. (4.22) these two relations are the main equations of the Breit Wigner approximation of the scattering matrix.



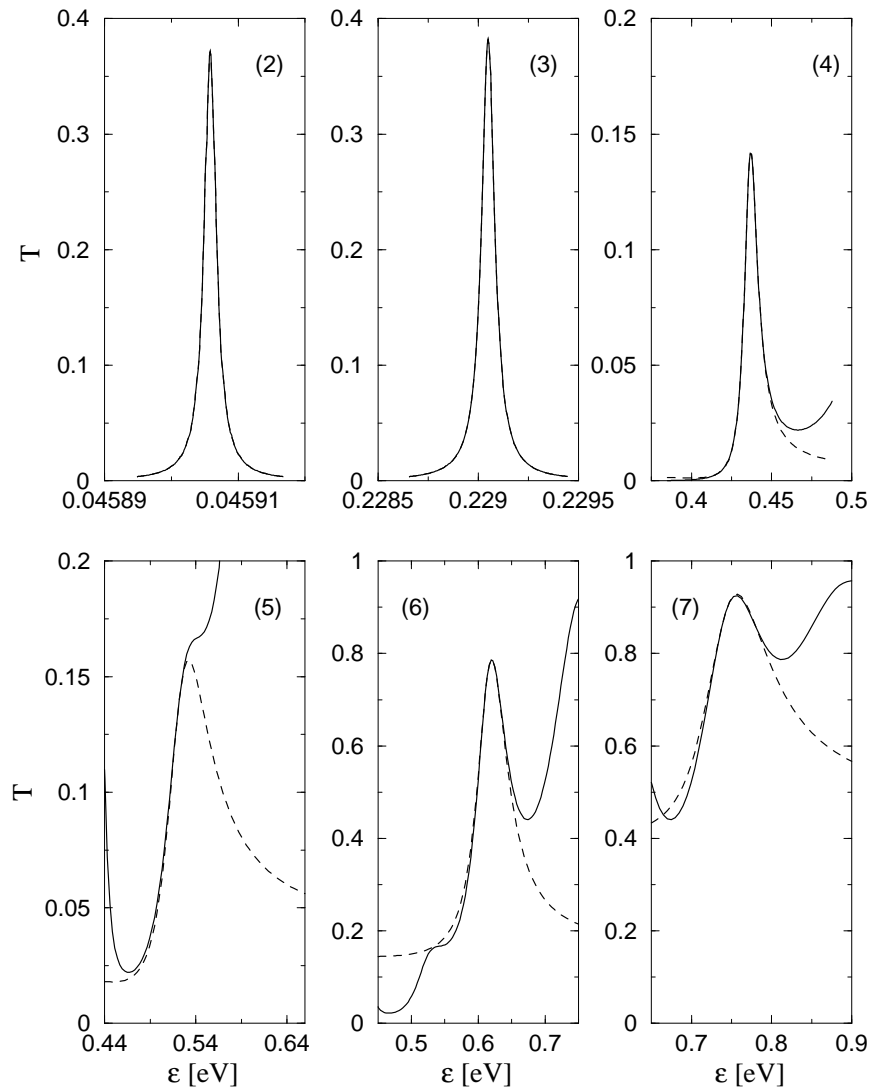


Figure 4.4: Transmission vs. energy from exact calculation (solid line) and approximation in Eq. (4.20) (dashed line) for the potential energy depicted in the middle part of Fig. 4.2. In the first two graphics the solid- and dashed curves practically coincide.

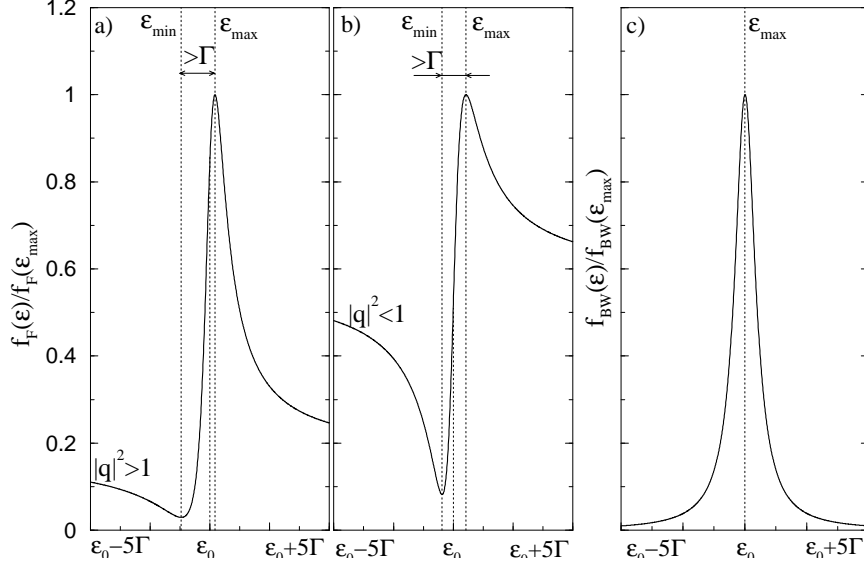


Figure 4.5: Fano distribution,  $f_F(\epsilon) = [(e + \text{Re}(q))^2 + (\text{Im}(q))^2]/[e^2 + 1]$  with  $e = 2(\epsilon - \epsilon_0)/\Gamma$ , for two values of the asymmetry parameter  $q$ : a.)  $|q|^2 > 1$ , b.)  $|q|^2 < 1$ ; c.) Breit Wigner distribution,  $f_{BW}(\epsilon) = 1/[e^2 + 1]$ .

In contrast to the Breit Wigner distribution, Fano function (4.20) is asymmetric and allows for two extreme points,

$$\epsilon_{\max} = \epsilon_0 + \frac{\Gamma}{4\text{Re}(q)} \left[ 1 - |q|^2 + \sqrt{(1 - |q|^2)^2 + 4[\text{Re}(q)]^2} \right], \quad (4.25)$$

$$\epsilon_{\min} = \epsilon_0 + \frac{\Gamma}{4\text{Re}(q)} \left[ 1 - |q|^2 - \sqrt{(1 - |q|^2)^2 + 4[\text{Re}(q)]^2} \right], \quad (4.26)$$

for which the transmission has the values  $T(\epsilon_{\max}) = T_{bg}[1 + \text{Re}(q)/\epsilon_{\max}]$  and  $T(\epsilon_{\min}) = T_{bg}[1 + \text{Re}(q)/\epsilon_{\min}]$ , respectively. The nonzero transmission minimum associated with the resonance is a consequence of the complex asymmetry parameter. These qualitative features, therefore, describe the interference of the resonant level with the background. An inspection of the line shapes of the exact calculation shows that there is an asymmetry which is correctly described in the Fano approximation. However, the results of our exact calculation (see Fig. 4.4) show no minimum associated with a resonance. This can be understood by noting that always  $\epsilon_{\max} - \epsilon_{\min} \geq \Gamma$  i. e. the minimum occurs in the tail of the distribution where it has no weight and where our linearization is less well justified.

A rigorous analysis of the resonance line shape requires an answer to the question if the Fano approximation is really better or the intensively used Breit Wigner profile is sufficient for describing quasiseparated resonances. While in the Fano approximation the slowly varying function of energy  $\bar{\mathcal{E}}_\lambda$  and  $\mathbf{Z}_\lambda$  are linearized in the

resonance domain, in the Breit Wigner approximation they are considered constant. For our test structure given in Fig. 4.2 we plot in Fig. 4.6 the derivative of  $\bar{\mathcal{E}}_\lambda$  with respect to the energy at  $\epsilon = \epsilon_0$  as a function of applied bias,  $V_{SD}$ . It is obvious

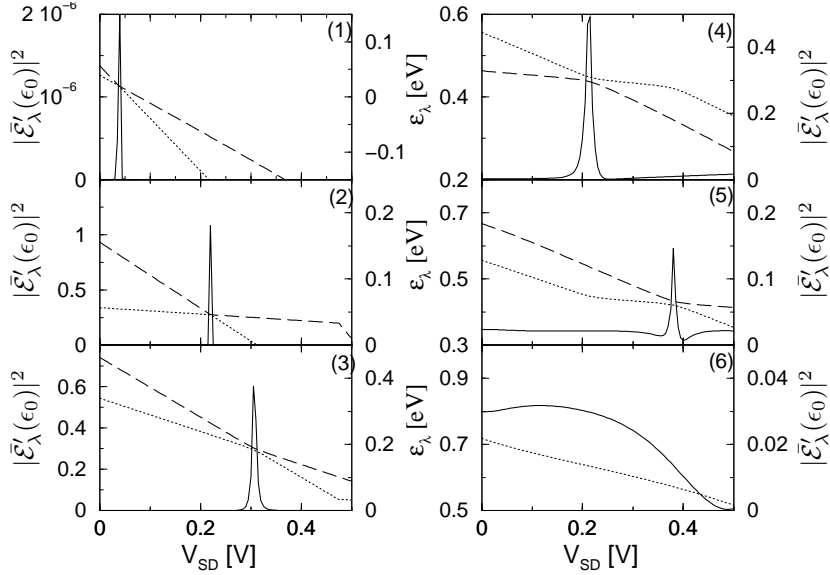


Figure 4.6:  $\bar{\mathcal{E}}'_\lambda(\epsilon_0) = d\bar{\mathcal{E}}_\lambda/d\epsilon$  at  $\epsilon = \epsilon_0$  (solid line) and Wigner Eisenbud energies  $\epsilon_\lambda$  next to the resonance energy  $\epsilon_0$  (dashed and dotted line) plotted against  $V_{SD}$ . The nonvanishing values of  $d\bar{\mathcal{E}}_\lambda/d\epsilon|_{\epsilon=\epsilon_0}$  are associated with the level crossing of Wigner Eisenbud energies with wave functions located before and between the barriers (see lower part of Fig. 4.7).

from this figure that there are double barrier systems for which the derivative of  $\bar{\mathcal{E}}_\lambda(\epsilon)$  and, implicitly, of  $\mathbf{Z}_\lambda(\epsilon)$  at the resonance energy can not be neglected even for narrow and well-separated peaks. As an example, we present in Fig. 4.7 the transmission around the second maximum given by exact calculation (Eq. (4.8)) and by the two approximations: Fano (Eq. (4.20)) and Breit-Wigner (Eq. (4.22)). For certain values of applied bias, the Breit Wigner approximation collapses although the asymmetry of the line shape is not so strong. These results seem unexpected, but are perfectly understandable in view of our method to determine the resonant contribution to the scattering matrix. The starting point is the so called closed scattering problem described by the Wigner Eisenbud functions and energies. For this problem, the energy spectrum is discrete, but the level crossing (see Fig. 4.6) is not forbidden. If  $\epsilon_\lambda$  and  $\epsilon_{\lambda+1}$  are close to each other the matrix  $\mathbf{\Omega}_\lambda$  (Eq. (4.3)), which contains  $(\epsilon - \epsilon_{\lambda+1})^{-1}$ , can not be considered constant around  $\epsilon_\lambda$ . In turn, the energy dependence of  $\bar{\mathcal{E}}_\lambda$  and  $\mathbf{Z}_\lambda$  is not negligible as it is presumed in the Breit Wigner approximation; these two functions have no singularities at  $\epsilon_\lambda$  or in its vicinity and the lowest approximation is a linear dependence on energy around  $\epsilon_\lambda$ .

Thus, for separated resonances, the position and the width are correctly given by Eqs. (4.12) and (4.13), i.e. in the Fano approximation. The most general form of

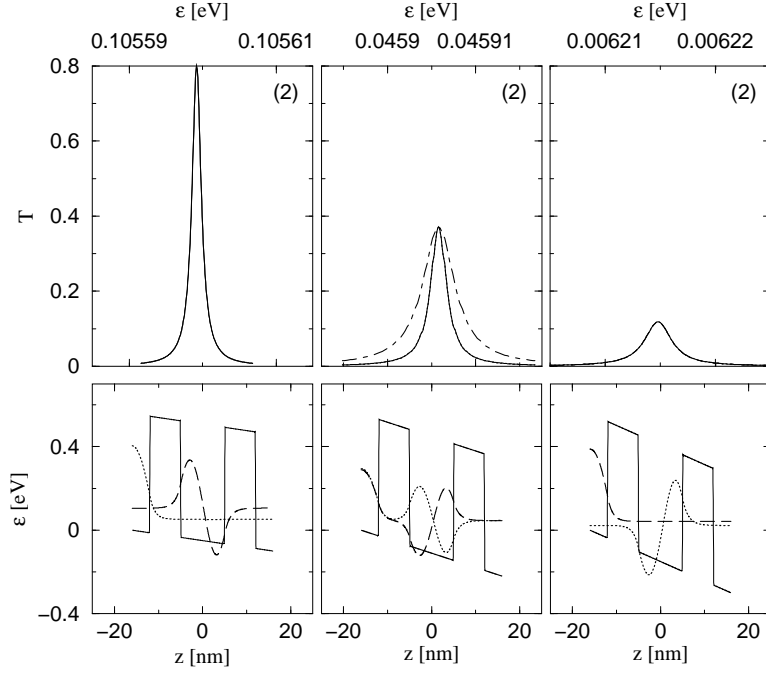


Figure 4.7: Upper part: Second transmission peak for the double barrier structure presented in Fig. 4.2 for three values of the applied bias:  $V_{SD} = 100$  mV (left),  $V_{SD} = 220$  mV (middle) and  $V_{SD} = 300$  mV (right). Solid line curves correspond to exact calculation (Eq. (4.8)), dotted curves to Fano approximation (Eq. (4.20)) and dot-dashed curves to Breit Wigner approximation (Eq. (4.22)). For  $V_{SD} = 100$  mV and  $V_{SD} = 300$  mV all three lines practically coincide, while in the middle graphic only the solid- and dotted curve appear identical. Lower part: Potential energy of the biased double barrier structure (solid line) and the Wigner Eisenbud functions (dotted and dashed lines) corresponding to the Wigner Eisenbud energies next to the resonance energy.

a quasi-isolated transmission peak is described by the Fano function given in Eq. (4.20). The numerical calculations in Fig. (4.8) confirm that the complex parameter  $q$  is a general finding. This seems to hold for narrow peaks as well as for broad and overlapping peaks. Similarly to the case of the Fano function with real parameter [53], we can establish a connection between the parameter  $q$  and the asymmetry of

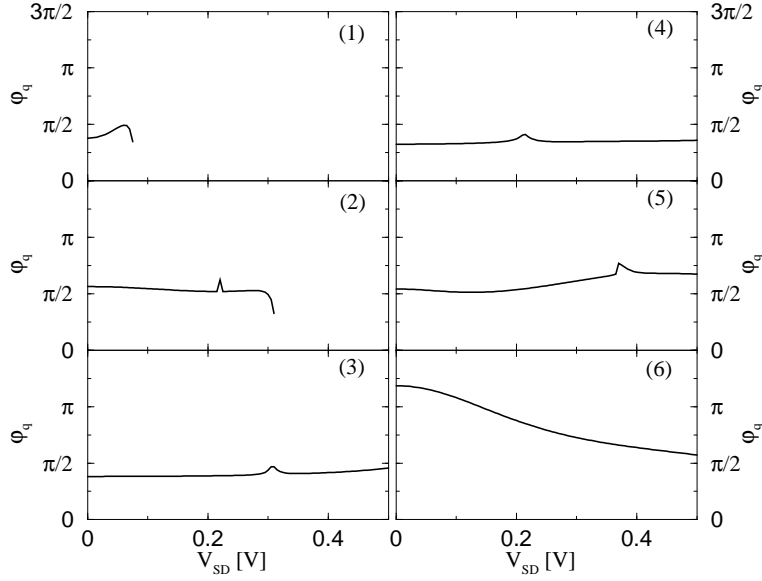


Figure 4.8: The argument of the complex asymmetry parameter  $q$  vs. applied bias for the first six transmission peaks. Even for the narrow transmission peaks corresponding to the quasibound states the imaginary part of  $q$  is big and thus, it is important for the description of the line shape.

the profile; Eq. (4.20) can be written into an equivalent form

$$T(\epsilon) = T_{bg} [\text{Im}(q)]^2 \frac{(\Gamma/2)^2}{(\epsilon - \epsilon_0)^2 + (\Gamma/2)^2} + T_{bg} [\text{Re}(q)]^2 \frac{\left[ \frac{1}{\text{Re}(q)} (\epsilon - \epsilon_0) + \Gamma/2 \right]^2}{(\epsilon - \epsilon_0)^2 + (\Gamma/2)^2} \quad (4.27)$$

which shows that the real part of  $q$  is responsible for the asymmetry of the transmission line shape. If  $\text{Re}(q)$  is large enough so that  $2(\epsilon - \epsilon_0)/[\Gamma \text{Re}(q)] \ll 1$  the asymmetric part of the transmission is negligible. In particular, this is the case of the second transmission maximum plotted in Fig. 4.7 for which  $\text{Re}(q) \sim 10^4$  (see Fig. 4.9) and which has no sizable asymmetry.

On the background of our systematic pole analysis we want to discuss a common practice in which an Ansatz for the S-matrix of the form of Eq. (4.19) with general  $\tilde{\mathbf{S}}_{bg}$  and  $\tilde{\mathbf{S}}(\epsilon_0)$  is made [51, 56, 57]. To restrict this Ansatz to physically meaningful cases the unitarity of  $\tilde{\mathbf{S}}$  is generally required for *all* real energies. In Appendix B it is shown that, in this case, the asymmetry parameter  $q_r$  is real and that  $\tilde{\mathbf{S}}_{bg}$  has only one real free parameter which can be chosen to be  $q_r$ . In our opinion, this requirement is an overconstraint since the aim is a good description of the main part of the transmission peak up to energies of about  $e \approx 1$ . Our pole analysis provides a systematic description of the line shape in this energy range. The resulting

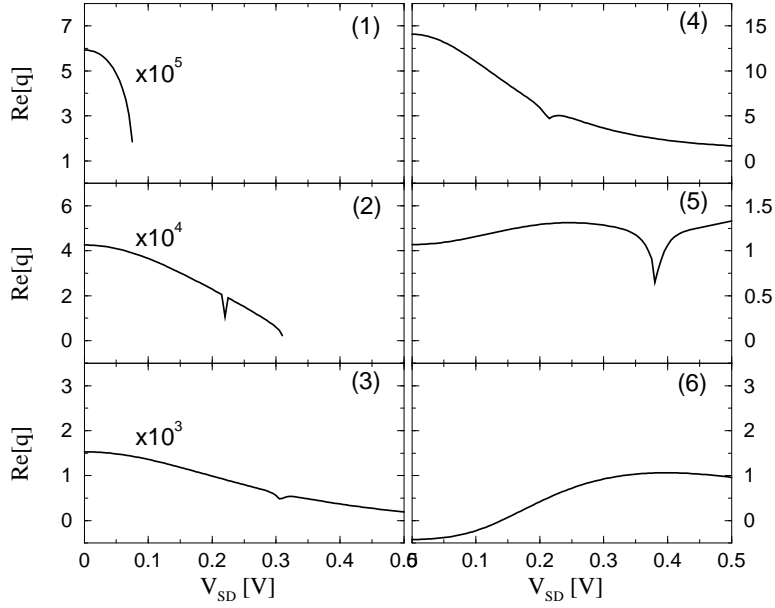


Figure 4.9: Real part of the complex parameter  $q$  vs. applied bias for the first six peaks. Large values of  $\text{Re}(q)$  lead to quasisymmetrical transmission peaks.

expression (4.19) preserves the unitarity of the scattering matrix only in linear order  $e$  (see Appendix B):

$$\tilde{\mathbf{S}}\tilde{\mathbf{S}}^\dagger = \tilde{\mathbf{S}}^\dagger\tilde{\mathbf{S}} \simeq \mathbf{1} + (\delta - \mathbf{1})\frac{e^2}{e^2 + 1}. \quad (4.28)$$

The background matrix  $\tilde{\mathbf{S}}_{bg}$  (Eq. (4.18)) is then characterized by three parameters. They can be chosen as the real- and the imaginary part of the complex asymmetry parameter  $q$ , given by Eq. (4.21), and the imaginary part of the complex asymmetry parameter  $q_R$  (Eq. B.4) describing the line shape of the resonance of the reflection probability. As shown in Fig. (4.10), the matrix elements of  $\delta - \mathbf{1}$  are small in comparison with 1. We expect that our approximation is valid as long as the second term on the right hand side of Eq. (4.28) is small compared to 1. Then, the deviation of  $\tilde{\mathbf{S}}$  from unitarity is small. This way, for each maximum we can estimate the range of validity for our approximation through the requirement  $(\delta - \mathbf{1})_{ij} e^2 / (e^2 + 1) \ll 1$ ,  $i, j = 1, 2$ .

## 4.2.2 Coherent and Noncoherent Contributions

The different contributions to the conductance through a quantum dot (Fig. 3.1) were analyzed thoroughly in Sec. 1.4. To each peak in the curve  $G(V_g)$ , it was assigned a resonance index  $(\nu_0, i_0)$  indicating the resonant channel and the number

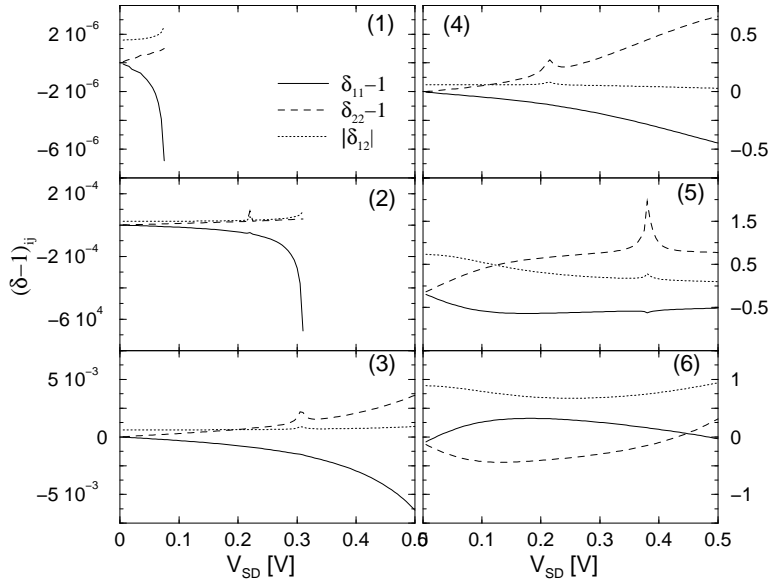


Figure 4.10: The deviation from the unitarity of the  $\tilde{S}$ -matrix given by the approximative expression (4.19):  $\hat{\delta}_{11} - 1$  (solid line),  $\hat{\delta}_{22} - 1$  (dashed line) and  $|\hat{\delta}_{12}|$  (dotted line) as a function of applied bias. The transmission peak order is indicated on each plot.

of the maximum in the transmission curve of the potential  $V(z) + V_g$ . The location of the conductance maximum  $V_g = V_0$  is connected through the relation (Eq. (3.7))

$$\epsilon_{i_0}^{V_0} = E_F - \epsilon_{\perp}^{\nu_0}, \quad (4.29)$$

to the energy of the  $i_0$ -th poles of the scattering matrix for the potential  $V(z) + V_0$ , where  $E_F$  is the Fermi energy and  $\epsilon_{\perp}^{\nu_0}$  the energy of the resonant channel. The coherent contribution to the conductance around this maximum is given by Eq. (3.9) and, for a narrow peak, it has approximately the form of the  $i_0$ -th transmission peak (Eq. (3.10)),

$$G_c(V_g) \simeq \frac{2e^2}{h} T^{V_0}(E_F - \epsilon_{\perp}^{\nu_0} - \delta V) = \frac{2e^2}{h} T^{V_0}(\epsilon_{i_0}^{V_0} - \delta V), \quad (4.30)$$

where  $\delta V = V_g - V_0$ . Inserting Eq. (4.20) into the above equation we obtain the coherent contribution to the conductance in the vicinity of the resonance as a Fano function with the complex asymmetry parameter  $q$  defined by (4.21),

$$G_c(V_g) = G_c^{bg} \frac{[\tilde{e} + \text{Re}(q)]^2 + [\text{Im}(q)]^2}{\tilde{e}^2 + 1}. \quad (4.31)$$

Here  $\tilde{e} = 2(V_g - V_0)/\Gamma$  is a function of the plunger gate potential  $V_g$ , the resonance position  $V_0$  and the resonance width  $\Gamma$  calculated as the imaginary part of the  $i_0$ -th pole of the scattering matrix for the potential  $V(z) + V_0$ . The background coherent contribution is related to the background transmission through

$$G_c^{bg} = \frac{2e^2}{h} T_{bg}. \quad (4.32)$$

The behavior of the dot analyzed here (Eq. (4.31)) shows that an asymmetric line shape arises, in general, when there is a coherent superposition of contributions to the S-matrix coming from different poles. This does not necessarily involve the coupling between two different channels, as in the usual scenario to explain Fano resonances.

After having evaluated the resonant part, we obtain for the total conductance

$$G = G_{n.c.}^{bg} + G_c^{bg} \frac{[\tilde{e} + \text{Re}(q)]^2 + [\text{Im}(q)]^2}{\tilde{e}^2 + 1}. \quad (4.33)$$

Here we assumed a small overlap of the conductance peaks, so that the contribution of the nonresonant channels can be approximated by a constant:

$$G_{n.c.}^{bg} = \frac{2e^2}{h} \sum_{\nu \neq \nu_0}^{\infty} T^{\nu_0}(E_F - \epsilon_{\perp}^{\nu}). \quad (4.34)$$

In our theory all parameters in Eq. (4.33) can be calculated microscopically.

### 4.2.3 Comparison with Experimental Data

Now we solve the inverse problem to extract the transmission through the resonant channel  $\nu_0$  from the experimental conductance data. Here we face the basic problem that the parameters  $q$ ,  $G_c^{bg}$ ,  $V_0$  and  $\Gamma$ , which enter Eq. (4.20), cannot be gained from a fit in a unique way. To see this we rewrite Eq. (4.33) into an equivalent form[54]

$$G = G_{of} + G_0 \frac{[\tilde{e} + q_F]^2}{\tilde{e}^2 + 1}. \quad (4.35)$$

This is a sum of a Fano line with a real asymmetry parameter,

$$q_F = \left[ |q|^2 - 1 + \sqrt{(|q|^2 - 1)^2 + 4(\text{Re}q)^2} \right] / 2\text{Re}q, \quad (4.36)$$

and a constant offset

$$G_{of} = G_{n.c.}^{bg} + G_c^{bg} - G_0, \quad (4.37)$$

where

$$G_0 = G_c^{bg} \frac{\text{Re}q}{q_F}. \quad (4.38)$$



The parameter  $q_F$  is obtained as a solution of a second order equation where we choose the value which leads to a positive  $G_0$ . The other choice for the sign in  $q_F$  yields an equivalent description. According to Eq. (4.35), a fit of the conductance line shape near a resonance can fix only the real parameters  $G_{of}$ ,  $G_0$ ,  $q_F$ ,  $V_0$ , and  $\Gamma$ , which are not enough for a unique separation of the coherent- from the noncoherent part of the conductance. In order to define a bijective mapping of the set of the five fitting parameters onto the six microscopic parameter set,  $G_{n.c.}^{bg}$ ,  $G_c^{bg}$ ,  $\text{Re}(q)$ ,  $\text{Im}(q)$ ,  $V_0$  and  $\Gamma$ , we need an additional variable which we call  $\alpha$ . We observe that the equivalence of the two conductance expressions (4.33) and (4.35) allows the variation of the background components of the conductance only inside a small domain: From Eqs. (4.36) and (4.38) it follows that  $G_c^{bg} \geq G_0$ . Taking into account that  $G_{n.c.}^{bg}$  is per construction positive, it immediately results from Eq. (4.37) that  $G_c^{bg} \leq G_0 + G_{of}$ . Thus, we can define the parameter  $\alpha$  as

$$G_c^{bg} = G_0 + \alpha G_{of} \quad (4.39)$$

where  $\alpha$  varies between zero and one. The complex asymmetry parameter and the noncoherent background component of the conductance can be expressed as a function of  $\alpha$  as well:

$$\text{Re}(q) = q_F \frac{G_0}{G_0 + \alpha G_{of}}, \quad (4.40)$$

$$\text{Im}(q) = \frac{G_{of}}{G_0 + \alpha G_{of}} \sqrt{\alpha^2 + (1 + q_F^2) \alpha \frac{G_0}{G_{of}}} \quad (4.41)$$

and

$$G_{n.c.}^{bg} = (1 - \alpha)G_{of}. \quad (4.42)$$

Using the values  $V_0$  and  $\Gamma$  from fitting and the expressions (4.39 - 4.41), it is very easy to construct the off-diagonal part of the  $S$ -matrix associated with the resonant channel  $\nu_0$  up to a global phase factor. This missing phase factor is expected because the absolute square has been taken in (4.20).

Using the expression (4.33) we have performed an analysis of the experimental conductance data in the Fano regime published by Göres et al [30]. We include a possible constant component due to incoherent transport ( $G_{inc}$  in Ref. [30]) in an effective noncoherent conductance background. In the experimental system the potential in the plane of the two-dimensional electron gas is not known in detail. The two major reasons are, first, the complexity of the geometry of the top gate electrodes. Second, experimentally the potential changes in an unpredictable way if the sample is heated and then cooled down again [30]. These changes are attributed to unknown metastabilities of electrons in the donor layer within the AlGaAs. Without sufficient knowledge of the electron potential it is clear that it is impossible to calculate the conductance exactly. Instead, we assume the correctness of a simple Ansatz for the potential. We then focus on the question of what can be learned

from the experimental peaks about the pole structure of the  $S$ -matrix which describes the resonance theoretically. As an Ansatz for the potential we choose the effectively one-dimensional model presented in Chap. 2 (see Eq. (2.2)). One reason for picking this model is that we can carry out an analytical analysis of the pole structure of the  $S$ -matrix which is independent of the particular shape of  $V(z)$  and  $V(\vec{r}_\perp)$ . Second, we adopt the discussion in Sect. II of Ref. [35] to argue that our model is suitable for the representation of the relevant part of the experimental structure: As shown in Fig. 3 of this reference, the scattering states are formed in the contacts which are widening into the reservoir. With the reservoir we associate the semi-infinite two-dimensional electron gases on the source and on the drain side of the quantum dot presented in Fig. 1 of Ref. [30]. The reservoirs have a low resistivity. With the contacts shown in Fig. 3 of Ref. [35] we associate the constrictions in the experimental samples between two split gates denoted by I in Fig. 1 of Ref. [30]. In our model the contacts have to be identified with the regions which lie between the reservoirs (source and drain) and the barrier in Fig. 3.1. In our simple model we neglect interactions between the one-dimensional channels in the contacts. In reality, this scattering is expected to have a significant impact. It is, however, plausible to assume in this first study that the conductance will have the same form and only the microscopic definitions of the parameters are modified by the new interaction. As a consequence, it is to be expected that under inclusion of channel scattering the asymmetry parameter  $q_F$  can vary in a wider range from zero, for the symmetrical dip of an antiresonance, to infinity, for a Breit-Wigner profile. In the case of decoupled channels we only find large values of  $q_F$  which correspond to maxima in the conductance.

Underlying our method we find for the first antiresonance presented in Fig. 2a of Ref. [30] that the offset conductance is not only generated by the incoherent processes as it is proposed there. Rather, from Eq. (4.39) it follows that the coherent contribution to the background conductance should have a value between  $0.131 e^2/h$  and  $0.210 e^2/h$  while the noncoherent background part  $G_{n.c.}^{bg}$  varies from 0 to  $0.210 e^2/h$ . We conclude that the offset term  $G_{inc}$ , given by Göres et al. [30] in Eq. (3), represents generally a number of different components which can be coherent or noncoherent.

From the experimental conductance data we can also extract the transmission curve  $T(\epsilon)$ , as used in Eq. (3.1) in the vicinity of a resonance, and verify that the energy dependence is given by a Fano function with a complex asymmetry parameter. For the case analyzed in Fig. (4.11) the line shape is a typical antiresonance ( $q_F = -0.06$ ). This demonstrates that the existence of many poles in the  $S$ -matrix leads to an asymmetry of the profile as we have shown in Section III and that the channel coupling increases the asymmetry.

We have provided in this section a systematic treatment of the conductance through a quantum dot embedded in a quantum wire. In our system the potential is decoupled in the transport- and in the lateral direction, which means that the scattering channels are also decoupled. The Fano function with a complex asymme-

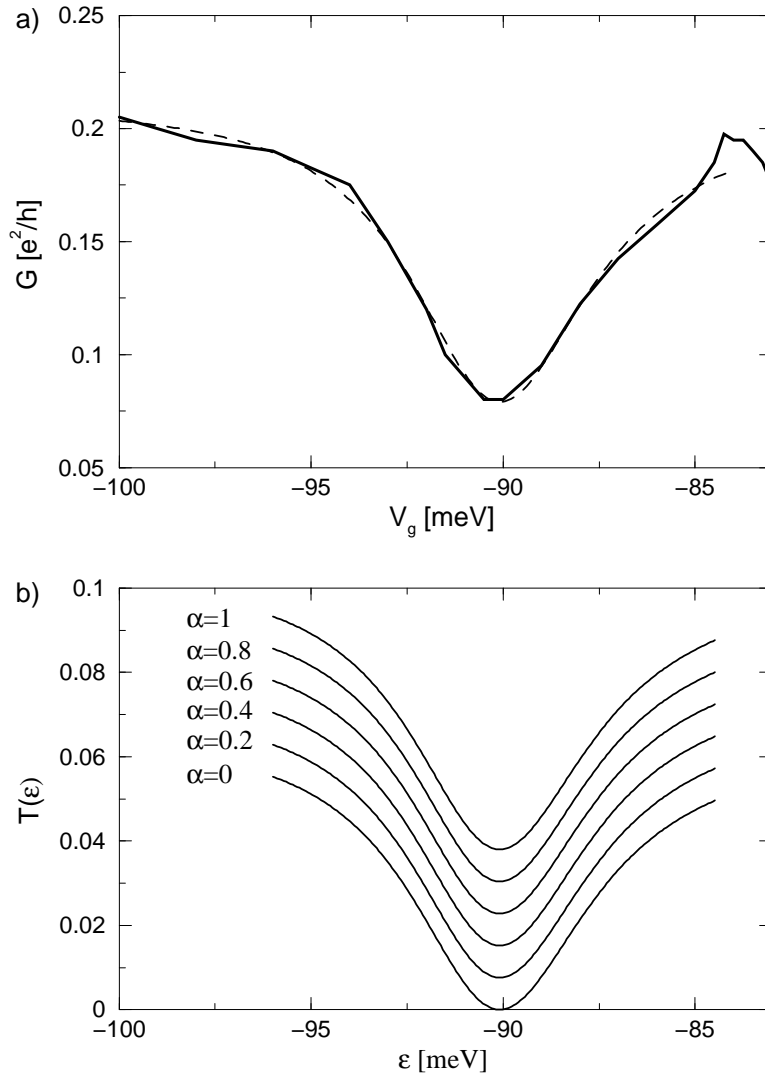


Figure 4.11: a) Conductance as a function of the plunger gate potential  $V_g$ : experimental curve from Ref. [30] (solid line) and theoretical calculation (dashed line) using Eq. (4.35). The parameters of the theoretical curve are:  $V_0 = -90.24$  meV,  $\Gamma = 5.76$  meV,  $q_F = -0.054$ ,  $G_0 = 0.131e^2/h$  and  $G_{of} = 0.079e^2/h$ . b) The transmission through the resonant channel  $\nu_0$  as a function of energy for a few values of  $\alpha$ .

try parameter arises as the most general resonance line shape under the assumption that the background can be considered constant over the width of the resonance. Our model provides microscopic expressions for the line shape parameters and predicts the coherent and noncoherent contributions to the background conductance. Also this method allows the reconstruction of the off-diagonal part in the scattering matrix from the experimental conductance data and shows that other measurements are necessary to determine S-matrix in an unique way.

### 4.3 Capacitance of a Field Induced 2DEG

We analyze further the two dimensional electron gas which is formed (for biases greater than a threshold value) at the interface between the GaAs spacer layer and the blocking barrier of the heterostructure presented in Fig. 2.2. As was shown in Sec. 3.2, for such a system the C-V curve takes the form of a broadened step located between a low voltage,  $V_g < V_-$ , and a high-voltage,  $V_g < V_+$ , plateau (Fig. 3.11). To demonstrate that this step and the subsequent high-voltage plateau are dominated by a single resonance which changes its character from an intermediate resonance (IR) to a quasibound state (QBS), we extend the resonance theory developed for the S matrix to the scattering functions. Inserting the relation (2.52) between R- and  $\tilde{S}$  matrix in the expression (2.60) we obtain

$$\begin{pmatrix} \psi^{(1)}(\epsilon, z) \\ \psi^{(2)}(\epsilon, z) \end{pmatrix} = \frac{i}{\sqrt{2\pi}} \Theta(\epsilon) \mathbf{K}^{1/2}(\epsilon) [\mathbf{1} - \tilde{\mathbf{S}}(\epsilon)] \mathbf{K}^{1/2}(\epsilon) \begin{pmatrix} R(\epsilon; -d, z) \\ R(\epsilon; d, z) \end{pmatrix} \quad (4.43)$$

for every  $|z| \leq d$ . Apparently the expression (4.43) of the scattering function has two types of singularities: poles in the complex energy plane, which are also poles of the  $\tilde{S}$  matrix and real poles of the R matrix for every Wigner Eisenbud energy  $\epsilon = \epsilon_\lambda$ . Following the method presented in Sec. 4.1.1, we perform an exact reformulation of Eq. (4.43) in a vicinity of the Wigner Eisenbud energy  $\epsilon_\lambda$ ,

$$\psi^{(s)}(\epsilon, z) = \frac{Z^{(s)}(\epsilon, z)}{\epsilon - \epsilon_\lambda - \bar{\mathcal{E}}_\lambda(\epsilon)}, \quad (4.44)$$

$s = 1, 2$ , with the regular functions  $\bar{\mathcal{E}}_\lambda(\epsilon)$  given by Eq. (4.6) and

$$\begin{pmatrix} Z^{(1)}(\epsilon, z) \\ Z^{(2)}(\epsilon, z) \end{pmatrix} = \frac{2i\Theta(\epsilon)}{\sqrt{2\pi}} (\epsilon - \epsilon_\lambda) \mathbf{K}^{1/2}(\epsilon) \frac{[\mathbf{1} + i\Omega^-(\epsilon)]}{\mathcal{D}_\lambda(\epsilon)} \mathbf{K}^{1/2}(\epsilon) \begin{pmatrix} R(\epsilon; -d, z) \\ R(\epsilon; +d, z) \end{pmatrix}, \quad (4.45)$$

where  $\Omega^- = \Omega^{-1} \det \Omega$ ,  $\mathcal{D}_\lambda(\epsilon)$  is given by Eq. (4.7) and the matrices  $\Theta$  and  $\mathbf{K}$  by Eqs. (2.26) and (2.37), respectively. As a first advantage, the expression (4.44) allows us to demonstrate that the Wigner Eisenbud energies are no singularities of the scattering functions. Per construction,  $\bar{\mathcal{E}}_\lambda(\epsilon)$  has this property and it is enough

to analyze the numerator function in Eq. (4.44). We split the R function, similarly to the  $\Omega$  matrix, into two parts,

$$R(\epsilon; z, z') = \frac{\beta_\lambda(z, z')}{\epsilon - \epsilon_\lambda} + R_\lambda(\epsilon; z, z'), \quad (4.46)$$

where  $\beta_\lambda(z, z') = (\hbar^2/2m^*)(\pi/2d)\chi_\lambda(z)\chi_\lambda(z')$  according to the definition (2.41), so that we can write Eq. (4.45) in the form

$$\begin{pmatrix} Z^{(1)}(\epsilon, z) \\ Z^{(2)}(\epsilon, z) \end{pmatrix} = \frac{2i\Theta}{\sqrt{2\pi}} \mathbf{K}^{1/2} [\mathbf{1} + i\Omega_\lambda]^{-1} \mathbf{K}^{1/2} \left[ (\epsilon - \epsilon_\lambda) \begin{pmatrix} R_\lambda(\epsilon; -d, z) \\ R_\lambda(\epsilon; +d, z) \end{pmatrix} + \begin{pmatrix} \beta_\lambda(-d, z) \\ \beta_\lambda(+d, z) \end{pmatrix} \right] - \frac{2\Theta}{\sqrt{2\pi}} \frac{\mathbf{K}^{1/2} \boldsymbol{\omega}_\lambda^- \mathbf{K}^{1/2}}{\mathcal{D}_\lambda(\epsilon)} \begin{pmatrix} R_\lambda(\epsilon; -d, z) \\ R_\lambda(\epsilon; +d, z) \end{pmatrix}. \quad (4.47)$$

which does not contain  $1/(\epsilon - \epsilon_\lambda)$  any more;  $(\boldsymbol{\omega}_\lambda^-)_{11} = (\boldsymbol{\omega}_\lambda)_{22}$ ,  $(\boldsymbol{\omega}_\lambda^-)_{22} = (\boldsymbol{\omega}_\lambda)_{11}$  and  $(\boldsymbol{\omega}_\lambda^-)_{12} = (\boldsymbol{\omega}_\lambda^-)_{21} = (\boldsymbol{\omega}_\lambda)_{12}$ . Therefore, Eqs. (4.8) and (4.44) show that the scattering functions  $\psi^{(s)}(\epsilon, z)$ ,  $s = 1, 2$ , and the scattering matrix  $S$  have the same poles  $\bar{\epsilon}_{0\lambda} = \epsilon_{0\lambda} - i\Gamma_\lambda/2$  in the complex energy plane which satisfy Eq. (4.11). According to the general theory [43, 8] we associate these poles with resonances; the real part of the pole gives the resonant energy and the imaginary part the width of the resonance.

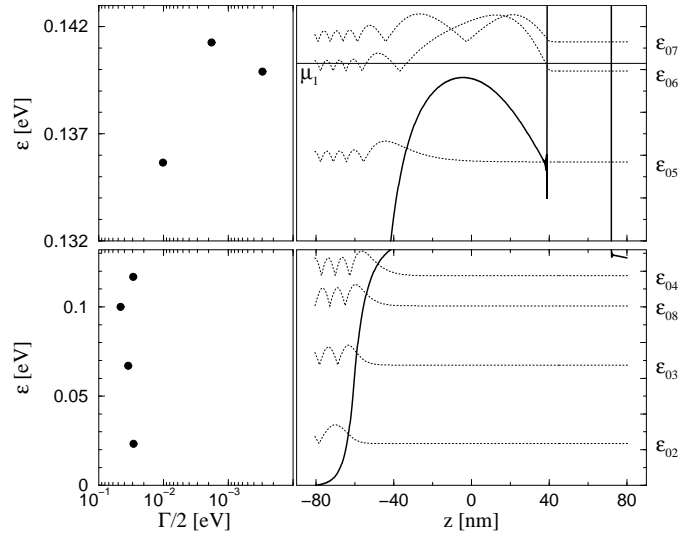


Figure 4.12: Left: Position of the resonance poles in the complex energy plane determined by Eq. (4.11). Right: Potential energy  $V(z)$  (solid line) for  $V_g = 0.016V$  and the probability distribution density,  $P_\epsilon(z) = |\psi^{(1)}(\epsilon, z)|^2$ , at the resonance energies (dotted line). The upper plots present in detail an energy domain around  $\mu_1$ .

For the scattering potential of the biased structure given in Fig. 2.2, we present in Fig. 4.12 the poles with the real part in the energy domain of the occupied states

and the probability distribution density at the resonance energies corresponding to these poles. The figure shows that there are two types of poles; the first one is associated to the scattering states of the electrons confined in the region close to the back contact and whose charge distribution varies very slowly with the applied bias [14, 41]. So these resonances do not play any role in the capacitance variation with  $V_g$ . The second type of poles, which have a smaller imaginary part, corresponds to the states of the electrons localized at the interface between the GaAs spacer layer and the blocking barrier. As discussed in Sec. 3.2, the charge accumulated there varies strongly with  $V_g$  and, consequently, the changes of the capacitance can be directly connected to the resonances of the second type. In our case there is a single pole with the resonance energy below the chemical potential  $\mu_1$  and for which the probability distribution density at the resonance energy has a maximum in the region of the potential quantum well, at the interface between the GaAs spacer and the blocking barrier. The imaginary part of this pole is smaller than that of the other poles and smaller than the gap between two adjacent resonance energies. So we can conclude that the charge accumulation in the field induced quantum well of the MIS type semiconductor structure given in Fig. 2.2 is characterized only by a narrow and quasi-isolated resonance; for simplicity we denote the complex energy of the corresponding pole by  $\bar{\epsilon}_0 = \epsilon_0 - i\Gamma/2$ . Therefore, in a vicinity of  $\bar{\epsilon}_0$  the functions  $Z^{(s)}(\epsilon, z)$  and  $\bar{\mathcal{E}}_\lambda(\epsilon)$  can be linearized and we obtain for the wave functions at a fixed  $z$  a Fano distribution

$$\psi^{(s)}(\epsilon, z) \simeq i\psi^{(s)}(\epsilon_0, z) \frac{\frac{1}{q^{(1)}(z)}e + 1}{e + i} \quad (4.48)$$

with a complex asymmetry parameter

$$\frac{1}{q^{(1)}(z)} = \frac{\Gamma/2}{Z^{(s)}(\epsilon_0, z)} \left. \frac{d}{d\epsilon} Z^{(s)}(\epsilon, z) \right|_{\epsilon=\epsilon_0}, \quad (4.49)$$

where  $e = 2(\epsilon - \epsilon_0)/\Gamma$ . The probability distribution density in the Fano approximation,

$$P_\epsilon(z) \simeq P_{\epsilon_0}(z) \frac{\left| \frac{1}{q^{(1)}(z)}e + 1 \right|^2}{e^2 + 1}, \quad (4.50)$$

yields a very accurate approximation for the numerically found maxima shown in Figs. 3.9 b.) and c.): for demonstration we plot in the middle part of Fig. 4.13 the energy of the maximum of the function  $P_\epsilon(z_{\max})$  given by Eq. (4.50),

$$\epsilon_{\max}^F = \epsilon_0 + \Gamma \frac{1 - |q^{(1)}(z_{\max})|^2 + \sqrt{(1 - |q^{(1)}(z_{\max})|^2)^2 + 4[\text{Re}(q^{(1)}(z_{\max}))]^2}}{4\text{Re}(q^{(1)}(z_{\max}))} \quad (4.51)$$

and the energies

$$\epsilon_{\pm}^F = \epsilon_0 + \Gamma \frac{2\text{Re}(q^{(1)}(z_{\max})) \pm \sqrt{[\text{Re}(q^{(1)}(z_{\max}))/e_{\max} + 1]^2 - 2[\text{Im}(q^{(1)}(z_{\max}))]^2}}{2[\text{Re}(q^{(1)}(z_{\max}))/e_{\max} - 1]} \quad (4.52)$$

at which the considered Fano function takes half the maximum value at constant  $z = z_{\max}$ ;  $e_{\max} = 2(\epsilon_{\max}^F - \epsilon_0)/\Gamma$  and as defined in Sec. 3.2  $z_{\max}$  is the position of the maximum of  $P_{\epsilon}(z)$ . There is an excellent agreement between  $\epsilon_{\max}^F$ ,  $\epsilon_{\pm}^F$  and its counterparts  $\epsilon_{\max}$ ,  $\epsilon_{\pm}$ , which results from the inspection of the complete numerical scattering functions (Eq. (4.48)). This agreement demonstrates that the wave functions, which are important for the step in the capacitance curve, are derived from a single resonance. For small applied biases ( $V_- < V_g < V_+$ ) this resonance has

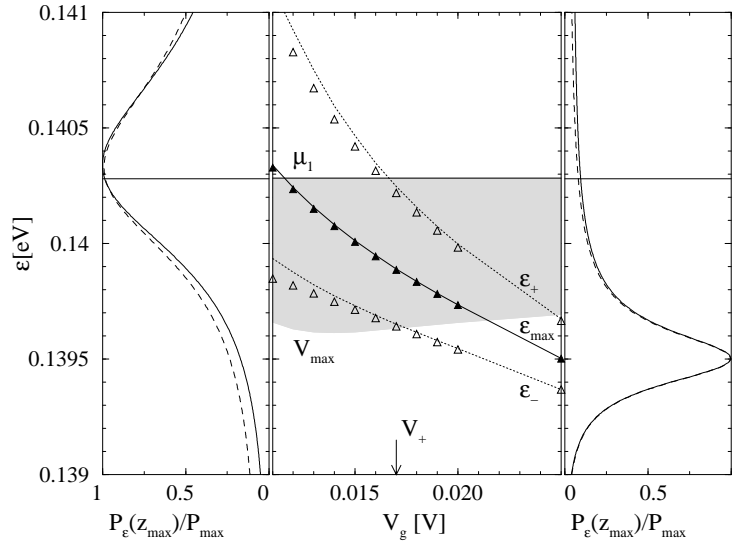


Figure 4.13: Left part: Probability distribution density at  $z = z_{\max}$ , normalized at its maximum value,  $P_{\epsilon}(z_{\max})/P_{\max}$  around the resonance energy  $\epsilon_0$ : numerical calculation (solid line) and Fano approximation (dashed line). Left part:  $V_g = 0.011$  V; Right part:  $V_g = 0.025$  V. Middle part: As the result of the complete numerical calculation the energy  $\epsilon_{\max}$  of the maximum of  $P_{\epsilon}(z)$  (solid line), and the energies  $\epsilon_{\pm}$  at which  $P_{\epsilon}$  takes half the maximum value at constant  $z = z_{\max}$  (dotted lines). The corresponding values  $\epsilon_{\max}^F$  (filled triangle) and  $\epsilon_{\pm}^F$  (triangle) in the Fano approximation. Shaded area: energies with  $\mu_1 > \epsilon > V_{\max}$ .

the character of an intermediate resonance [14]: i) its energy lies in the classically allowed range (Fig. 4.13, middle part) and, therefore, is a Fabry-Perot type resonance; ii) it is located in the space between the contact and the region where an isolated 2DEG is formed at large values of  $V_g$  (Figs. 3.9 b.) and 3.10 b.); iii) its

shape is strongly asymmetric (Fig. 4.13, left part). With increasing  $V_g$  the intermediate resonance turns into a quasibound state which, in contrast to the intermediate resonance, is connected to the back contact only via the tunneling effect. The resonance line of  $P_\epsilon(z)$  narrows and tends to become symmetric (Fig. 4.13, right part). To demonstrate the continuous transformation of the intermediate resonance to a quasibound state by decreasing the coupling strength between the back contact and the accumulation layer, i.e. increasing  $V_g$ , we plot in the upper part of Fig. 4.14 the imaginary part of the poles closest to the real axis in dependence on the gate voltage. It is clearly seen that the step in the capacitance corresponds to a domain

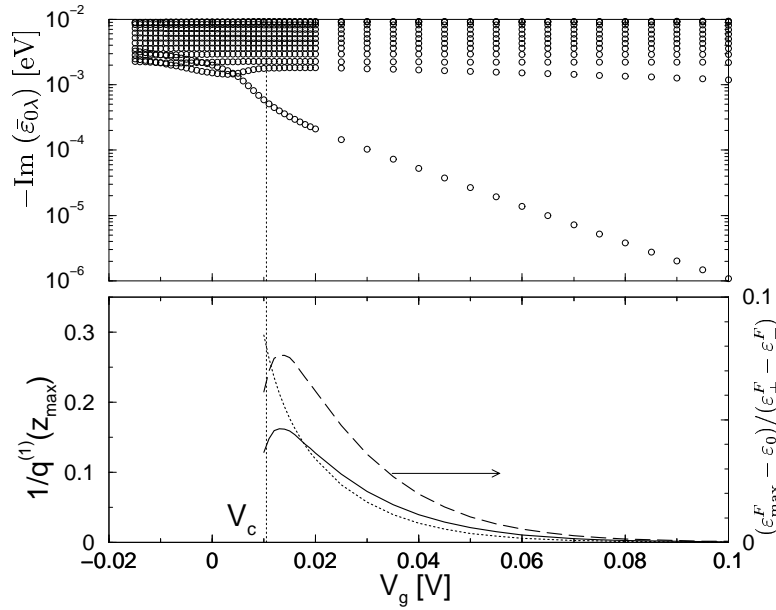


Figure 4.14: Upper part: The imaginary part of  $\bar{\epsilon}_0$  vs. gate voltage  $V_g$ . Lower part: Real part (solid line) and imaginary part (dotted line) of the complex asymmetry parameter  $1/q^{(1)}(z_{\max})$  and the deviation of the maximum of the Fano distribution from the pole energy (dashed line) at gate voltages for which the Fano approximation of the wave functions is valid. The dotted vertical line indicates the center of the step in the C-V characteristic,  $V_c = 0.0105$  V.

of the gate voltages where a single pole becomes separated from all other and the width of this resonant poles decreases very strongly and continuously with the applied bias. To characterize quantitatively this resonance we plot in Fig. 4.14 the real and the imaginary part of the asymmetry parameter  $1/q^{(1)}$ . For gate voltages in the step region, in the case of the intermediate resonance, both quantities are large and we find from Eq. (4.50) that there is a strong asymmetry in center of the resonance, i. e. for  $e \leq 1$ . Furthermore, the strong asymmetry in the line shape causes a distinct separation of  $\epsilon_0$  and  $\epsilon_{\max}$ . With increasing voltage the asymme-



try decreases to become negligible in the high-voltage plateau when the quasibound state is formed. From Eq. (4.50) we obtain a standard Breit-Wigner distribution for the probability distribution density with the symmetry center given by  $\epsilon_0$ . Since  $\Gamma$  decreases rapidly with increasing voltage the Breit-Wigner distribution turns into a  $\delta$ -function expected for an isolated two-dimensional electron gas.

## 4.4 Summary

We develop an analytical theory of the quasi-isolated transport resonances and identify the signature of these resonances in the conductance and capacitance measurements performed on semiconductor heterostructures.

Our starting point is a noninteracting model for the effectively one dimensional transport through semiconductor nanostructures. We use the S-matrix description of coherent transport in which a Fano resonance is obtained from a pole of the S-matrix in the complex energy plane of the standard form Eq. (4.19). The advantage of our model is that, dissimilar to other approaches [8, 51, 56, 57], it is possible to derive explicit expressions for the S-matrix in Eq. (4.19) starting from the Schrödinger equation. In contrast to the situation in Refs. [45, 46, 47, 48, 49], there is only one (conserved) channel per contact for a given energy so that the usual picture to explain asymmetric lines, which invokes coupling between two different channels, does not apply. Nevertheless, we obtain Fano profiles in our model.

In Sec. 4.2 we analyze the conductance of a quantum dot embedded in a quantum wire. We demonstrate that to each conductance peak a resonant channel can be associated which provides the resonant part of the conductance. The other channels yield a noncoherent contribution which for narrow resonances can be approximated as a constant. The contribution of the resonant channel is described by a Fano profiles with a complex asymmetry parameter. The coherent background component  $\tilde{\mathbf{S}}_{bg}$  of the S-matrix, which is necessary for an asymmetric line shape (Eq. (4.19)), is the natural consequence of the existence of other poles of the S-matrix in the complex energy plane which are different from the resonant pole. The imaginary part of the asymmetry parameter results from the following consideration: We obtain Eq. (4.19) for the S-matrix by a linearization of the S-matrix around the conductance maximum. Our description of the resonances, therefore, is correct in the center of the resonances i. e. for  $e \leq 1$ . This is sufficient since, if there is an overlap of the experimental resonances like in [30], a single pole approximation of the matrix as in (4.19) cannot be expected to be valid outside the center of the resonances. Therefore, in contrast to the standard approach which requires unitarity of  $\tilde{\mathbf{S}}$  in the whole energy range (even where Eq. (4.19) cannot be expected to hold anymore), our linearization yields unitarity of the S-matrix only in linear order of  $e$ . Therefore,  $\tilde{\mathbf{S}}_{bg}$  does not have to be a unitary matrix and we gain one more free parameter for the line shape. We demonstrate that this parameter consists of the imaginary part of the asymmetry parameter. From numerical calculation we conclude that a complex

asymmetry parameter is a general finding even for extremely narrow and strongly isolated resonances. We discuss our results in the context of the experiments from Ref. [30]. Since the contacts in the experiments are two-dimensional, there is the possibility of channel interaction which is not considered in our model. Nevertheless, we expect that the basic structure of our results carries over to the experimental geometry. It is then demonstrated that within certain limits, it is possible to reconstruct from the experimental data the off-diagonal part of the  $S$ -matrix, as given in Eq. (4.19) up to a natural global phase.

In Sec. 4.3 we demonstrate that the scattering functions and the scattering matrix have the same poles in the complex energy plane. This finding allows for obtaining Fano lines with a complex asymmetry parameter for the probability distribution density,  $P_\epsilon(z) = |\psi^{(1)}(\epsilon, z)|^2$ , at a given space coordinate  $z$ . Based on the resonance theory generalized for the scattering functions we discuss the measured step in the C-V characteristic of a MIS type semiconductor heterostructure. Contrary to the well-known statistical limit, we find that the formation of a field induced two dimensional electron gas (2DEG) in the considered system is dominated by only one relevant resonance and there is no channel mixing. Since for the open system the coupling between contact and the accumulation layer in front of the blocking barrier is strong, this resonance has the character of an intermediate resonance; It is a new type of resonance, with distinct characteristics: i) it is localized in the space between the probe and the isolated quantum system, ii) its energy lies in the classically allowed regime, and iii) its line shape is strongly asymmetric. At the transition from the open to nearly closed system the intermediate resonance develops into the quasibound state known for an isolated 2DEG. Excellent quantitative agreement shows that this transition is seen in capacitance experiments.

# Chapter 5

## Optical Phonons in Uniaxial Slabs

The electron-optical phonon interaction plays a dominant role in determining the various electronic properties of the quasi-two dimensional electronic systems of polar crystals. Since the work of Lucas et al [59] and continuing with studies of Wang and Mahan [60], Evans and Mills [61], Licari and Evrard [62], Wendler [63], Mori and Ando [64], Chen et al [65], Hai et al [66], Pokatilov et al [67] and others, this problem has stirred up a large interest, justified in the last period by the works of Lee et al [68] and Weinan and Huang [69]. With the development of modern growth techniques [6, 70], it has become possible to grow not only very thin layers but also perfect epitaxial structures containing semiconductor layers with unequal lattice constants. Such structures contain layers with elastically strained crystal lattice and the strain will affect both the properties of the electrons and holes [17, 71] and the properties of the phonons [72], allowing the fabrication of devices with enhanced performances. The high-speed modulation-doped field effect transistor and the low-threshold quantum well laser are two examples which benefited from the technique used to exploit the effects of the built-in strain distribution on the electronic properties of semiconductor devices.

Our main purpose is to discuss both the spectra of optical phonons and their interaction with a conduction electron in strained semiconductor heterostructures. But to achieve this goal we have to overcome difficulties, mainly determined by the anisotropic features of the pseudomorphic semiconductor layer of the heterostructure, layer which, in certain conditions, is uniaxially deformed. Thus, in order to elucidate the role of the uniaxial anisotropy on the spectra of optical phonons and the electron-phonon interaction, we shall first discuss a much simpler system, namely a uniaxial semiconductor slab. We use the dielectric continuum model of Born and Huang [15] with electrostatic boundary conditions. Investigation of the normal modes have been carried out excluding the retardation of the Coulomb interaction. This method was presented in detail in Refs. [72, 73, 74].

A slab is a system of finite thickness oriented normal to the  $z$  axis and extending to infinity in the  $x$  and  $y$  directions. Because of the translational symmetry in directions parallel to the plane of the slab, one assumes normal modes in which the

ionic displacement amplitudes are wavelike in these directions. The problem is then to determine both how the frequencies  $\omega$  of these normal modes depend on the two-dimensional wave vector  $\vec{k}$  in the plane of the slab and how the ionic displacements amplitudes vary in the direction perpendicular to the slab for each normal mode.

The normal modes of the slab can be classified as either confined modes or surface modes. According to Jones and Fuchs [75] we define the confined modes as normal modes for which the variation of the ionic displacement amplitudes in the direction perpendicular to the slab is wavelike in character (given by a sine or a cosine function of  $z$ ). Surface modes are ones in which the ionic displacement amplitudes decrease with increasing distance into the slab from the surface, i.e. they are localized at the surfaces. Both confined and surface modes can be also characterized as acoustical or optical and as transverse or longitudinal depending upon the direction of the ionic displacements at  $\vec{k} = 0$ .

We consider an anisotropic uniaxial slab lying between  $\pm l/2$  with the faces normal to  $z$  axis and with the optical axis directed along the normal to the slab; as usual, the slab extends to infinity in the  $x$  and  $y$  directions. The geometry of the system is given in Fig. 5.1.

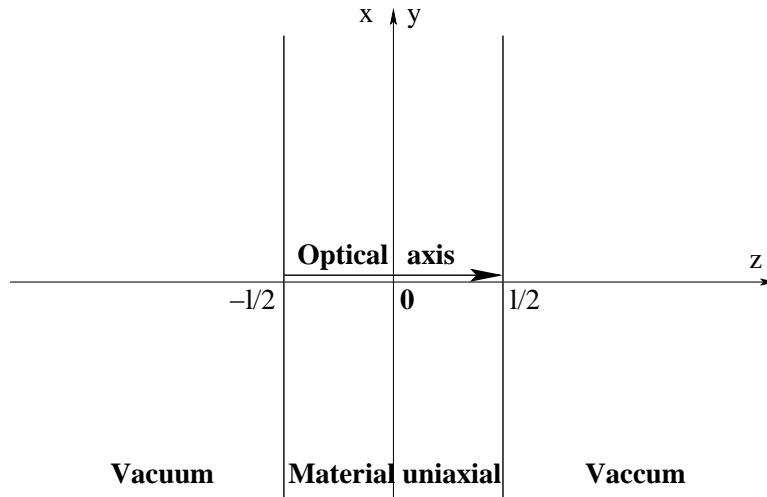


Figure 5.1: Geometry relevant to the discussion of the dielectric slab.

## 5.1 Equations of Motion

For the sake of simplicity, the generalization being easy to perform, we shall suppose the slab to be composed of an ionic crystal or a polar semiconductor having one pair of ions per primitive cell and surrounded by vacuum.

The optical phonon modes of the uniaxial slab will be calculated in the frame of the dielectric continuum model [62, 75, 76]. The optical modes will be found in the long-wave approximation; the displacement of the positive and negative ions are slowly varying functions of position, and it is meaningful to introduce a macroscopic polarization,  $\vec{\mathcal{P}}(\vec{r}, t)$ , and an average electric field,  $\vec{\mathcal{E}}(\vec{r}, t)$ . In the absence of free charges, the only two contributions to the total charge density are the bulk and the surface polarization charges so that, in the electrostatic approximation

$$\vec{\mathcal{E}}(\vec{r}, t) = -\nabla\phi(\vec{r}, t), \quad (5.1)$$

and the equation for the scalar potential [63, 77] is

$$\phi(\vec{r}, t) = \frac{1}{4\pi\epsilon_0} \sum_{i=x,y,z} \int d\vec{r}' \frac{\partial}{\partial r_i} \frac{1}{|\vec{r} - \vec{r}'|} \vec{\mathcal{P}}_i(\vec{r}', t), \quad (5.2)$$

where  $\epsilon_0$  is the dielectric permittivity of the vacuum.

In order to avoid the difficulty of obtaining an equivalent of the Lorentz relation between the local field and the macroscopic electric field, for the anisotropic case we are referring directly to the equations of the Born-Huang model. Denoting the optical phonon field by the vectors  $\vec{\mathcal{U}}(\vec{r}, t)$  the equations of the model are [78]

$$\begin{aligned} \ddot{\mathcal{U}}_i(\vec{r}, t) &= \beta_{11,i} \mathcal{U}_i(\vec{r}, t) + \beta_{12,i} \mathcal{E}_i(\vec{r}, t) \\ \mathcal{P}_i(\vec{r}, t) &= \beta_{12,i} \mathcal{U}_i(\vec{r}, t) + \beta_{22,i} \mathcal{E}_i(\vec{r}, t) \end{aligned} \quad (5.3)$$

where  $i = x, y, z$ . Taking into account the axial symmetry of the system, we introduce the symbols  $\parallel$  and  $\perp$  corresponding to a direction that is either parallel or orthogonal to the optical axis, respectively. The coefficients  $\beta$  which appear in Eqs. (5.3), in fact elements of some diagonal matrices [78], have the expressions

$$\beta_{11,i} = \begin{cases} -\omega_{TO,\perp}^2, & i = x, y \\ -\omega_{TO,\parallel}^2, & i = z \end{cases} \quad (5.4)$$

$$\beta_{12,i} = \begin{cases} \omega_{TO,\perp} [\epsilon_0 (\epsilon_{\perp}(0) - \epsilon_{\perp}(\infty))]^{1/2}, & i = x, y \\ \omega_{TO,\parallel} [\epsilon_0 (\epsilon_{\parallel}(0) - \epsilon_{\parallel}(\infty))]^{1/2}, & i = z \end{cases} \quad (5.5)$$

$$\beta_{22,i} = \begin{cases} \epsilon_0 [\epsilon_{\perp}(\infty) - 1], & i = x, y \\ \epsilon_0 [\epsilon_{\parallel}(\infty) - 1], & i = z \end{cases} \quad (5.6)$$

where  $\omega_{TO,\alpha}$ , are the frequencies of the transverse phonon modes on the principal directions,  $\alpha = \parallel, \perp$ , and  $\epsilon_{\alpha}(0)$  and  $\epsilon_{\alpha}(\infty)$  are the low and high frequencies dielectric constants, respectively, along the same directions.

Assuming a sinusoidal dependence on time for the fields,

$$\begin{aligned} \vec{\mathcal{E}}(\vec{r}, t) &= \vec{E}(\vec{r})e^{-i\omega t}, \\ \vec{\mathcal{P}}(\vec{r}, t) &= \vec{P}(\vec{r})e^{-i\omega t}, \\ \vec{\mathcal{U}}(\vec{r}, t) &= \vec{u}(\vec{r})e^{-i\omega t}, \end{aligned} \quad (5.7)$$

where  $\omega$  is the normal frequency of vibration, we obtain from the first equation of the system (5.3) the relation between the macroscopic electric field and the vector which describes the ions displacement,

$$E_i(\vec{r}) = \frac{\omega_{TO,i}^2 - \omega^2}{\beta_{12,i}} u_i(\vec{r}), \quad i = x, y, z. \quad (5.8)$$

Taking into account the definition relation of the electrical polarization,

$$P_i(\vec{r}) = \epsilon_0 \chi_i(\omega) E_i(\vec{r}), \quad i = x, y, z, \quad (5.9)$$

where  $\chi_i(\omega)$  is the dielectric susceptibility,

$$\chi_i(\omega) = \begin{cases} \epsilon_{\perp}(\omega) - 1, & i = x, y \\ \epsilon_{\parallel}(\omega) - 1, & i = z \end{cases}, \quad (5.10)$$

the second equation of the system (5.3) yields the components of the dielectric tensor

$$\epsilon_{\alpha}(\omega) = \epsilon_{\alpha}(\infty) \frac{\omega_{LO,\alpha}^2 - \omega^2}{\omega_{TO,\alpha}^2 - \omega^2}. \quad (5.11)$$

The frequencies of the longitudinal phonon modes on the principal directions,  $\omega_{LO,\alpha}$  ( $\alpha = \parallel, \perp$ ), verify the well-known relation Lyddane-Sachs-Teller:

$$\omega_{LO,\alpha}^2 = \omega_{TO,\alpha}^2 \frac{\epsilon_{\alpha}(0)}{\epsilon_{\alpha}(\infty)}. \quad (5.12)$$

Inserting the relations deduced from Eqs. (5.3) and the expression (5.2) of the scalar potential in Eq. (5.1) we obtain an integral equation for the components of the phonon field:

$$\frac{\omega_{TO,i}^2 - \omega^2}{\beta_{12,i}} u_i(\vec{r}) = \sum_{j=x,y,z} \chi_j(\omega) \frac{\omega_{TO,j}^2 - \omega^2}{\beta_{12,j}} \int d\vec{r}' \Gamma_{ij}(\vec{r} - \vec{r}') u_j(\vec{r}') \quad (5.13)$$

with

$$\Gamma_{ij}(\vec{r} - \vec{r}') = \frac{1}{4\pi} \frac{\partial^2}{\partial r_i \partial r_j} \left( \frac{1}{|\vec{r} - \vec{r}'|} \right), \quad i = x, y, z. \quad (5.14)$$

The translational symmetry of the system in the directions parallel to the plane of the slab allows for the definition of a 2D wave vector  $\vec{k}$ . To write the integral on the right side of Eq. (5.13) in a more transparent form, one can introduce the two dimensional Fourier transform [62]

$$\vec{u}(\vec{r}) = \sum_{\vec{k}} \frac{e^{i\vec{k}\vec{r}_{\perp}}}{\sqrt{A}} \vec{u}(\vec{k}, z), \quad (5.15)$$

where  $A$  is the area of the slab surface and  $\vec{r}_\perp$  is the component of  $\vec{r}$  in the plane of the slab,

$$\vec{r}_\perp = x\vec{e}_x + y\vec{e}_y. \quad (5.16)$$

$\{\vec{e}_x, \vec{e}_y, \vec{e}_z\}$  is the Cartesian basis corresponding to the coordinate system given in Fig. 5.1. Using also the Fourier transform [62] of the kernel

$$\frac{1}{4\pi|\vec{r} - \vec{r}'|} = \frac{1}{2A} \sum_{\vec{k}} e^{i\vec{k}(\vec{r}_\perp - \vec{r}'_\perp)} \frac{e^{-k|z-z'|}}{k}, \quad (5.17)$$

the integral equations (5.13) are written into a more convenient form

$$\begin{aligned} g_\perp(\omega)u_x(\vec{k}, z, \omega) &= -\frac{k_x}{2} \int_{-l/2}^{l/2} dz' e^{-k|z-z'|} \left\{ \chi_\perp(\omega)g_\perp(\omega) \left[ u_x(\vec{k}, z', \omega) \frac{k_x}{k} + u_y(\vec{k}, z', \omega) \frac{k_y}{k} \right] \right. \\ &\quad \left. + i \operatorname{sgn}(z-z') \chi_\parallel(\omega)g_\parallel(\omega)u_z(\vec{k}, z', \omega) \right\}, \\ g_\perp(\omega)u_y(\vec{k}, z, \omega) &= -\frac{k_y}{2} \int_{-l/2}^{l/2} dz' e^{-k|z-z'|} \left\{ \chi_\perp(\omega)g_\perp(\omega) \left[ u_x(\vec{k}, z', \omega) \frac{k_x}{k} + u_y(\vec{k}, z', \omega) \frac{k_y}{k} \right] \right. \\ &\quad \left. + i \operatorname{sgn}(z-z') \chi_\parallel(\omega)g_\parallel(\omega)u_z(\vec{k}, z', \omega) \right\}, \\ \epsilon_\parallel(\omega)g_\parallel(\omega)u_z(\vec{k}, z, \omega) &= -\frac{k}{2} \int_{-l/2}^{l/2} dz' e^{-k|z-z'|} \left\{ i \operatorname{sgn}(z-z') \chi_\perp(\omega)g_\perp(\omega) \left[ u_x(\vec{k}, z', \omega) \frac{k_x}{k} \right. \right. \\ &\quad \left. \left. + u_y(\vec{k}, z', \omega) \frac{k_y}{k} \right] - \chi_\parallel(\omega)g_\parallel(\omega)u_z(\vec{k}, z', \omega) \right\}, \end{aligned} \quad (5.18)$$

where

$$g_\alpha(\omega) = \frac{\omega_{TO,\alpha}^2 - \omega^2}{\beta_{12,\alpha}}, \quad \alpha = \perp, \parallel \quad (5.19)$$

and

$$\operatorname{sgn}(z-z') = \begin{cases} 1, & z > z' \\ -1, & z < z' \end{cases}. \quad (5.20)$$

According to L. Wendler [63] we introduce the Cartesian basis

$$\begin{aligned} \vec{e}_\perp &= \frac{k_x}{k} \vec{e}_x + \frac{k_y}{k} \vec{e}_y, \\ \vec{e}_s &= \frac{k_y}{k} \vec{e}_x - \frac{k_x}{k} \vec{e}_y, \\ \vec{e}_\parallel &= \vec{e}_z \end{aligned} \quad (5.21)$$

and the components of the phonon field with respect to the new basis satisfy the integral equations:

$$\begin{aligned}
g_{\perp}(\omega)u_s(\vec{k}, z, \omega) &= 0 \\
g_{\perp}(\omega)u_{\perp}(\vec{k}, z, \omega) &= -\frac{k}{2} \int_{-l/2}^{l/2} dz' e^{-k|z-z'|} \left[ \chi_{\perp}(\omega)g_{\perp}(\omega)u_{\perp}(\vec{k}, z', \omega) \right. \\
&\quad \left. + i \operatorname{sgn}(z-z')\chi_{\parallel}(\omega)g_{\parallel}(\omega)u_{\parallel}(\vec{k}, z', \omega) \right] \\
\epsilon_{\parallel}(\omega)g_{\parallel}(\omega)u_{\parallel}(\vec{k}, z, \omega) &= -\frac{k}{2} \int_{-l/2}^{l/2} dz' e^{-k|z-z'|} \left[ i \operatorname{sgn}(z-z')\chi_{\perp}(\omega)g_{\perp}(\omega)u_{\perp}(\vec{k}, z', \omega) \right. \\
&\quad \left. - \chi_{\parallel}(\omega)g_{\parallel}(\omega)u_{\parallel}(\vec{k}, z', \omega) \right]
\end{aligned} \tag{5.22}$$

The new basis (5.21) allows for the separation of the phonon field into a  $s$ -polarized part,  $u_s$ , and a  $p$ -polarized part,  $u_p = u_{\perp}\vec{e}_{\perp} + u_{\parallel}\vec{e}_{\parallel}$ , which are completely decoupled. Using the linear dependence between  $P_i$  and  $u_i$ ,  $i = x, y, z$ , (Eqs. (5.8) and (5.9)), it is easy to write Eqs. (5.22) in terms of the  $s$ - and  $p$ -polarized components of  $\vec{P}(\vec{k}, z)$ , having thus a generalization of the integral equations obtained for the isotropic case by Wendler [63]. Due to the form of the Hamiltonian density, however, in the following, we shall prefer to work with the components of the phonon field, in a manner similar to that developed in Ref. [64] for isotropic systems.

## 5.2 Normal Modes

The normal modes are obtained as particular solutions of Eqs. (5.22).

### 5.2.1 $s$ -Polarized Phonon Modes

The first equation of the system (5.22), which is not coupled to the others, can be solved immediately. The eigenvalues are

$$\omega_j = \omega_{TO,\perp}, \tag{5.23}$$

and  $u_s(\vec{k}, z, \omega_j)$  are arbitrary function of  $z$ . Since the  $s$  component of the phonon field does not produce polarization charges on the surfaces, the finite slab behaves as if it were an infinite medium. They are purely transverse and degenerate modes and their eigenfrequency is associated with the infrared resonance of the crystal. In addition these modes have no coupling with the conduction electrons.

### 5.2.2 $p$ -Polarized Phonon Modes

For these normal modes  $\omega \neq \omega_{TO,\perp}$  and the component  $u_s(\vec{k}, z)$  of the phonon field should be zero. The other two components,  $u_{\perp}$  and  $u_{\parallel}$ , are obtained as solutions of



the two coupled integral equations of the system (5.22) using the method developed by Fuchs and Kliewer [76]. With the notations

$$K(z, z') = ke^{-k|z-z'|}, \quad (5.24)$$

$$K_A(z, z') = -k \operatorname{sgn}(z - z')e^{-k|z-z'|}, \quad (5.25)$$

the system (5.22) becomes

$$\begin{aligned} g_{\perp}(\omega)u_{\perp}(\vec{k}, z, \omega) &= -\frac{1}{2}\chi_{\perp}(\omega)g_{\perp}(\omega)\int_{-l/2}^{l/2} dz' K(z, z')u_{\perp}(\vec{k}, z', \omega) \\ &\quad + \frac{i}{2}\chi_{\parallel}(\omega)g_{\parallel}(\omega)\int_{-l/2}^{l/2} dz' K_A(z, z')u_{\parallel}(\vec{k}, z', \omega), \\ \epsilon_{\parallel}(\omega)g_{\parallel}(\omega)u_{\parallel}(\vec{k}, z, \omega) &= \frac{i}{2}\chi_{\perp}(\omega)g_{\perp}(\omega)\int_{-l/2}^{l/2} dz' K_A(z, z')u_{\perp}(\vec{k}, z', \omega) \\ &\quad + \frac{1}{2}\chi_{\parallel}(\omega)g_{\parallel}(\omega)\int_{-l/2}^{l/2} dz' K(z, z')u_{\parallel}(\vec{k}, z', \omega). \end{aligned} \quad (5.26)$$

Using the relation between the phonon field and the polarization field (Eqs. (5.8) and (5.9)), we find that the system (5.26) is equivalent with the following eigenvalue problem:

$$\sum_{\beta=\perp, \parallel} \eta_{\alpha\beta}(\omega)P_{\beta}(\vec{k}, z, \omega) = \sum_{\beta=\perp, \parallel} \int_{-l/2}^{l/2} dz' \mathbf{M}_{\alpha\beta}(z, z')P_{\beta}(\vec{k}, z', \omega) \quad (5.27)$$

where

$$\eta_{\alpha\beta}(\omega) = \begin{cases} \chi_{\perp}^{-1}(\omega), & \alpha = \beta = \perp \\ 1 + \chi_{\parallel}^{-1}(\omega), & \alpha = \beta = \parallel \\ 0, & \alpha \neq \beta \end{cases} \quad (5.28)$$

and the kernel

$$\mathbf{M}(z, z') = \frac{1}{2} \begin{pmatrix} -K(z, z') & iK_A(z, z') \\ iK_A(z, z') & K(z, z') \end{pmatrix} \quad (5.29)$$

is a Hermitian one,

$$\mathbf{M}_{\alpha\beta}^{\dagger}(z, z') = \mathbf{M}_{\beta\alpha}^*(z', z) = \mathbf{M}_{\alpha\beta}(z, z'). \quad (5.30)$$

The system (5.27) is a generalization of the equations given by Wendler [63] for the isotropic case.

Based on the Hermitian property of the kernel  $\mathbf{M}(z, z')$  we obtain from the relation (5.27) written for two values of the frequencies,  $\omega_i$  and  $\omega_j$ , the equations verified by the components of the polarization field,

$$\int_{-l/2}^{l/2} dz \sum_{\alpha, \beta=\perp, \parallel} [\eta_{\alpha\beta}(\omega_i) - \eta_{\alpha\beta}(\omega_j)] P_{\alpha}^*(\vec{k}, z, \omega_j) P_{\beta}(\vec{k}, z, \omega_i) = 0. \quad (5.31)$$

Replacing in Eq. (5.31) the polarization by its expression given by Eqs. (5.8) and (5.9), it follows the orthogonality relation for the components of the phonon field

$$(\omega_j^2 - \omega_i^2) \int_{-l/2}^{l/2} dz \sum_{\alpha, \beta=\perp, \parallel} u_\alpha^*(\vec{k}, z, \omega_j) u_\beta(\vec{k}, z, \omega_i) = 0. \quad (5.32)$$

In contrast to the phonon field eigenvectors, the polarization eigenvectors do not satisfy an orthogonality relation (Eq. (5.31)) and, therefore, do not form a basis as in the isotropic case [63]. We need an orthogonal and complete system of functions in order to write the Hamiltonian in the second quantization and it is more convenient in the anisotropic case to solve the eigenvalue problem of the phonon field.

Further, the Fredholm-type integral equations (5.26) are transformed into a system of differential equations using the following properties of the kernels  $K(z, z')$  and  $K_A(z, z')$  [62]:

$$\frac{d}{dz} \int_{-l/2}^{l/2} dz' K(z, z') f(z') = k \int_{-l/2}^{l/2} dz' K_A(z, z') f(z'), \quad (5.33)$$

$$\frac{d}{dz} \int_{-l/2}^{l/2} dz' K_A(z, z') f(z') = k \int_{-l/2}^{l/2} dz' K(z, z') f(z') - 2k f(z), \quad (5.34)$$

valid for all  $f$  defined on the interval  $[-l/2, l/2]$ . If Eqs. (5.26) are differentiated once with respect to  $z$ , it follows

$$\begin{aligned} g_\perp(\omega) \frac{d}{dz} u_\perp(\vec{k}, z, \omega) &= ik g_\parallel(\omega) u_\parallel(\vec{k}, z, \omega), \\ \epsilon_\parallel(\omega) g_\parallel(\omega) \frac{d}{dz} u_\parallel(\vec{k}, z, \omega) &= -ik \epsilon_\perp(\infty) g_\perp(\omega) u_\perp(\vec{k}, z, \omega). \end{aligned} \quad (5.35)$$

It is easy to see that, strictly in this anisotropic case,  $\omega_{LO, \perp}$ ,  $\omega_{LO, \parallel}$ ,  $\omega_{TO, \perp}$ ,  $\omega_{TO, \parallel}$  are not eigenfrequencies of the  $p$ -polarized phonon field. If we suppose that  $\omega_{LO, \perp}$  is an eigenfrequencies and impose the condition to have nonzero solutions for  $u_\perp$  and  $u_\parallel$ , then  $\omega_{LO, \perp} = \omega_{LO, \parallel}$  and this corresponds to an isotropic system. We can analogously demonstrate that  $\omega_{TO, \perp}$  is an eigenfrequency if and only if  $\omega_{TO, \perp} = \omega_{TO, \parallel}$ . Differentiating once the first equation in (5.35), the system (5.35) can be written in the equivalent form

$$\frac{d^2}{dz^2} u_\perp(\vec{k}, z, \omega) = k^2 \frac{\epsilon_\perp(\omega)}{\epsilon_\parallel(\omega)} u_\perp(\vec{k}, z, \omega), \quad (5.36)$$

$$u_\parallel(\vec{k}, z, \omega) = -\frac{i}{k} \frac{g_\perp(\omega)}{g_\parallel(\omega)} \frac{d}{dz} u_\perp(\vec{k}, z, \omega). \quad (5.37)$$

Eq. (5.36) shows that, depending on the sign of the ratio

$$r(\omega) = \frac{\epsilon_\perp(\omega)}{\epsilon_\parallel(\omega)} \quad (5.38)$$

the phonon modes can be classified as surface modes for  $r(\omega) > 0$  and confined modes for  $r(\omega) < 0$ . Thus, we find the same mode types as for isotropic slabs [62].

**Surface phonon (SO) modes**

In the case  $r(\omega) > 0$  the solution of Eqs. (5.36) and (5.37) are of the form

$$\begin{aligned} u_{\perp}(\vec{k}, z, \omega) &= Ae^{\gamma(\omega)kz} + Be^{-\gamma(\omega)kz}, \\ u_{\parallel}(\vec{k}, z, \omega) &= -i\gamma(\omega)\frac{g_{\perp}(\omega)}{g_{\parallel}(\omega)} \left[ Ae^{\gamma(\omega)kz} - Be^{-\gamma(\omega)kz} \right], \end{aligned} \quad (5.39)$$

where

$$\gamma(\omega) = [r(\omega)]^{1/2}. \quad (5.40)$$

Requiring that the functions defined by Eqs. (5.39) also satisfy the system (5.22) we obtain the dispersion law for the surface phonon modes,

$$e^{\gamma(\omega)kl} = p \frac{\epsilon_{\parallel}(\omega)\gamma(\omega) - 1}{\epsilon_{\parallel}(\omega)\gamma(\omega) + 1}, \quad p = \pm \quad (5.41)$$

and the relation between the constants  $A$  and  $B$

$$B = A \frac{\epsilon_{\parallel}(\omega)\gamma(\omega) - 1}{\epsilon_{\parallel}(\omega)\gamma(\omega) + 1} e^{-\gamma(\omega)kl}. \quad (5.42)$$

Inserting the dispersion law in Eq. (5.42) we find

$$\begin{aligned} A &= B & \text{for } p = + \\ A &= -B & \text{for } p = - \end{aligned} \quad (5.43)$$

By definition  $\gamma(\omega)$  (Eq. (5.40)) is a positive quantity and consequently  $e^{\gamma(\omega)kl} > 1$ . Requiring that the term on the right-hand side of Eq. (5.41) has values greater than 1, two types of surface phonon modes are obtained corresponding to the inequalities

$$\begin{aligned} \epsilon_{\parallel}(\omega)\gamma(\omega) &< -1 & \text{for } p = + \\ -1 < \epsilon_{\parallel}(\omega)\gamma(\omega) &< 0 & \text{for } p = -. \end{aligned} \quad (5.44)$$

For here follows the condition

$$\epsilon_{\parallel}(\omega) < 0 \quad (5.45)$$

which should be satisfied for both types of modes. So, the frequencies of the surface modes denoted by  $\omega_{0,p}(k)$  are the solutions of the equation

$$\cosh[\gamma(\omega)kl] = p \frac{\epsilon_{\perp}(\omega)\epsilon_{\parallel}(\omega) + 1}{\epsilon_{\perp}(\omega)\epsilon_{\parallel}(\omega) - 1} \quad (5.46)$$

(equivalent to Eq. (5.41)) verifying for the two values of the parity index  $p$  the conditions:

$$\begin{aligned} \epsilon_{\parallel}(\omega)\epsilon_{\perp}(\omega) &> 1 & \text{for } p = + \\ 0 < \epsilon_{\parallel}(\omega)\epsilon_{\perp}(\omega) &< 1 & \text{for } p = -. \end{aligned} \quad (5.47)$$

Eigenvalues	Eigenvectors $\vec{u}^{(0,p)}(\vec{k}, z) = (u_{\perp}^{(0,p)}(\vec{k}, z), u_{\parallel}^{(0,p)}(\vec{k}, z))$
$\omega_{0,+}$	$\vec{u}^{(0,+)}(\vec{k}, z) = C_{0,+} \left( -i \frac{\cosh[\gamma(\omega_{0,+})kz]}{g_{\perp}(\omega_{0,+})}, -\gamma(\omega_{0,+}) \frac{\sinh[\gamma(\omega_{0,+})kz]}{g_{\parallel}(\omega_{0,+})} \right)$
$\omega_{0,-}$	$\vec{u}^{(0,-)}(\vec{k}, z) = C_{0,-} \left( -i \frac{\sinh[\gamma(\omega_{0,-})kz]}{g_{\perp}(\omega_{0,-})}, -\gamma(\omega_{0,-}) \frac{\cosh[\gamma(\omega_{0,-})kz]}{g_{\parallel}(\omega_{0,-})} \right)$

Table 5.1: Phonon field eigenvalues and eigenvectors associated with the surface optical phonon modes for a uniaxial slab with the optical axis directed along the normal to the surface.

The eigenvectors corresponding to the eigenvalues  $\omega_{0,p}(k)$ ,  $p = \pm$ , are given in Table 5.1 and the normalization constants  $C_{0,p}$ ,  $p = \pm$ , have the expressions

$$\begin{aligned}
C_{0,p} &= \left\{ \frac{\epsilon_0 l}{4\omega_{0,p}} \left[ p \left( \frac{d\epsilon_{\perp}}{d\omega} - \gamma^2(\omega) \frac{d\epsilon_{\parallel}}{d\omega} \right) + \frac{\sinh[\gamma(\omega)kl]}{\gamma(\omega)kl} \left( \frac{d\epsilon_{\perp}}{d\omega} + \gamma^2(\omega) \frac{d\epsilon_{\parallel}}{d\omega} \right) \right] \Big|_{\omega=\omega_{0,p}} \right\}^{-1/2} \\
&= \left\{ \frac{l}{2} \left[ p \left( \frac{1}{g_{\perp}^2(\omega)} - \frac{\gamma^2(\omega)}{g_{\parallel}^2(\omega)} \right) + \frac{\sinh[\gamma(\omega)kl]}{\gamma(\omega)kl} \left( \frac{1}{g_{\perp}^2(\omega)} + \frac{\gamma^2(\omega)}{g_{\parallel}^2(\omega)} \right) \right] \Big|_{\omega=\omega_{0,p}} \right\}^{-1/2}.
\end{aligned} \tag{5.48}$$

These eigenvectors satisfy the orthogonality relation

$$\sum_{\alpha=\perp,\parallel} \int_{-l/2}^{l/2} dz \left( u_{\alpha}^{(0,p)}(\vec{k}, z) \right)^* u_{\alpha}^{(0,p')}(\vec{k}, z) = \delta_{pp'}. \tag{5.49}$$

According to Licari and Evrard [62] the parity index  $p = \pm$  is related to the symmetry of the component  $u_{\perp}^{(0,p)}$  of the phonon field. This choice will be justified by the form of the electron-phonon interaction Hamiltonian.

As in the isotropic case we can define a polarization charge density associated to the optical phonon modes,

$$\sigma_{0,p}(\vec{r}) \Big|_{z=\pm \frac{l}{2}} = P_{\parallel}^{0,p}(\vec{r}) \Big|_{z=\pm \frac{l}{2}}, \tag{5.50}$$

where  $P_{\parallel}$  is the component of the polarization field in the direction normal to the slab surface.

### Confined phonon modes in the uniaxial slab

In the case  $r(\omega) < 0$  the solutions of Eqs. (5.36) and (5.37) are of the form

$$\begin{aligned}
u_{\perp}(\vec{k}, z, \omega) &= A e^{i\gamma(\omega)kz} + B e^{-i\gamma(\omega)kz} \\
u_{\parallel}(\vec{k}, z, \omega) &= \gamma(\omega) \frac{g_{\perp}(\omega)}{g_{\parallel}(\omega)} \left[ A e^{i\gamma(\omega)kz} - B e^{-i\gamma(\omega)kz} \right]
\end{aligned} \tag{5.51}$$

where  $\gamma(\omega)$  is defined here as

$$\gamma(\omega) = |r(\omega)|^{1/2}. \quad (5.52)$$

The components of the phonon field given by Eqs. (5.51) are eigenfunctions if and only if they satisfy the system (5.22). This condition yields the dispersion law of the confined modes

$$e^{i\gamma(\omega)kl} = p \frac{i\gamma(\omega)\epsilon(\omega) - 1}{i\gamma(\omega)\epsilon(\omega) + 1}, \quad p = \pm \quad (5.53)$$

and the relation between the constants  $A$  and  $B$ ,

$$B = A \frac{i\gamma(\omega)\epsilon_{\parallel}(\omega) - 1}{i\gamma(\omega)\epsilon_{\parallel}(\omega) + 1} e^{-i\gamma(\omega)kl}. \quad (5.54)$$

Using Eq. (5.53) the above relation becomes

$$\begin{aligned} A &= B & \text{for } p &= + \\ A &= -B & \text{for } p &= - \end{aligned} \quad (5.55)$$

The dispersion law (5.53) is equivalent to the relations

$$\cos[\gamma(\omega)kl] = p \frac{\epsilon_{\parallel}(\omega)\epsilon_{\perp}(\omega) + 1}{\epsilon_{\parallel}(\omega)\epsilon_{\perp}(\omega) - 1}, \quad (5.56)$$

$$\sin[\gamma(\omega)kl] = -p \frac{2\gamma(\omega)\epsilon_{\parallel}(\omega)}{\epsilon_{\parallel}(\omega)\epsilon_{\perp}(\omega) - 1}. \quad (5.57)$$

Irrespective of the frequencies  $\omega_{TO,\perp}$ ,  $\omega_{TO,\parallel}$ ,  $\omega_{LO,\perp}$ ,  $\omega_{LO,\parallel}$  there are always two domains in which  $\gamma(\omega)$  takes values from 0 to  $\infty$  and the ratio  $r(\omega)$  is negative. For each of these two frequency intervals we introduce a branch index  $\mu$  which takes the values

$$\begin{aligned} \mu &= 1 & \text{for } \epsilon_{\parallel}(\omega) &> 0, \\ \mu &= 2 & \text{for } \epsilon_{\parallel}(\omega) &< 0. \end{aligned} \quad (5.58)$$

In Fig. 5.2 we present the dependence of  $\gamma$  on the frequency  $\omega$  for a material with  $\omega_{TO,\perp} < \omega_{LO,\perp} < \omega_{TO,\parallel} < \omega_{LO,\parallel}$ .

Further we solve the equations (5.56) and (5.57) on each frequency interval labelled with  $\mu$ . The function

$$f(\omega) = p \frac{\epsilon_{\parallel}(\omega)\epsilon_{\perp}(\omega) + 1}{\epsilon_{\parallel}(\omega)\epsilon_{\perp}(\omega) - 1} = F_{\mu}(\gamma(\omega)) \quad (5.59)$$

has the property  $-1 < f(\omega) < 1$  for all values of  $\omega$  with  $r(\omega) < 0$ . If  $\mu$  is fixed, then there exist a bijective mapping of  $\omega$  onto  $\gamma(\omega)$  and Eq. (5.56) can be regarded as an equation for  $\gamma$ ,

$$\cos[\gamma kl] = F_{\mu}(\gamma), \quad (5.60)$$

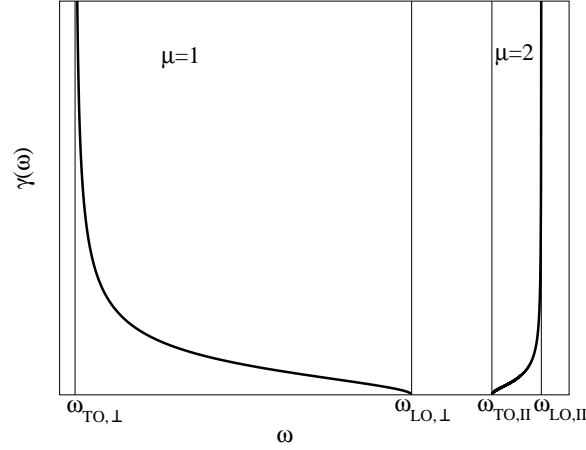


Figure 5.2:  $\gamma$  vs. frequency on the intervals for which  $r(\omega) < 0$  and for a material with  $\omega_{TO,\perp} < \omega_{LO,\perp} < \omega_{TO,\parallel} < \omega_{LO,\parallel}$ .

with  $\gamma \in (0, \infty)$ ,  $\mu = 1, 2$ . Because  $F_\mu(\gamma)$  has per construction values between  $-1$  and  $+1$ , Eq. (5.60) has an infinite number of solutions, two solutions for each interval  $\left(\frac{2(m-1)\pi}{kl}, \frac{2m\pi}{kl}\right)$ ,  $m = 1, 2, 3, \dots$ . However, eigenfrequencies are only the solutions which also satisfy Eq. (5.57). On the frequencies intervals of the confined modes  $r(\omega) < 0$  and from Eq. (5.57) follows that  $\sin[\gamma(\omega)kl]$  and  $p\epsilon_\parallel(\omega)$  have the same sign. Thus, we can write for each value of the branch index  $\mu$  and of the parity index  $p$  the conditions:

$$\begin{aligned} \sin[\gamma(\omega)kl] > 0 & \quad \text{for} \quad \begin{cases} \mu = 1, & p = + \\ \mu = 2, & p = - \end{cases}, \\ \sin[\gamma(\omega)kl] < 0 & \quad \text{for} \quad \begin{cases} \mu = 1, & p = - \\ \mu = 2, & p = + \end{cases}. \end{aligned} \quad (5.61)$$

Fig. 5.3 shows a graphic method to find the eigenfrequencies of the confined phonon modes solving Eq. (5.60).

We put together all the above conditions and the dispersion law will be written in a compact form. In the case  $r(\omega) < 0$ , i.e. in the domains of the confined modes, the eigenfrequencies  $\omega_{m,\mu,p}$  are the solutions of the equation

$$\cos[\gamma(\omega)kl] = p \frac{\epsilon_\parallel(\omega)\epsilon_\perp(\omega) + 1}{\epsilon_\parallel(\omega)\epsilon_\perp(\omega) - 1} \quad (5.62)$$

which satisfy the condition

$$kl\gamma(\omega) \in ((m-1)\pi, m\pi) \quad (5.63)$$

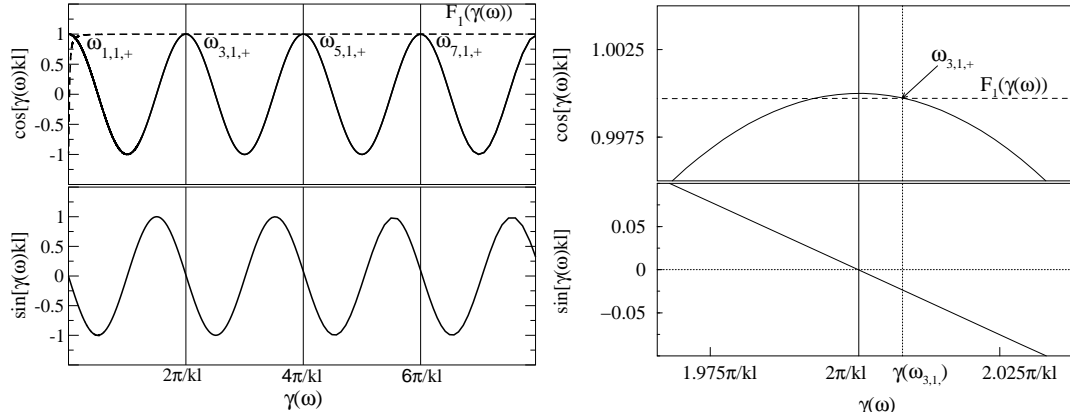


Figure 5.3: Left side: Graphic method to find the eigenfrequencies of the modes with the parity  $p = +$  and the branch index  $\mu = 1$ . Characteristic frequencies of the slab material satisfy the inequalities  $\omega_{TO,\perp} < \omega_{LO,\perp} < \omega_{TO,\parallel} < \omega_{LO,\parallel}$ . Right side: Detail around  $\gamma(\omega) = 2\pi/kl$ . From the two crossing points of the curves  $\cos[\gamma(\omega)kl]$  and  $F_\mu(\gamma(\omega))$  only that with  $\sin[\gamma(\omega)kl] < 0$  can be associated with an eigenfrequency.

and the labels  $(m, \mu, p)$  are assigned according to the following rule

$$p = + \quad \begin{cases} m = 1, 3, 5, \dots; & \mu = 1 \\ m = 2, 4, 6, \dots; & \mu = 2 \end{cases} \quad (5.64)$$

$$p = - \quad \begin{cases} m = 2, 4, 6, \dots; & \mu = 1 \\ m = 1, 3, 5, \dots; & \mu = 2 \end{cases} \quad (5.65)$$

In contrast to the case of an isotropic slab where the confined modes are degenerate and have the frequencies of the bulk optical phonons,  $\omega_{TO}$  and  $\omega_{LO}$  [62], for the uniaxial slab the anisotropy lifts the degeneracy; the eigenfrequencies are distributed in the two intervals indexed by  $\mu = 1, 2$ .

The eigenvectors corresponding to the eigenvalues  $\omega_{m,\mu,p}$  are periodical functions of  $z$  inside the slab and their expressions are given in Table 5.2. The normalization constants  $C_{m,\mu,p}$ ,  $m = 1, 2, 3, \dots$ ,  $\mu = 1, 2$ ,  $p = \pm$ , are given as

$$\begin{aligned} C_{m,\mu,p} &= \sqrt{\frac{2}{l}} \left\{ \frac{\epsilon_0 k^2 l^2}{4\omega_{m,\mu,p}} \left[ \frac{d\epsilon_\perp}{d\omega} + \gamma^2(\omega) \frac{d\epsilon_\parallel}{d\omega} + p \frac{\sin[\gamma(\omega)kl]}{\gamma(\omega)kl} \left( \frac{d\epsilon_\perp}{d\omega} - \gamma^2(\omega) \frac{d\epsilon_\parallel}{d\omega} \right) \right] \Big|_{\omega=\omega_{m,\mu,p}} \right\}^{-1/2} \\ &= \sqrt{\frac{2}{l}} \left\{ \left[ \frac{k^2 l^2}{g_\perp^2(\omega)} + \gamma^2(\omega) \frac{k^2 l^2}{g_\parallel^2(\omega)} + p \frac{\sin[\gamma(\omega)kl]}{\gamma(\omega)kl} \left( \frac{k^2 l^2}{g_\perp^2(\omega)} - \gamma^2(\omega) \frac{k^2 l^2}{g_\parallel^2(\omega)} \right) \right] \Big|_{\omega=\omega_{m,\mu,p}} \right\}^{-1/2}. \end{aligned} \quad (5.66)$$

The values of the normalization constant (Eqs. (5.48) and (5.66)) for both types of optical phonon modes depend strongly on the slab thickness  $l$ .

Eigenvalues	Eigenvectors $\vec{u}^{(m,\mu,p)}(\vec{k}, z) = \left( u_{\perp}^{(m,\mu,p)}(\vec{k}, z), u_{\parallel}^{(m,\mu,p)}(\vec{k}, z) \right)$
$\omega_{m,\mu,+}$	$\vec{u}^{(m,\mu,+)}(\vec{k}, z) = C_{m,\mu,+} \left( -ikl \frac{\cos[\gamma(\omega_{m,\mu,+})kz]}{g_{\perp}(\omega_{m,\mu,+})}, kl\gamma(\omega_{m,\mu,+}) \frac{\sin[\gamma(\omega_{m,\mu,+})kz]}{g_{\parallel}(\omega_{m,\mu,+})} \right)$
$\omega_{m,\mu,-}$	$\vec{u}^{(m,\mu,-)}(\vec{k}, z) = C_{m,\mu,-} \left( -ikl \frac{\sin[\gamma(\omega_{m,\mu,-})kz]}{g_{\perp}(\omega_{m,\mu,-})}, -kl\gamma(\omega_{m,\mu,-}) \frac{\cos[\gamma(\omega_{m,\mu,-})kz]}{g_{\parallel}(\omega_{m,\mu,-})} \right)$

Table 5.2: Phonon field eigenvalues and eigenvectors corresponding to optical phonon modes confined in the uniaxial slab with the optical axis directed along the normal to the surface.

The eigenvectors associated with the confined modes satisfy the orthogonality condition:

$$\sum_{\alpha=\perp,\parallel} \int_{-l/2}^{l/2} dz \left( u_{\alpha}^{(m,\mu,p)}(\vec{k}, z) \right)^* u_{\alpha}^{(m',\mu',p')}(\vec{k}, z) = \delta_{mm'} \delta_{\mu\mu'} \delta_{pp'}. \quad (5.67)$$

For each optical phonon mode confined in the slab and labelled with  $(m, \mu, p)$ ,  $m = 1, 2, 3, \dots$ ,  $\mu = 1, 2$ ,  $p = \pm$ , we can define two polarization charge densities, a surface one

$$\sigma_{m,\mu,p}(\vec{r}) \Big|_{z=\pm\frac{l}{2}} = P_{\parallel}^{m,\mu,p}(\vec{r}) \Big|_{z=\pm\frac{l}{2}} \quad (5.68)$$

and a volume one

$$\rho_{m,\mu,p}(\vec{r}) = \nabla \cdot \vec{P}^{(m,\mu,p)}(\vec{r}). \quad (5.69)$$

This charge acts as a source for the fields associated with the confined modes.

The eigenvectors of the  $p$ -polarized phonon field, i.e. those which correspond to the surface and confined modes of the slab, are orthogonal (Eqs. (5.49) and (5.67)) and verify the closure relation

$$\begin{aligned} & \sum_{p=\pm} \left( u_{\alpha}^{(0,p)}(\vec{k}, z) \right)^* u_{\beta}^{(0,p)}(\vec{k}, z') \\ & + \sum_{m=1,2,3,\dots} \sum_{\mu=1,2} \sum_{p=\pm} \left( u_{\alpha}^{(m,\mu,p)}(\vec{k}, z) \right)^* u_{\beta}^{(m,\mu,p)}(\vec{k}, z') = \delta_{\alpha\beta} \delta(z - z'). \end{aligned} \quad (5.70)$$

### 5.3 Hamiltonian of the Optical Phonon Field

In the absence of free charges, the Hamiltonian density of the optical phonon field, in this anisotropic uniaxial case, has the form given in Ref. [79]:

$$H_{ph} = \frac{1}{2} \sum_{\alpha=\perp,\parallel} \left[ \Pi_{\alpha}^2(\vec{r}) + \omega_{TO,\alpha}^2 u_{\alpha}^2(\vec{r}) - \beta_{12,\alpha} E_{\alpha}(\vec{r}) u_{\alpha}(\vec{r}) \right] \quad (5.71)$$

where  $\vec{\Pi}(\vec{r})$  is the momentum density canonically conjugate to the phonon field. We disregard the contribution of the s-polarized phonon modes because they are purely transverse and do not interact with the conduction electrons.



Further, we expand the operators which appear in the Hamiltonian expression (5.71) in terms of the eigenvectors of the  $p$ -polarized phonon field:

$$\vec{u}(\vec{r}) = \sum_{\vec{k}} \frac{e^{i\vec{k}\vec{r}_\perp}}{\sqrt{A}} \sum_{\nu} B_{\nu}(\vec{k}) \vec{u}^{(\nu)}(\vec{k}, z) [a_{\nu}(\vec{k}) + a_{\nu}^{\dagger}(-\vec{k})], \quad (5.72)$$

$$\vec{\Pi}(\vec{r}) = \sum_{\vec{k}} \frac{e^{i\vec{k}\vec{r}_\perp}}{\sqrt{A}} \sum_{\nu} A_{\nu}(\vec{k}) \vec{u}^{(\nu)}(\vec{k}, z) [a_{\nu}(\vec{k}) - a_{\nu}^{\dagger}(-\vec{k})], \quad (5.73)$$

where  $\nu$  represents the index set  $(m, \mu, p)$ ,  $m = 1, 2, 3, \dots$ ,  $\mu = 1, 2$ ;  $p = \pm$  for the confined modes and  $(0, p)$ ,  $p = \pm$  for the surface modes and  $\vec{r}_\perp$  is the component of  $\vec{r}$  in the plane parallel to the surface of the slab.  $a_{\nu}(\vec{k})$  and  $a_{\nu}^{\dagger}(\vec{k})$  are the creation and annihilation operators, respectively, and satisfy the bosonic-type commutation relations:

$$\begin{aligned} [a_{\nu}(\vec{k}), a_{\nu'}(\vec{k}')] &= 0, \\ [a_{\nu}^{\dagger}(\vec{k}), a_{\nu'}^{\dagger}(\vec{k}')] &= 0, \\ [a_{\nu}(\vec{k}), a_{\nu'}^{\dagger}(\vec{k}')] &= \delta_{\nu\nu'} \delta_{\vec{k}\vec{k}'}. \end{aligned} \quad (5.74)$$

Using the relation (5.8) between  $\vec{E}(\vec{r})$  and  $\vec{u}(\vec{r})$ , we express also the macroscopic electric field in terms of creation and annihilation operators for the phonon modes:

$$\vec{E}(\vec{r}) = \sum_{\vec{k}} \frac{e^{i\vec{k}\vec{r}_\perp}}{\sqrt{A}} \sum_{\nu} B_{\nu}(\vec{k}) [a_{\nu}(\vec{k}) + a_{\nu}^{\dagger}(-\vec{k})] \sum_{\alpha=\perp, \parallel} \frac{\omega_{TO, \alpha}^2 - \omega_{\nu}^2}{\beta_{12, \alpha}} u_{\alpha}^{(\nu)}(\vec{k}, z) \vec{e}_{\alpha}(\vec{k}), \quad (5.75)$$

where  $\vec{e}_{\perp}(\vec{k})$  and  $\vec{e}_{\parallel}(\vec{k})$  are defined by the relations (5.21).

The phonon field and the canonically conjugate momentum density are dynamical variables which correspond to observables and the associated operators  $\vec{u}(\vec{r})$  and  $\vec{\Pi}(\vec{r})$  should be Hermitian. From this condition follows the conditions which should be satisfied by the expansion coefficients  $A_{\nu}(\vec{k})$  and  $B_{\nu}(\vec{k})$ ,

$$B_{\nu}^*(-\vec{k}) \left( u_{\alpha}^{(\nu)}(-\vec{k}, z) \right)^* [\vec{e}_{\alpha}(-\vec{k})]_i = B_{\nu}(\vec{k}) u_{\alpha}^{(\nu)}(\vec{k}, z) [\vec{e}_{\alpha}(\vec{k})]_i \quad (5.76)$$

$$-A_{\nu}^*(-\vec{k}) \left( u_{\alpha}^{(\nu)}(-\vec{k}, z) \right)^* [\vec{e}_{\alpha}(-\vec{k})]_i = A_{\nu}(\vec{k}) u_{\alpha}^{(\nu)}(\vec{k}, z) [\vec{e}_{\alpha}(\vec{k})]_i \quad (5.77)$$

for  $\alpha = \perp, \parallel$  and  $i = x, y, z$ . Using the expressions of the phonon field eigenvectors given in Tables 5.1 and 5.2 and the definition relations (5.21) of the basis vectors  $\vec{e}_{\perp}(\vec{k})$  and  $\vec{e}_{\parallel}(\vec{k})$  we find

$$B_{\nu}^*(-\vec{k}) = B_{\nu}(\vec{k}), \quad (5.78)$$

$$A_{\nu}^*(-\vec{k}) = -A_{\nu}(\vec{k}). \quad (5.79)$$

The operators  $\vec{u}(\vec{r})$  and  $\vec{\Pi}(\vec{r})$  satisfy the commutation relation

$$[u_i(\vec{x}), \Pi_j(\vec{x}')] = i\hbar\delta_{ij}\delta(\vec{x} - \vec{x}') \quad (5.80)$$

which yields

$$A_\nu(\vec{k}) = -\frac{i\hbar}{2B_\nu(\vec{k})}. \quad (5.81)$$

Inserting Eqs. (5.72) and (5.73) in the expression (5.71) of the Hamilton operator and requiring that the coefficients of the operators which do not correspond to the energy conservation are zero, we find

$$|B_\nu(\vec{k})|^2 = \frac{\hbar}{2\omega_\nu(k)}. \quad (5.82)$$

The relation (5.81) between  $A_\nu(\vec{k})$  and  $B_\nu(\vec{k})$  was also taken into account.  $B_\nu(\vec{k})$  depends only on the modulus of  $\vec{k}$  and from Eqs. (5.79) yields that this quantity is real,

$$B_\nu(\vec{k}) = \left( \frac{\hbar}{2\omega_\nu(k)} \right)^{1/2}. \quad (5.83)$$

The expansion coefficients  $A_\nu(\vec{k})$  and  $B_\nu(\vec{k})$  being determined, we can write the Hamiltonian density in the diagonal form

$$H_{ph} = \sum_{\vec{k}, \nu} \hbar\omega_\nu(k) \left[ a_\nu^\dagger(\vec{k})a_\nu(\vec{k}) + \frac{1}{2} \right]. \quad (5.84)$$

## 5.4 Electron-Phonon Interaction

The Hamiltonian which describes the electron-optical phonon interaction has the form

$$H_{e-ph} = -e\phi(\vec{r}^e), \quad (5.85)$$

where  $(-e)$  is the electron charge and  $\phi(\vec{r}^e)$  is the scalar potential (5.2) generated by the polarization charge;  $\vec{r}^e$  gives the position of the electron. Inserting the relation (5.17) in Eq. (5.2) we obtain

$$\phi(\vec{r}^e) = -\frac{1}{\epsilon_0} \sum_{j=x,y,z} \sum_{\vec{k}} \frac{1}{2k} \frac{\partial}{\partial r_j} \frac{e^{i\vec{k}\vec{r}^e}}{\sqrt{A}} \int_{-l/2}^{l/2} dz' e^{-k|z-z'|} P_j(\vec{k}, z'). \quad (5.86)$$

Using the relation (5.9) between the electric- and the polarization field and the expression (5.75) of  $\vec{E}(\vec{r})$ , we can also write  $P_j(\vec{k}, z)$  in terms of creation and annihilation operators:

$$\vec{P}_j(\vec{k}, z) = \epsilon_0 \sum_{\nu} \sqrt{\frac{\hbar}{2\omega_{\nu}(k)}} \sum_{\alpha=\perp,\parallel} \chi_{\alpha}(\omega_{\nu}) g_{\alpha}(\omega_{\nu}) u_{\alpha}^{(\nu)}(k, z) \left( \vec{e}_{\alpha}(\vec{k}) \right)_j \left[ a_{\nu}(\vec{k}) + a_{\nu}^{\dagger}(-\vec{k}) \right], \quad (5.87)$$

where  $\chi_{\alpha}(\omega_{\nu})$  is the dielectric susceptibility (5.10) and  $g_{\alpha}(\omega_{\nu})$  is given by Eq. (5.19). From here the potential of the electric field is obtained as

$$\begin{aligned} \phi(\vec{r}^e) = & - \sum_{j=x,y,z} \sum_{\vec{k}} \frac{e^{i\vec{k}\vec{r}_e}}{2k\sqrt{A}} \sqrt{\frac{\hbar}{2\omega_{\nu}(k)}} \left[ i\chi_{\perp}(\omega_{\nu}) g_{\perp}(\omega_{\nu}) \int_{-l/2}^{l/2} dz' K(z^e, z') u_{\perp}^{(\nu)}(k, z') \right. \\ & \left. + \chi_{\parallel}(\omega_{\nu}) g_{\parallel}(\omega_{\nu}) \int_{-l/2}^{l/2} dz' K_A(z^e, z') u_{\parallel}^{(\nu)}(k, z') \right] \\ & \left[ a_{\nu}(\vec{k}) + a_{\nu}^{\dagger}(\vec{k}) \right], \quad (5.88) \end{aligned}$$

where  $K(z, z')$  and  $K_A(z, z')$  are defined by Eqs. (5.24) and (5.25), respectively.

### 5.4.1 Interaction with the Surface Modes

Using the eigenvectors corresponding to the surface phonon modes (Table 5.1), the Hamiltonian density which describes the interaction of these modes with the conduction electron placed at  $\vec{r} = \vec{r}^e$  is found as

$$H_{e-ph}^{SO} = \sum_{\vec{k}} \sum_{p=\pm} e^{i\vec{k}\vec{r}_e} \Gamma_{0,p}(k, z^e) \left[ a_{0,p}(\vec{k}) + a_{0,p}^{\dagger}(\vec{k}) \right], \quad (5.89)$$

where  $a_{0,p}(\vec{k})$  and  $a_{0,p}^{\dagger}(\vec{k})$  are the creation and annihilation operators of the phonon mode  $(\vec{k}, 0, p)$  and the coupling constant  $\Gamma_{0,p}$  is

$$\Gamma_{0,p}(k, z^e) = - \left( \frac{\hbar e^2}{2A\omega_{0,p}(k)} \right)^{1/2} \frac{C_{0,p}}{k} F_{0,p}(k, \omega_{0,p}, z^e). \quad (5.90)$$

$C_{0,p}$  is the normalization constants defined by Eq. (5.48) and the functions  $F_{0,p}(k, \omega, z)$  are given in Table 5.3.

Imposing the isotropy conditions on the above expressions ( $\omega_{LO,\perp} = \omega_{LO,\parallel}$ ,  $\omega_{TO,\perp} = \omega_{TO,\parallel}$ ,  $\epsilon_{\perp}(\infty) = \epsilon_{\parallel}(\infty)$ ) the dispersion law and the electron-phonon coupling constants for the surface modes of the isotropic slab are easily obtained.

$J$	$F_J$		
	$z < -l/2$	$ z  \leq l/2$	$z > l/2$
$J=0,+$	$\cosh[\gamma(\omega)kl/2]e^{k(z+l/2)}$	$\cosh[\gamma(\omega)kz]$	$\cosh[\gamma(\omega)kl/2]e^{-k(z-l/2)}$
$J=0,-$	$-\sinh[\gamma(\omega)kl/2]e^{k(z+l/2)}$	$\sinh[\gamma(\omega)kz]$	$\sinh[\gamma(\omega)kl/2]e^{-k(z-l/2)}$
$J=+$	$\cos[\gamma(\omega)kl/2]e^{k(z+l/2)}$	$\cos[\gamma(\omega)kz]$	$\cos[\gamma(\omega)kl/2]e^{-k(z-l/2)}$
$J=-$	$-\sin[\gamma(\omega)kl/2]e^{k(z+l/2)}$	$\sin[\gamma(\omega)kz]$	$\sin[\gamma(\omega)kl/2]e^{-k(z-l/2)}$

Table 5.3:  $F_{0,p}(k, \omega, z)$  and  $F_p(k, \omega, z)$  for  $z$  inside and outside the slab.

### 5.4.2 Interaction with the Confined Modes

The coupling between a conduction electron at  $\vec{r} = \vec{r}^e$  and the confined phonon modes is described by the Hamiltonian density

$$H_{e-ph}^{conf} = \sum_{\vec{k}} \sum_{(m,\mu,p)} e^{i\vec{k}\vec{r}^e} \Gamma_{m,\mu,p}(k, z^e) [a_{m,\mu,p}(\vec{k}) + a_{m,\mu,p}^\dagger(\vec{k})], \quad (5.91)$$

where  $a_{m,\mu,p}(\vec{k})$  and  $a_{m,\mu,p}^\dagger(\vec{k})$  are the creation and annihilation operators of the phonon mode  $(\vec{k}, m, \mu, p)$  and the coupling constant  $\Gamma_{m,\mu,p}$  has the form

$$\Gamma_{m,\mu,p}(k, z^e) = - \left( \frac{\hbar e^2}{2A\omega_{m,\mu,p}(k)} \right)^{1/2} l C_{m,\mu,p} F_p(k, \omega_{m,\mu,p}, z^e). \quad (5.92)$$

$C_{m,\mu,p}$  are the normalization constants defined by Eq. (5.66) and the functions  $F_{m,\mu,p}(k, \omega, z)$  are given in Table 5.3.

For a uniaxial slab the confined modes are not degenerate anymore and for each of the two branches ( $\mu = 1, 2$ ) they yield an electric field with a nonzero potential inside and outside the slab. So, as an effect of the anisotropy the optical phonon modes confined in the slab are coupled with external conduction electrons.

Following the method presented by Licari and Evrard [62], in the limit  $l \rightarrow \infty$ , one proves the equivalence between the expression (5.91) and the form of the electron-phonon interaction Hamiltonian density of a uniaxial bulk system [79].

## 5.5 Normal Modes for Different Uniaxial Materials

Depending on the values of the transverse- and longitudinal phonon mode frequencies,  $\omega_{TO,\alpha}$  and  $\omega_{LO,\alpha}$ ,  $\alpha = \perp, \parallel$ , respectively, the anisotropic uniaxial materials can be classified as

## 1. Uniaxial materials with surface optical phonon modes

- (a) for all values of the modulus of the 2D wave vector  $\vec{k}$ . Characteristic frequencies of the material satisfy in this case the inequality:

$$\omega_{TO,\parallel} < \omega_{TO,\perp} < \omega_{LO,\parallel} < \omega_{LO,\perp}; \quad (5.93)$$

- (b) for values of  $k$  greater than a limit value,  $k > k_{lim}$ . This situation corresponds to the materials for which

$$\omega_{TO,\perp} < \omega_{TO,\parallel} < \omega_{LO,\perp} < \omega_{LO,\parallel}; \quad (5.94)$$

## 2. Uniaxial materials without surface optical phonon modes. For this kind of materials

$$\omega_{TO,\parallel} < \omega_{LO,\parallel} < \omega_{TO,\perp} < \omega_{LO,\perp} \quad (5.95)$$

or

$$\omega_{TO,\perp} < \omega_{LO,\perp} < \omega_{TO,\parallel} < \omega_{LO,\parallel}. \quad (5.96)$$

Because the characteristic frequencies of an uniaxial material have only to satisfy the condition  $\omega_{TO,\alpha} < \omega_{LO,\alpha}$ ,  $\alpha = \perp, \parallel$ , theoretically it is possible to find the other two types of materials according to the fulfillment of one of the following two inequalities

$$\omega_{TO,\parallel} < \omega_{TO,\perp} < \omega_{LO,\perp} < \omega_{LO,\parallel}, \quad (5.97)$$

$$\omega_{TO,\perp} < \omega_{TO,\parallel} < \omega_{LO,\parallel} < \omega_{LO,\perp}. \quad (5.98)$$

However, we are not aware of the existence of these types of materials.

A slab with the thickness  $l = Nc$ , where  $c$  is the lattice constant along the optical axis, supports  $3N$  optical phonon modes for every value of the wave vector  $\vec{k}$  if the material is diatomic. These  $3N$  modes can be classified as:

1.  $N$  purely transverse modes, labelled  $(\vec{k}, j)$ ;
2.  $(N-1)$  confined modes in the first branch if the system supports surface modes; if not there are  $N$  confined modes in the first branch. They are labelled with  $(\vec{k}, m, 1, p)$ ;
3.  $(N-1)$  confined modes in the second branch if the system supports surface modes; if not there are  $N$  confined modes in the second branch. They are labelled with  $(\vec{k}, m, 2, p)$ ;
4. if they exist, 2 surface modes, labelled  $(\vec{k}, 0, p)$ .

The total number of optical phonon modes is a constant for a fixed  $l$  and does not depend on the material if the number of atoms or ions per primitive cell is the same. Consequently, the number of confined modes in a uniaxial slab is smaller for a material which supports surface modes than that for a material without surface modes. This assumption is verified in the case of the slab of  $\text{PbI}_2$  (Fig. 5.6) for which the first confined mode of each branch ( $\mu = 1, 2$ ) changes its character and becomes a surface mode at  $k = k_{lim}^{(\mu)}$ .

### 5.5.1 Uniaxial Materials with Surface Modes

#### Materials with Surface Modes for all Values of $k$

As an example we consider a hexagonal CdS (würtzite) slab in vacuum, even though it has a weak asymmetry. For this material there is a single type of infrared active optical modes [79] and, thus, the hypothesis of the diatomic material is justified.

In Fig. 5.4 the dispersion laws for the surface and confined modes in the case of a CdS slab with  $l = 6c$  ( $c$  being the lattice constant along the optical axis) are presented. The material parameters are:  $\omega_{TO,\parallel} = 234 \text{ cm}^{-1}$ ,  $\omega_{TO,\perp} = 242 \text{ cm}^{-1}$ ,  $\omega_{LO,\parallel} = 305 \text{ cm}^{-1}$ ,  $\omega_{LO,\perp} = 307 \text{ cm}^{-1}$ ,  $\epsilon_{\parallel}(\infty) = \epsilon_{\perp}(\infty) = 5.27$ ,  $c = 5.82 \text{ \AA}$  and  $a = 4.13 \text{ \AA}$ , where  $a$  is the lattice constant in the slab plane.

Similarly to the case of an isotropic slab [62], there are two interface modes which has dispersion. The branch of symmetrical surface modes starts from  $\omega_{TO,\perp}$  at  $kl = 0$  and reaches for  $kl \rightarrow \infty$  the value  $\omega_{\infty}$ , solution of the equation

$$\epsilon_{\perp}(\omega)\epsilon_{\parallel}(\omega) = 1. \quad (5.99)$$

For the second branch, that of the symmetrical surface modes, the frequency  $\omega_{0,-}(k)$  decreases from  $\omega_{LO,\parallel}$  for  $kl \rightarrow 0$  to the common value  $\omega_{\infty}$ . The eigenfrequencies of these modes depend strongly on the slab thickness  $l$  for a fixed value of the wave vector  $\vec{k}$  and, therefore, the relevant parameter to characterize is the quantity  $kl$ .

Unlike the situation encountered in the case of an isotropic slab, the eigenfrequencies of the confined modes are spread out between  $\omega_{LO,\parallel}$  and  $\omega_{LO,\perp}$  for  $\mu = 1$  - the domain of the quasilongitudinal modes - and between  $\omega_{TO,\parallel}$  and  $\omega_{TO,\perp}$  for  $\mu = 2$  - the domain of the quasitransverse modes. Thus, the anisotropy lifts the degeneracy and yields the dispersion of the confined optical phonon modes. As follows from the analysis of the spatial dependence of the electron-phonon coupling constants (Fig. 5.5) an electron (inside or outside the slab) interacts with the surface modes and with all types of confined modes. But for a weak anisotropic material as CdS the coupling with the quasilongitudinal modes is much stronger than the coupling with the quasitransverse modes.

#### Isotropic limit

We can find the dispersion laws and the electron-phonon coupling constants for an isotropic slab as a limit case of the results obtained for an uniaxial slab imposing the conditions:

$$\begin{aligned} \omega_{TO,\perp} &\simeq \omega_{TO,\parallel} = \omega_{TO} \\ \omega_{LO,\perp} &\simeq \omega_{LO,\parallel} = \omega_{LO} \\ \epsilon_{\perp}(\infty) &\simeq \epsilon_{\parallel}(\infty) = \epsilon(\infty). \end{aligned} \quad (5.100)$$

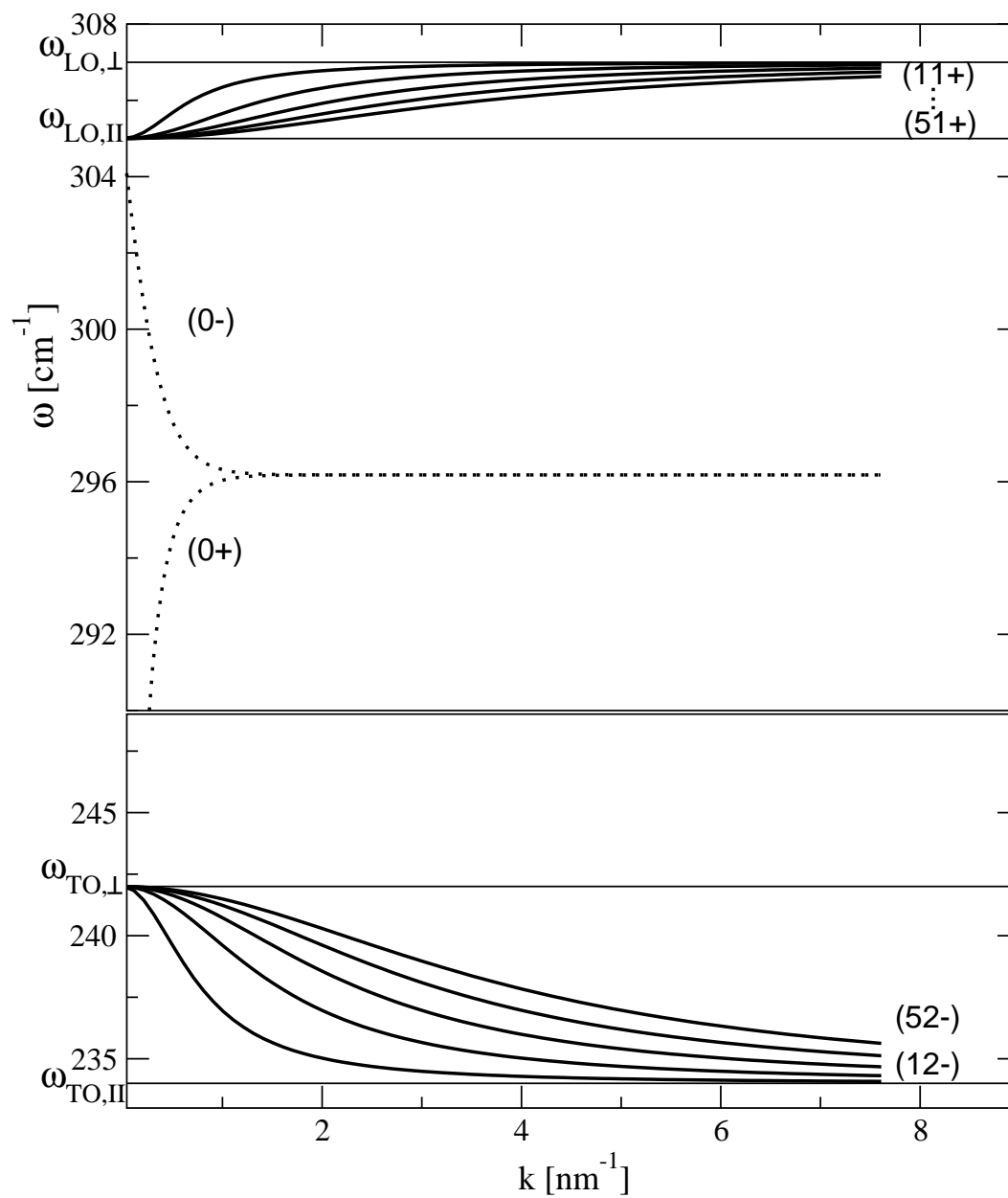


Figure 5.4: Dispersion curves of the surface- (Eqs. (5.46) and (5.47)) and confined phonon modes (Eqs. (5.62), (5.63), (5.64) and (5.65)) for the hexagonal CdS slab with  $l = 6c = 4.05$  nm.

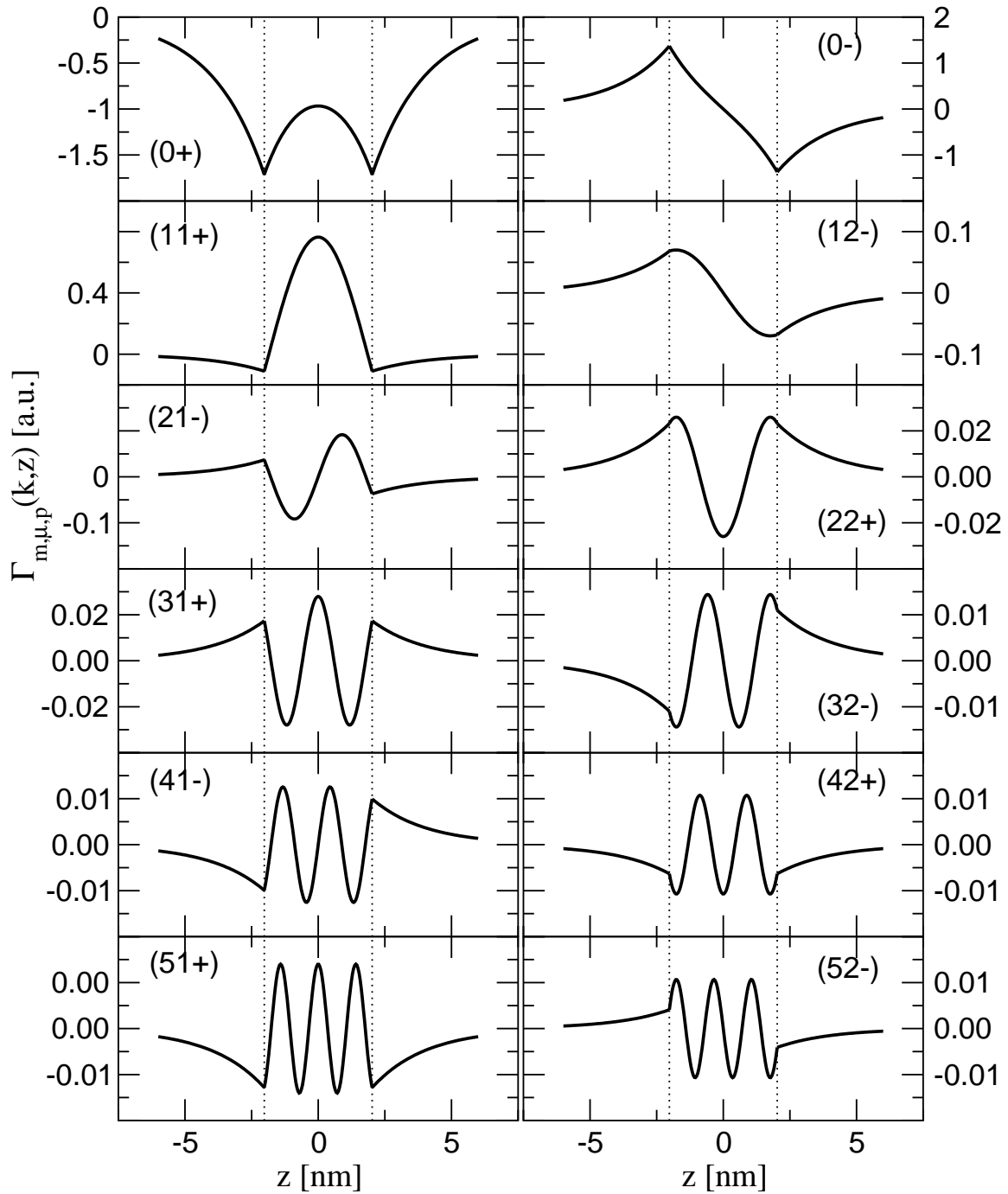


Figure 5.5: Spatial dependence of the electron-phonon coupling constants in the case of the surface modes (Eq. (5.90)) and confined modes (Eq. (5.92)) for the hexagonal CdS slab with  $l = 6c = 4.05$  nm and for  $k = 0.5$  nm<sup>-1</sup>.



Eigenvalues	Eigenvectors $\vec{u}^{(0,p)}(\vec{k}, z) = (u_{\perp}^{(0,p)}(\vec{k}, z), u_{\parallel}^{(0,p)}(\vec{k}, z))$
$\omega_{0,+}$	$\vec{u}^{(0,+)}(\vec{k}, z) = C_0 (-i \cosh(kz), -\sinh(kz))$
$\omega_{0,-}$	$\vec{u}^{(0,-)}(\vec{k}, z) = C_0 (-i \sinh(kz), -\cosh(kz))$

Table 5.4: Surface modes of an isotropic slab placed in vacuum.

In the case of the surface modes, the particularization is straightforward:

$$\begin{aligned} \epsilon_{\perp}(\omega) &\rightarrow \epsilon(\omega) = \epsilon(\infty) \frac{\omega_{TO}^2 - \omega^2}{\omega_{TO}^2 - \omega^2} \\ \epsilon_{\parallel}(\omega) &\rightarrow \epsilon(\omega) \\ \gamma(\omega) &\rightarrow 1 \end{aligned} \quad (5.101)$$

and the dispersion law (5.46) becomes

$$e^{-kl} = p \frac{\epsilon(\omega) + 1}{\epsilon(\omega) - 1}, \quad (5.102)$$

where the two values of the parity index  $p$  satisfy

$$\begin{aligned} \epsilon(\omega) < -1 &\quad \text{for } p = +, \\ -1 < \epsilon(\omega) < 0 &\quad \text{for } p = -. \end{aligned} \quad (5.103)$$

Eq. (5.102) yields directly the frequencies of the two surface modes of the slab

$$\omega_{0,p}^2 = \omega_{TO}^2 \frac{p[\epsilon(0) + 1] + [\epsilon(0) - 1]e^{-kl}}{p[\epsilon(\infty) + 1] + [\epsilon(\infty) - 1]e^{-kl}} \quad (5.104)$$

and the expression of the dielectric function

$$\epsilon(\omega) = \frac{e^{-kl} + p}{e^{-kl} - p}. \quad (5.105)$$

The eigenvectors of the phonon field corresponding to the surface modes have in the case of the isotropic slab the expressions given in Table 5.4 and the normalization constant is

$$C_0 = \left( \frac{1}{k \sinh(kz)} \right)^{1/2}. \quad (5.106)$$

These relations are identical with those given in Ref. [62] for an isotropic slab in vacuum.

In the case of the confined modes we should perform the isotropic limit more carefully.

For  $\omega \in (\omega_{TO,\parallel}, \omega_{TO,\perp})$ , the condition (5.100) yields

$$\begin{aligned} \epsilon_{\parallel}(\omega) &\rightarrow -\infty \\ \epsilon_{\perp}(\omega) &\rightarrow \infty \end{aligned} \quad \begin{aligned} (5.59) \\ \Rightarrow \end{aligned} \quad f(\omega) \rightarrow p, \quad (5.107)$$

and the dispersion law (5.62) becomes

$$\cos[\gamma(\omega_{m,2,p})kl] = p. \quad (5.108)$$

From here we obtain

$$\gamma(\omega_{m,2,p}) = \frac{m\pi}{kl}, \quad \begin{array}{ll} m = 2, 4, 6, \dots & \text{for } p = + \\ m = 1, 3, 5, \dots & \text{for } p = -. \end{array} \quad (5.109)$$

Because the isotropic limit means  $\omega_{TO,\parallel} \simeq \omega_{TO,\perp} = \omega_{TO}$  it makes no sense to use the bijection between  $\omega$  and  $\gamma(\omega)$  in order to calculate the eigenfrequencies  $\omega_{m,2,p}$  from the interval  $(\omega_{TO,\parallel}, \omega_{TO,\perp})$ . Instead, we can directly write  $\omega_{m,2,p} \simeq \omega_{TO}$  for all pairs  $(m, p)$  given by the rules (5.64) and (5.65) for  $\mu = 2$ , but we have to keep in mind that  $\gamma(\omega_{m,2,p})$  has the values given by Eq. (5.109). So, these modes become purely transverse and degenerate.

In the isotropic limit (5.100), the normalization constant  $C_{m,2,p}$  (Eq. (5.66)) vanishes,

$$C_{m,2,p} \xrightarrow[\text{limit}]{\text{isotropic}} 0, \quad (5.110)$$

but the quantity  $C_{m,2,p}/g_{\alpha}(\omega_{m,2,p})$ ,  $\alpha = \perp, \parallel$  which appears in the expressions of the eigenvectors is nonzero. Using Eq. (5.66) we find

$$\begin{aligned} \frac{C_{m,\mu,p}}{g_{\alpha}(\omega_{m,\mu,p})} &\xrightarrow[\text{limit}]{\text{isotropic}} \frac{\frac{1}{g_{\alpha}(\omega_{m,\mu,p})}}{\left| \frac{1}{g_{\alpha}(\omega_{m,\mu,p})} \right|} \sqrt{\frac{2/l}{k^2 l^2 + (m\pi)^2 + p \frac{\sin(m\pi)}{m\pi} [k^2 l^2 - (m\pi)^2]}} \\ &= \frac{\frac{1}{g_{\alpha}(\omega_{m,\mu,p})}}{\left| \frac{1}{g_{\alpha}(\omega_{m,\mu,p})} \right|} C_m \end{aligned} \quad (5.111)$$

with

$$C_m = \left( \frac{2/l}{k^2 l^2 + (m\pi)^2} \right)^{1/2}. \quad (5.112)$$

For the quasitransverse confined modes we have  $\omega_{TO,\parallel} < \omega_{m,2,p} < \omega_{TO,\perp}$  and in the isotropic limit  $\omega_{m,2,p} \simeq \omega_{TO}$ ; it follows  $g_{\perp}(\omega_{TO}) \rightarrow \infty$ ,  $g_{\parallel}(\omega_{TO}) \rightarrow -\infty$  and from Eq. (5.111) we obtain

$$\frac{C_{m,2,p}}{g_{\alpha}(\omega_{m,2,p})} \xrightarrow{\omega_{m,2,p} \rightarrow \omega_{TO}} \begin{cases} C_m, & \alpha = \perp \\ -C_m, & \alpha = \parallel \end{cases}. \quad (5.113)$$

Eigenvalues	Eigenvectors $\vec{u}^{(m,p)}(\vec{k}, z) = \left( u_{\perp}^{(m,p)}(\vec{k}, z), u_{\parallel}^{(m,p)}(\vec{k}, z) \right)$
$\omega_{TO}$	$\vec{u}^{(m,+)}(\vec{k}, z) = C_m \left( -im\pi \cos\left(\frac{m\pi}{l}z\right), -kl \sin\left(\frac{m\pi}{l}z\right) \right)$ $m = 2, 4, 6, \dots$
	$\vec{u}^{(m,-)}(\vec{k}, z) = C_m \left( -im\pi \sin\left(\frac{m\pi}{l}z\right), kl \sin\left(\frac{m\pi}{l}z\right) \right)$ $m = 1, 3, 5, \dots$
$\omega_{LO}$	$\vec{u}^{(m,+)}(\vec{k}, z) = C_m \left( ikl \cos\left(\frac{m\pi}{l}z\right), -m\pi \sin\left(\frac{m\pi}{l}z\right) \right)$ $m = 1, 3, 5, \dots$
	$\vec{u}^{(m,-)}(\vec{k}, z) = C_m \left( ikl \sin\left(\frac{m\pi}{l}z\right), m\pi \sin\left(\frac{m\pi}{l}z\right) \right)$ $m = 2, 4, 6, \dots$

Table 5.5: Purely transverse (TO) and purely longitudinal (LO) confined modes of an isotropic slab placed in vacuum.

Now we can directly obtain from the expressions given in Table 5.2 the eigenvectors associated with the purely transverse modes of the isotropic slab in vacuum (see Table 5.5). They are identical with the eigenvectors obtained by Licari and Evrard [62] in the frame of a model for the isotropic slab.

The purely transverse modes of the isotropic slab are not coupled with the conduction electrons as follows from Eqs. (5.92) and (5.110),

$$\Gamma_{m,2,p}(k, z) \xrightarrow{\omega_{m,2,p} \rightarrow \omega_{TO}} 0. \quad (5.114)$$

If we consider now the domain of the quasilongitudinal modes,  $\omega \in (\omega_{LO,\parallel}, \omega_{LO,\perp})$ , in the isotropic limit the dielectric functions tend to zero,

$$\begin{aligned} \epsilon_{\parallel}(\omega) \rightarrow 0, \quad \epsilon_{\parallel}(\omega) > 0 & \quad (5.59) \\ \epsilon_{\perp}(\omega) \rightarrow 0, \quad \epsilon_{\perp}(\omega) < 0 & \quad \Rightarrow \quad f(\omega) \rightarrow -p. \end{aligned} \quad (5.115)$$

and the dispersion law (5.62) becomes

$$\cos[\gamma(\omega_{m,1,p})kl] = -p \quad (5.116)$$

or

$$\gamma(\omega_{m,1,p}) = \frac{m\pi}{kl}, \quad \begin{array}{ll} m = 1, 3, 5, \dots & \text{for } p = + \\ m = 2, 4, 6, \dots & \text{for } p = -. \end{array} \quad (5.117)$$

Similarly to the case of the quasitransverse modes, we can argue that  $\omega_{m,1,p} \simeq \omega_{LO}$  for all  $m$  and  $p$  given by the rules (5.64) and (5.65) for  $\mu = 1$  and that these eigenfrequencies correspond to the degenerate purely longitudinal modes. If  $\omega_{m,1,p} \simeq \omega_{LO}$  then  $g_{\alpha}(\omega_{LO}) < 0$  and Eq. (5.111) becomes

$$\frac{C_{m,1,p}}{g_{\alpha}(\omega_{m,1,p})} \xrightarrow{\omega_{m,1,p} \rightarrow \omega_{LO}} -C_m \quad \alpha = \perp, \parallel \quad (5.118)$$

and from here the expression of the eigenvectors associated with the purely longitudinal phonon modes of the isotropic slab (Table 5.5) are directly found. In the isotropic limit (5.100) the normalization constant  $C_{m,1,p}$  is

$$C_{m,1,p} \xrightarrow{\omega_{m,1,p} \rightarrow \omega_{LO}} \omega_{LO} \left[ \frac{1}{\epsilon_0} \left( \frac{1}{\epsilon(\infty)} - \frac{1}{\epsilon(0)} \right) \right]^{1/2} C_m \quad (5.119)$$

and the electron-phonon coupling constant (5.92) becomes

$$\Gamma_{m,1,p} \longrightarrow - \left[ \frac{e^2 \hbar \omega_{LO}}{Al \epsilon_0} \left( \frac{1}{\epsilon(\infty)} - \frac{1}{\epsilon(0)} \right) \frac{1}{k^2 + \left( \frac{m\pi}{l} \right)^2} \right]^{1/2} \begin{cases} 0, & z^e < -l/2 \\ \cos \left( \frac{m\pi}{l} z^e \right), & |z^e| \leq l/2 \\ 0, & z^e > l/2 \end{cases} \quad (5.120)$$

as well-known for an isotropic slab in vacuum [62]. The purely longitudinal modes are not coupled with the conduction electrons outside the slab because the functions  $F_+(k, \omega_{m,1,p}, z^e)$  and  $F_-(k, \omega_{m,1,p}, z^e)$  (Table 5.3) vanish for  $|z^e| > l/2$ , if  $\gamma(\omega_{m,1,p}) = m\pi/l$ ,  $m = 1, 2, 3, \dots$ , as given by Eq. (5.117).

### Materials with surface modes for $k > k_{\text{lim}}$

Further we consider the slab of  $\text{PbI}_2$ . This material has a strong anisotropy which is responsible for the existence of the surface modes only for  $k > k_{\text{lim}}$ . It is a material with a lamellar structure and with 3 atoms/primitive cell. The optical phonon modes of the bulk are of two types: infrared active and Raman active [80] and, consistently with the model for the dielectric function, we analyze further the influence of the low dimensionality only on the infrared active optical phonon modes.

In Fig 5.6 we present the dispersion curves of the confined- and surface optical phonons for a slab of  $\text{PbI}_2$  with the thickness  $l = 6c$  placed in vacuum. The material parameters [80] used for the numerical calculations are  $\omega_{TO,\parallel} = 96 \text{ cm}^{-1}$ ,  $\omega_{TO,\perp} = 52 \text{ cm}^{-1}$ ,  $\omega_{LO,\parallel} = 121 \text{ cm}^{-1}$ ,  $\omega_{LO,\perp} = 108 \text{ cm}^{-1}$ ,  $\epsilon_{\parallel}(\infty) = 5.9$ ,  $\epsilon_{\perp}(\infty) = 6.1$ ,  $a = 4.557 \text{ \AA}$ ,  $c = 6.899 \text{ \AA}$ ,  $a$  and  $c$  being the lattice constants on the directions perpendicular and parallel to the optical axis, respectively. In addition to the general properties of the dispersion law of an anisotropic slab (there are nondegenerate confined modes which have dispersion) in the case of a slab of  $\text{PbI}_2$  there are two modes which change (continuously) their character at the variation of  $k$ . For small values of  $k$  these modes have the character of the confined modes (the associated eigenfunctions have a sinusoidal dependence on  $z$ ) and are labelled with  $(1, 1, +)$  and  $(1, 2, -)$ . Starting from the values  $k_{\text{lim}}^{(1)}$  and  $k_{\text{lim}}^{(2)}$ , respectively, the corresponding eigenfunctions tend to be localized at the surface and the modes have the character of surface modes labelled with  $(0, +)$  and  $(0, -)$ , respectively. Therefore, we can conclude that a normal mode changes its character from confined- to surface mode and that this transformation preserves the parity of the mode.

For each branch  $\mu = 1, 2$  the value of the wave vector at which the surface mode appears,  $k = k_{\text{lim}}^{(\mu)}$ , depends strongly on the slab thickness. We plot in Fig. 5.7 the limit value  $k = k_{\text{lim}}^{(1)}$  for the quasitransverse phonon branch as a function of  $l$ . With increasing  $l$  the limit value of  $k$  decreases strongly and the slab practically supports surface modes for all the values of  $k$  relevant for the optical phonons.

To analyze the material properties which lead to the character change of the phonon modes we introduce an anisotropy parameter  $\lambda$  which allows for a continuous

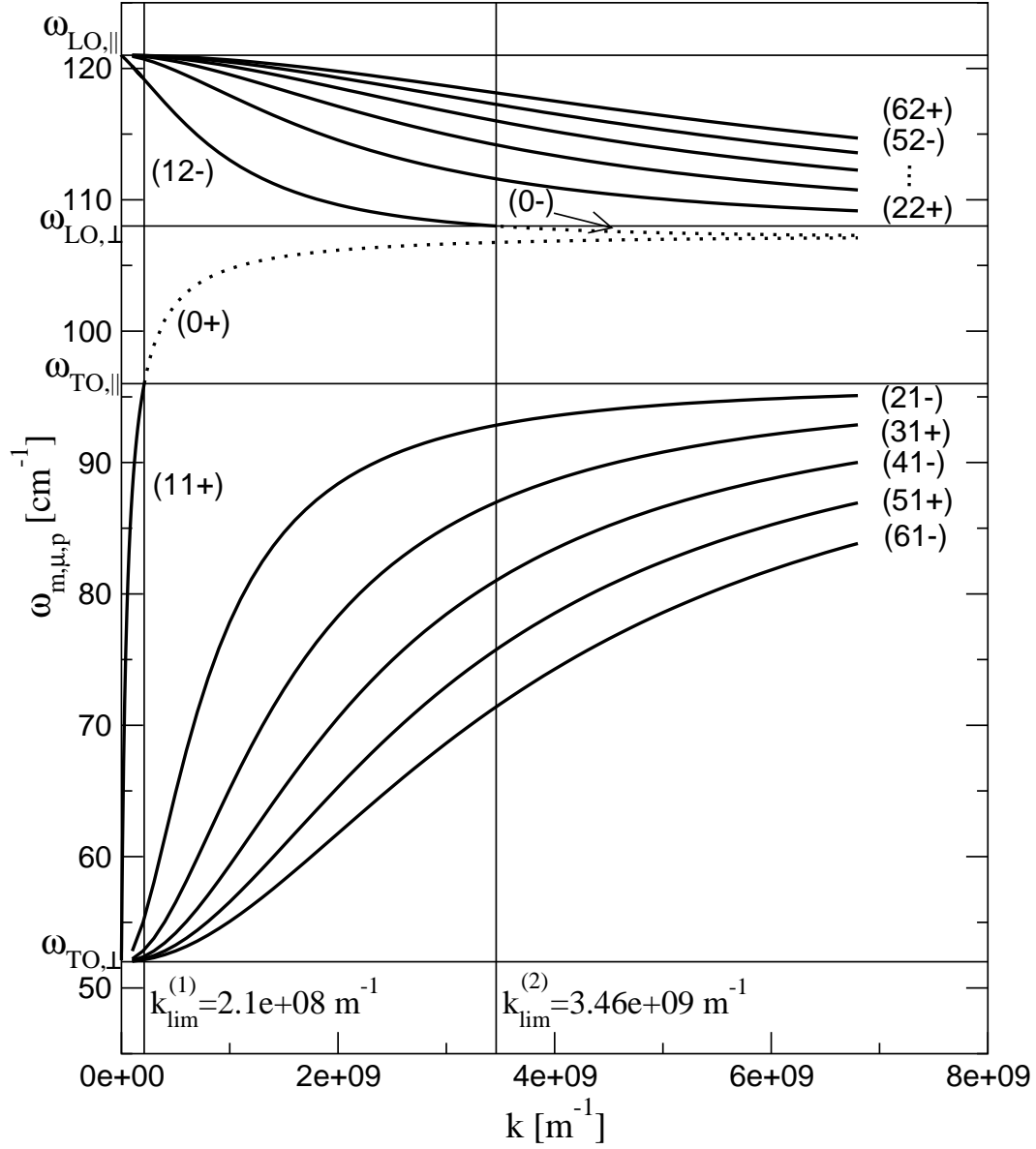


Figure 5.6: Dispersion curves of the surface- (Eqs. (5.46) and (5.47)) and confined- (Eqs. (5.62), (5.63), (5.64) and (5.65)) optical phonon modes for a slab of  $\text{PbI}_2$  with  $l = 6c = 4.14 \text{ nm}$ .

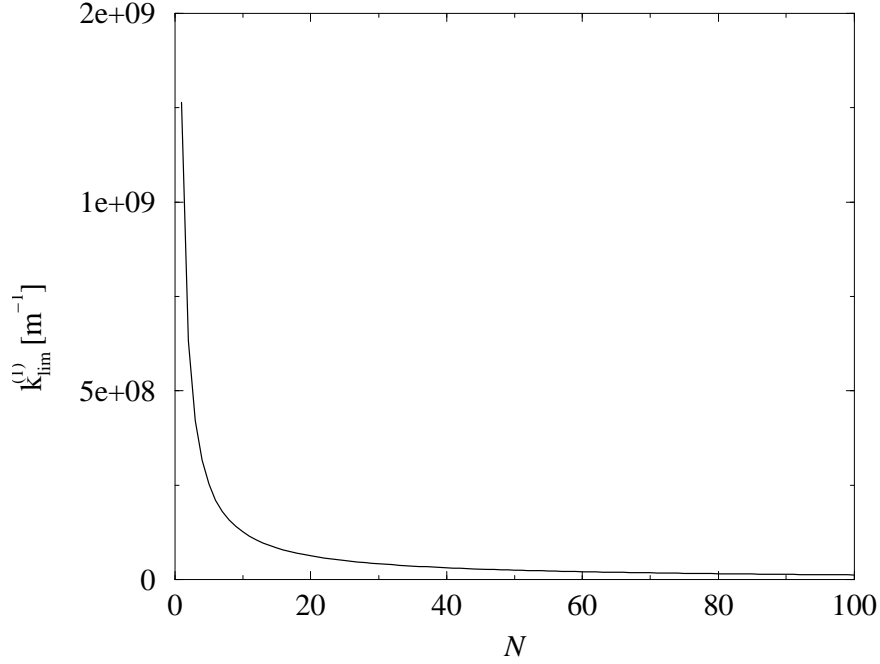


Figure 5.7: The limit value of the wave vector at which the first phonon mode of the quasitransverse branch changes its character from confined- to surface mode,  $k_{\text{lim}}^{(1)}$ , vs.  $N = l/c$  for a slab of  $\text{PbI}_2$ .

variation of the frequencies  $\omega_{TO,\alpha}$  and  $\omega_{LO,\alpha}$  on the principal directions  $\alpha = \perp, \parallel$ ,

$$\omega_{TO,\perp}(\lambda) = \omega_{TO,\perp} + \lambda(\omega_{TO,\parallel} - \omega_{TO,\perp}), \quad (5.121)$$

$$\omega_{LO,\perp}(\lambda) = \omega_{LO,\perp} + \lambda(\omega_{LO,\parallel} - \omega_{LO,\perp}), \quad (5.122)$$

$$\omega_{TO,\parallel}(\lambda) = \omega_{TO,\parallel} - \lambda(\omega_{TO,\parallel} - \omega_{TO,\perp}), \quad (5.123)$$

$$\omega_{LO,\parallel}(\lambda) = \omega_{LO,\parallel} - \lambda(\omega_{LO,\parallel} - \omega_{LO,\perp}). \quad (5.124)$$

Thus, for  $\lambda = 0$  we find the material parameters of  $\text{PbI}_2$  and for  $\lambda = 0.5$  the parameters of an isotropic material with  $\omega_{TO} = (\omega_{TO,\perp} + \omega_{TO,\parallel})/2$  and  $\omega_{LO} = (\omega_{LO,\perp} + \omega_{LO,\parallel})/2$ . For simplicity we consider here the high frequencies limit of the dielectric functions,  $\epsilon_{\perp}(\infty)$  and  $\epsilon_{\parallel}(\infty)$ , independent from  $\lambda$ . Using the dispersion laws of the surface- (Eqs. (5.46) and (5.47)) and confined modes (Eqs. (5.62), (5.63), (5.64) and (5.65)) we analyze further what kind of modes exists for a given value of  $k$  and  $\lambda \in [0, 0.5]$ . If the mode  $(1, 1, +)$  appears, then the component  $u_{\perp}(k, z)$  of the phonon field has a sinusoidal dependence on  $z$  inside the slab,  $u_{\perp}^{(1,1,+)} \sim \cos[\gamma(\omega_{1,1,+})kz]$ . In the opposite case, in which the surface mode  $(0, +)$  exists, the component  $u_{\perp}(k, z)$  has inside the slab a dependence on  $z$  given by  $u_{\perp}^{(0,+)} \sim \cosh[\gamma(\omega_{0,+})kz]$ . We plot in Fig. 5.8  $u_{\perp}(k, z)$  at the same  $k$  for  $|z| \leq l/2$

and for different values of the anisotropy parameter  $\lambda$ . From here we infer that the localization of a mode at the surface decreases with continuous increase of the anisotropy from  $\lambda = 0.5$  toward that of  $\text{PbI}_2$  crystal and the change of the mode character,  $(0, +) \rightarrow (1, 1, +)$ , appears as a direct consequence. For a fixed value of  $k$ , there is a value of  $\lambda$  for which the component  $u_{\perp}$  of the phonon field is practically constant inside the slab.

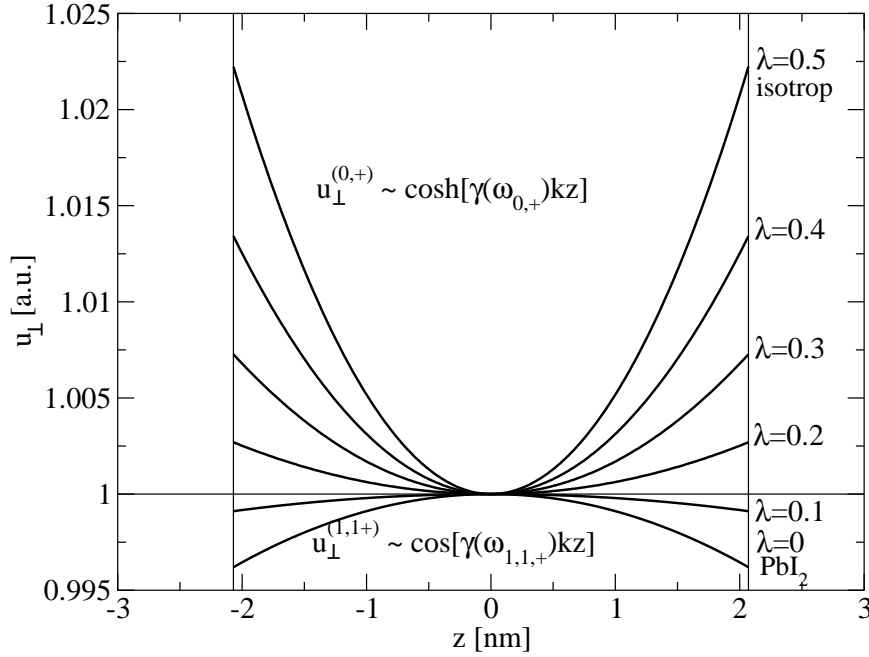


Figure 5.8: Spatial dependence of the component  $u_{\perp}$  of the phonon field for  $k = 10^8 \text{ m}^{-1}$  and for different values of the anisotropy parameter  $\lambda$ . The system is a slab with  $l = 6c$ . For  $\lambda < 0.14$  the eigenvector  $u_{\perp}^{(1,1,+)}$  corresponds to a confined mode in the slab and for  $\lambda > 0.14$  the eigenvector  $u_{\perp}^{(0,+)}$  corresponds to a surface mode.

The coupling functions of the electron-phonon interaction (Eqs. (5.90) and (5.92)) present the same property of continuity at  $k = k_{\text{lim}}^{(\mu)}$ . To illustrate this we present in Fig. 5.9 the coupling functions of the electron on the slab surface with the modes  $(1, 1, +)$ ,  $(1, 2, -)$ ,  $(0, +)$  and  $(0, -)$  in dependence on the wave vector  $k$ . For the rest of the confined modes, i.e. for  $m \geq 2$ , the electron-phonon coupling functions are presented in Fig. 5.10; in comparison with the first ones, these modes are weakly coupled to an electron placed on the slab surface. Due to the strong anisotropy, the phonon mode  $(1, 1, +)$  carries the main contribution to the electron-phonon interaction Hamiltonian, although it belongs to the branch of the quasitransverse modes. Thus, the uniaxial materials have normal modes with the frequencies in the domain of the quasitransverse modes and these modes are

coupled to the conduction electrons; for strong anisotropy this coupling can be even dominant.

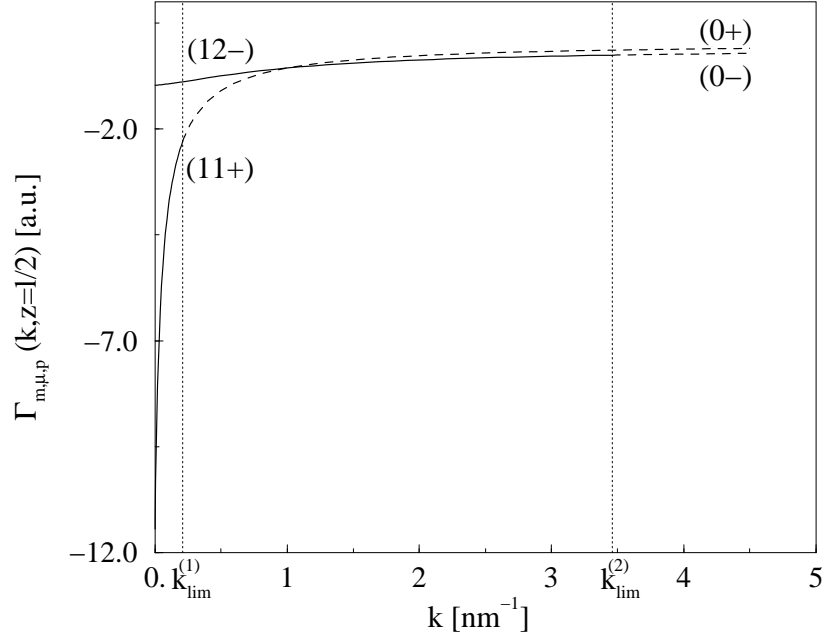


Figure 5.9: Coupling functions of the phonon modes  $(1, 1, +)$ ,  $(1, 2, -)$ ,  $(0, +)$  and  $(0, -)$  with an electron on the slab surface in dependence on  $k$ . These functions are continuous at  $k = k_{\text{lim}}^{(1)}$  and  $k = k_{\text{lim}}^{(2)}$  where the symmetric- and antisymmetric mode, respectively, changes its character from confined to surface mode. The system is a slab with  $l = 6c = 4.14$  nm.

In Fig. 5.11 we present the spatial dependence of the electron-phonon coupling functions  $\Gamma_{m,\mu,p}(k, z)$  (Eqs. (5.90) and (5.92)) for a fixed value of  $k$  and for every mode of the slab. We analyze a case for which there exist the surface mode  $(0, +)$ , but  $k$  is in the vicinity of the limit value  $k_{\text{lim}}^{(1)}$ . The coupling function  $\Gamma_{0,+}$  is nearly constant inside the slab and we can not really speak about the localization of the mode at the surface. As shown in Fig. 5.12, this property of the mode  $(0, +)$  can be identified only for values of  $k$  which satisfy  $k \gg k_{\text{lim}}^{(1)}$ . On the right side of Fig. 5.12 it is illustrated the transformation of the antisymmetric mode  $(1, 2, -)$  to  $(0, -)$  with increasing  $k$  and it is obvious that a typical surface mode is only obtained for large value of  $k$ ,  $k \gg k_{\text{lim}}^{(2)}$ .

As in the case of the CdS slab, we can perform the isotropic limit and obtain the dispersion laws, the eigenvectors and the electron-phonon coupling functions given in Ref. [62].



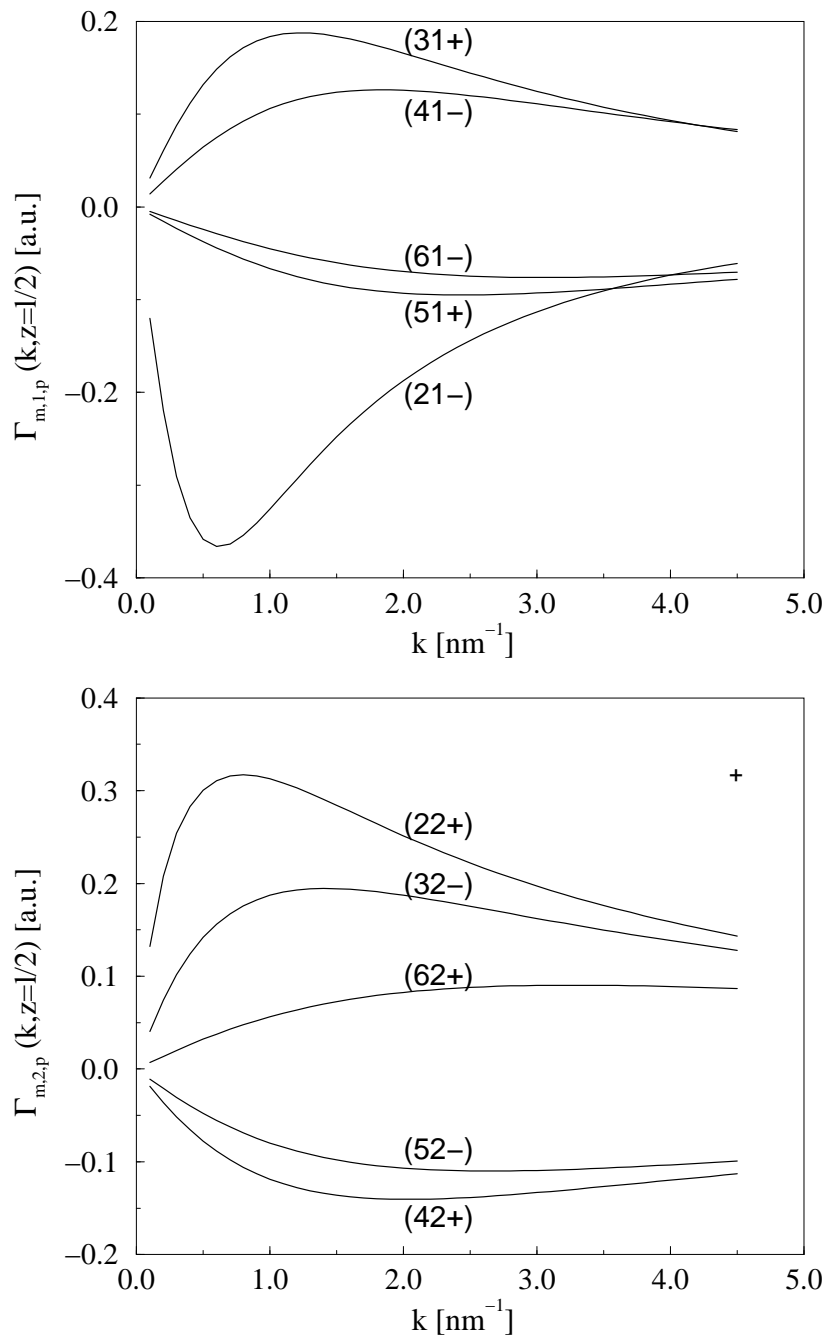


Figure 5.10: Coupling functions of the confined modes  $(m, \mu, p)$  with  $m \geq 2$  with an electron placed on the slab surface as a function of the wave vector  $k$ . The slab of  $\text{PbI}_2$  has  $l = 6c = 4.14$  nm.

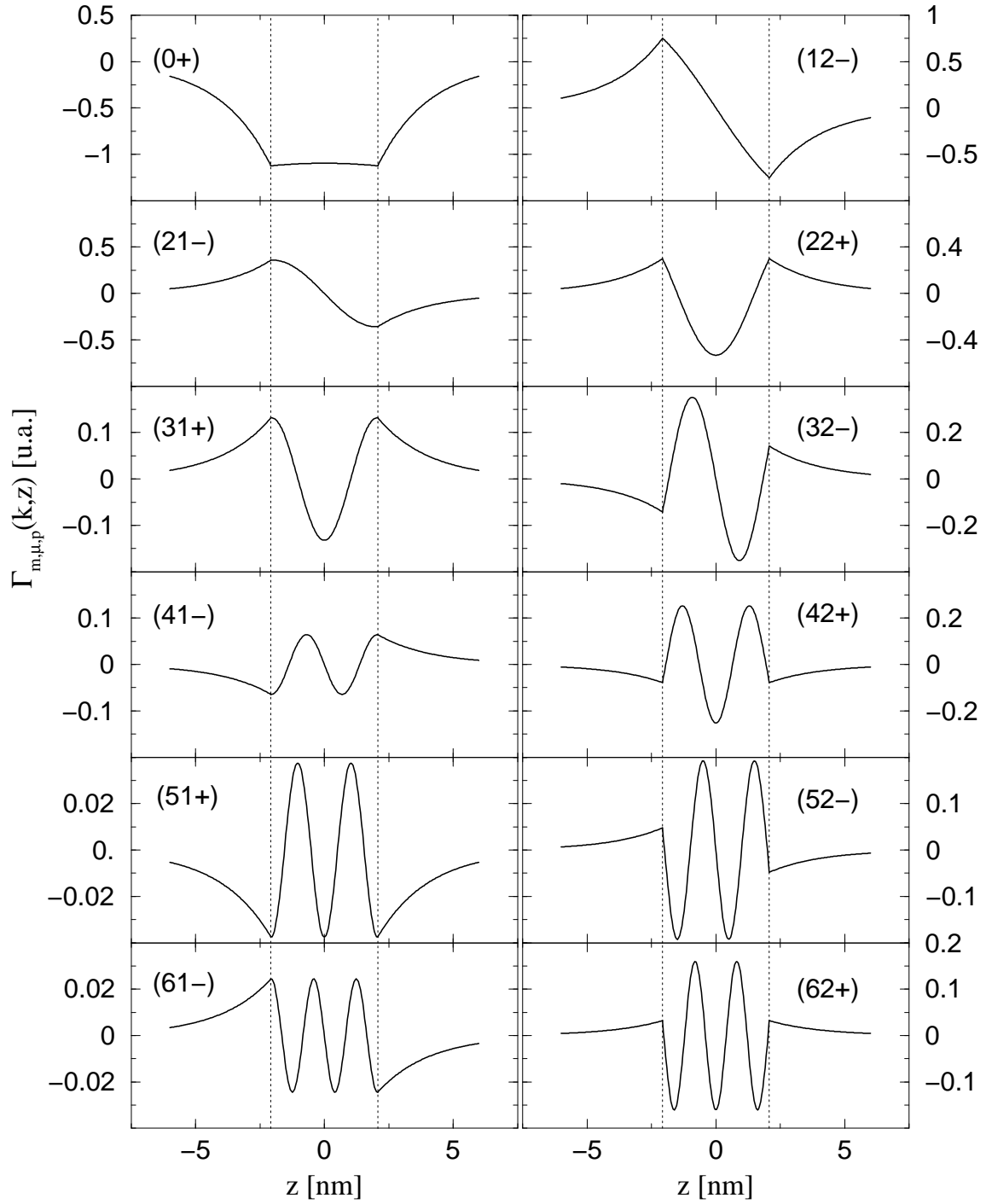


Figure 5.11: Spatial dependence of the electron-phonon coupling constants in the case of the surface modes (Eq. (5.90)) and confined modes (Eq. (5.92)) for the  $\text{PbI}_2$  slab with  $l = 6c = 4.14 \text{ nm}$  and for  $k = 0.5 \text{ nm}^{-1}$ .

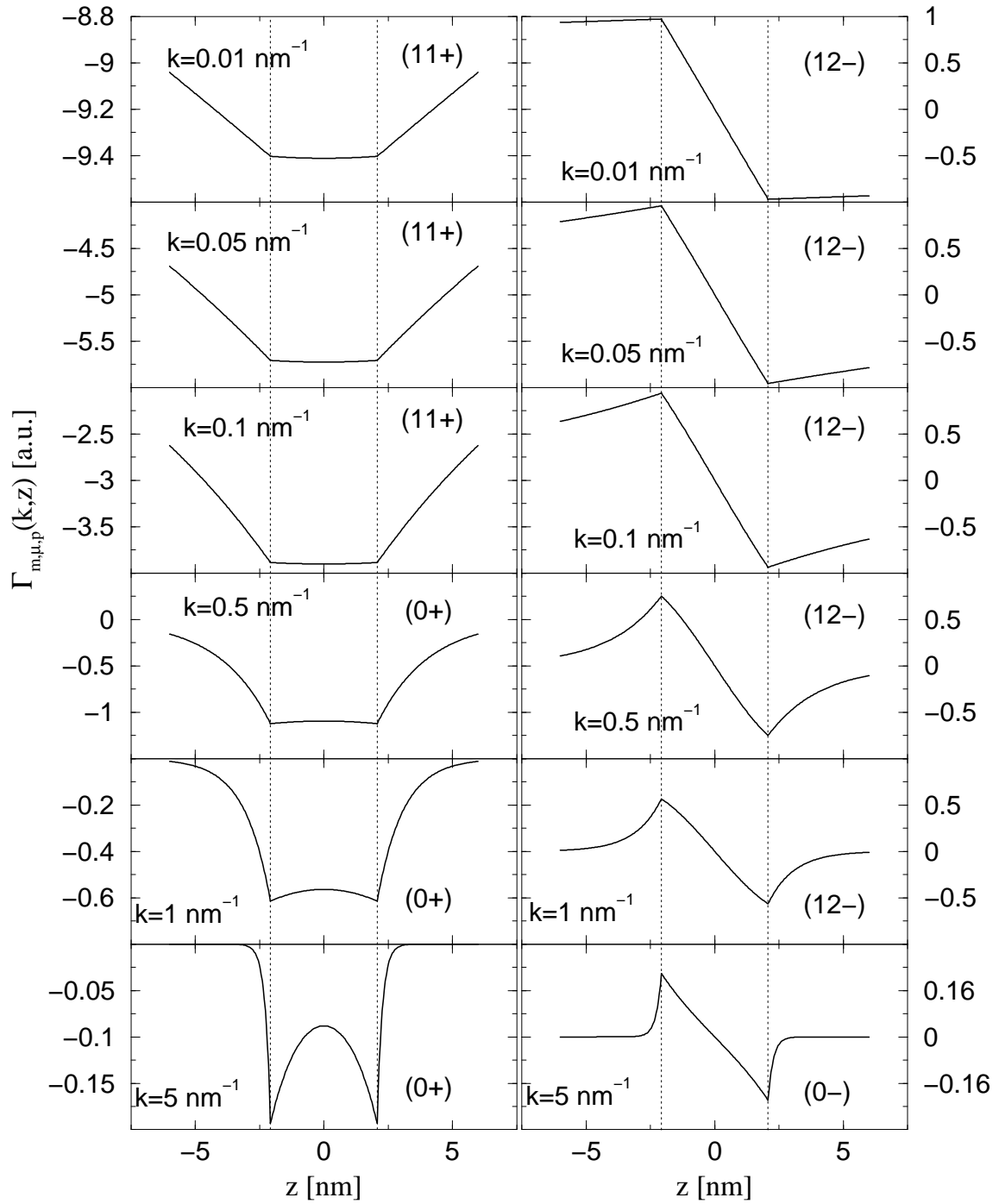


Figure 5.12: Spatial dependence of the electron-phonon coupling constants for the first two strongest coupled modes of the  $\text{PbI}_2$  slab with  $l = 6c = 4.14$  nm and for different values of  $k$ .

### 5.5.2 Uniaxial Materials without Surface Modes

Although Licari and Evrard [62] have considered the surface phonon modes as being a characteristic of all systems with low dimensionality, the existence of these modes is conditioned not only by the presence of the surfaces or interfaces but also by the material properties. For the uniaxial material SnS<sub>2</sub> the dielectric continuum model predicts that the strong anisotropy does not allow for the surface modes. SnS<sub>2</sub> is a lamellar material with 3 atoms per primitive cell. For the calculations performed here we consider only the infrared active modes with the frequencies [80]:  $\omega_{TO,\parallel} = 314 \text{ cm}^{-1}$ ,  $\omega_{TO,\perp} = 205 \text{ cm}^{-1}$ ,  $\omega_{LO,\parallel} = 340 \text{ cm}^{-1}$ ,  $\omega_{LO,\perp} = 356 \text{ cm}^{-1}$  and with the high frequencies dielectric constants  $\epsilon_{\parallel}(\infty) = 5.7$  and  $\epsilon_{\perp}(\infty) = 7.6$ . The lattice constants of SnS<sub>2</sub> are  $a = 3.639 \text{ \AA}$  and  $c = 5.868 \text{ \AA}$ .

The dispersion laws of the confined modes in the slab of SnS<sub>2</sub> are given in Fig. 5.13. The eigenfrequencies are distributed inside the intervals  $(\omega_{TO,\perp}, \omega_{LO,\perp})$  and  $(\omega_{TO,\parallel}, \omega_{LO,\parallel})$  and, therefore, we can not define anymore the domains of the quasi-longitudinal and quasitransverse modes. The two frequencies intervals are large and, therefore, the dispersion is very important.

An electron on the slab surface is coupled with all the confined modes. The coupling functions depending on  $k$  are given in Fig. 5.14. The strongest coupling corresponds to the mode  $(1, 1, +)$ . From the spatial dependence of the coupling function for a fixed  $k$  (Fig. 5.15) it follows that the electrons outside the slab are also coupled with all the confined modes.

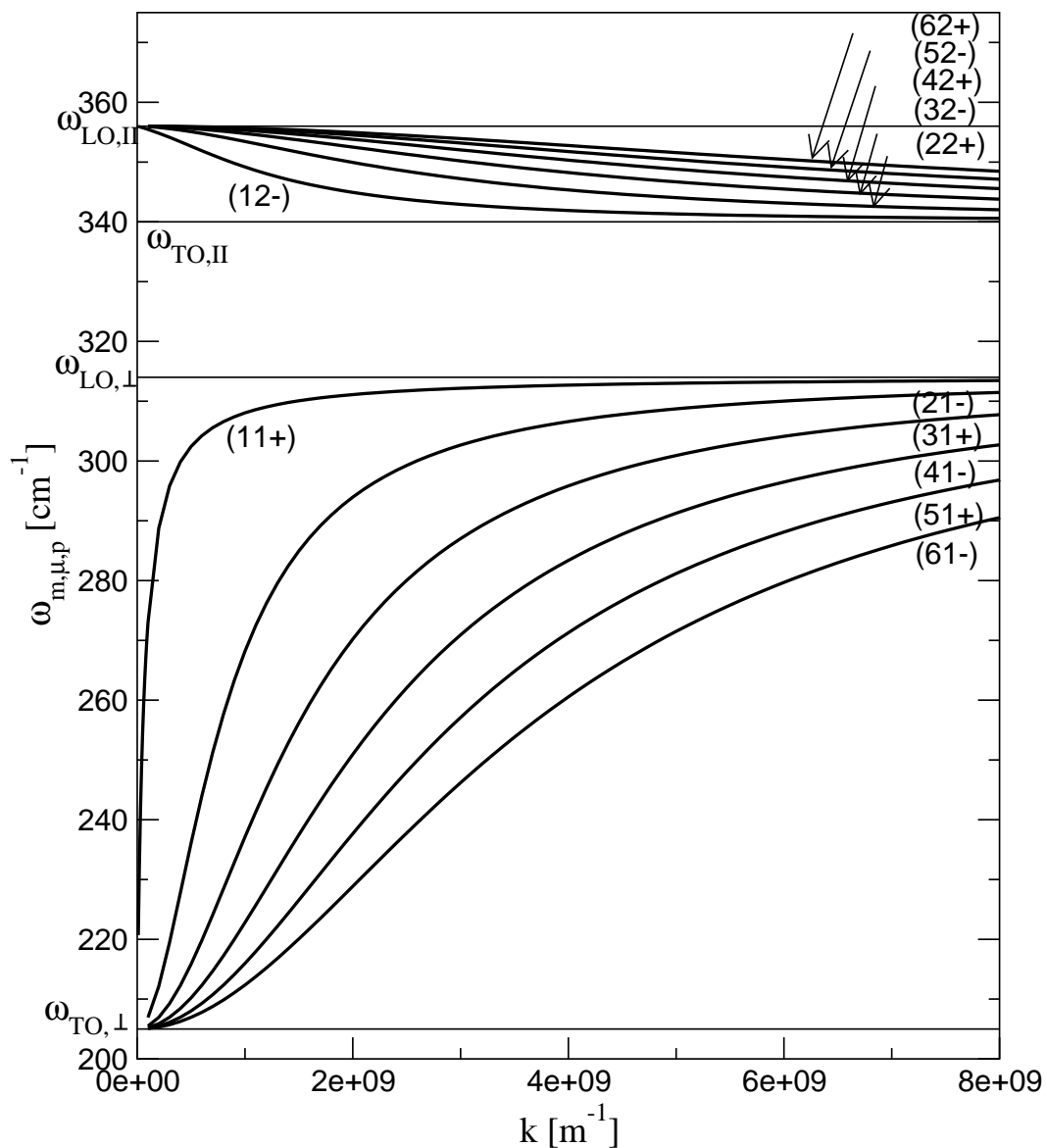


Figure 5.13: Dispersion curves of the surface- (Eqs. (5.46) and (5.47)) and confined optical phonon modes (Eqs. (5.62), (5.63), (5.64) and (5.65)) for a slab of SnS<sub>2</sub> with  $l = 6c = 3.52$  nm.

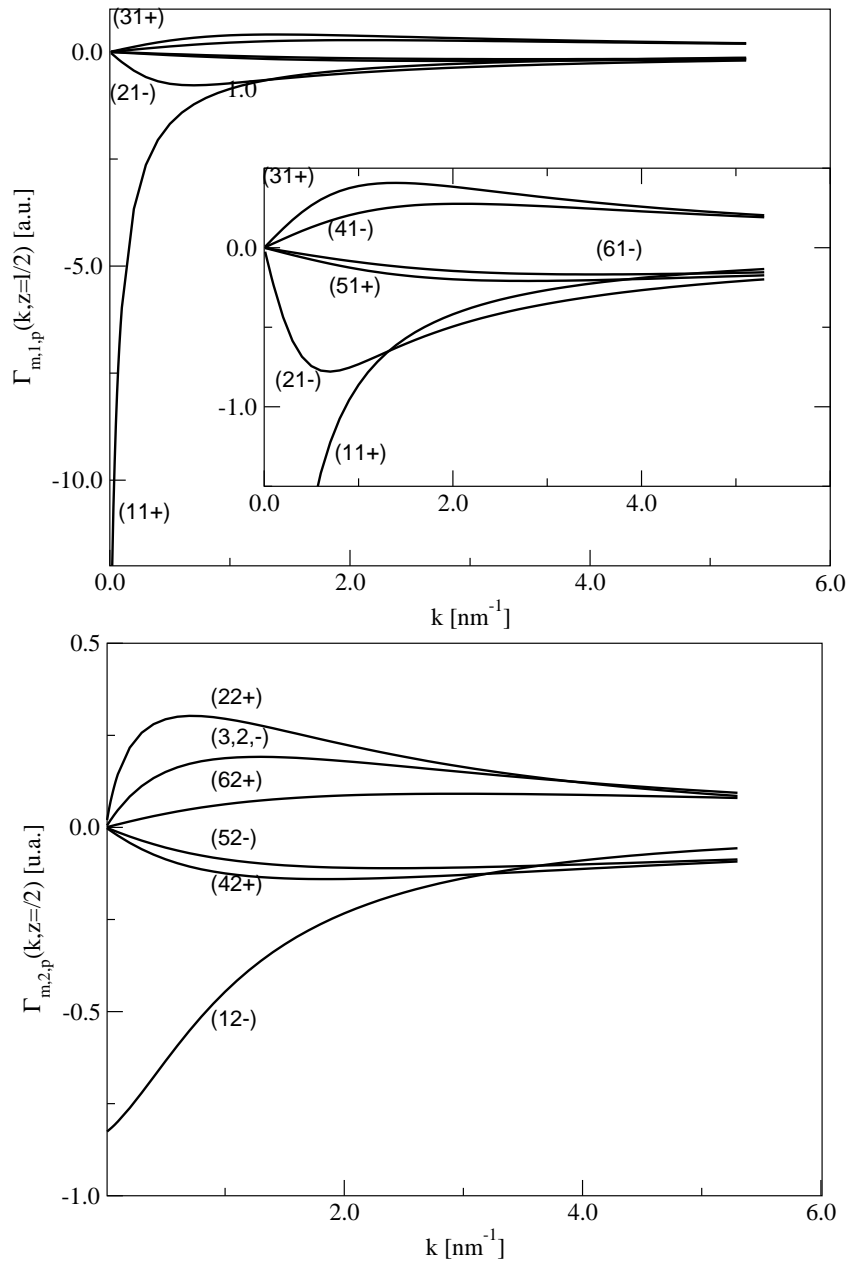


Figure 5.14: Coupling functions of the confined modes  $(m, \mu, p)$  with an electron placed on the slab surface, as a function of the wave vector  $k$ . The slab of  $\text{SnS}_2$  has  $l = 6c = 3.52$  nm.

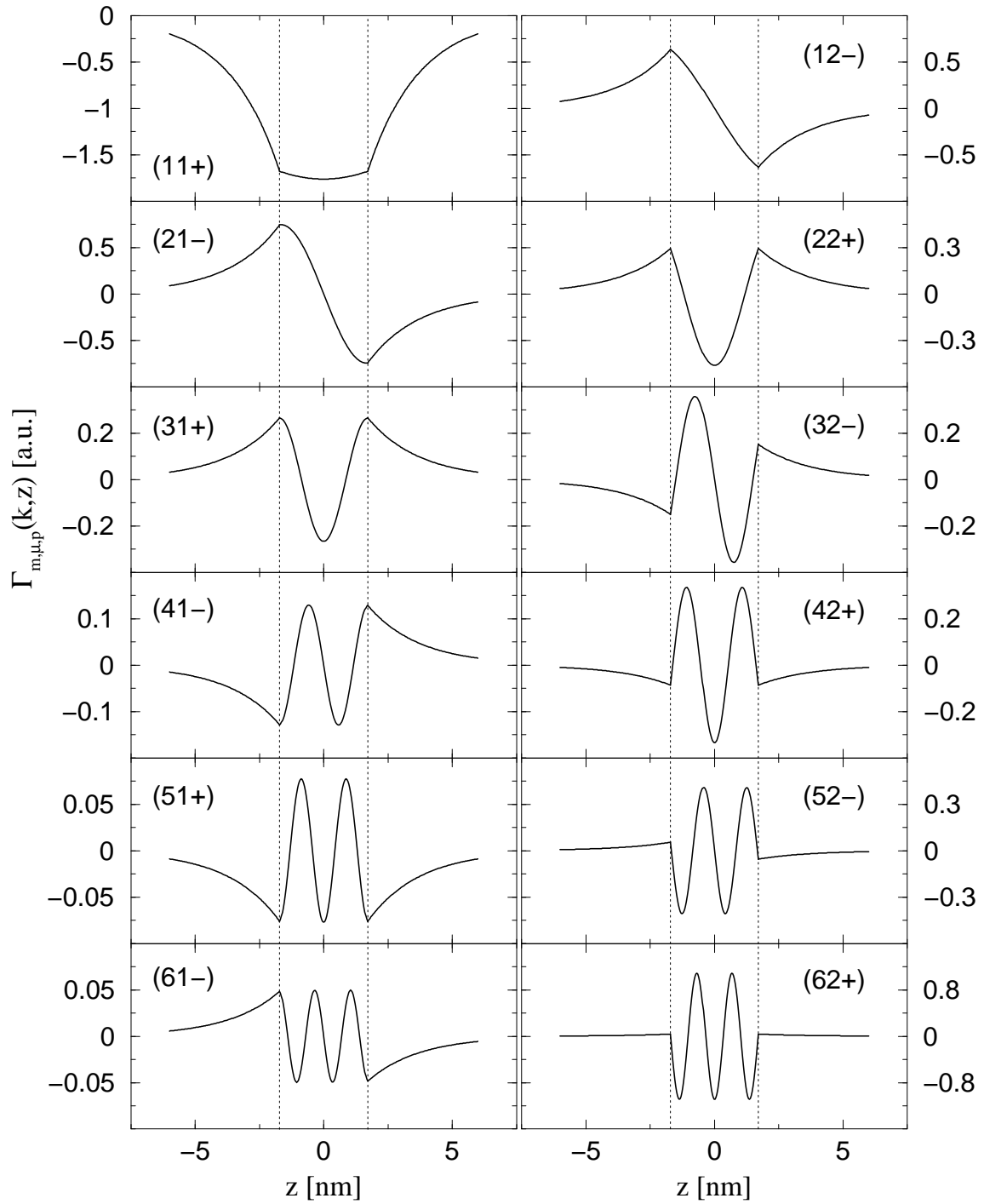


Figure 5.15: Spatial dependence of the electron-phonon coupling constants in the case of the confined modes (Eq. (5.92)) for the  $\text{SnS}_2$  slab with  $l = 6c = 3.52$  nm and for  $k = 0.5 \text{ nm}^{-1}$ .

## 5.6 Summary

We have discussed here, in the context of the dielectric continuum model, the optical phonon modes of a slab made of an anisotropic uniaxial material and their interaction with a conduction electron. In contrast to the situation encountered in the case of an isotropic slab, for an uniaxial one with the optical axis normal to the surface new features are found:

- the degeneracy of the confined modes is lifted and these modes have dispersion. There are not purely transverse or purely longitudinal modes anymore;
- for some anisotropic materials the existence of the surface modes depends on the value of the in-plane wave vector  $\vec{k}$ . If the whole domain of  $\vec{k}$  is analyzed, the continuous transformation of a confined mode into a surface mode can be observed;
- there are materials with an uniaxial anisotropy which can not support surface modes, even though the system has free surfaces;
- an electron placed outside the slab interacts with all the confined modes;
- for some materials it is obtained an unexpected large interaction between an electron situated on the slab surface and the first phonon mode which belongs to the branch of the so-called quasitransverse modes.

Some of these properties can be also found in the case of the anisotropic uniaxial heterostructures.

In the particular case of a slab made from a material with the property  $\omega_{TO,\alpha} < \omega_{LO,\beta}$ ,  $\forall \alpha, \beta = \perp, \parallel$ , we can impose the isotropic limit and obtain the dispersion laws, the eigenvectors of the phonon field and the electron-phonon coupling functions known for the isotropic slab [62].



## Chapter 6

# Optical Phonons in Uniaxial Double Heterostructures

The results obtained in the previous chapter for an anisotropic uniaxial slab can be generalized for the case of a double semiconductor heterostructure having as median layer an anisotropic uniaxial polar material with the optical axis directed along the normal to the interfaces [72, 73].

For a 3D system, a lot of experimental and theoretical work [81, 82, 83] has been done in the past to study the morphic effects ( particularly those effects induced by a homogeneous stress distribution) on both the lattice dynamics and the electronic bands. In the early 1980s, the field concerned with the electronic properties of the strained layer superlattices [84] and, subsequently, that of the strained heterostructures [71, 16] came to the attention of the researchers due to their potentiality in manufacturing devices with enhanced performances.

We present here, in the context of the dielectric continuum model, the phonon modes and their interaction with the conduction electrons, in an anisotropic semiconductor double heterostructure. Pistol et al [17] have investigated, in the backscattering geometry, the Raman spectra of the strained layers of GaAs with estimated thicknesses of 18 and 28 Å, grown on (001) oriented InP substrates; a strain shift of the LO phonon frequency is obtained and this shift agrees, within 10%, with the theoretical value predicted by the continuum models (dielectric, elastic). Based on the work of Pistol et al [17], we apply our results to the cases of strained semiconductor heterostructures InP/GaAs/InP obtained by growing the pseudo-morphic layers of GaAs, uniaxially distorted, on the faces (001) and (111). We are limiting ourselves to the dielectric continuum model because the presence of the anisotropy and of the interfaces makes hopeless any attempt to improve the treatment along the lines of the more elaborate models [85, 86] considered for simpler systems.

## 6.1 Geometry of the Problem

We consider a double heterostructure containing a zincblende-type semiconductor layer grown on the faces (001) or (111) of the same type material, 2. The geometry of the system is given in Fig. 6.1. Due to the difference between the lattice parameters of the adjacent materials, the median layer of the heterostructure is strained and, if its thickness  $l$  does not exceed the critical thickness  $l_c$  [87], a uniaxial anisotropy appears. The optical axis of the system is along the normal to the interfaces. We assume the thicknesses of the buffer and cladding layers of the heterostructure large enough ( $l_2 \gg l$ ) so that their structures are not affected by the lattice mismatching and remain isotropic.

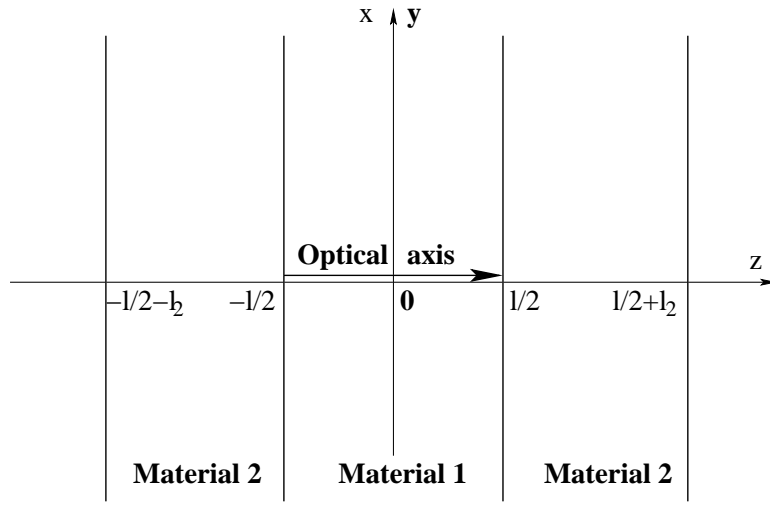


Figure 6.1: Geometry of the double heterostructure with the interfaces normal to  $z$  axis.

For simplicity sake we consider the two polar semiconductors as diatomic materials. The heterostructure is made from different adjacent layers and the material parameters are functions of the space coordinate  $z$ :

$$\begin{aligned}
 \omega_{TO,\alpha}(z) &= \omega_{TO}^{(2)}[\theta(-l/2 - z) + \theta(z - l/2)] + \omega_{TO,\alpha}^{(1)}[\theta(z + l/2) - \theta(z - l/2)], \\
 \omega_{LO,\alpha}(z) &= \omega_{LO}^{(2)}[\theta(-l/2 - z) + \theta(z - l/2)] + \omega_{LO,\alpha}^{(1)}[\theta(z + l/2) - \theta(z - l/2)], \\
 \epsilon_{\alpha}(\infty, z) &= \epsilon_{\alpha}^{(2)}(\infty)[\theta(-l/2 - z) + \theta(z - l/2)] + \epsilon_{\alpha}^{(1)}(\infty)[\theta(z + l/2) - \theta(z - l/2)],
 \end{aligned} \tag{6.1}$$

where  $\alpha = \perp, \parallel$  and  $\theta(z)$  is the Heviside function

$$\theta(z) = \begin{cases} 1, & z \geq 0 \\ 0, & z < 0 \end{cases} . \tag{6.2}$$

## 6.2 Equation of Motion

In the absence of free charges, the only two contributions to the total charge density are the bulk and the surface polarization charges. Thus, in the electrostatic approximation, the scalar potential of the electric field is given by Eq. (5.2). Also, in the case of the double heterostructure with an uniaxial layer, it is convenient to use the equations of the Born-Huang model [78]

$$\begin{aligned}\ddot{\mathcal{U}}_i(\vec{r}, t) &= \beta_{11,i}(z)\mathcal{U}_i(\vec{r}, t) + \beta_{12,i}(z)\mathcal{E}_i(\vec{r}, t), \\ \mathcal{P}_i(\vec{r}, t) &= \beta_{12,i}(z)\mathcal{U}_i(\vec{r}, t) + \beta_{22,i}(z)\mathcal{E}_i(\vec{r}, t),\end{aligned}\quad (6.3)$$

where  $i = x, y, z$  and  $\mathcal{P}(\vec{r}, t)$  and  $\vec{\mathcal{E}}(\vec{r}, t)$  are the polarization- and the electric field, respectively; the coefficients  $\beta_{ij}$ ,  $i, j = 1, 2$  are given by

$$\beta_{11,i}(z) = \begin{cases} -\omega_{TO,\perp}^2(z), & i = x, y \\ -\omega_{TO,\parallel}^2(z), & i = z \end{cases}, \quad (6.4)$$

$$\beta_{12,i}(z) = \begin{cases} \omega_{TO,\perp}(z) [\epsilon_0 (\epsilon_{\perp}(0, z) - \epsilon_{\perp}(\infty, z))]^{1/2}, & i = x, y \\ \omega_{TO,\parallel}(z) [\epsilon_0 (\epsilon_{\parallel}(0, z) - \epsilon_{\parallel}(\infty, z))]^{1/2}, & i = z \end{cases}, \quad (6.5)$$

$$\beta_{22,i}(z) = \begin{cases} \epsilon_0 [\epsilon_{\perp}(\infty, z) - 1], & i = x, y \\ \epsilon_0 [\epsilon_{\parallel}(\infty, z) - 1], & i = z \end{cases}. \quad (6.6)$$

Similarly to the uniaxial slab in vacuum the system considered here is translation invariant in the directions parallel to the interfaces ( $x$  and  $y$  directions) and one can introduce the 2D Fourier transforms of the space dependent functions. Following the method described thoroughly in Sec. 5.1, we obtain the equations satisfied by the components of the phonon field:

$$g_{\perp}(\omega, z)u_s(\vec{k}, z, \omega) = 0, \quad (6.7)$$

$$\begin{aligned}g_{\perp}(\omega, z)u_{\perp}(\vec{k}, z, \omega) &= -\frac{k}{2} \int_{-l/2}^{l/2} dz' e^{-k|z-z'|} \left[ \chi_{\perp}(\omega, z')g_{\perp}(\omega, z')u_{\perp}(\vec{k}, z', \omega) \right. \\ &\quad \left. + i \operatorname{sgn}(z - z')\chi_{\parallel}(\omega, z')g_{\parallel}(\omega, z')u_{\parallel}(\vec{k}, z', \omega) \right],\end{aligned}\quad (6.8)$$

$$\begin{aligned}\epsilon_{\parallel}(\omega, z)g_{\parallel}(\omega, z)u_{\parallel}(\vec{k}, z, \omega) &= -\frac{k}{2} \int_{-l/2}^{l/2} dz' e^{-k|z-z'|} \left[ i \operatorname{sgn}(z - z')\chi_{\perp}(\omega, z')g_{\perp}(\omega, z') \right. \\ &\quad \left. \cdot u_{\perp}(\vec{k}, z', \omega) - \chi_{\parallel}(\omega, z')g_{\parallel}(\omega, z')u_{\parallel}(\vec{k}, z', \omega) \right],\end{aligned}\quad (6.9)$$

where  $\vec{k}$  is the in-plane wave vector. The dielectric functions  $\epsilon_{\alpha}(\omega)$  (Eq. (5.11)), dielectric susceptibilities  $\chi_{\alpha}$  (Eq. (5.10)) and the functions  $g_{\alpha}(\omega)$  (Eq. (5.19)),  $\alpha = \perp, \parallel$ , depend on  $z$  through the TO and LO frequencies on the principal directions and through the high frequency dielectric constants (Eqs. (6.1)).

The eigenvectors of the phonon field obtained as solutions of the system (6.7)-(6.9) satisfy, per construction, the conditions which lead from the continuity of

the macroscopic electric field at the interfaces [77]. Thus, at each interface of the heterostructure, the normal component of the displacement field and the tangential components of the electric field are conserved.

### 6.3 Normal Modes

We are not taking into consideration the problem of the *s*-polarized part of the phonon field, which verifies Eq. (6.7), because the associated modes do not interact with the conduction electrons.

Following the procedure used in Ref. [88], where the Fredholm-type equations (6.8)-(6.9) are transformed in differential equations, the eigenfrequencies and the eigenvectors of the phonon field are obtained. The equation for the component  $u_{\perp}$  of the phonon field is obtained differentiating (6.8) twice and replacing  $du_{\parallel}/dz$  by the derivative of (6.9). It is easy to see that, strictly in this anisotropic uniaxial case,  $\omega_{TO,\perp}^{(1)}$ ,  $\omega_{TO,\parallel}^{(1)}$ ,  $\omega_{LO,\perp}^{(1)}$  and  $\omega_{LO,\parallel}^{(1)}$  can not be eigenfrequencies and the integral equations (6.7)-(6.9) are equivalent to the following system of differential equations:

$$\frac{d^2}{dz^2}u_{\perp}(\vec{k}, z, \omega) = k^2 \frac{\epsilon_{\perp}(\omega, z)}{\epsilon_{\parallel}(\omega, z)} u_{\perp}(\vec{k}, z, \omega) \quad (6.10)$$

$$u_{\parallel}(\vec{k}, z, \omega) = -\frac{i}{k} \frac{g_{\perp}(\omega, z)}{g_{\parallel}(\omega, z)} \frac{d}{dz} u_{\perp}(\vec{k}, z, \omega) \quad (6.11)$$

Based on Eq. (6.10) we infer that, depending on the sign of the ratio

$$r(\omega) = \frac{\epsilon_{\perp}^{(1)}(\omega)}{\epsilon_{\parallel}^{(1)}(\omega)} \quad (6.12)$$

and similarly to the case of an isotropic heterostructure [64], the phonon modes of an anisotropic heterostructure with uniaxial layer are classified as interface modes for  $r(\omega) > 0$  and as confined modes in the uniaxial layer for  $r(\omega) < 0$ . Obviously, there are, also, the so-called half-space modes [64] which characterize the lateral parts of the heterostructure, and which are not affected by the induced anisotropy of the median layer.

Substituting in the integral equations (6.8)-(6.9) the solutions given by Eqs. (6.10)-(6.11) the dispersion laws and the expressions of the eigenvectors of the phonon field are obtained.

#### 6.3.1 Interface Modes

The eigenfrequencies  $\omega_{0,\mu,p}(k)$  are the solutions of the equation [72]:

$$\cosh[\gamma(\omega)kl] = p \frac{\epsilon_{\perp}^{(1)}(\omega)\epsilon_{\parallel}^{(1)}(\omega) + (\epsilon^{(2)}(\omega))^2}{\epsilon_{\perp}^{(1)}(\omega)\epsilon_{\parallel}^{(1)}(\omega) - (\epsilon^{(2)}(\omega))^2} \quad (6.13)$$

Eigenvalues	Eigenvectors $\vec{u}^{(0,\mu,p)}(\vec{k}, z) = \left( u_{\perp}^{(0,\mu,p)}(\vec{k}, z), u_{\parallel}^{(0,\mu,p)}(\vec{k}, z) \right)$
$\omega_{0,\mu,+}$	$\vec{u}^{(0,\mu,+)}(\vec{k}, z) = C_{0,\mu,+} \begin{pmatrix} -i \frac{F_{0,+}(k, \omega_{0,\mu,+}, z)}{g_{\perp}(\omega_{0,\mu,+}, z)}, \\ -\gamma(\omega_{0,\mu,+}) \frac{\epsilon_{\parallel}^{(1)}(\omega_{0,\mu,+}) F_{0,-}(k, \omega_{0,\mu,+}, z)}{\epsilon_{\parallel}(\omega_{0,\mu,+}, z) g_{\parallel}(\omega_{0,\mu,+}, z)} \end{pmatrix}$
$\omega_{0,\mu,-}$	$\vec{u}^{(0,\mu,-)}(\vec{k}, z) = C_{0,\mu,-} \begin{pmatrix} -i \frac{F_{0,-}(k, \omega_{0,\mu,-}, z)}{g_{\perp}(\omega_{0,\mu,-}, z)}, \\ -\gamma(\omega_{0,\mu,-}) \frac{\epsilon_{\parallel}^{(1)}(\omega_{0,\mu,-}) F_{0,+}(k, \omega_{0,\mu,-}, z)}{\epsilon_{\parallel}(\omega_{0,\mu,-}, z) g_{\parallel}(\omega_{0,\mu,-}, z)} \end{pmatrix}$

Table 6.1: Interface modes of a double heterostructure with uniaxial layer. The optical axis of the anisotropic layer is directed along the normal to the interfaces.

on the intervals where the following inequalities are satisfied:

$$\epsilon_{\parallel}^{(1)}(\omega)\epsilon^{(2)}(\omega) < 0 \Leftrightarrow \begin{cases} \epsilon_{\parallel}^{(1)}(\omega) > 0, & \epsilon^{(2)}(\omega) < 0 & \text{for } \mu = 1 \\ \epsilon_{\parallel}^{(1)}(\omega) < 0 & \epsilon^{(2)}(\omega) > 0 & \text{for } \mu = 2 \end{cases} \quad (6.14)$$

and verify, for the two values of the parity index  $p$ , the conditions:

$$\begin{aligned} \epsilon_{\parallel}^{(1)}(\omega)\epsilon_{\perp}^{(1)}(\omega) &> (\epsilon^{(2)}(\omega))^2 && \text{for } p = + \\ 0 < \epsilon_{\parallel}^{(1)}(\omega)\epsilon_{\perp}^{(1)}(\omega) &< (\epsilon^{(2)}(\omega))^2 && \text{for } p = -. \end{aligned} \quad (6.15)$$

Similarly to the case of an isotropic heterostructure [64], the interface modes are associated with the index  $m = 0$ ; the values  $+$  and  $-$  of the parity index correspond to the symmetric and antisymmetric character of the component  $u_{\perp}$  of the phonon vector, respectively. The condition (6.14) introduces a branch index  $\mu$  for the interface modes. For the particular case of a heterostructure made of materials having well separated reststrahlen bands, the interface modes can be considered as interface-like substrate and interface-like pseudo-morphic layer modes.

The eigenvectors corresponding to the interface modes are given in Table 6.1 and the normalization constant  $C_{0,\mu,p}$  has the form

$$C_{0,\mu,p} = \left\{ \frac{\epsilon_0 l}{4\omega_{0,\mu,p}} \left[ p \left( \frac{d\epsilon_{\perp}^{(1)}}{d\omega} - \gamma^2(\omega) \frac{d\epsilon_{\parallel}^{(1)}}{d\omega} \right) + \frac{\sinh[\gamma(\omega)kl]}{\gamma(\omega)kl} \left( \frac{d\epsilon_{\perp}^{(1)}}{d\omega} + \gamma^2(\omega) \frac{d\epsilon_{\parallel}^{(1)}}{d\omega} \right) - 2 \frac{\sinh[\gamma(\omega)kl]}{kl} \frac{\gamma(\omega)\epsilon_{\parallel}^{(1)}(\omega)}{\epsilon^{(2)}(\omega)} \frac{d\epsilon^{(2)}}{d\omega} \right] \Big|_{\omega=\omega_{0,\mu,p}} \right\}^{-\frac{1}{2}}, \quad (6.16)$$

where  $\gamma(\omega) = |r(\omega)|^{1/2}$ . The expressions of the functions  $F_{0,\pm}$  given in Table 6.4 show that these eigenvectors decrease rapidly with the distance to the interface.

### 6.3.2 Normal Modes Confined in the Uniaxial Layer

For the case  $r(\omega) < 0$ , in which there are periodical solutions (confined modes) in the anisotropic region of the heterostructure, the eigenfrequencies  $\omega_{m,\mu,p}$  are obtained as

Eigenvalues	Eigenvectors $\vec{u}^{(m,\mu,p)}(\vec{k}, z) = \left( u_{\perp}^{(m,\mu,p)}(\vec{k}, z), u_{\parallel}^{(m,\mu,p)}(\vec{k}, z) \right)$
$\omega_{m,\mu,+}$	$\vec{u}^{(m,\mu,+)}(\vec{k}, z) = C_{m,\mu,+} \begin{pmatrix} -ikl \frac{F_+(k, \omega_{m,\mu,+}, z)}{g_{\perp}(\omega_{m,\mu,+}, z)}, \\ kl\gamma(\omega_{m,\mu,+}) \frac{\epsilon_{\parallel}^{(1)}(\omega_{m,\mu,+})}{\epsilon_{\parallel}(\omega_{m,\mu,+}, z)} \frac{F_-(k, \omega_{m,\mu,+}, z)}{g_{\parallel}(\omega_{m,\mu,+}, z)} \end{pmatrix}$
$\omega_{m,\mu,-}$	$\vec{u}^{(m,\mu,-)}(\vec{k}, z) = C_{m,\mu,-} \begin{pmatrix} -ikl \frac{F_-(k, \omega_{m,\mu,-}, z)}{g_{\perp}(\omega_{m,\mu,-}, z)}, \\ -kl\gamma(\omega_{m,\mu,-}) \frac{\epsilon_{\parallel}^{(1)}(\omega_{m,\mu,-})}{\epsilon_{\parallel}(\omega_{m,\mu,-}, z)} \frac{F_+(k, \omega_{m,\mu,-}, z)}{g_{\parallel}(\omega_{m,\mu,-}, z)} \end{pmatrix}$

Table 6.2: Normal modes confined in the uniaxial region of the double heterostructure.

solutions of the equation

$$\cos[\gamma(\omega)kl] = p \frac{\epsilon_{\perp}^{(1)}(\omega)\epsilon_{\parallel}^{(1)}(\omega) + (\epsilon^{(2)}(\omega))^2}{\epsilon_{\perp}^{(1)}(\omega)\epsilon_{\parallel}^{(1)}(\omega) - (\epsilon^{(2)}(\omega))^2} \quad (6.17)$$

satisfying the condition

$$kl\gamma(\omega) \in ((m-1)\pi, m\pi) \quad (6.18)$$

with  $\gamma(\omega) = |r(\omega)|^{1/2}$ . The parity and the branch indices are chosen according to the following rules:

$$\text{for } p = + \begin{cases} m = 1, 3, 5, \dots, & \mu = 1 & \text{for } \epsilon_{\parallel}^{(1)}(\omega)\epsilon^{(2)}(\omega) > 0 \\ m = 2, 4, 6, \dots, & \mu = 2 & \text{for } \epsilon_{\parallel}^{(1)}(\omega)\epsilon^{(2)}(\omega) < 0 \end{cases} \quad (6.19)$$

$$\text{for } p = - \begin{cases} m = 2, 4, 6, \dots; & \mu = 1 & \text{for } \epsilon_{\parallel}^{(1)}(\omega)\epsilon^{(2)}(\omega) > 0 \\ m = 1, 3, 5, \dots; & \mu = 2 & \text{for } \epsilon_{\parallel}^{(1)}(\omega)\epsilon^{(2)}(\omega) < 0 \end{cases} \quad (6.20)$$

The corresponding eigenvectors given in Table 6.2 are periodical functions inside the uniaxial layer and decrease strongly with the distance to the interfaces, outside this layer [72]. For the different regions of the heterostructure, the functions  $F_{\pm}$  have the expressions given in Table 6.4 and the normalization constant  $C_{m,\mu,p}$  are given as

$$C_{m,\mu,p} = \sqrt{\frac{2}{l}} \left\{ \frac{\epsilon_0 l^2 k^2}{4\omega_{m,\mu,p}} \left[ \frac{d\epsilon_{\perp}^{(1)}}{d\omega} + \gamma^2(\omega) \frac{d\epsilon_{\parallel}^{(1)}}{d\omega} + p \frac{\sinh[\gamma(\omega)kl]}{\gamma(\omega)kl} \left( \frac{d\epsilon_{\perp}^{(1)}}{d\omega} - \gamma^2(\omega) \frac{d\epsilon_{\parallel}^{(1)}}{d\omega} \right) + 2p \frac{\sinh[\gamma(\omega)kl]}{kl} \frac{\gamma(\omega)\epsilon_{\parallel}^{(1)}(\omega)}{\epsilon^{(2)}(\omega)} \frac{d\epsilon^{(2)}}{d\omega} \right] \right\}_{\omega=\omega_{m,\mu,p}}^{-1/2}. \quad (6.21)$$

In contrast to the situation encountered for the isotropic heterostructures, where the confined modes are degenerate having the frequencies  $\omega_{TO}^{(1)}$  and  $\omega_{LO}^{(1)}$  [64], for the anisotropic heterostructures discussed here the degeneracy is lifted and the frequencies of the confined modes are distributed in two domains of frequencies, corresponding to the values  $\mu = 1, 2$  of the branch index (Eqs. (6.19) and (6.20)).

Eigenvalues	Eigenvectors $\vec{u}(\vec{k}, k_z, z) = (u_{\perp}(\vec{k}, k_z, z), u_{\parallel}(\vec{k}, k_z, z))$
$\omega_{LO}^{(2)}$	$\vec{u}^{LO}(\vec{k}, k_z, z) = C(\vec{k}, k_z) (ikF_{h,-}(k, k_z, z), k_z F_{h,+}(k, k_z, z))$
$\omega_{TO}^{(2)}$	$\vec{u}^{TO}(\vec{k}, k_z, z) = C(\vec{k}, k_z) (ik_z F_{h,+}(k, k_z, z), kF_{h,-}(k, k_z, z))$

Table 6.3: Half-space modes of a double heterostructure with anisotropic uniaxial layer.

J	$F_J$		
	$z < -l/2$	$ z  < l/2$	$z > l/2$
$J = +$	$\cos[\gamma(\omega)kl/2]e^{k(z+l/2)}$	$\cos[\gamma(\omega)kz]$	$\cos[\gamma(\omega)kl/2]e^{-k(z-l/2)}$
$J = -$	$-\sin[\gamma(\omega)kl/2]e^{k(z+l/2)}$	$\sin[\gamma(\omega)kz]$	$\sin[\gamma(\omega)kl/2]e^{-k(z-l/2)}$
$J = 0, +$	$\cosh[\gamma(\omega)kl/2]e^{k(z+l/2)}$	$\cosh[\gamma(\omega)kz]$	$\cosh[\gamma(\omega)kl/2]e^{-k(z-l/2)}$
$J = 0, -$	$-\sinh[\gamma(\omega)kl/2]e^{k(z+l/2)}$	$\sinh[\gamma(\omega)kz]$	$\sinh[\gamma(\omega)kl/2]e^{-k(z-l/2)}$
$J = h, +$	$\cos[k_z(z+l/2)]$	0	$\cos[k_z(z-l/2)]$
$J = h, -$	$-\sin[k_z(z+l/2)]$	0	$\sin[k_z(z-l/2)]$

Table 6.4: Functions  $F_J(k, \omega, z)$  for the different regions of the heterostructure [72].

### 6.3.3 Half-Space Modes

The modes of the isotropic bulk layers (lateral layers) of the heterostructure have the eigenfrequencies  $\omega_{LO}^{(2)}$  and  $\omega_{TO}^{(2)}$  and, therefore, are purely longitudinal and purely transverse modes, respectively. The eigenvectors corresponding to these modes (Table 6.3) are periodical functions for  $z$  outside the uniaxial layer of the heterostructure and vanish inside. Thus, they are identical with those of the isotropic heterostructure given in Ref. [89]. For the half-space modes, the normalization constant is

$$C(\vec{k}, k_z) = \frac{1/\sqrt{l_2}}{\sqrt{k^2 + k_z^2}}, \quad (6.22)$$

where  $l_2$  is the width of a lateral layer of the heterostructure and  $(\vec{k}, k_z)$  is a 3D wave vector with  $k_z = n\pi/l_2$ ,  $n \in \mathbf{N}$ . We have considered here  $l_2 \gg l$  and it follows that  $k_z$  varies practically quascontinuously; in this case it is appropriate to speak about a three dimensional wave vector  $(\vec{k}, k_z)$ .

The eigenvectors corresponding to the interface modes (Table 6.1), to the modes confined in the uniaxial region of the heterostructure (Table 6.2) and to the half-space modes (Table 6.3) verify the orthogonality and the closure relations and, therefore, form a basis.

We can obtain the eigenvectors and eigenvalues of the  $p$ -polarized phonon field for a uniaxial slab in vacuum as a particular case of a double heterostructure with uniaxial layer, for which the material in the lateral regions has the dielectric function  $\epsilon^{(2)}(\omega) = 1$  for every value of the frequency  $\omega$ .

## 6.4 Hamiltonian of the Optical Phonon Field

Expressing the fields from the expression of the energy density (5.85) (appropriate also for an uniaxial double heterostructure) in terms of the obtained eigenvectors, one finds the diagonal form of the Hamiltonian of optical phonons

$$\begin{aligned}
 H_{ph} = & \sum_{\vec{k}, m, \mu, p} \hbar \omega_{m, \mu, p}(k) \left[ a_{m, \mu, p}^\dagger(\vec{k}) a_{m, \mu, p}(\vec{k}) + \frac{1}{2} \right] \\
 & + \sum_{\vec{k}, k_z} \hbar \omega_{LO}^{(2)} \left[ a_{LO}^\dagger(\vec{k}, k_z) a_{LO}(\vec{k}, k_z) + \frac{1}{2} \right] + \sum_{\vec{k}, k_z} \hbar \omega_{TO}^{(2)} \left[ a_{TO}^\dagger(\vec{k}, k_z) a_{TO}(\vec{k}, k_z) + \frac{1}{2} \right].
 \end{aligned} \tag{6.23}$$

$a_{m, \mu, p}^\dagger(\vec{k})$  and  $a_{m, \mu, p}(\vec{k})$  are the creation and annihilation operators, respectively, for the modes  $(m, \mu, p)$ , satisfying bosonic type commutation relations. The index  $m$  has the values  $1, 2, 3, \dots$  for the confined modes and  $0$  for the interface modes;  $\mu = 1, 2$ ,  $p = \pm$ .  $a_{LO/TO}^\dagger(\vec{k}, k_z)$  and  $a_{LO/TO}(\vec{k}, k_z)$  are the creation and annihilation operators for the longitudinal and transverse half-space modes, respectively, and, also, satisfy bosonic type commutation relations.

We neglect the contribution given by the  $s$ -polarized part of the phonon field because the associated modes are purely transverse and not coupled with the conduction electrons.

## 6.5 Electron-Phonon Interaction

The Hamiltonian which describes the electron-phonon interaction has the form

$$H_{e-ph} = -e\Phi(\vec{r}^e), \tag{6.24}$$

where  $(-e)$  is the electron charge and  $\Phi(\vec{r}^e)$  is the scalar potential (5.2) generated by the polarization charge only.

Expressing the scalar potential, in terms of the creation and annihilation operators for the phonon modes, the Hamiltonian (6.24) has the expression

$$\begin{aligned}
 H_{e-ph} = & \sum_{\vec{k}, m, \mu, p} \exp(i\vec{k}\vec{r}_\perp^e) \Gamma_{m, \mu, p}(k, z^e) \left[ a_{m, \mu, p}(\vec{k}) + a_{m, \mu, p}^\dagger(\vec{k}) \right] \\
 & + \sum_{\vec{k}, k_z} \exp(i\vec{k}\vec{r}_\perp^e) \Gamma_{LO}(k, k_z, z^e) \left[ a_{LO}(\vec{k}, k_z) + a_{LO}^\dagger(\vec{k}, k_z) \right],
 \end{aligned} \tag{6.25}$$

with the coupling function given by

$$\Gamma_{0, \mu, p}(k, z^e) = - \left( \frac{\hbar e^2}{2A\omega_{0, \mu, p}(k)} \right)^{1/2} \frac{C_{0, \mu, p}}{k} F_{0, p}(k, \omega_{0, \mu, p}, z^e) \tag{6.26}$$



for the interface modes,

$$\Gamma_{m,\mu,p}(k, z^e) = - \left( \frac{\hbar e^2}{2A\omega_{m,\mu,p}(k)} \right)^{1/2} l C_{m,\mu,p} F_p(k, \omega_{m,\mu,p}, z^e) \quad (6.27)$$

for the modes confined in the uniaxial region of the heterostructure ( $m \geq 1$ ), and

$$\Gamma_{LO}(k, k_z, z^e) = - \left[ \frac{\hbar e^2 \omega_{LO}^{(2)}}{V \epsilon_0} \left( \frac{1}{\epsilon^{(2)}(\infty)} - \frac{1}{\epsilon^{(2)}(0)} \right) \right]^{1/2} \frac{1}{k^2 + k_z^2} F_{h,-}(k, k_z, z^e) \quad (6.28)$$

for the half-space modes;  $A$  is the area of the heterostructure in the  $(x, y)$  plane and  $V = 2Al_2$  is the volume of the isotropic domains of the heterostructure. The normalization constants  $C_{0,\mu,p}$  and  $C_{m,\mu,p}$  are given by Eqs. (6.16) and (6.21), respectively and the functions  $F$  have the expressions given in Table 6.4.

In contrast to the situation encountered in the case of the isotropic heterostructures, for the anisotropic ones some differences are found: i.) an electron placed in the lateral regions of the heterostructure (Fig. 6.1) is coupled with the phonon modes confined in the median layer; ii.) an electron situated inside the anisotropic region interacts with the confined modes having the frequency between  $\omega_{TO,\parallel}^{(1)}$  and  $\omega_{TO,\perp}^{(1)}$ ; in the case of a very thick heterostructure, these modes correspond to the quasitransverse modes of a 3D anisotropic uniaxial crystal. For a 3D uniaxial crystal, a measure of the interaction strength is given by the angular average of the dimensionless Fröhlich coupling constants,  $\langle \alpha_\mu(\theta) \rangle_{AV}$ . Although for a slightly anisotropic crystal of würtzite type, like CdS, the value of the polaronic constant for these quasitransverse modes is negligibly small [79], for layered-type semiconductors such as  $\alpha$ -HgI<sub>2</sub> the polaronic constant, corresponding to the same type of phononic mode, has an unexpectedly large value [90].

## 6.6 Bisotropically Strained Double Heterostructures

As specified at the beginning of this chapter, we consider the double heterostructures made of zincblende type materials 1 and 2, arranged in the geometry 2/1/2 (Fig. 6.1). For a thickness  $l$  of the median layer smaller than the critical value  $l_c$  [87], the difference between the lattice parameters of the adjacent materials induces an anisotropy in the layer 1. In the particular case of the material 1 grown on the faces (001) and (111) of the material 2, an uniaxial anisotropy appears; the optical axis of the strained layer being directed along the normal to the interfaces. The lateral layers of the heterostructure are very large and can be considered isotropic.

In the context of the bisotropic strain model [16] for the pseudo-morphic layer uniaxially distorted, the components  $\epsilon_\perp^{(1)}$  and  $\epsilon_\parallel^{(1)}$  of the dielectric tensor are obtained

in terms of the phonon deformation potentials (PDPs),  $K_{ij}^{(LO)}$  and  $K_{ij}^{(TO)}$ , where  $LO$  and  $TO$  are indices standing for the longitudinal and transverse optical phonons, and also in terms of the high frequency photoelastic coefficients,  $k_{ij}^e$  and  $k_{ij}^e$ .

### 6.6.1 Heterostructures Grown on the Face (001)

For the geometry given in Fig. 6.1 and the growth direction  $[001]$ , the distorted layer parameters are obtained from the parameter of the isotropic material,  $\omega_{TO}^{(1)}$ ,  $\omega_{LO}^{(1)}$  and  $\epsilon^{(1)}(\infty)$ , using the relations [91]:

$$\begin{aligned} \left(\omega_{\alpha,\parallel}^{(1)}\right)^2 &= \omega_{\alpha}^2 + K_{11}^{(\alpha)} \epsilon_3 + 2K_{12}^{(\alpha)} \epsilon_1, \\ \left(\omega_{\alpha,\perp}^{(1)}\right)^2 &= \omega_{\alpha}^2 + K_{12}^{(\alpha)} \epsilon_3 + (K_{11}^{(\alpha)} + K_{12}^{(\alpha)}) \epsilon_1 \end{aligned} \quad (6.29)$$

$\alpha$  being  $LO$  or  $TO$ , and

$$\begin{aligned} \epsilon_{\parallel}^{(1)}(\infty) &= \epsilon^{(1)}(\infty) + k_{11}^e \epsilon_3 + 2k_{12}^e \epsilon_1, \\ \epsilon_{\perp}^{(1)}(\infty) &= \epsilon^{(1)}(\infty) + k_{12}^e \epsilon_3 + (k_{11}^e + k_{12}^e) \epsilon_1, \end{aligned} \quad (6.30)$$

where  $\epsilon_1$  and  $\epsilon_3$  are the diagonal components of the strain tensor [16]:

$$\begin{aligned} \epsilon_1 &= \epsilon_2 = \delta, \\ \epsilon_3 &= -2\delta C_{12}/C_{11}, \\ \epsilon_i &= 0 \text{ for } i = 4, 5, 6. \end{aligned} \quad (6.31)$$

$\delta$  is the parameter which characterizes the lattice mismatching of the two materials contained by the heterostructure,

$$\delta = \frac{a_2}{a_1} - 1 \quad (6.32)$$

and the coefficients  $C_{ij}$ ,  $i, j = 1, 2, \dots, 6$  are the elastic constants of the material 1. We replace here the indices  $ij$  of the symmetrical strain tensor,  $i, j = x, y, z$ , by  $i = 1, 2, \dots, 6$  according to the well-known convention used in the elasticity theory.

For the zincblende-type heterostructures the built-in strain distribution determines frequency shifts  $|\omega_{TO,\parallel}^{(1)} - \omega_{TO,\perp}^{(1)}|$  and  $|\omega_{LO,\parallel}^{(1)} - \omega_{LO,\perp}^{(1)}|$  which are small in comparison to  $\omega_{LO}^{(1)} - \omega_{TO}^{(1)}$  and, therefore, the induced anisotropy is weak, like in würtzite-type crystals.

Further, we analyze the double heterostructure InP/GaAs/InP with the GaAs layer grown on the face (001) of the InP substrate [17, 92, 93, 94]. The parameters of the pseudo-morphic layer in this particular case are [72]:  $\omega_{TO,\parallel}^{(1)} = 252 \text{ cm}^{-1}$ ,  $\omega_{TO,\perp}^{(1)} = 255.6 \text{ cm}^{-1}$ ,  $\omega_{LO,\parallel}^{(1)} = 273.3 \text{ cm}^{-1}$ ,  $\omega_{LO,\perp}^{(1)} = 281.1 \text{ cm}^{-1}$ ,  $\epsilon_{\parallel}^{(1)}(\infty) = 11.5$  and  $\epsilon_{\perp}^{(1)}(\infty) = 11.8$ . For the isotropic GaAs, we have considered [91, 95]:  $\omega_{TO}^{(1)} = 269 \text{ cm}^{-1}$ ,  $\omega_{LO}^{(1)} = 292 \text{ cm}^{-1}$ ,  $\epsilon^{(1)}(\infty) = 10.9$ ,  $K_{11}^{TO} = -2.4$ ,  $K_{12}^{TO} = -2.7$ ,  $K_{44}^{TO} =$

$-0.9$ ,  $K_{11}^{LO} = -1.7$ ,  $K_{12}^{LO} = -2.4$ ,  $K_{44}^{LO} = -0.55$ ,  $k_{11}^e = 19.60$ ,  $k_{12}^e = 16.63$ ,  $k_{44}^e = 8.55$ ,  $C_{11} = 118.8$  GPa,  $C_{12} = 53.8$  GPa,  $C_{44} = 59.4$  GPa and the lattice constant  $a_1 = 5.654$  Å. The material parameters of InP are [91]:  $\omega_{TO}^{(2)} = 304$  cm<sup>-1</sup>,  $\omega_{LO}^{(2)} = 351$  cm<sup>-1</sup>,  $\epsilon^{(2)}(\infty) = 9.61$  and  $a_2 = 5.869$  Å.

If the GaAs layer of the considered heterostructure is thin enough ( $l < 5c$  as given in Ref. [17]), then, practically, it has the lattice constant of the InP substrate in the plane normal to the growth direction. Because InP has a larger lattice constant than that of GaAs, the frequencies of the transverse modes of the distorted GaAs layer (related in the Born-Huang model to the elastic interaction between the nearest neighbors) should be smaller than those of its isotropic counterpart.

GaAs and InP are materials with well separated reststrahlen bands and this property remains also valid when the built-in strain distribution is considered. In this case, the interface modes can be classified as interface-like substrate modes and interface-like pseudo-morphic layer modes. The dispersion laws of these modes are given in Fig. 6.2. For comparison, we present on the right side of Fig. 6.2 the dispersion laws of the interface phonon modes for a InP/GaAs/InP heterostructure, for which the effects of the built-in strain distribution are neglected. The interface modes occurring in the domain of the reststrahlen band of InP (the branch index = 1) are modified only to a very little extent by the effect of the strains. The opposite situation is found for the modes which occur in the reststrahlen band of GaAs; their frequency domain ( $\omega_{TO}^{(1)}, \omega_{LO}^{(1)}$ ) is well marked by the effect of the strains, thus, becoming ( $\omega_{TO,\perp}^{(1)}, \omega_{LO,\parallel}^{(1)}$ ). In a rough estimation, one can say that the dispersion curves for both symmetric- and antisymmetric interface-like pseudo-morphic layer modes ( $\mu = 2$ ) are shifted to lower frequencies with 14 and 20 cm<sup>-1</sup>, respectively.

As an effect of the built-in strain distribution, the degeneracy of the normal modes, confined in the heterostructure median layer, is lifted and these modes have dispersion. The purely longitudinal modes of the isotropic system, with the frequency  $\omega_{LO}^{(1)}$ , correspond in the anisotropic case to the modes labelled with  $(m, 1, p)$ , whose frequencies are distributed in the interval ( $\omega_{LO,\parallel}^{(1)}, \omega_{LO,\perp}^{(1)}$ ); the purely transverse modes with  $\omega_{TO}^{(1)}$  become the confined modes of the branch  $\mu = 2$  with the frequencies in the interval ( $\omega_{TO,\parallel}^{(1)}, \omega_{TO,\perp}^{(1)}$ ), when the uniaxial distortion is taken into account.

The electron-phonon interaction in the considered heterostructure is also affected by the built-in strain distribution. The coupling functions of the interface phonon modes and the modes confined in the uniaxial layer of the heterostructure, with an electron at the interface are plotted in Fig. 6.3 as a function of the wave vector  $k$ . In contrast to an isotropic system [89], the confined modes  $(m, \mu, p)$  of the distorted heterostructure are also coupled with the electron at the interface. A comparative analysis of the two plots in Fig. 6.3 show that the interface modes give the main contribution to the coupling constants, especially for small values of  $\vec{k}$ .

In Fig. 6.4 we present the effect of the strain distribution on the electron-interface phonons coupling functions,  $\Gamma_{0,\mu,p}(k, z = l/2)$  (Eq. (6.26)), by plotting the relative

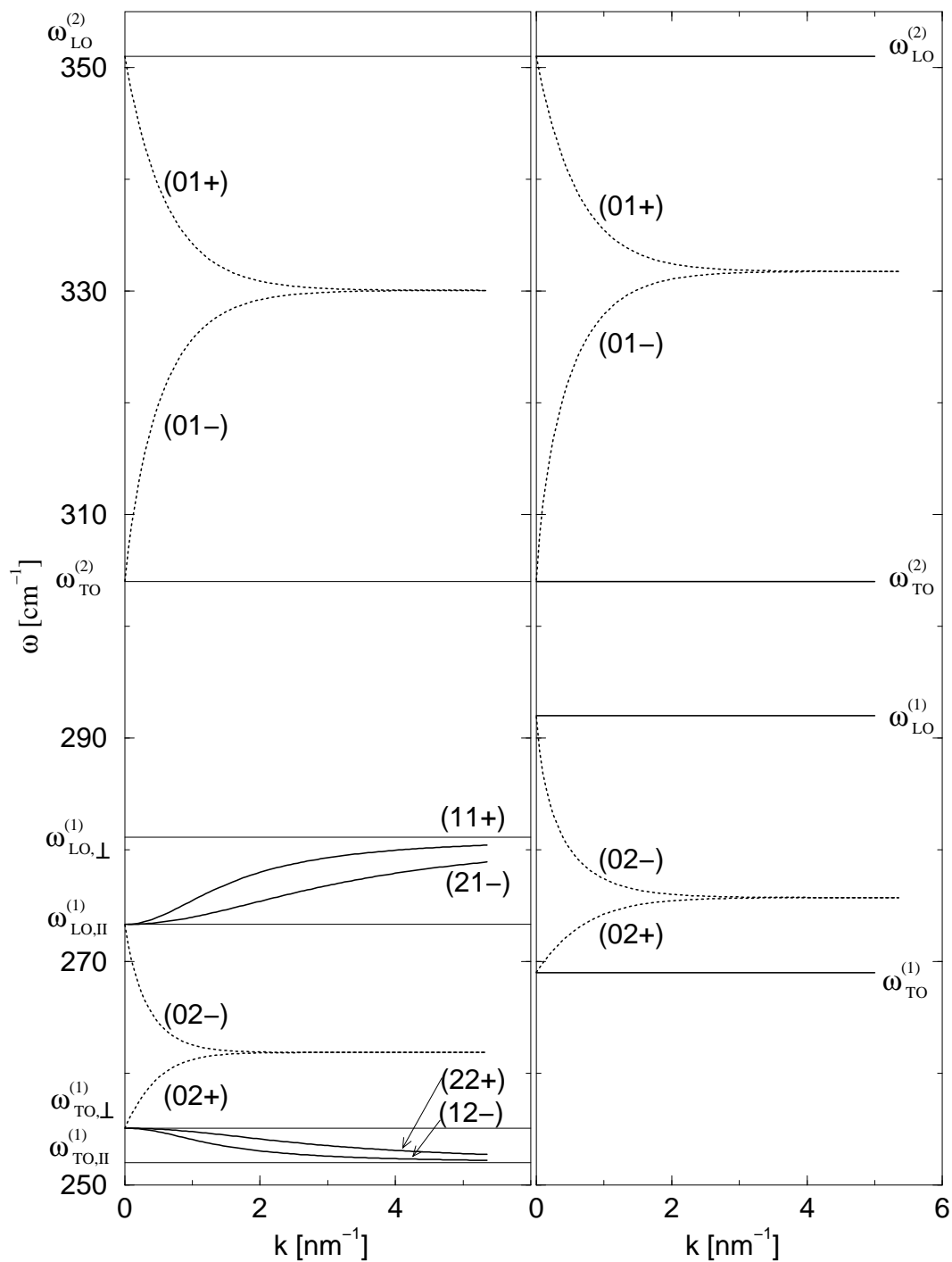


Figure 6.2: Dispersion curves of the phonon modes of the InP/GaAs/InP heterostructure grown on the face (001): interface modes, normal modes confined in the GaAs layer, and half-space modes. The thickness of the GaAs layer is  $l = 3a_1 = 1.8$  nm. Left side: the induced anisotropy of the GaAs layer is taken into account; Right side: GaAs layer is assumed isotropic.

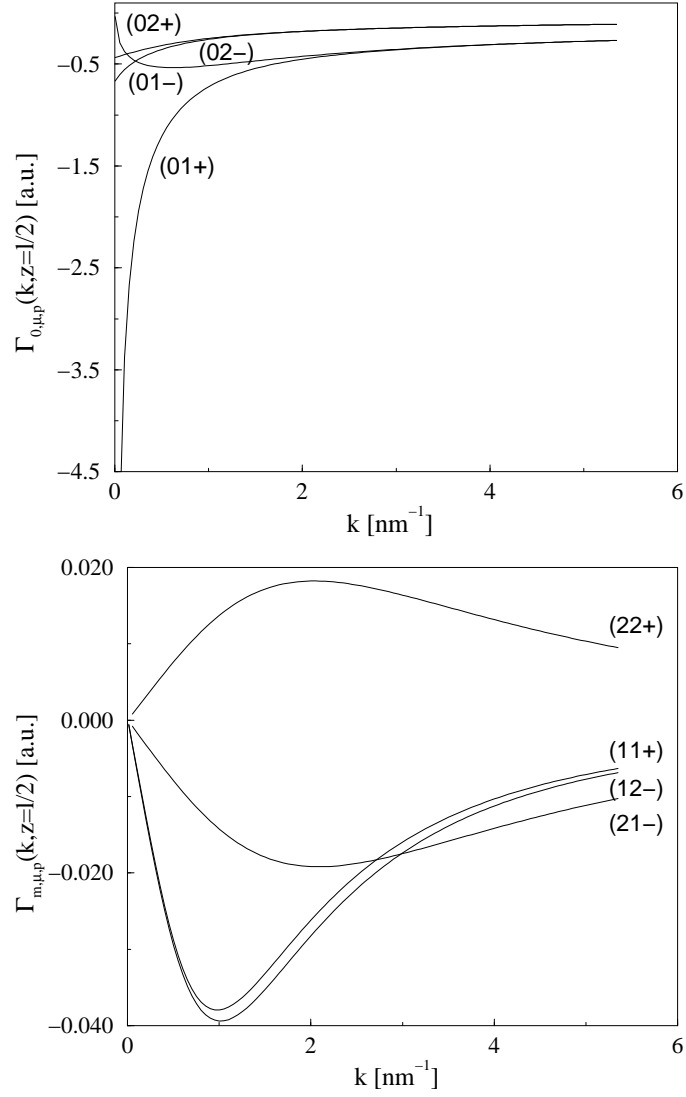


Figure 6.3: Coupling functions of the interface- and confined modes of the InP/GaAs/InP heterostructure grown on the face (001), uniaxially distorted, as a function of the 2D wave vector  $k$ . The thickness of the GaAs layer is  $l = 3a_1 = 1.8 \text{ nm}$ .

variation

$$\Delta\Gamma_{0,\mu,p}/\Gamma_{0,\mu,p}^{\text{is}}(k, z = l/2) = \Gamma_{0,\mu,p}(k, z = l/2)/\Gamma_{0,\mu,p}^{\text{is}}(k, z = l/2) - 1, \quad (6.33)$$

where  $\Gamma_{0,\mu,p}^{\text{is}}$ ,  $\mu = 1, 2$ ,  $p = \pm$ , are the values of  $\Gamma_{0,\mu,p}$  at the isotropic limit (Eqs. (5.100)). Except for the mode (0, 1, +), for all the other interface modes the strength of the electron-phonon interaction is considerably modified by the strain distribution.

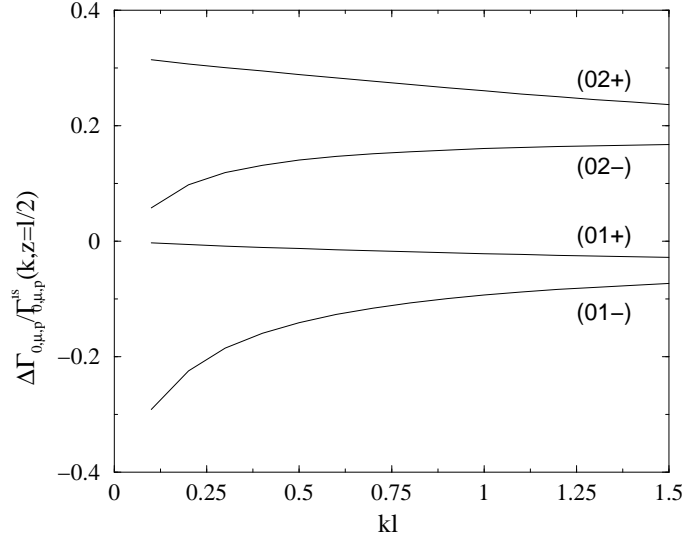


Figure 6.4:  $kl$  dependence of the relative variation  $\Delta\Gamma_{0,\mu,p}/\Gamma_{0,\mu,p}^{\text{is}}(k, z = l/2)$  for all the interface phonon modes of the InP/GaAs/InP heterostructure grown on the face (001). The thickness of the GaAs layer is  $l = 3a_1 = 1.8$  nm.

## 6.6.2 Heterostructures Grown on the Face (111)

We consider, further, a double heterostructure of the type 2/1/2 with the material 1 grown on the face (111) of the material 2. If the median layer of this heterostructure is uniaxially distorted due to the lattice mismatching of the adjacent materials, the parameters of the pseudo-morphic layer are given by the relations [91]:

$$\begin{aligned} (\omega_{\alpha,\parallel}^{(1)})^2 &= (\omega_{\alpha}^{(1)})^2 + K'_{33}(\alpha)\epsilon_3 + 2K'_{13}(\alpha)\epsilon_1, \\ (\omega_{\alpha,\perp}^{(1)})^2 &= (\omega_{\alpha}^{(1)})^2 + K'_{13}(\alpha)\epsilon_3 + (K'_{11}(\alpha) + K'_{12}(\alpha))\epsilon_1 \end{aligned} \quad (6.34)$$

$\alpha$  being *LO* or *TO*, and

$$\begin{aligned} \epsilon_{\parallel}^{(1)}(\infty) &= \epsilon^{(1)}(\infty) + k'_{33}{}^e\epsilon_3 + 2k'_{13}{}^e\epsilon_1, \\ \epsilon_{\perp}^{(1)}(\infty) &= \epsilon^{(1)}(\infty) + k'_{13}{}^e\epsilon_3 + (k'_{11}{}^e + k'_{12}{}^e)\epsilon_1, \end{aligned} \quad (6.35)$$

where  $\epsilon_1$  and  $\epsilon_3$  are the diagonal components of the strain tensor [16]:

$$\begin{aligned}\epsilon_1 &= \epsilon_2 = \delta \\ \epsilon_3 &= -2\delta \left( \frac{C_{11}+2C_{12}-2C_{44}}{C_{11}+2C_{12}+4C_{44}} \right) \delta \\ \epsilon_i &= 0 \text{ for } i = 4, 5, 6.\end{aligned}\quad (6.36)$$

with  $\delta$  defined by Eq. (6.32). The coefficients  $C_{ij}$ ,  $i, j = 1, 2, \dots, 6$  are the elastic constants of the material 1. We replace here the indices  $ij$  of the symmetrical strain tensor,  $i, j = x, y, z$ , by  $i = 1, 2, \dots, 6$  according to the well-known convention used in the elasticity theory. The coefficients  $K'_{ij}^{(\alpha)}$  used here are connected to the components of the PDP tensor,  $K_{ij}^{(\alpha)}$ ,  $\alpha = LO, TO$ , through the relations [91]:

$$\begin{aligned}K'_{11}^{(\alpha)} &= \frac{1}{2} \left( K_{11}^{(\alpha)} + K_{12}^{(\alpha)} + 2K_{44}^{(\alpha)} \right), \\ K'_{12}^{(\alpha)} &= \frac{1}{6} \left( K_{11}^{(\alpha)} + 5K_{12}^{(\alpha)} - 2K_{44}^{(\alpha)} \right), \\ K'_{13}^{(\alpha)} &= \frac{1}{3} \left( K_{11}^{(\alpha)} + 2K_{12}^{(\alpha)} - 2K_{44}^{(\alpha)} \right), \\ K'_{33}^{(\alpha)} &= \frac{1}{3} \left( K_{11}^{(\alpha)} + 2K_{12}^{(\alpha)} - 4K_{44}^{(\alpha)} \right).\end{aligned}\quad (6.37)$$

There are analogous relations between  $k'_{ij}{}^e$  and the photoelastic constants  $k_{ij}{}^e$ :

$$\begin{aligned}k'_{11}{}^e &= \frac{1}{2} (k_{11}{}^e + k_{12}{}^e + 2k_{44}{}^e), \\ k'_{12}{}^e &= \frac{1}{6} (k_{11}{}^e + 5k_{12}{}^e - 2k_{44}{}^e), \\ k'_{13}{}^e &= \frac{1}{3} (k_{11}{}^e + 2k_{12}{}^e - 2k_{44}{}^e), \\ k'_{33}{}^e &= \frac{1}{3} (k_{11}{}^e + 2k_{12}{}^e - 4k_{44}{}^e).\end{aligned}\quad (6.38)$$

In the particular case of the heterostructure InP/GaAs/InP with a GaAs layer grown on the face (111) [17], the parameter of the pseudo-morphic layer are:  $\omega_{TO,\parallel}^{(1)} = 257.3 \text{ cm}^{-1}$ ,  $\omega_{TO,\perp}^{(1)} = 242.8 \text{ cm}^{-1}$ ,  $\omega_{LO,\parallel}^{(1)} = 279.2 \text{ cm}^{-1}$ ,  $\omega_{LO,\perp}^{(1)} = 269.7 \text{ cm}^{-1}$ ,  $\epsilon_{\parallel}^{(1)}(\infty) = 11.3$  and  $\epsilon_{\perp}^{(1)}(\infty) = 12.25$ . The dispersion laws of the interface- and confined modes of the considered heterostructure, given by Eqs. (6.13) and (6.17), respectively, are plotted in Fig. 6.5. In contrast to the heterostructure InP/GaAs/InP with the GaAs layer grown on the face (001), in this case the characteristic frequencies of the system satisfy the inequality

$$\omega_{TO,\perp} < \omega_{TO,\parallel} < \omega_{LO,\perp} < \omega_{LO,\parallel} \quad (6.39)$$

corresponding to an uniaxial material for which the surface/interface modes exist only for values of the wave vector  $k$  greater than a limit value  $k_{\text{lim}}$ . As shown in Fig. 6.5 for the heterostructure InP/GaAs/InP grown on the face (111) of the substrate, for  $k = k_{\text{lim}}^{(1)}$ , the confined mode (1, 1, +) changes its character by becoming the interface mode (0, 2, +). Analogously, for  $k_{\text{lim}}^{(2)}$  the confined mode (1, 2, -) becomes the interface modes (0, 2, -). Similarly to the case of the uniaxial slab (Sec. 5.5.1), the transformation from a confined mode to an interface mode preserves the parity.

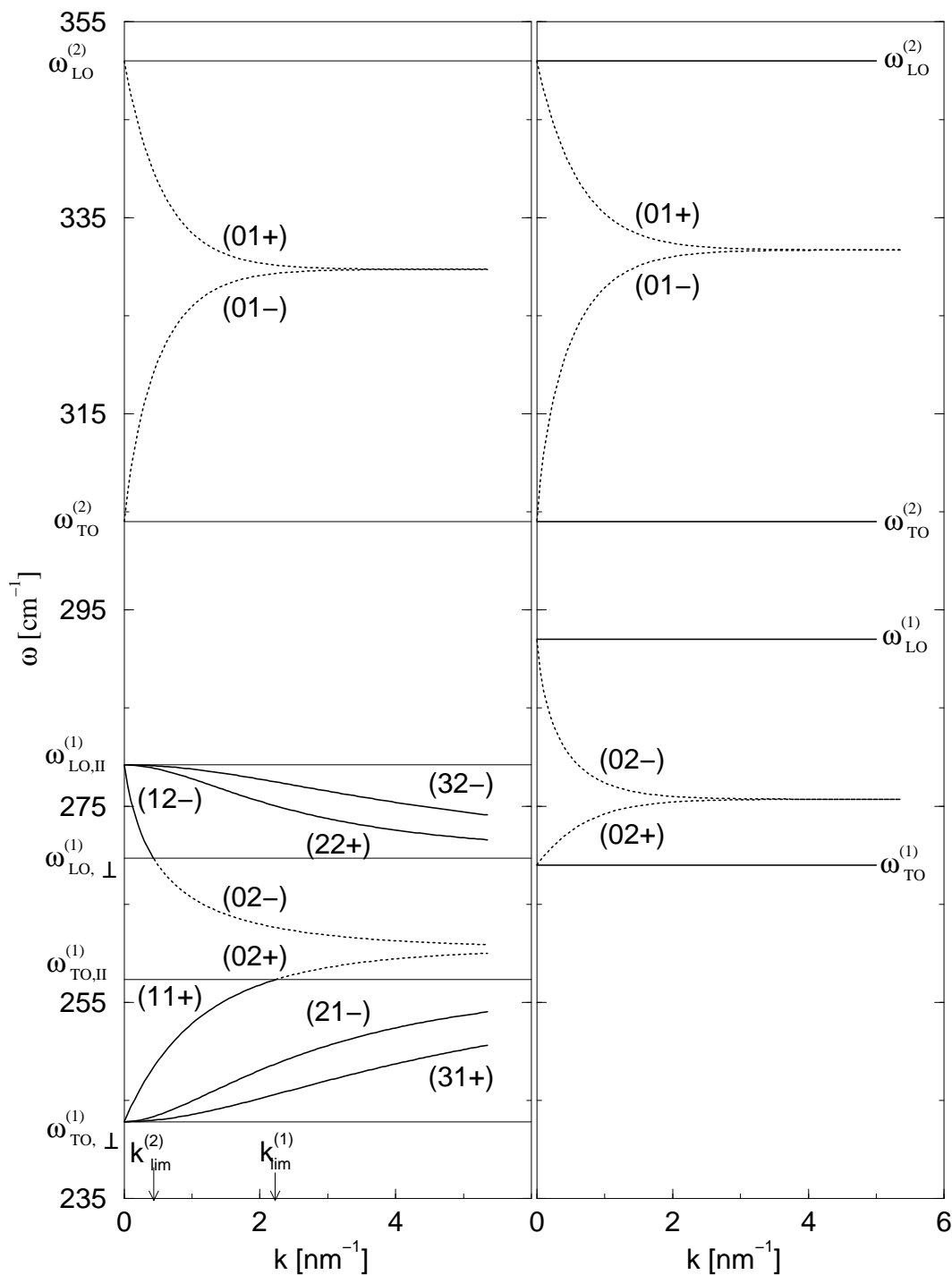


Figure 6.5: Dispersion curves of the phonon modes of the InP/GaAs/InP heterostructure grown on the face (111): interface modes, normal modes confined in the GaAs layer, and half-space modes. The thickness of the GaAs layer is  $l = 3a_1 = 1.8$  nm. Left side: the induced anisotropy of the GaAs layer is taken into account; Right side: GaAs layer is presumed isotropic.



Also, in the case of the heterostructure grown on the face (111) of the substrate, the frequencies of the interface modes and of normal modes confined in the pseudomorphic layer are shifted towards low frequencies due to lattice mismatching ( $a_{InP} > a_{GaAs}$ ). The degeneracy of the confined modes is lifted and their frequencies are distributed inside the intervals  $(\omega_{TO,\perp}^{(1)}, \omega_{TO,\parallel}^{(1)})$  and  $(\omega_{LO,\perp}^{(1)}, \omega_{LO,\parallel}^{(1)})$ . As an effect of the induced anisotropy, an electron at the interface is coupled not only with the interface modes but also with the modes confined in the uniaxial layer of the heterostructure. The coupling functions of the phonon modes  $(m, \mu, p)$ ,  $m \geq 0$ ,  $\mu = 1, 2$ ,  $p = \pm$ , with an electron at the interface are given in Fig. 6.6 and, as shown in this figure, they are also continuous at  $k = k_{\text{lim}}^{(\mu)}$ ,  $\mu = 1, 2$ . The main contribution to the electron-phonon interaction Hamiltonian is given by interface-like substrate modes, especially for small values of  $k$ , and by the modes which change their character from confined to interface modes at  $k = k_{\text{lim}}^{(\mu)}$ .

## 6.7 Summary

The dispersion laws and the normal modes of the optical phonons have been obtained in the case of a double semiconductor heterostructure having as median layer a uniaxial polar material with the optical axis directed along the normal to the interfaces. We have found, also, the form of the Hamiltonian describing electron-optical phonon interactions, thus, generalizing to this anisotropic case the results presented in Ref. [64] for isotropic heterostructures. To apply the results obtained to some particular cases we have considered, in the context of the bisotropic strain model [16], a strained semiconductor double heterostructure made by zincblende-type semiconductors, with pseudomorphic layer uniaxially distorted by the built-in strain distribution. The system cumulates both the effect of the anisotropy and that of the confinement. As a result of the anisotropy, the degeneracy of the LO and TO confined modes of an isotropic heterostructure are lifted; thus, the obtained quasilongitudinal and quasitransverse confined modes have the frequencies distributed between  $\omega_{LO,\parallel}^{(1)}$  and  $\omega_{LO,\perp}^{(1)}$  and  $\omega_{TO,\parallel}^{(1)}$  and  $\omega_{TO,\perp}^{(1)}$ , respectively. The effect of the built-in strain distribution on the confined modes leads to anisotropic features, comparable in magnitude to those found in some slightly anisotropic semiconductors as CdS and InSe. The main effect is obtained on the dispersion curves and on the electron-phonon coupling constants for the interface modes.

These results can be applied for the case of a natural anisotropic heterostructure as well as for that of a strained heterostructure. Referring to the latter case, we believe that for very narrow median layers, when discussing the effects determined by the electron-optical phonon interaction (polaron selfenergy, scattering rate), the anisotropic features of the interfacephonon spectra have to be considered in the future.

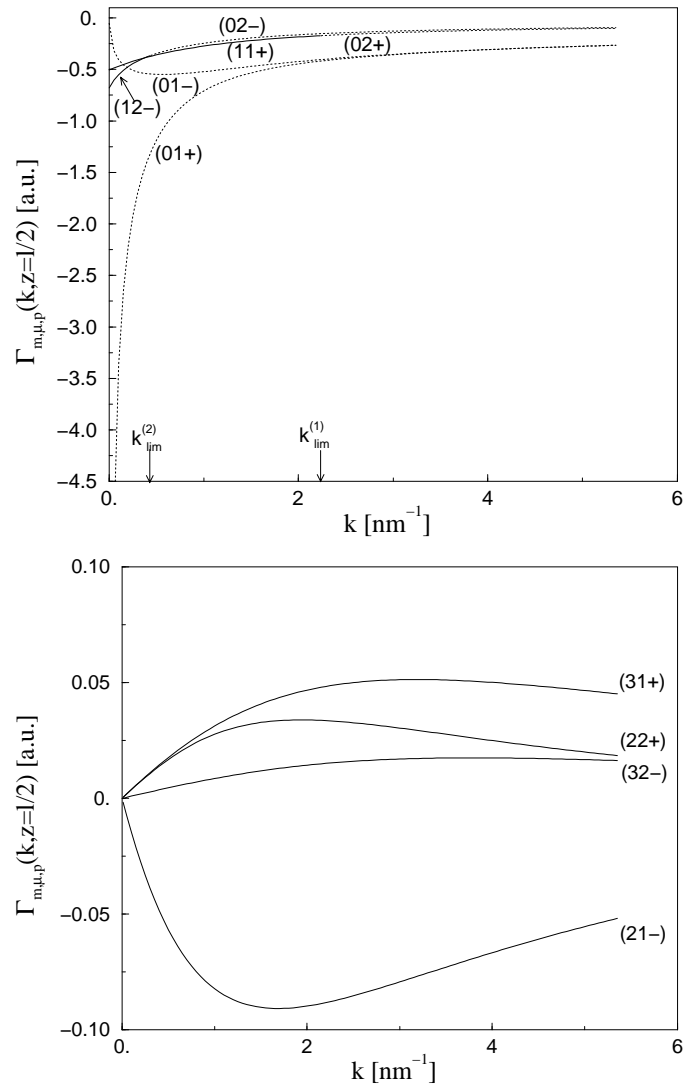


Figure 6.6: Coupling functions of the interface- and confined modes of the InP/GaAs/InP heterostructure grown on the face (111), uniaxially distorted, as a function of the 2D wave vector  $k$ . The thickness of the GaAs layer is  $l = 3a_1 = 1.8$  nm.

# Chapter 7

## Conclusions

The domain of semiconductor heterostructures, including quantum wells, quantum wires, and quantum dots, is a huge field of research, however this thesis is focused only on two aspects: i) elastic scattering of the conduction electrons in low-dimensional systems and its contribution to the transport properties; and ii) changes of the optical phonon spectra and of their coupling functions to the conduction electrons due to the existence of the interfaces and the lattice mismatching at the interfaces.

We analyze first the electronic scattering states in semiconductor nanostructures and, on this basis, the transport properties of the electron gas: conductance and capacitance. The considered systems are mesoscopic and the transport is supposed ballistic. We concentrate our attention especially on heterostructures with a very small active region (quantum systems with nanometer size) connected to contacts (probes) not only by tunneling barriers but also through a classically allowed channel for the electron motion. The physics of these systems is often dominated by resonances which are broadened due to the open character of the systems. We develop a theory of resonant transport in semiconductor nanostructures valid for all coupling regimes between the quantum system and contacts, i.e. for open systems as well as for almost-closed quantum systems. To separate weakly from strongly energy dependent contributions on the scale of the width of the resonance we employ a representation of the S matrix in terms of the R matrix. We find a simple procedure to determine the poles of the S matrix in the complex energy plane which gives the position and the width of the resonances. Numerical results show the remarkable accuracy of our procedure which is applied to a great variety of resonances types: quasibound states, Fowler-Nordheim, and Fabry-Perot resonances. In the case of separated resonances, the linearization of the weakly energy dependent part in S matrix yields an analytical expression of the line shape which is a Fano profile with a complex asymmetry parameter.

The resonant theory of transport is applied to study the conductance through a quantum dot embedded in a quantum wire and the capacitance of a 2DEG formed at the interface between the spacer layer and the blocking barrier in a MIS-type

semiconductor heterostructure. For the quantum dot the potential is decoupled in the the transport- and in the lateral directions, which means that the scattering channels are also decoupled. In the framework of the Landauer-Büttiker formalism we find two basic contributions to the conductance: first, a resonant one depending strongly on the gate voltage and second, a noncoherent background. The Fano function with a complex asymmetry parameter arises as the most general resonance line shape, under the assumption that the background can be considered constant over the entire width of the resonance. In addition, we establish a method to reconstruct S matrix from the experimental conductance data and use it to explain the measurements presented in Ref. [30]. For the second considered system we study the continuous transition from weak to strong coupling between the quantum system and contacts. Opposite to the well-known statistical limit, this transition is dominated by a single relevant resonance and there is no channel mixing. As expected, in the weak coupling regime the bound state of the quantum system turns into a narrow quasi bound state with nearly identical location in space. We find that with increasing coupling the quasibound state turns into an intermediate resonance. In contrast to the quasibound state, the intermediate resonance has the following properties: First, it is located in the space between the probes and the isolated quantum system. Second, dissimilar to the case of the quantum bound state which is coupled to the probes only via the tunneling effect, the intermediate resonance occurs in the open system where there is a channel of classically allowed motion. Third, since the decay of the intermediate resonance into the probe is classically allowed, it has the character of a Fabry-Perot resonance. Fourth, the intermediate resonance is strongly asymmetric and can be described well by a Fano distribution with a complex asymmetry parameter. Finally, if the coupling becomes too strong a resonant state cannot exist any more. Because of the excellent quantitative agreement with our theory, we can demonstrate that the transition from a quasibound state to an intermediate resonance is directly seen in capacitance experiments by Dolgoplov et al.[41].

In the second part of this work, we have discussed, in the context of the dielectric continuum model, the optical phonon modes of a slab made of an anisotropic uniaxial material and their interaction with a conduction electron. In contrast to the situation encountered in the case of an isotropic slab, for an uniaxial one with the optical axis normal to the surface new features are found: i) the degeneracy of the confined modes is lifted and these modes have dispersion. There are not purely transverse or purely longitudinal modes anymore; ii) for some anisotropic materials the existence of the surface modes depends on the value of the in-plane wave vector  $\vec{k}$ . If the whole domain of  $\vec{k}$  is analyzed, the continuous transformation of a confined mode into a surface mode can be observed. There are materials with an uniaxial anisotropy which can not support surface modes, even though the system has free surfaces; iii) an electron placed outside the slab interacts with all the confined modes; iv) for some materials it is obtained an unexpected large interaction between an electron situated on the slab surface and the first phonon mode which

belongs to the branch of the so-called quasitransverse modes. These properties are also found in the case of a double semiconductor heterostructure having as median layer a uniaxial polar material with the optical axis directed along the normal to the interfaces. To apply the results obtained to some particular cases we have considered, in the context of the bisotropic strain model, a strained semiconductor double heterostructure made by zincblende-type materials. The pseudo-morphic layer of such a heterostructure is uniaxially distorted by the built-in strain distribution. The dispersion laws and the electron-phonon coupling functions are calculated for the heterostructures presented in Ref. [17], InP/GaAs/InP grown on the faces (001) and (111).



# Appendix A

## Hamilton Operator of a Bound System

As it is specified in the second postulate of the quantum mechanics every observable of a physical system is represented by a linear self-adjoint operator which acts in the Hilbert space associated with the considered physical system [9]. So that the Hamilton operator which is associated to the energy of the system should be a self-adjoint one.

Further we analyze a 1D system for which the Hamiltonian is given by

$$H = \frac{1}{2m^*} P_z^2 + V(z), \quad (\text{A.1})$$

with  $P_z = -i\hbar d/dz$  the momentum operator and  $V(z)$  the potential energy which is supposed to be an analytical function of the  $z$ -coordinate. If the system is infinite it is demonstrate in the quantum mechanics [9] that the operators  $V(z)$  and  $P_z$  are self-adjoint and consequently  $H$  is also self-adjoint.

The situation becomes more delicate when we consider a bound system ( $z \in [z_1, z_2]$ ). The Hamilton operator (in units  $\hbar^2/2m^*$ ) is defined in the Hilbert space  $\mathcal{H} = L^2(z_1, z_2)$  by

$$(\bar{H}\psi)(z) = -\frac{d^2\psi}{dz^2} + \mathcal{V}(z). \quad (\text{A.2})$$

with the domain

$$\mathcal{D}(\bar{H}) = \left\{ \psi \in \mathcal{H} : \psi, \psi' \text{ absolutely continuous, } \int_{z_1}^{z_2} dz |\psi(z)|^2 < \infty, \right. \\ \left. \int_{z_1}^{z_2} dz |\psi'(z)|^2 < \infty, \int_{z_1}^{z_2} dz |\psi''(z)|^2 < \infty, \text{ boundary condition} \right\} \quad (\text{A.3})$$

$\mathcal{D}(\bar{H})$  contains the set of infinitely differentiable functions with compact support and therefore is a dense domain in  $L^2(z_1, z_2)$  [9]. Because the system is bound the wave functions should satisfy a boundary condition and we want to establish what kind

of boundary conditions are compatible with the property of the Hamilton operator to be Hermitian.

In this point it is essential to emphasize the difference between a symmetrical operator,

$$\langle \psi | \bar{H} | \phi \rangle = \langle \bar{H} \psi | \phi \rangle \quad \Leftrightarrow \quad \mathcal{D}(\bar{H}) \subseteq \mathcal{D}(\bar{H}^\dagger) \quad (\text{A.4})$$

and a self-adjoint one,

$$\mathcal{D}(\bar{H}^\dagger) \subseteq \mathcal{D}(\bar{H}) \quad \text{and} \quad \mathcal{D}(\bar{H}) \subseteq \mathcal{D}(\bar{H}^\dagger). \quad (\text{A.5})$$

For two arbitrary wave functions  $\psi$  and  $\phi$  in  $\mathcal{D}(\bar{H})$  the matrix element  $\langle \psi | \bar{H} | \phi \rangle$  is defined as

$$\langle \psi | \bar{H} | \phi \rangle = \int_{z_1}^{z_2} dz \psi^*(z) \left( -\frac{d^2\phi}{dz^2} + \mathcal{V}(z)\phi(z) \right). \quad (\text{A.6})$$

Using this definition and performing an integration by parts we find that the Hamilton operator  $\bar{H}$  is symmetric if and only if the condition

$$\left[ \psi^*(z) \frac{d\phi}{dz} - \frac{d\psi^*}{dz} \phi(z) \right] \Big|_{z=z_1} = \left[ \psi^*(z) \frac{d\phi}{dz} - \frac{d\psi^*}{dz} \phi(z) \right] \Big|_{z=z_2} \quad (\text{A.7})$$

is satisfied for each pair of functions  $\psi, \phi \in \mathcal{D}(\bar{H})$ .

Further we define the domain of the operator  $\bar{H}$  as the set of the wave functions in  $L^2(z_1, z_2)$  which are absolutely continuous and bound, with the first derivative absolutely continuous and bound, and any two wave functions of this set must verify the boundary condition (A.7). The next step is to show that  $\bar{H}$  with the imposed boundary condition is self-adjoint, i.e. to demonstrate that  $\mathcal{D}(\bar{H}^\dagger) \subseteq \mathcal{D}(\bar{H})$ . To this end consider a function  $\psi \in \mathcal{D}(\bar{H}^\dagger)$  and define  $\psi_1 = \bar{H}^\dagger \psi$ ; then

$$\langle \psi | \bar{H} | \phi \rangle = \langle \psi_1 | \phi \rangle, \quad \forall \phi \in \mathcal{D}(\bar{H}) \quad (\text{A.8})$$

can be written as

$$\langle \psi | \bar{H} | \phi \rangle = \int_{z_1}^{z_2} dz \psi_1^*(z) \phi(z) = \int_{z_1}^{z_2} dz \left[ \frac{d}{dz} \left( \int_{z_1}^z dz' \psi_1(z') + c_1 \right) \right]^* \phi(z), \quad (\text{A.9})$$

where  $c_1$  is an arbitrary constant. Taking into account that  $\phi(z)$  is an infinitely differentiable function and integrating by parts, we obtain

$$\langle \psi | \bar{H} | \phi \rangle = \phi(z_2) \psi_2^*(z_2) - \int_{z_1}^{z_2} dz \psi_2^*(z) \frac{d\phi}{dz}, \quad (\text{A.10})$$

where  $\psi_2(z) \stackrel{\text{def}}{=} \int_{z_1}^z dz' \psi_1(z')$ . We write the integral on the right side of the above equation as in Eq. (A.9) and finally find

$$\langle \psi | \bar{H} | \phi \rangle = \phi(z_2) \psi_2^*(z_2) - \frac{d\phi}{dz} \Big|_{z=z_2} \int_{z_1}^{z_2} dz \psi_2^*(z) - \int_{z_1}^{z_2} dz \int_{z_1}^z dz' \psi_2^*(z') \left( -\frac{d^2\phi}{dz^2} \right). \quad (\text{A.11})$$



On the other hand, using the definition (A.6) of  $\langle \psi | \bar{H} | \phi \rangle$  and writing in this expression the matrix element of  $\mathcal{V}$  in a similar form as  $\langle \psi_1 | \phi \rangle$  it results

$$\begin{aligned} \langle \psi | \bar{H} | \phi \rangle &= \int_{z_1}^{z_2} dz \psi^*(z) \left( -\frac{d^2\phi}{dz^2} \right) + \phi(z_2) \int_{z_1}^{z_2} dz \mathcal{V}(z) \psi^*(z) \\ &\quad - \left. \frac{d\phi}{dz} \right|_{z=z_2} \int_{z_1}^{z_2} dz \int_{z_1}^z dz' \mathcal{V}(z') \psi^*(z') + \int_{z_1}^{z_2} dz \int_{z_1}^z dz' \int_{z_1}^{z'} dz'' \mathcal{V}(z'') \psi^*(z'') \frac{d^2\phi}{dz^2}. \end{aligned} \quad (\text{A.12})$$

Equating the two expressions (A.11) and (A.12) of  $\langle \psi | \bar{H} | \phi \rangle$  we obtain

$$\begin{aligned} &\int_{z_1}^{z_2} dz \left[ \psi(z) + \int_{z_1}^z dz' \int_{z_1}^{z'} dz'' [\psi_1(z'') - \mathcal{V}(z'')\psi(z'')] \right]^* \left( -\frac{d^2\phi}{dz^2} \right) \\ &= \phi(z_2) \int_{z_1}^{z_2} dz [\psi_1^*(z) - \mathcal{V}(z)\psi^*(z)] - \left. \frac{d\phi}{dz} \right|_{z=z_2} \int_{z_1}^{z_2} dz \int_{z_1}^z dz' [\psi_1^*(z') - \mathcal{V}(z')\psi^*(z')] \end{aligned} \quad (\text{A.13})$$

Since  $\phi \in \mathcal{D}(\bar{H})$  and  $\mathcal{D}(\bar{H})$  is dense in  $L^2(z_1, z_2)$ , the first factor of the integrand in (A.13) must be a linear function of  $z$  and we can write for points between  $z_1$  and  $z_2$

$$\psi(z) = c_1 + c_2(z - z_2) - \int_{z_1}^z dz' \int_{z_1}^{z'} dz'' [\psi_1(z'') - \mathcal{V}(z'')\psi(z'')] \quad (\text{A.14})$$

with  $c_1$  and  $c_2$  arbitrary constants. From (A.14) we identify

$$\frac{d\psi}{dz} = c_2 - \int_{z_1}^z dz' [\psi_1(z') - \mathcal{V}(z')\psi(z')] \quad (\text{A.15})$$

and

$$\frac{d^2\psi}{dz^2} = -\psi_1(z) + \mathcal{V}(z)\psi(z) \quad \Leftrightarrow \quad \psi_1(z) = (\bar{H}\psi)(z). \quad (\text{A.16})$$

The wave function defined by (A.14) should also satisfy Eq. (A.13) which can be written into the equivalent form

$$\left[ \psi^*(z) \frac{d\phi}{dz} - \frac{d\psi^*}{dz} \phi(z) \right] \Big|_{z=z_1} = \left[ \psi^*(z) \frac{d\phi}{dz} - \frac{d\psi^*}{dz} \phi(z) \right] \Big|_{z=z_2} \quad \forall \phi \in \mathcal{D}(\bar{H}) \quad (\text{A.17})$$

using Eqs. (A.14-A.16). This relation is identical with Eq. (A.7) which defines the boundary condition of the wave functions from  $\mathcal{D}(\bar{H})$ . With other words,  $\psi(z)$  from  $\mathcal{D}(\bar{H}^\dagger)$  must verify the condition imposed on the wave functions from  $\mathcal{D}(\bar{H})$ . Taking also into account the relation  $\psi_1(z) = (\bar{H}\psi)(z)$  deduced above we can conclude that  $\mathcal{D}(\bar{H}^\dagger) \subseteq \mathcal{D}(\bar{H})$ . So it is demonstrated that considering the Hilbert space

$\mathcal{H} = L^2(z_1, z_2)$  the operator  $\bar{H}$  defined by formula (A.2) and the boundary condition (A.7) is self-adjoint.

Two interesting properties follow directly from the boundary condition. First, if  $\psi \in \mathcal{D}(\bar{H})$  then  $\psi^*$  belongs also to the domain of  $\bar{H}$ ; Second, if the definition interval is symmetric ( $z_1 = -d, z_2 = d$ ) and the Hamilton operator is also symmetric on this interval,  $\bar{H}(z) = \bar{H}(-z)$ , then  $\psi(-z) \in \mathcal{D}(\bar{H})$  for any  $\psi(z)$  from  $\mathcal{D}(\bar{H})$ .

The relation (A.7) gives the most general boundary condition imposed on the wave function of a bound system, but in practice restrictions of this condition are usually used. The most obvious choice [96] is

$$\begin{pmatrix} \left. \frac{d\psi}{dz} \right|_{z=z_1} \\ \left. \frac{d\psi}{dz} \right|_{z=z_2} \end{pmatrix} = A \begin{pmatrix} \psi(z_1) \\ \psi(z_2) \end{pmatrix}, \quad (\text{A.18})$$

where  $A$  is a  $2 \times 2$  matrix with the property  $A_{ij} = (-1)^{i+j} A_{ji}$ ,  $i, j = 1, 2$ . This form of the  $A$  matrix follows direct from the condition (A.7); two arbitrary functions  $\psi$  and  $\phi$  which satisfy the boundary condition (A.18) should also verify the relation (A.7) and it results  $A_{ij} = (-1)^{i+j} A_{ji}^*$ ,  $i, j = 1, 2$ . The property of  $\mathcal{D}(\bar{H})$  to contain  $\psi$  and  $\psi^*$  leads to  $A_{12} = A_{12}^*$ . In addition, for a symmetrical operator,  $\bar{H}(z) = \bar{H}(-z)$ ,  $\forall z \in [-d, d]$ ,  $\psi(z)$  and  $\psi(-z)$  belong both to  $\mathcal{D}(\bar{H})$  and this fact imposes a new restriction on the  $A$  matrix:  $A_{11} = -A_{22}$ .

The definition of the matrix  $A$  ensures the symmetry of the operator  $\bar{H}$ . In order to prove that  $\bar{H}$  is self-adjoint we have only to show that a wave function  $\psi \in \mathcal{D}(\bar{H}^\dagger)$  satisfies also the boundary condition (A.18). If  $\psi \in \mathcal{D}(\bar{H}^\dagger)$  then it verifies the relation (A.17) for each  $\phi \in \mathcal{D}(\bar{H})$ . Taking into account the boundary condition (A.18) satisfied by  $\phi$  and the property of  $A$ , Eq. (A.17) becomes

$$\phi(z_2) \left[ \left. \frac{d\psi}{dz} \right|_{z=z_2} - A_{21}\psi(z_1) - A_{22}\psi(z_2) \right]^* - \phi(z_1) \left[ \left. \frac{d\psi}{dz} \right|_{z=z_1} - A_{11}\psi(z_1) - A_{12}\psi(z_2) \right]^* = 0. \quad (\text{A.19})$$

Because  $\phi$  is an arbitrary function in  $\mathcal{D}(\bar{H})$  the coefficients of  $\phi(z_2)$  and  $\phi(z_1)$  should be zero. Thus  $\psi$  satisfies also the condition (A.18) and that implies  $\mathcal{D}(\bar{H}^\dagger) \subset \mathcal{D}(\bar{H})$ .

As a particular case we can obtain the well-known von Neumann boundary conditions,

$$\left. \frac{d\psi}{dz} \right|_{z=z_1} = 0, \quad \left. \frac{d\psi}{dz} \right|_{z=z_2} = 0. \quad (\text{A.20})$$

for a particular choice of  $A$  for which

$$A \begin{pmatrix} \psi(z_1) \\ \psi(z_2) \end{pmatrix} \rightarrow 0. \quad (\text{A.21})$$

The last conditions lead to

$$\psi(z_2) = \frac{A_{11}}{A_{12}}\psi(z_1), \quad (\text{A.22})$$

$$0 = A_{11}A_{22} + A_{12}^2. \quad (\text{A.23})$$

$\psi(z_1)$  is usually fixed by the normalization condition. The above relations are fulfilled for each real value of  $A_{11}/A_{12}$  so that there exists a matrix  $A$  for which the Hamilton operator with von Neumann boundary conditions is self-adjoint. Even in the case of a symmetrical operator ( $\bar{H}(z) = \bar{H}(-z)$ ,  $z \in [-d, d]$ ) such a matrix exists,  $A_{11} = -A_{22} = \pm A_{12}$ .

The most important advantage of using the boundary conditions (A.20) is that they allow for a nondegenerate energy spectrum of the Hamilton operator. We suppose that there are two eigenfunctions,  $\psi$  and  $\phi$  corresponding to the same eigenvalue of  $\bar{H}$ ,

$$(\bar{H}\psi)(z) = \epsilon\psi(z) \quad (\text{A.24})$$

and

$$(\bar{H}\phi)(z) = \epsilon\phi(z). \quad (\text{A.25})$$

Multiplying the first equation by  $\phi^*(z)$  and the complex conjugate of the second one by  $\psi(z)$  and subtracting one from the other it results

$$\phi^*(z) \left( -\frac{d^2\psi}{dz^2} \right) - \psi(z) \left( -\frac{d^2\phi^*}{dz^2} \right) = 0 \quad (\text{A.26})$$

or

$$\frac{d}{dz} \left[ -\phi^*(z) \frac{d\psi}{dz} + \psi(z) \frac{d\phi^*}{dz} \right] = 0. \quad (\text{A.27})$$

Performing an integration of the above relation we find

$$-\phi^*(z) \frac{d\psi}{dz} + \psi(z) \frac{d\phi^*}{dz} = -\phi^*(z_1) \frac{d\psi}{dz} \Big|_{z=z_1} + \psi(z_1) \frac{d\phi^*}{dz} \Big|_{z=z_1} \quad (\text{A.28})$$

The quantity on the right side of this equation vanishes due to the boundary conditions and it follows directly that

$$\psi(z) = c\phi^*(z) \quad (\text{A.29})$$

with  $c$  an arbitrary constant. Thus the two wave functions  $\psi$  and  $\phi$  correspond to the same physical states and consequently the energy level  $\epsilon$  is nondegenerate.



# Appendix B

## Unitarity of the $\tilde{\mathbf{S}}$ -matrix

From Eq. (4.19) we obtain for all energies:

$$\begin{aligned} \tilde{\mathbf{S}}(\epsilon)\tilde{\mathbf{S}}^\dagger(\epsilon) &\simeq \tilde{\mathbf{S}}_{bg}\tilde{\mathbf{S}}_{bg}^\dagger\frac{e^2}{e^2+1} + \tilde{\mathbf{S}}(\epsilon_0)\tilde{\mathbf{S}}^\dagger(\epsilon_0)\frac{1}{e^2+1} \\ &\quad -i\left[\tilde{\mathbf{S}}_{bg}\tilde{\mathbf{S}}^\dagger(\epsilon_0) - \tilde{\mathbf{S}}(\epsilon_0)\tilde{\mathbf{S}}_{bg}^\dagger\right]\frac{e}{e^2+1}, \end{aligned} \quad (\text{B.1})$$

where  $e = 2(\epsilon - \epsilon_0)/\Gamma$ . Here

$$\tilde{\mathbf{S}}(\epsilon_0)\tilde{\mathbf{S}}^\dagger(\epsilon_0) = \mathbf{1} \quad (\text{B.2})$$

is exactly fulfilled because the linearization is exact at the real energy  $\epsilon_0$ . Taking into account the definition (4.18) of  $\tilde{\mathbf{S}}_{bg}$  we find the first step in

$$\left[\tilde{\mathbf{S}}_{bg}\tilde{\mathbf{S}}^\dagger(\epsilon_0) - \tilde{\mathbf{S}}(\epsilon_0)\tilde{\mathbf{S}}_{bg}^\dagger\right] = \frac{i\Gamma/2 \frac{d}{d\epsilon}(\mathbf{Z}_\lambda\mathbf{Z}_\lambda^\dagger)\big|_{\epsilon=\epsilon_0}}{|\epsilon_0 - \epsilon_\lambda - \bar{\mathcal{E}}_\lambda(\epsilon_0)|^2} = 0, \quad (\text{B.3})$$

and the second step is obtained differentiating the relation (4.10) with respect to the energy. The condition (B.3) is sufficient for the unitarity of  $\tilde{\mathbf{S}}$  in first order in  $e$ . Thus our linearization of  $\mathbf{Z}_\lambda$  and  $\bar{\mathcal{E}}_\lambda$  leads to a consistent theory.

In general the symmetrical complex matrix  $\tilde{\mathbf{S}}_{bg}$  can be written in the form

$$\tilde{\mathbf{S}}_{bg} = \begin{pmatrix} \frac{i}{q_R}(\tilde{\mathbf{S}}(\epsilon_0))_{11} & \frac{i}{q}(\tilde{\mathbf{S}}(\epsilon_0))_{12} \\ \frac{i}{q}(\tilde{\mathbf{S}}(\epsilon_0))_{12} & \frac{i}{q'_R}(\tilde{\mathbf{S}}(\epsilon_0))_{22} \end{pmatrix} \quad (\text{B.4})$$

using the (complex) asymmetry parameters for transmission,  $q$  defined in (4.21) and for reflection,  $q_R$  and  $q'_R$ . In the limit of our linear approximation  $\tilde{\mathbf{S}}_{bg}$  has to satisfy the Hermitian condition (B.3) and thus only three real parameters can be chosen freely, for example  $\text{Im}(1/q_R)$ ,  $\text{Re}(1/q)$  and  $\text{Im}(1/q)$ :

$$\tilde{\mathbf{S}}_{bg} = \frac{i}{q}\tilde{\mathbf{S}}(\epsilon_0) - \begin{pmatrix} \tau(\tilde{\mathbf{S}}(\epsilon_0))_{11} & 0 \\ 0 & -\tau^*(\tilde{\mathbf{S}}(\epsilon_0))_{22} \end{pmatrix}, \quad (\text{B.5})$$

with

$$\tau = \text{Im} \left( \frac{1}{q_R} \right) - \text{Im} \left( \frac{1}{q} \right) + \frac{i}{1 - T(\epsilon_0)} \text{Re} \left( \frac{1}{q} \right) \quad (\text{B.6})$$

and  $T(\epsilon_0)$  is the transmission probability at the energy  $\epsilon_0$ . As can be seen from Eq. (4.12)  $\epsilon_0$  is only an approximative value of the resonance energy so that  $T(\epsilon_0) < 1$  and  $\tau$  has no singularity.

Using Eq. (B.3) we obtain directly Eq. (4.28) from Eq. (B.1) if we identify the first term on the right hand side of (B.1) with  $\delta e^2/(e^2 + 1)$  in (4.28). Using (B.5) we obtain for the matrix elements of  $\delta$

$$\delta_{11} = [1 - T(\epsilon_0)] \left| \frac{i}{q} - \tau \right|^2 + T(\epsilon_0) \left| \frac{i}{q} \right|^2, \quad (\text{B.7})$$

$$\delta_{22} = [1 - T(\epsilon_0)] \left| \frac{i}{q^*} - \tau \right|^2 + T(\epsilon_0) \left| \frac{i}{q} \right|^2, \quad (\text{B.8})$$

$$\delta_{12} = 2\tau \text{Im} \left( \frac{1}{q} \right) (\tilde{\mathbf{S}}(\epsilon_0))_{11} (\tilde{\mathbf{S}}(\epsilon_0))_{12}^*. \quad (\text{B.9})$$

If we artificially impose the unitarity condition on  $\tilde{\mathbf{S}}_{bg}$  ( $\delta \rightarrow \mathbf{1}$ ) there remains only one free variable which describes the background matrix. This can be chosen as the real Fano asymmetry parameter denoted with  $q_r$ :

$$\tilde{\mathbf{S}}_{bg} = \frac{i}{q_r} \tilde{\mathbf{S}}(\epsilon_0) - \begin{pmatrix} \tau_r (\tilde{\mathbf{S}}(\epsilon_0))_{11} & 0 \\ 0 & -\tau_r^* (\tilde{\mathbf{S}}(\epsilon_0))_{22} \end{pmatrix}, \quad (\text{B.10})$$

with

$$\tau_r = \frac{1}{1 - T(\epsilon_0)} \left[ \pm \sqrt{1 - T(\epsilon_0) \left( 1 + \frac{1}{q_r^2} \right)} + \frac{i}{q_r} \right]. \quad (\text{B.11})$$

The real parameter  $q_r$  should satisfy the inequality  $T(\epsilon_0)(1 + 1/q_r^2) \leq 1$ .

We can also remark here that assuming in Eq. (4.19) the background contribution to the  $S$ -matrix as zero the relation (B.1) becomes:

$$\tilde{\mathbf{S}}(\epsilon) \tilde{\mathbf{S}}^\dagger(\epsilon) = \frac{\mathbf{1}}{e^2 + 1}. \quad (\text{B.12})$$

The unitarity of the scattering matrix (2.55) restricts strongly ( $e^2/(e^2 + 1) \ll 1$ ) the domain inside which the common Wigner-Breit profile yields a good description of the transmission even for extremely narrow and isolated peaks.

Often the background matrix  $\tilde{\mathbf{S}}_{bg}$  is assumed to be absent leading to a symmetrical Wigner-Breit shape of the transmission peak[58].

# Bibliography

- [1] T. Ando, Y. Arakawa, K. Furuya, S. Komiyama, H. Nakashima (Eds.), *Mesoscopic Physics and Electronics*, Springer Verlag, Berlin, 1998.
- [2] D. K. Ferry and S. M. Goodnick, *Transport in Nanostructures*, Cambridge University Press, Cambridge 1999.
- [3] Z. I. Alferov, *Nobel Lecture: The double heterostructure concept and its applications in physics, electronics, and technology*, Rev. Mod. Phys. **73**, 767 (2001).
- [4] H. Kroemer, *Nobel Lecture: Quasielectric fields and band offsets: teaching electrons new tricks*, Rev. Mod. Phys. **73**, 783 (2001).
- [5] H. L. Stormer, *Nobel Lecture: The fractional quantum Hall effect*, Rev. Mod. Phys. **71**, 875 (1999).
- [6] L. L. Chang and K. Ploog (Eds.), *Molecular Beam Epitaxy and Heterostructures*, M. Nijhof, Dordrecht, The Netherlands 1985.
- [7] M. L. Goldberger and K. Watson, *Collision Theory*, John Wiley and sons, New York, 1964.
- [8] A. Bohm, *Quantum Mechanics*, Springer, New York, 1993, Chap. 18 *Resonance Phenomena*.
- [9] A. Galindo and P. Pascual, *Quantum Mechanics I*, Springer Verlag, Berlin, 1990, Cap. 2.
- [10] L. Smrcka, *R-matrix and the coherent transport in mesoscopic systems*, Superlattices Microstruct. **8**, 221 (1990).
- [11] R. A. Jalabert, A. D. Stone, and Y. Alhassid, *Statistical theory of Coulomb blockade oscillations: Quantum chaos in quantum dots*, Phys. Rev. Lett. **68**, 3468 (1992); H. Fukuyama and T. Ando (Eds.) *Transport phenomena in Mesoscopic Systems*, Springer-Verlag, Berlin, 1992, p. 39.
- [12] U. Wulf, J. Kucera, P. N. Racec, and E. Sigmund, *Transport through quantum systems in the R-matrix formalism*, Phys. Rev. B **58**, 16209 (1998).

- [13] E. R. Racec and U. Wulf, *Resonant quantum transport in semiconductor nanostructures*, Phys. Rev. B **64**, 115318 (2001).
- [14] P. N. Racec, E. R. Racec, and U. Wulf, *Capacitance in open quantum structures*, Phys. Rev. B **65**, 193314 (2002).
- [15] M. Born and K. Huang, *Dynamical Theory of Crystal Lattices*, Clarendon, Oxford, 1968.
- [16] E. Anastassakis, *Strained superlattices and heterostructures: Elastic consideration*, J.Appl.Phys. **68**, 4561 (1990).
- [17] M. E. Pistol, M. Gerling, D. Hessman and L. Samuelson, *Properties of thin strained layers of GaAs grown on InP*, Phys.Rev. B **45**, 3628 (1992).
- [18] N. W. Ashcroft and N. D. Mermin, *Solid State Physics*, CBS Publishing Asia Ltd., Philadelphia, 1988.
- [19] C. Weisbuch and B. Vinter, *Quantum Semiconductor Structures*, Academic Press, Inc., Boston, 1991.
- [20] T. Ando, A. B. Fowler, and F. Stern, *Electronic properties of two-dimensional systems*, Rev. Mod. Phys. **54**, 437-672 (1982).
- [21] T. Schmidt, R.J. Haug, K. v. Klitzing, A. Förster and H. Lüth, *Single-electron transport in small resonant-tunneling diodes with various barrier-thickness asymmetries*, Phys. Rev. B **55**, 2230, (1997).
- [22] S. Tarucha, D. G. Austing, T. Honda, R. J. van der Hage, and L. P. Kouwenhoven, *Shell Filling and Spin Effects in a Few Electron Quantum Dot*, Phys. Rev. Lett. **77**, 3613, (1996).
- [23] R. C. Ashoori, H. L. Stoermer, J. S. Weiner, L. N. Pfeiffer, K. W. Baldwin, and K. W. West, *N-electron ground state energies of a quantum dot in magnetic field*, Phys. Rev. Lett. **71**, 613 (1993); R. C. Ashoori, *Electrons in artificial atoms*, Nature (London) **379**, 413 (1996).
- [24] B. J. van Wees, H. van Houten, C. W. Beenakker, and J. G. Williamson, L. P. Kouwenhoven and D. van der Marel, C. T. Foxton, *Quantized conductance of point contacts in two-dimensional electron gas*, Phys. Rev. Lett. **60**, 848 (1988).
- [25] M.J. Kelly, *Low-dimensional Semiconductors*, Clarendon Press, Oxford, 1995.
- [26] D. Goldhaber-Gordon, H. Shtrikman, D. Mahalu, D. Abusch-Magder, U. Meirav, and M. A. Kastner, *Kondo effect in a single-electron transistor*, Nature, **391**, 156 (1998); D. Goldhaber-Gordon, J. Göres, and M. A. Kastner,



- H. Shtrikman, D. Mahalu, and U. Meirav, *From the Kondo Regime to the Mixed-Valence Regime in a Single-Electron Transistor*, Phys. Rev. Lett. **81**, 5225 (1998).
- [27] Y. Alhassid, *The statistical theory of quantum dots*, Rev. Mod. Phys. **72**, 895 (2000).
- [28] P.N. Racec, Ph.D. Thesis, University of Technology Cottbus, 2002.
- [29] G.Bastard, J.A.Brum, and R.Ferreira, *Electronic States in semiconductor Heterostructures*, Sol.State Phys. **44**, 229 (1991).
- [30] J. Göres, D. Goldhaber-Gordon, S. Heemeyer, and M.A. Kastner, H. Shtrikman, D. Mahalu, and U. Meirav, *Fano resonances in electronic transport through a single-electron transistor*, Phys. Rev. B **62**, 2188 (2000).
- [31] R. Landauer, *Spatial variation of currents and fields due to localized scatterers in metallic conduction*, IBM J. Res. Develop. **1**, 223 (1957); R. Landauer, *Electrical transport in open and closed systems*, Z. Phys. **B 68**, 217 (1987); D. S. Fisher and P. A. Lee, *Relation between conductivity and transmission matrix*, Phys. Rev. **B 23**, 6851 (1981); M. Büttiker, *Four-Terminal Phase-Coherent Conductance*, Phys. Rev. Lett. **57**, 1761 (1986); M. Büttiker, *Basic concepts in quantum and stochastic transport - preface*, IBM J. Res. Develop. **32**, 317 (1988); A. D. Stone and A. Szafer, *What is measured when you measure a resistance - the Landauer formula revisited*, IBM J. Res. Develop. **32**, 384 (1988).
- [32] A.G.Sitenko, *Lectures in scattering theory*, Pergamon Press, Oxford 1971, p. 32
- [33] E. P. Wigner and L. Eisenbud, *Higher Angular Momenta and Long Range Interaction in Resonance Reactions*, Phys. Rev. **72**, 29 (1947).
- [34] A. M. Lane and R. G. Thomas, *R-Matrix Theory of Nuclear Reactions*, Rev. Mod. Phys. **30**, 257 (1958).
- [35] M. Büttiker, *Scattering theory of current and intensity noise correlations in conductors and wave guides*, Phys. Rev. B **46**, 12485 (1992).
- [36] Albert Messiah, *Quantum Mechanics*, Dover Publications, Inc., Mineola, New York 1999, pp. 179-188.
- [37] M. Büttiker, Y. Imry, R. Landauer, and S. Pinhas, *Generalized many-channel conductance formula with application to small rings*, Phys. Rev. B **31**, 6207 (1985).
- [38] F. Mandl, *Statistical Physics*, John Wiley & Sons, New York, 1988.

- [39] M. A. Kastner, *Artificial atoms*, Phys. Today **46**, 24 (1993); D. Goldhaber-Gordon, J. Göres, M. A. Kastner, H. Shtrikman, D. Mahalu, and U. Meirav, *From the Kondo Regime to the Mixed-Valence Regime in a Single-Electron Transistor*, Phys. Rev. Lett. **81**, 5225 (1998).
- [40] P. N. Racec, E. R. Racec, and U. Wulf, *Capacitance theory of open quantum systems with classical contacts*, Computational Material Science **21**, 475 (2001).
- [41] V.T. Dolgoplov et al., *Nonlinear Screening in Two-Dimensional Electron System*, Phys. Low-Dim. Struct. **6**, 1 (1996).
- [42] R. E. Cavicchi and R. H. Silsbee, *Dynamics of tunneling to and from small metal particles*, Phys. Rev. **B 37**, 706 (1988).
- [43] V. I. Kukuljin, V. M. Krasnopolsky, J. Horacek, *Theory of Resonances - Principles and Applications*, Kluwer Academic Publishers, Dordrecht, 1989.
- [44] Y. V. Fyodorov and H. J. Sommers, *Statistics of resonance poles, phase shifts and time delays in quantum chaotic scattering: Random matrix approach for systems with broken time-reversal invariance*, J. Math. Phys. **38**, 1918 (1997).
- [45] E. Tekman and P. F. Bagwell, *Fano resonances in quasi-one-dimensional electron waveguides*, Phys. Rev. B **48**, 2553 (1993).
- [46] P. F. Bagwell, *Evanescent modes and scattering in quasi-one-dimensional wire*, Phys. Rev. B **41**, 10354 (1993); C. S. Kim, A. M. Satanin, Y. S. Joe, and R. M. Cosby, *Resonant tunneling in a quantum waveguide: Effect of a finite-size attractive impurity*, Phys. Rev. B **60**, 10962 (1999); C. S. Kim and A. M. Satanin, *Tunneling through a quantum channel with impurities: An exactly solvable model*, Physica E **4**, 211 (1999).
- [47] R. C. Bowen, W. R. Frensley, G. Klimeck, and R. Lake, *Transmission resonances and zeros in multiband model*, Phys. Rev. B **52**, 2754 (1995).
- [48] W. Porod, Z. Shao, and C. S. Lent, *Resonance-antiresonance line shape for transmission in quantum waveguides with resonantly coupled cavities*, Phys. Rev. B **48**, 8495 (1993); Z. Shao, W. Porod, and S. Lent, *Transmission resonances and zeros in quantum waveguide systems with attached resonators*, Phys. Rev. B **49**, 7453 (1994); R. Akis, P. Vasilopoulos, and P. Debray, *Bound states and transmission antiresonances in parabolically confined cross structures: Influence of weak magnetic fields*, Phys. Rev. B **56**, 9594 (1997); K. Nikolic and R. Sordan, *Electronic transport in quantum waveguide systems with attached stubs*, Phys. Rev. B **58**, 9631 (1998); H. Chen and Y. Shi, *Antiresonances modulated by magnetic flux in an Aharonov-Bohm ring*, Physics Letters A **262**, 76 (1999);

- [49] A. Yacoby, M. Heiblum, D. Mahalu, and H. Shtrikman, *Coherence and Phase Sensitive Measurements in a Quantum Dot*, Phys. Rev. Lett. **74**, 4047 (1995); C. Ryu and S. Y. Cho, *Phase evolution of the transmission coefficient in an Aharonov-Bohm ring with Fano resonance*, Phys. Rev. B **58**, 3572 (1998).
- [50] J. U. Nöckel and A. D. Stone, *Fano resonances in transport across a quantum well in a tilted magnetic field*, Phys.Rev. B **51**, 17219 (1995).
- [51] J. U. Nöckel and A. D. Stone, *Resonance line shape in quasi-one-dimensional scattering* , Phys. Rev. B **50** 17415 (1994).
- [52] H. Mizuta and T. Tanoue, *The Physics and Applications of Resonant Tunneling Diodes*, Cambridge University Press, Cambridge, 1995, Chapt. 2; C. Presilla and J. Sjöstrand, *Transport properties in resonant tunneling heterostructures*, J. Math. Phys. **37**, 4816 (1996).
- [53] U. Fano, *Effects of Configuration Interaction on Intensities and Phase Shifts*, Phys. Rev. **124**, 1866 (1961).
- [54] G. Abstreiter, M. Cardona, and A. Pinczuk, in *Light Scattering in Solids*, edited by M. Cardona and G. Güntherodt , Topics in Applied Physics Vol. 54 (Springer, Berlin, 1984), p.127; K. J. Jin, S. H. Pan, and G. Z. Yang, *Fano effect of resonant Raman scattering in semiconductor quantum well*, Phys. Rev. B **50**, 8584 (1994).
- [55] G. S. Agarwal, S. L. Haan, and J. Cooper, *Radiative decay of autoionizing states in laser fields. I. General Theory* , Phys. Rev. A **29**, 2552 (1984).
- [56] M. Büttiker, *Negative resistance fluctuations at resistance minimum in narrow quantum Hall conductors*, Phys. Rev. B **38**, 12724 (1988).
- [57] L. D. Landau and E. M. Lifschitz, *Quantum Mechanics (Non-Relativistic Theory)*, Pergamon, Oxford, 1977.
- [58] Y. Alhassid and H. Attias, *Universal correlations of Coulomb blockade conductance peaks and the rotation scaling in quantum dots* , Phys. Rev. B **54**, 2696 (1996); Y. Alhassid and H. Attias, *Universal Parametric Correlations of Conductance Peaks in Quantum Dots*, Phys. Rev. Lett. **76**, 1711 (1996).
- [59] A. A. Lucas, E. Khartheuser, and R. G. Badro, *Electron-Phonon Interaction in Dielectric Films. Application to Electron Energy Loss and Gain Spectra*, Phys. Rev. B **2**, 2488 (1970).
- [60] S. Q. Wang and D. G. Mahan, *Electron Scattering from Surface Excitations*, Phys. Rev. B **6**, 4517 (1972).

- [61] E. Evans and D. L. Mills, *Interaction of Slow Electrons with the Surface of a Model Dielectric: Theory of Surface Polarons*, Phys. Rev. B **8**, 4004 (1973).
- [62] J.J. Licari and R. Evrard, *Electron-phonon interaction in a dielectric slab: Effect of the electronic polarizability*, Phys. Rev. B **15**, 2254 (1977).
- [63] L.Wendler, *Electron-Phonon Interaction in Dielectric Bilayer Systems*, Phys.Stat.Sol. (b) **129**, 513 (1985).
- [64] N.Mori and T.Ando, *Electron-optical-phonon interaction in single and double heterostructures*, Phys.Rev.B **40**, 6175 (1989).
- [65] R. Chen, D. L. Lin, and T. F. George, *Optical-phonon modes in a double heterostructure of polar crystals*, Phys. Rev. B **41**, 1435 (1990).
- [66] G. Q. Hai, F. M. Peters, and J. T. Devreese, *Polaron energy and effective mass in a quantum well*, Phys. Rev. B **42**, 11063 (1990).
- [67] E. P. Pokatilov, V. M. Fomin, N. N. Semenovskaya, and S. I. Beril *Interaction Hamiltonian between an electron and polar surface vibrations in a symmetrical three-layer structure*, Phys. Rev. B **47**, 16597 (1993).
- [68] B. C. Lee and K. W. Kim, M. Dutta and M. A. Stroscio, *Electron-optical-phonon scattering in wurtzite crystals*, Phys. Rev. B **56**, 997 (1997); B. C. Lee, K. W. Kim, M. A. Stroscio, and M. Dutta, *Optical-phonon confinement and scattering in wurtzite heterostructures*, Phys. Rev. B **57**, 4860 (1998).
- [69] Weinan E and Zhongyi Huang, *Matching Conditions in Atomistic-Continuum Modeling of Materials*, Phys. Rev. Lett. **87**, 135501 (2001).
- [70] M. L. Ludowise, *Metalorganic chemical vapor-deposition of III-V semiconductors*, J. Appl. Phys. **58**, R31 (1985).
- [71] J. Los, A. Fasolino, and A. Catellani, *Generalization of the kp approach for strained layered semiconductor structures grown on high-index-planes*, Phys. Rev. B **53**, 4630 (1996).
- [72] E.R. Racec and D.E.N. Brancus, *Electron-phonon interaction in anisotropic uniaxial double heterostructures*, J.Phys.: Condens. Matter **10**, 3845 (1999).
- [73] D.E.N. Brancus and E.R. Racec, *Phonon modes in strained double heterostructures, a comparative analysis*, Balkan Phys. Lett. **7**, 40 (1999).
- [74] D.E.N. Brancus and E.R. Racec, *Electron-optical phonon interaction in an anisotropic uniaxial slab*, Rom. Journ. Phys. **45**, 99 (2000).
- [75] W.E.Jones and Ronald Fuchs, *Surface Modes of Vibration and Optical Properties of an Ionic - Crystal Slab*, Phys. Rev. **B 4**, 3581 (1971).

- [76] R. Fuchs and K. L. Kliewer, *Optical Modes of Vibration in Ionic Crystal Slab*, Phys.Rev. **140**, A2076 (1965).
- [77] R. Englman and R. Ruppin, *Optical lattice vibrations in finite ionic crystals*, J.Phys. C (Proc.Phys.Soc) **1**, 614 (1968)
- [78] L. Merten, in *Atomic Structure and Properties of Solids* Academic Press, New York, 1972.
- [79] D. E. N. Brancus and A. C. Mocuta, *Anisotropic optical polaron in crystals with complex structure*, Can.J. Phys. **B 73**, 126 (1995).
- [80] H. J. L. van der Valk and C. Haas, *Anisotropy of lattice-vibrations of layered compounds*, Phys. Stat. So. (b) **80**,321 (1977).
- [81] F. Cerdeira, C.J. Buchenauer, F. H. Pollak, and M. Cardona, *Stress-Induced Shifts of First-Order Raman Frequencies of Diamond- and Zinc-Blende-Type Semiconductors*, Phys. Rev. B **5**, 580 (1972).
- [82] F. Cerdeira, E. Anastassakis, W. Kauschke, and M. Cardona, *Stress-induced doubly resonant Raman scattering in GaAs*, Phys. Rev. Lett. **57**, 3209 (1986).
- [83] E. Anastassakis, Y. S. Raptis, M. Humlnermann, W. Richter, and M. Cardona, *Raman and infrared phonon piezospectroscopy in InP*, Phys. Rev. B **38**, 7702-7709 (1988).
- [84] D. L. Smith and C. Mailhot, *Theory of semiconductor superlattice electronic structure*, Rev. Mod. Phys. **62**, 173-234 (1990).
- [85] C. Trallero-Giner, F. Garcia-Moliner, V. R. Velasco, and M. Cardona, *Analysis of the phenomenological models for long-wavelength polar optical modes in semiconductor layered systems*, Phys.Rev. B **45** 11944 (1992).
- [86] B. K. Ridley, O. Al-Dossary, N. C. Constantinou, and M. Babiker, *Continuum model of the optical modes of vibration of an ionic crystal slab*, Phys. Rev. B **50**, 11701 (1994).
- [87] J. W. Matthews and A. E. Blabescu, J. Cryst. Growth **27**, 118 (1974).
- [88] L. Wendler and E. Jäger, *Phonon-Polaritons in Bilayer Systems*, Phys.Stat.Sol. **b 120**, 235 (1983).
- [89] L. Wendler and R. Pechstedt, *Dynamic screening, collective excitations, and electron phonon interaction in heterostructures and semiconductor quantum-wells - application to double heterostructures*, Phys.Stat.Sol. **b 141**, 129 (1987).
- [90] D. E. N. Brancus and G. Stan, *Cyclotron resonance in uniaxial polar crystals with complex structure*, Phys. Rev. B **57**, 3411 (1998).

- [91] E. Anastassakis, *Strains and optical phonons in material systems*, Acta Physica Hungarica **74**, 83-105 (1994).
- [92] S. J. J. Teng, J. M. Ballingall, and F. J. Rosenbaum, *Vapor phase epitaxial growth and characterization of InP on GaAs*, Appl.Phys.Lett **48**, 1217 (1986).
- [93] S. Agarwala, M. B. Patil, C. K. Peng, and H. Morkoç, *Al<sub>0.3</sub>Ga<sub>0.7</sub>As/GaAs metal-insulator-semiconductor-type field-effect transistor fabricated on an InP substrate*, Appl.Phys.Lett. **53**, 493 (1988).
- [94] A. Freundlich, J. C. Grenet, G. Neu, G. Landa, and R. Carles, *Photoluminescence and Raman studies of residual stresses in GaAs directly grown on InP*, Appl.Phys.Lett. **55**, 1558 (1989).
- [95] M. Hünemann, W. Richter, J. Saalmüller, and E. Anastassakis, *Phonon and plasmon deformation potentials of GaAs: Far-infrared study under uniaxial stress*, Phys. Rev. B **34**, 5381 (1986).
- [96] S. Albeverio, F. Haake, P. Kurasov, M. Kus, P. Seba, *S-matrix, resonances, and wave functions for transport through billiards with leads*, J. Math. Phys. **37** 4888 (1996).

## Danksagung

An dieser Stelle möchte ich mich bei all denen bedanken, die mich in den vergangenen Jahren unterstützt haben.

Herrn Prof. Dr. Ernst Sigmund danke ich für seine großzügige Unterstützung und für die Aufnahme an seinem Lehrstuhl.

Daß mein Aufenthalt in Cottbus in wissenschaftlicher wie auch persönlicher Hinsicht ein Gewinn für mich war, verdanke ich auch herzlich Herrn Dr. Ulrich Wulf. Mit seiner Hilfe konnte ich mich in das Gebiet der Transport Phenomena einarbeiten. Er hat viel getan, damit ich mich in Cottbus wohlfühlen konnte.

Special thanks go to Prof. Dr. Dan Brancus, who gave me invaluable insights into the secrets of the solid state theory. The many discussions and his knowledge have contributed greatly to the success of my work. He offered me the opportunity to start the research in a very interesting field of physics and encouraged and supported me during all the years of my thesis work.

I would like to express my gratitude to Prof. Dr. Gheorghe Ciobanu from the University of Bucharest for the valuable discussions.

Herrn Dr. Jan Kučera danke ich für die hilfreichen Diskussionen über das R-matrix Formalismus und die Transport Theorie.

Meinen Kollegen an den Lehrstühlen der Theoretischen Physik der BTU Cottbus gilt mein Dank für die angenehme und kollegiale Arbeitsatmosphäre.

I am also very grateful to my colleagues from the Department of Solid State Physics of the University of Bucharest for helping me during my PhD study.

Ein großer und persönlicher Dank an Frau Dr. Renate Kranzusch und Herrn Dr. Jochen Schöttner die mir die deutsche Sprache beigebracht haben und die Schönheit dieser Sprache gezeigt haben.

Schließlich möchte ich mich bei Paul und bei meinen Eltern bedanken. Sie waren mir die ganzen Jahre die wichtigste Stütze.





## Lebenslauf

Name: ELENA ROXANA RACEC  
Geburtsname: Tepus  
Geburtsdatum: 2.01.1972  
Geburtsort: Filipestii de Tirg, Rumänien  
Nationalität: Rumänisch

### Ausbildung:

September 1978 - Juni 1982 Grundschule Nr.2 Campina, Prahova  
September 1982 - Juni 1986 Gymnasium Nr.2 Campina, Prahova  
September 1986 - Juni 1990 Industriegymnasium Nr. 5 Campina, Prahova  
Juni 1990 Abitur  
September 1990 - Juni 1995 Fakultät für Physik  
Universität Bukarest, Rumänien  
Juni 1995 Diplom  
September 1995 - Juni 1996 Vertiefende Studien (Master Program),  
Universität Bukarest, Rumänien

Spezialisierung: Festkörperphysik

### Berufstätigkeit

Oktober 1995 - September 1996 Forschungsassistentin -Nationalinstitut  
für Physik der Materialien, Bukarest, Rumänien  
seit Oktober 1996 Hochschulassistentin - Fakultät für Physik,  
Universität Bukarest, Rumänien  
Oktober 1999 - Juli 2000 Gastwissenschaftlerin an der Technische Universität  
Cottbus; DAAD Stipendium  
seit August 2000 Wissenschaftliche Mitarbeiterin am Lehrstuhl  
Theoretische Physik, Technische Universität  
Cottbus